Testing General Relativity with the next generation of cosmological surveys

Teboho Abram Moloi

Department of Mathematics, as part of ACGC
University of Cape Town

This dissertation is submitted in fulfillment of the requirements for the *Doctor of Philosophy degree*

Supervisor:Dr Julien Larena
Cosupervisor:Dr Chris Clarkson June 2019

To Nkosingiphile and our son Pheello.

Abstract

The late-time acceleration expansion of the Universe is conceptually considered the great burdensome issue in theoretical physics (cosmological problem) dubbed dark energy (DE) problem. In general relativity (GR) framework view point, there are two ways to explain where this acceleration might originate from; this riddle might either emerge from some unknown dark energy models or general relativity is a mistake on cosmological scale and dark energy is insubstantial. Innovative efforts have been carried out to comprehend the origin of the cosmic acceleration, involving surveys such as baryon acoustic oscillations (BAOs), Type Ia supernovae, weak gravitational lensing and the abundance of galaxy clusters. The next generation of cosmological surveys including LSST, DES, eBOSS, DESI, PFS, SKA and WFIRST; are aimed to provide percent-level or higher measurement of history of expansion and growth of structure over a volume which is sizable fraction of the whole observable Universe, these measurements provides strong constrains on DE.

In this analysis, we investigate the Horndeski scalar-tensor theories and beyond which has been recently described in the generilized dark energy (DE) or scalar-tensor paradigm - dubbed *unified dark energy* (UDE). This applies the 3+1 Arnowitt-Deser-Misner (ADM) formalism where a general action in unitary gauge depends on the lapse function and geometrical scalar quantities. This approach is convenient since it generates a unified framework of modified theories based on UDE or effective field theory (EFT) of linear cosmological perturbations on Friedmann-Lemaitre-Robertson-Walker (FLRW) background, this are generally characterized by five free time-dependent functions α_i ($\alpha_B, \alpha_H, \alpha_K, \alpha_M, \alpha_T$) each describing different properties of unified dark energy physical outcome. The evolution equations for the given UDE which assimilates beyond-Horndeski paradigms appear to correspond to a non-conservative DE scenario, in which the total energy-momentum tensor is not conserved.

Furthermore, we evaluate the large-scale imprint of this UDE, by probing the two-point correlation function or power spectrum of galaxy number counts and the magnification of galaxies, on horizon scales; making sure to include the full relativistic corrections in the observed overdensity and convergence. This yield new observables which gives

independent insights regarding the peculiar velocity of galaxies, the growth of structure of the Universe etc.

Declaration

Whilst registered as a candidate for the above degree, I have not been registered for any other research award. The results and conclusions embodied in this thesis are the work of the author under the supervision of Chris Clarkson (Queen Mary University of London) and Julien Larena (University of Cape Town) and in collaboration with Didam Duniya (University of Cape Town), Amanda Weltman (University of Cape Town), David Bacon (University of Portsmouth), Roy Maartens (University of Western Cape), Camille Bonvin (European Organization For Nuclear Research (CERN)), Sambatra Andrianomena (South African Radio Astronomy Observatory (SARAO)) and Philip Bull (University of Oslo). The following published papers resulted from my collaboration with these people

1. Bonvin C., Andrianomena S., Bacon D., Clarkson C., Maartens R., **Moloi T**., Bull P.,"Dipolar modulation in the size of galaxies: The effect of Doppler magnification ". MNRAS, 472, 3936. arXiv:1610.05946 [astro-ph.CO]

2. Andrianomena. Sambatra, Bonvin. Camille, Bacon, David, Bull. Philip, Clarkson. Chris, Maartens. Roy and **Moloi. Teboho**, "Testing General Relativity with the Doppler magnification effect." Mnras.(2018), arXiv:1810.12793 [astro-ph.CO]

Chapter. 5 is absolutely based on "Probing beyond-Horndeski gravity on horizon scales" Didam G.A. Duniya, Chris Clarkson, Amanda Weltman, Roy Maartens, and Teboho Moloi, in preparation.
Chapter. 6 consists of two main sections, section. 6.1 entirely new results based on "Probing beyond-Horndeski theories in Quasi-static limit approximation" Teboho Moloi, Didam G.A. Duniya Julien Larena, Chris Clarkson, Sambatra Andrianomena, Camille Bonvin, David Bacon, Roy Maartens, Philip Bull. in preparation.
section. 6.2 is based on second paper given above.

I hereby declare that the contents of this dissertation are original and have not been submitted in whole or in part for consideration for any other degree or qualification in this, or any other university.

Teboho Abram Moloi

June 2019

Acknowledgements

First of all, I would like to thank my supervisors Chris Clarkson and Julien Larena, for their support and guidance, for all useful hours of the skype discussions and for proof reading parts of this thesis.

I would also like to thank Didam G.A. Duniya, for all the answers to my uncountable inquiries, for help with things related to coding, for motivational words and mentoring. Many thanks to Sambatra Andrianomena, for his time and for the kind mentoring. Additionally, Many thanks to my collaborators Amanda Weltman, David Bacon, Roy Maartens, Camille Bonvin, and Philip Bull for their great work and many useful skype discussions.

I would like to thank National Institute for Theoretical Physics (NITheP), for funding my studies and research. Thanks to the cosmology group, University of Cape Town, for pleasant academic environment.

Many thanks to my family, for the support, love and encouragement they give me.

Table of contents

List of figures

List of tables

Chapter 1

Introduction

> *A book, too, can be a star, a living fire to lighten the darkness, leading out into the expanding Universe.*
>
> — Madeleine L'Engle

The centerpiece of the galaxy clustering studies has been two point correlation function (2PCF) over years, the importance of this statistical quantity has been rigorously discussed by [199]. 2PCF in modern physics describes the way in which the actual distribution of galaxies deviates from a simple Poisson distribution. Nevertheless, 2PCF is not the only statistical quantity in cosmology there are many descriptors like genus topology, three point correlation function which dubbed as bispectrum and so forth, unfortunately in this thesis we won't go in to details on other statistical quantities but 2PCF.

There are two kinds of 2PCF: (i) describes the clustering in space known as the spatial correlation function $\xi(r)$. (ii) Describes the clustering as projected on the sky, thus describing the angular distribution of galaxies in a typical galaxy catalogue dubbed the angular distribution $\omega(\theta)$. The matter power spectrum is the Fourier transform of the correlation function. We know that power spectrum is the basic outcome of the structure formation, growth and the large scale structure of the Universe. 2PCF could be used to test unknowns like dark energy DE and dark matter DM, it should be noted that here when we refer to DE this include modification of gravity. It is in our believe or guess that if modified gravity MG could be a source candidate for acceleration of our Universe, then it can definitely be described in term of the background dark energy density.

Lets give a picture from concordance model of the Universe, of about 4% matter of the Universe is what is known as baryons in cosmology (neutrinos and radiation),

then 73% of the energy density is composed of DE and the remaining 23% is dark matter. This is a driving factor for us to get our hands dirty with DE, reason being the majority of our Universe is dominated by this unknown. Additional motivation we have strong believe that the solution to this mystery might give us the more details of our Universe's fundamentals. It is our hope that this could give a better explanation for the expansion of the Universe.

1.1 Dark Energy experiments

What do we get from observations? From [204, 209] provided the exiting news that our Universe is accelerating. What really makes DE a key factor is that it has a negative pressure, now this negative pressure opposes the gravitational force this leads to the accelerating expansion of the Universe. For years there where many attempts to understand DE, One of the candidates is called cosmological constant Λ, which has a constant energy density [242]. (See for more details [7]) focusing on particle physics perspective, vacuum energy density describes the cosmological constant. At Planck scale, the vacuum energy density is much larger than the observed value of the Λ energy density dubbed as dark energy. Furthermore, several experiments have been conducted in order to constrain this most favored model of the Universe.

1.1.1 Cosmic Microwave Background

Unquestionably the gold of cosmological observable is the cosmic microwave background (CMB). As specified by Big bang theory—that the Universe began hot and dense, then expanded and cooled. The early Universe in hot, dense conditions the photons and matter were coupled together. When the Universe was about 300.000 years old the temperature dropped to $T_{dec} \sim 3000K$ this leads to the formation of atomic hydrogen and photons decouple from matter. These decoupled photons propagate freely through the Universe makes up observed cosmic microwave background (CMB) today [3]. The recent Planck the joint constraint with BAO measurements on spatial curvature is consistent with a flat universe, $\Omega_K = 0.001 \pm 0.002$. And with the addition of Type Ia supernovae (SNe), the DE equation of state parameter is measured to be $w_0 = -1.03 \pm 0.03$, consistent with a cosmological constant [4].

1.1.2 Type Ia Supernovae

Supernovae are an explosion of massive stars, which are generally classified into two types: Type I or Type II depending upon the shape of their light curves and the nature of their spectra, the commonly used in modern physics is Type Ia which occurs when accretion white dwarf (descendant of a low mass star) goes above Chandrasekhar limit and collapses, causes carbon-fusion and explodes in a supernova. Due to the fact that this objects are well studied and all their mass is the same during the explosion, this can be used as the standard candle to measure luminosity distance $d_L(z)$. Since the intrinsic luminosity L of such events are constants and one can measure the flux F directly from the supernova, then luminosity distance can easily evaluated from the relation [87, 204, 209, 222],

$$d_L(z) = \sqrt{\frac{L}{4\pi F}} = (1+z)\int_0^z \frac{dz'}{H(z')}. \tag{1.1}$$

In modern physics we determine the luminosity distance from the distance modulus of the apparent magnitude m of the object [1] and the absolute magnitude M [2] given by, $m - M = 5\log_{10}\left(\frac{d_L}{10pc}\right)$. Type Ia supernovae at high redshift, measure higher derivatives of $d_L(z)$, which we use to measure the time evolution of the Dark Energy equation of state parameter w_{DE} from supernova without involving CMB and without worrying about any degeneracies Turner and Huterer [234].

1.1.3 Baryon Acoustic Oscillations

Over years it have been shown that the matter power spectrum (its Fourier transform 2PCF) is not the only key diagnose feature that could be evaluated as function of redshift [103, 221, 235]. This oscillations appear in the 2PCF because the acoustic perturbations in the era prior to recombination, era where the Universe has been filled with transparent fluid of coupled (baryons, photons and electrons) dubbed as photon-baryon fluid provide new feature. Furthermore, even though the magnitude of the baryon oscillations are small—they are more distinct than 2PCF. Thus, provide a very useful standard ruler even at low signal-to-noise.

[1] proportional to the log of the flux

[2] proportional to the log of the intrinsic luminosity (we note that 5 astronomical magnitudes correspond to a factor of 100 in flux or a factor of 10 in luminosity distance)

1.1.4 Weak Lensing Surveys

When light rays emitted by a distant source get deflected by passing the matter distribution along the line of sight of the observer. The deflection results in some distortions of the image of the object, that involves both **shear** and **magnification** (or **demagnification**). It is worth mentioning that shear and convergence are observables. Furthermore, weak-lensing associate with distortions of the images of distant source by primordial fluctuations in the line of sight but does not correspond to lens. Therefore, weak-lensing is able to probe the intervening matter through the gravitational potential which can be compared to theory. Weak-lensing also yields a unique ways of probing the Dark Energy [17, 109, 180, 189, 223, 226, 231]. (More comprehensive review of Weak-Lensing is provided in chapter. 2)

1.1.5 Cluster Surveys

The most large-scale structure objects are galaxy clusters, which has redshift distribution that is given by [136, 142, 161, 185, 239, 244]

$$\frac{dN}{dz}(z) = \Delta\Omega \frac{dV}{dz d\Omega} \int_{M_{\rm lim}}^{\infty} \frac{dn(M,z)}{dM} dM \tag{1.2}$$

Where $dV/(dzd\Omega)$ is the comoving volume element and $\Delta\Omega$ is the solid angle of the survey. This allow for the prediction of mass function $dN/(dMdV)$ for the abundance of clusters, these can be used to be compared to observations from galaxy surveys. Furthermore, making use comoving volume element one can extract the dependence on DE, which depends on scale factor. Hence, tracks the cosmological history. Additional dependence can be extracted from the way the mass function depends on the growth of perturbations, which are very turn sensitive to the Hubble factor. Correspondence to the magnitude of perturbations in the CMB enable us to consider the dependency in prediction of the expected mass function [40].
Later on the thesis, this review will be reintroduced when we evaluate the galaxy number count in chapter. 5

1.1.6 Alcock-Paczynski test

Alcock-Paczynski test is one of the interesting cosmological test due to the fact that it does not depends on the evolution of galaxies, but only on the geometry of the Universe dubbed as assumption free. The key diagnose is to measure an evaluation of the ratio of observed angular size to radial size given both as a function of redshift [5, 173].

1.2 Fundamental topics of this work

In this thesis we are mostly anxious with testing standard theory of gravity at largest possible observable scale through estimation of the velocity field or the formation of structure at late-time cosmology. Moreover, we show a unified framework which allow us to deliver theoretically reliable forecasts for growth of structure for possible contending scalar-tensor theories to general relativity GR. Thus, we exploit two phases of the explored aspects. *First phase*: Priority being predictions of cosmological probes such as Euclid [159] and the SKA [175], we investigate the large-scale imprint of DE by means of joint correlations between the observed density contrast and the magnification of galaxies. Furthermore, from this we extricate diverse multipoles which yields new observables which give independent information about the growth of structure, the velocity field of galaxies and so forth. We evaluate all this in GR, as a means of more accurately using galaxy surveys to calculate the parameters of the concordance model.

Second phase: After we've resolved the variability of all new observables, we generalize them into more generic modified theories or effective field theories. Many theories of gravity can be encompassed within a broader context whereby deviations from GR can be parameterized by free functions, it is this we aim to constraint observationally. We sought combinations of the correlation functions to isolate these free functions so as to determine them observationally. These can be considered as providing null tests for the standard theory of gravity. We provide predictions for the measurability of these parameters for cosmological probes such as SKA[3] and DESI [4].

1.3 Configuration of this thesis

The structure of this thesis is as follows; in chapter. 2 we review the cosmological perturbation theory and it's applications we mainly center our attention to the scalar, vector and tensor modes. We analyze the gauge problem, we also provide the Einstein equations and we make available the experience of the generalized fluid systems. We discuss the basic on weak gravitational lensing which will be of importance later on in this dissertation.

In chapter. 3 we outline the large scale fluctuation spectra and we describe the magnification bias in the large-scale structure

[3] https://www.skatelescope.org
[4] https://www.desi.lbl.gov/

In chapter. 4 we introduce the effective field theory of DE, we also discuss the UDE formalism and provide the generalized action for linear cosmological perturbations.

We apply this apparatus in chapter. 5 by probing beyond-Horndeski gravity on horizon scales. The evolution equations for the given UDE appear to correspond to a non-conservative DE scenario, in which the total energy-momentum tensor is not conserved. We investigate the large-scale imprint of this UDE, by probing the angular power spectrum of galaxy number counts, on horizon scales; taking are to include the full relativistic corrections in the observed overdensity. Additionally, we probe two-point correlation functions for Doppler magnification. This whole chapter is mainly based on my on work. The recent published work on this chapter my collaborators focused on cls while here I just looked into two point correlation funtions.

Finally, in chapter. 6 we look into the modification of gravity signature in quasistatic limit approximation. firstly We investigate the large-scale imprint of this UDE, by probing the 2PCF of galaxy overdensity-convergence-galaxy; taking are to include the full relativistic corrections in the observed overdensity and convergence. Secondly We show that the next generation of spectroscopic galaxy redshift surveys will be able to measure the Doppler magnification effect with sufficient signal-to-noise to test GR on large scales. We illustrate this with forecasts for the constraints that can be achieved on parametrised deviations from GR for forthcoming low-redshift galaxy surveys with DESI and SKA2.

In chapter. 7 we give general conclusions and discuss the possible future work to follow up on the research presented here.

Appendix.A provides the detailed GR evaluation of galaxy overdensity. Appendix. B provides the useful function or parameters used in computing the correlation functions. In Appendix. C we evaluate some of the multipoles. Lastly, in Appendix. D we give the modified perturbed Einstein equations, beyond-Horndeski parameters and we also provide the quasi-static limit approximation

Chapter 2

Linear cosmological perturbation theory and weak-lensing

In this chapter we review the basic background equations based in the Friedmann-Lemaitre-Robertson-Walker (FLRW) background and we review in component context the scalar, vector and tensor linear perturbations equations—this will serve as very useful tools for the analysis of some of upcoming chapters. We begin by introducing the non interacting space-like hypersurfaces then discuss the Arnorwitt-Deser-Misner (ADM) formulation of general relativity (GR) and make available their useful action and Lagrangian. After we review the spatially homogeneous and isotropic background of our Universe and the perturbations around it, we also provide their perturbed metric and we also addressed the gauge problem in the perturbation theory. We give the small review of the geodesic equations and their perturbed equations that are very important in the derivation of galaxy number count in Appendix. A. We provide the scalar, vector and tensor Einstein field equations and introduce the multi-component interactions of fluids in the perturbed Universe—this are all within Newtonian gauge; which we particularly used throughout this thesis. We finish off the section by providing the basics of gravitational lensing.

2.1 Hypersurfaces and the ADM formalism

In this section, we describe the foliation (The non-interacting space-like hypersurfaces $\sum_t$ where t is scalar function such that $t =$ arbitrary const) of co-dimension space-like hypersurfaces, which results into a time-like gradient involving the scalar field ϕ. The decomposition of time vector t^μ in the basis provided by the normal and the tangent

vector [1] demonstrated in Eq. (2.1) ;

$$t^\mu = Nn^\mu + N^\mu e^\mu{}_\mu \tag{2.1}$$

Where *lapse function* is denoted by $N(\vec{x},t)$ as the normalized and *shift vector* is $N^\mu(\vec{x},t)$. The normal vector to the foliation $n_\mu \equiv -N\nabla_\mu\phi$. We note that this curves are not geodesics nor intersect orthogonality. Furthermore, we introduce the extrinsic curvature tensor and acceleration vector field given by

$$K_{\mu\nu} \equiv D_\mu n_\nu \quad \text{and} \quad a_\mu \equiv D_\mu \ln N \tag{2.2}$$

Which are respectively in correspondent with the components of $\nabla_\nu n_\mu$ which are parallel and perpendicular to the hypersurfaces, where the induced metric on the hypersurfaces yields $h_{\mu\nu} \equiv g_{\mu\nu} + n_\mu n_\nu$, with D_μ being the intrinsic covariant derivative associated with $h_{\mu\nu}$.Thus, we can express the second derivatives of ϕ and the extrinsic curvature tensor as follows

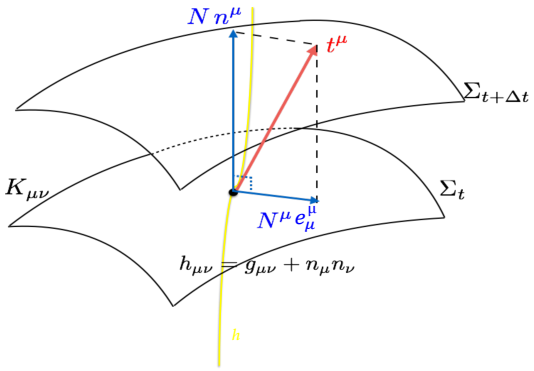

Fig. 2.1 Schematic for 3+1 Decomposition of the vector t^μ into lapse function N (the normalized coefficient) and shift vector N^μ.

$$K_{\mu\nu} = -N\nabla_\mu\nabla_\nu\phi + n_\mu a_\nu + n_\nu a_\mu + \frac{1}{2X} n_\mu n_\nu n^\gamma \nabla_\gamma X \tag{2.3}$$

Where $X \equiv g^{\rho\sigma}\nabla_\rho\phi\nabla_\sigma\phi$.
In the ADM formalism, we express the 3+1 decomposition by the following metric (see

[1] Reader should note that basis $e^\mu{}_\mu$ is equal in specified coordinates to the Kronecker's delta δ^μ_μ, the same applies for t^μ and δ^μ_t

[13, 128–130] for comprehensive review)

$$ds^2_{ADM} = -(N^2 - N_i N^i)dt^2 + 2N_i dx^i dt + h_{ij}dx^i dx^j \tag{2.4}$$

Where h_{ij} is the spatial metric, we use this to lower and raise indices. additionally, we define the components of the metric as follows; $g_{00} = -(N^2 - N_i N^i)$, $g_{0i} = N_i$ and $g_{ij} = h_{ij}$.Then the inverse of the metric components are; $g^{00} = -\frac{1}{N^2}$, $g^{0i} = \frac{N^i}{N^2}$ and $g^{ij} = h^{ij} + \frac{N^i N^j}{N^2}$. A normal unit vector orthogonal to constant time hypersurface $\sum_t$ is denoted by

$$n^\mu \equiv \left(\frac{1}{N}, \frac{N^i}{N}\right), \quad n_\mu \equiv (-N, 0, 0, 0) \tag{2.5}$$

The extrinsic curvature of hypersurface $\sum_t$ is defined as

$$K_{ij} = D_i n_j = \Gamma^\mu{}_{ij} n_\mu = -N\Gamma^0{}_{ij} \tag{2.6}$$

Where covariant derivatives and Christoffel[2] symbols are respectively[3] denote by

$$D_\mu n_\nu \equiv \partial_\mu n_\nu - \Gamma^\alpha{}_{\mu\nu} n_\alpha \tag{2.7}$$

And

$$\Gamma^\alpha{}_{\mu\nu} = g^{\alpha\beta}\Gamma_{\beta\mu\nu} = \frac{1}{2}g^{\alpha\beta}(\partial_\mu g_{\beta\nu} + \partial_\nu g_{\beta\mu} - \partial_\beta g_{\mu\nu}) \tag{2.8}$$

The extrinsic curvature tensor satisfies the following characteristics

1. The space-like metric h_{ij} and its covariant derivative D_k is always commutative; this can be deduced from Eq. (2.6)

$$K_{ij} = h_j{}^l h_i{}^k D_k n_l \equiv h_i{}^k D_k n_j + n_j n^l h_i{}^k D_k n_l \tag{2.9}$$

2. The extrinsic curvature tensor is symmetric; $K_{ij} = K_{ji}$, which yields $K_{ij} = \frac{1}{2}(K_{ij} + K_{ji})$

[2] $\Gamma^\alpha{}_{\mu\nu}$ goes by multiple names Levi-Civita connections, connection coefficient or affline connections.

[3] Note also that the curvature tensor in theories with non-metric connection can be viewed as an (exact at second order) variation of the Riemannian one with respect to the connection being varied from its Levi-Civita value by non-metricity and contortion tensors Golovnev [120]

3. The extrinsic curvature is half of the Lie derivative of the intrinsic metric along the unit normal (detailed by [83, 236]):

$$2K_{ij} = n^k D_k h_{ij} + h_{kj} D_i n^k + h_{ik} D_j n^k = \mathscr{L}_n h_{ij} \tag{2.10}$$

The above expression can be reformulated as follows $K_{ij} = \frac{1}{2N} h_i{}^k h_j{}^l (\mathscr{L}_t h_{kl} - \mathscr{L}_N h_{kl})$

Making use of the four properties and Eq. (2.1) and with some algebra the extrinsic curvature tensor finally becomes

$$K_{ij} = \frac{1}{2N}(\dot{h}_{ij} - D_i N_j - D_j N_i) \tag{2.11}$$

This vasty contribute to velocity of the spatial metric and hence a good candidate for its momentum. Furthermore, the 4-dimensional curvature is often involved in Lagrangian for gravitational theories, using the Gauss-Codazzi equation and Ricci equation together with the symmetry of the Riemann tensor we arrive at

$${}^{(4)}R = K_{ij}K^{ij} - (K^i{}_i)^2 - 2\nabla_i v^i + R \tag{2.12}$$

Henceforth, we will consider the general gravitational actions which we express in term of the geometrical quantities given as

$$S_g = \int d^4x \sqrt{-g} \mathcal{L}(N, k_{ij}, R_{ij}, h_{ij}, D_i; t) \tag{2.13}$$

In GR we Neglecting total time derivative and covariant divergence[4] terms, we finally obtain the Einstein-Hilbert action in the ADM formalism:

$$S_{EH} = \frac{1}{16\pi G} \int d^4x \sqrt{-\det g}\, R = \int dt \mathcal{L}_{GR} \tag{2.14}$$

The Lagrangian in term of the extrinsic curvature and the 4 Ricci scalar is denoted by

$$\mathcal{L}_{GR} = \frac{1}{16\pi G} \int d^3x\, N \sqrt{-\det h} \left(K_{ij}K^{ij} - (K^i{}_i)^2 + R \right) \tag{2.15}$$

Where the determinants $\det g = -N^2 \det h$. Henceforth, the results given Eq. (2.13) made active for more complicated modified gravity models such as (Quintessence, $f({}^4R)$

[4]Note that the vector field v^i is defined as follows : $v^i = -n^i D_k n^k + n^k D_k n^i$

theories, Horava-Lifshitz theories, Horndeski theories, Beyond Horndeski theories and so forth).

2.2 FLRW metric perturbations

Observations have shown [43] that the geometry of the Universe is roughly homogeneous and isotropic, this can be best described by the homogeneous and isotropic FLRW space-time metric [110, 160, 211, 237]. On large-scale the observable Universe is effectively described by cosmological paradigms based on FLRW geometry. However, this fails to explain the 'real' Universe well in an essential way, due to their conceptualized degree of symmetry which in comparison does not compare with the 'lumpy' real Universe. Thus, this needs to be perturbed in order to get realistic 'almost-FLRW' Universe paradigm, which will be useful in evaluation of the inhomogeneities and anisotropies arising during structure formation so as the comparison of this an the observations.

The linearized cosmological perturbation theory around FLRW background metric has quiet a history, which originated or introduced by [166], summarized by [167], additional crucial extensions was introduced by [21] which shines a light on gauge-invariant potentials to describe the metric perturbations, other motivated by this work are given by [121, 188]. This theory provide important tools when we confront dark energy paradigm with observations of the cosmic microwave background (CMB) and large-scale structure (LSS) and this will enable one to make theoretical predictions. Throughout out this thesis our computation are with in linearized cosmological perturbation theory [7, 87, 95, 96, 151, 176, 188, 214]—via the following underlying action *Einstein-Hilbert action*

$$S_{EH}[g_{\mu\nu}] = \frac{1}{2K}\int_{\mathcal{M}} d^4x\sqrt{-g}(R - 2\Lambda + \mathcal{L}_m) \tag{2.16}$$

Where the dynamical variable is the metric $g_{\mu\nu}$ of the spacetime manifold $\mathcal{M}$, with $K = \frac{8\pi G}{c^4}$, $g = \det[g_{\mu\nu}]$ is the determinant of the metric tensor, R is the Ricci scalar, $\mathcal{L}_m$ is denoted by Lagrangian of matter and finally Λ is the cosmological constant. The action above results in *Einstein's field equations*

$$R_{\mu\nu} - \frac{R}{2}g_{\mu\nu} + \Lambda g_{\mu\nu} = -K\frac{2}{\sqrt{-g}}\frac{\delta(\sqrt{-g}\mathcal{L}_m)}{\delta g^{\mu\nu}} \implies G_{\mu\nu} + \Lambda g_{\mu\nu} = \frac{8\pi G}{c^4}T_{\mu\nu} \tag{2.17}$$

Where $R_{\mu\nu}$ and $g_{\mu\nu}$ are the Ricci and metric tensors respectively, Ricci scalars are denoted by $R \equiv R^{\alpha}{}_{\alpha}$. We define stress-energy tensor as follows

$$T_{\mu\nu} \equiv \frac{-2}{\sqrt{-g}} \frac{\delta(\sqrt{-g}\mathcal{L}_m)}{\delta g^{\mu\nu}} \tag{2.18}$$

We also define the Einstein tensor to be given by

$$G_{\mu\nu} = R_{\mu\nu} - \frac{1}{2} R g_{\mu\nu}, \qquad G_{\mu\nu} = \frac{8\pi G}{c^4} T_{\mu\nu} \tag{2.19}$$

The combination of Bianchi identity $\nabla_{\mu} G_{\mu\nu} = 0$ and $\nabla_{\mu} g_{\mu\nu} = 0$ lead to *energy-momentum conservation* $\nabla_{\mu} T_{\mu\nu} = 0$. Prior to evaluation of expressions above we introduce perturbations in FLRW Universe, described by the line element in polar coordinates.

$$ds^2_{FRW} = a^2(\eta)[-c^2 d\eta^2 + \frac{dr^2}{1 - Kr^2} + r^2 d\theta^2 + r^2 \sin^2\theta d\phi^2] \tag{2.20}$$

Where η is the conformal time related to proper time t by the relation $a\, d\eta = dt$, $a(\eta)$ is the scale factor and (r, θ, ϕ) denotes polar coordinates. We choose the spacetime curvature constant K to take only discrete values -1, $+1$ and 0 corresponding to closed, open and flat geometries, μ and ν indices range from 1 to 3. Throughout this dissertation our work is enclosed by FLRW Universe framework. Furthermore, in subsections to follow we outline the linear cosmological perturbations theory in FLRW Universe.

2.2.1 Metric fluctuations

The metric tensor about the perturbed FLRW Universe may be decomposed by

$$g_{\mu\nu} = \bar{g}_{\mu\nu} + \delta g_{\mu\nu} \tag{2.21}$$

This can be decomposed into scalar, vector and 2-rank tensor fluctuations. The background term $g_{\mu\nu}(\eta)$ is time dependent and its components are given as follows; $\bar{g}_{00} = -a^2$, $\bar{g}_{0i} = 0$ and $\bar{g}_{ij} = a^2 \gamma_{ij}$. Where γ_{ij} is the metric on the 3-dimensional space with fixed curvature K. Henceforth, the vertical bar (e.g $X_{ab..|i}$) denote the covariant spatial derivative. Furthermore, the components of *scalar* fluctuation metric might be parametrized by scalar quantities (i.e metric fluctuations follow the notation of [24, 179, 188], apart from [24, 179] they make use of ϕ rather than A as the perturbation

in the lapse function $\phi = \phi(\eta, x^i)$, $\psi = \psi(\eta, x^i)$, $B = B(\eta, x^i)$ and $E = E(\eta, x^i)$ with x^i being the space vector), correspondently as follows;

$$\delta g_{00} = -2a^2\phi, \quad \delta g_{0i} = a^2 B_{|i}, \quad \delta g_{ij} = 2a^2(\psi\delta_{ij} - E_{|ij}) \tag{2.22}$$

The components of metric *vector* fluctuations which are given by

$$\delta g_{00} = 0, \quad \delta g_{0i} = S_i, \quad \delta g_{ij} = F_{i|j} - F_{j|i} \tag{2.23}$$

Where F_i and S_i are non-divergence vectors.
Lastely we have the component of metric *tensor* which reads $\delta g_{ij} = a^2 h_{ij}$, where h_{ij} is the trace-free and divergence-free. Thus, the linearly perturbed FLRW Universe metric is given as

$$\begin{aligned} ds^2 &= a^2(\eta)\{-(1+2\phi)d\eta^2 + 2(B_{|i} - S_i)dx^i d\eta \\ &\quad +[(1-2\psi)\delta_{ij} + 2E_{|ij} + 2F_{(i|j)} + h_{ij}]dx^i dx^j \end{aligned} \tag{2.24}$$

The intrinsic Ricci scalar curvature of $\sum_t$ constant time hypersurfaces and acceleration are given by

$$R = \frac{4}{a^2}\partial^2\phi, \quad a_i = \phi_{,i} \tag{2.25}$$

Where $\partial^2 = \delta^{ij}\partial_i\partial_j$ is the spatial Laplacian. Hence we refer to ϕ as the curvature perturbation. Throughout this thesis we will consider all this introduced (scalar, vector and tensor) perturbations: due to the fact that tensor mode result in gravitational waves and this will also help to feather our understanding of the generalized theories of linear cosmological perturbations which we will look at later on the thesis.

2.2.2 Energy-momentum stress-tensor perturbations

In this subsection, we treat the energy-momentum to be a perfect fluid which involves baryonic and dark matter fluids, on the subsection. (2.2.6) we will provide the more generalized scenarios that includes dark fluids. The perfect fluid energy-momentum stress $T_{\mu\nu}$ is given by

$$T_{\mu\nu} = u_\mu u_\nu(\rho + p) + p\delta_{\mu\nu} + \pi_{\mu\nu} \tag{2.26}$$

Where the matter density fluctuation is defined by $\delta = \frac{\delta\rho}{\bar{\rho}}$. With the total energy density ρ and total pressure p and u_μ is the four-velocity which we can break down as $u_\mu = \bar{u}_\mu + \delta u_\mu$, making use of $u_\mu u^\mu = -1$, the linear perturbed velocity and its inverse becomes

$$u_\mu = a[-(1+\phi), (v+B)_{|i} + (v-S)_i], \qquad u^\mu = \frac{1}{a}[(1-\phi), v_|{}^i + v^i] \tag{2.27}$$

This introduce the irrotational peculiar velocities. From Eq. (2.26) where we have included the gauge invariant anisotropic stress tensor which split into (scalar Π, vector π_i and tensor ${}^{(tensor)}\pi_{ij}$) [7, 95, 176]

$$\pi_{ij} = \Pi_{|ij} - \frac{1}{3}\nabla^2\delta_{ij} + \frac{1}{2}(\pi_{i|j} + \pi_{j|i}) + {}^{(T)}\pi_{ij} \tag{2.28}$$

Note that in [95] this is expressed slightly different since they neglect the vector modes and tensor modes, whereas from [7] the anisotropic stress tensor is set to zero. Now elaborating on the perfect fluid energy-momentum stress tensor in perturbed FLRW Universe which we can decompose into backgrounds and perturbations to take the form

$$T_{\mu\nu} = \bar{T}_{\mu\nu} + \delta T_{\mu\nu} \tag{2.29}$$

The energy-momentum stress tensor backgrounds and perturbations components respectively yields

$$\bar{T}_{00} = -\frac{1}{a^2}\bar{\rho}, \qquad \bar{T}_{i0} = 0, \qquad \bar{T}_{ij} = \frac{1}{a^2}\bar{p}\delta_{ij} \tag{2.30}$$

And

$$\delta T_{00} = -\frac{1}{a^2}\delta\rho, \tag{2.31}$$

$$\delta T_{i0} = \frac{1}{a^2}[(\bar{\rho}+\bar{p})(v_| + v)_i], \tag{2.32}$$

$$\delta T_{0i} = \frac{1}{a^2}\{(\bar{\rho}+\bar{p})[(v+B)_{|i}, (v-S)_i]\} \tag{2.33}$$

$$\delta T_{ij} = \frac{1}{a^2}(\delta\rho\,\delta_{ij} + \pi_{ij}) \tag{2.34}$$

As initiated in section. (2.2) Bianchi identity $\nabla_\mu G_{\mu\nu} = 0$ and $\nabla_\mu g_{\mu\nu} = 0$, result into the covariant derivative of the total energy-momentum tensor vanishing, explicitly

given by

$$\nabla_\mu T^\mu{}_\nu = \nabla_\mu \bar{T}^\mu{}_\nu + \nabla_\mu \delta T^\mu{}_\nu \tag{2.35}$$

The background part yields (called energy density continuity equation)

$$\bar{\rho}' + 3\mathcal{H}(\bar{\rho}+\bar{p}) = 0 \tag{2.36}$$

Where $\mathcal{H}$ is comoving Hubble parameter, which we define as

$$\mathcal{H} = \frac{a'}{a} = aH \quad \text{with} \quad H = \frac{\dot{a}}{a} \tag{2.37}$$

Then the perturbations part (scalar, vector and tensor fluctuations) of Eq, (2.35) which results into conservation equations for energy density and momentum density in *scalar mode* respectively denoted by

$$\delta\rho' + 3\mathcal{H}(\delta\rho+\delta p) - 3(\bar{\rho}+\bar{p})\psi' + (\bar{\rho}+\bar{p})\nabla^2(v+E') = 0 \tag{2.38}$$

$$[(\bar{\rho}+\bar{p})(v+B)]' + \delta p + \frac{2}{3}(\nabla^2+3K)\Pi + (\bar{\rho}+\bar{p})[\phi + 3\mathcal{H}(v+B)] = 0 \tag{2.39}$$

In *vector modes* there is no energy conservation equation only momentum conservation equation which read

$$[(\bar{\rho}+\bar{p})(v_i - S_i)]' + 4\mathcal{H}(\bar{\rho}+\bar{p})(v_i - S_i) = (\nabla^2 + 2K)\pi_i \tag{2.40}$$

In *tensor mode* there is no energy (scalar quantity) nor momentum (vector quantity) conservation equations, since both this quantities are dissociate from tensor quantities.

2.2.3 The gauge problem

In general relativity we relate the space-time background points and perturbation points through some coordinate system, this does not favor any particular coordinate, One can choose the coordinate system however one pleases - hence in modern physics we refer to this as freedom of choice of coordinate. However, for spacetime background coordinate system, there are countless plausible space-time perturbed coordinate system which are vey close to each other. (for comprehensive see reviews by [55, 177–179, 183, 210]). Now we introducing the two space-time manifolds - (i) FLRW Universe background $\bar{\mathcal{M}}$ and the physical Universe $\mathcal{M}$ with inhomogeneities - this coordinates choice can be considered to mapping x between the manifolds background $\bar{\mathcal{M}}$ and $\mathcal{M}$. (ii) Mapping

the same point in $\bar{\mathcal{M}}$ into different point in $\mathcal{M}$ - considering the inverse of the maps x and $\tilde{x}$, one may assign two different set of points in $\mathcal{M}$.
Provided a set of coordinates x, then a perturbation of a quantity Q (i.e., Ricci scalar, metric ...) on $\mathcal{M}$ and $\bar{Q}$ on $\bar{\mathcal{M}}$, we define this as the variance between the quantity and fixed function at the fixed point given as

$$\delta Q(x) = Q(x) - \bar{Q}(x), \quad \delta\tilde{Q}(\tilde{x}) = \tilde{Q}(\tilde{x}) - \bar{Q}(\tilde{x}) \tag{2.41}$$

The above gauge artifact carries not importance physically. However, this can be made meaningful by studying the coordinate transformation on the metrics (in subsection. (2.2.1) certain degrees of freedom of the perturbations are gauge artifacts). Considering the gauge transformation (given a set of coordinate $x^\mu = (\eta, x^i)$)composed of temporal and spatial parts

$$x^\mu \to \tilde{x}^\mu = (\tilde{\eta}, \tilde{x}^i), \quad \tilde{\eta} = \eta + \xi^0(\eta, \xi^i), \quad \tilde{x}^i = x^i + \bar{\xi}^i(\eta, \xi^i) + \xi_{|}{}^i(\eta, \xi^i) \tag{2.42}$$

Where $\xi^\mu = (\xi^0, \xi^i = \xi_{|}{}^i + \bar{\xi}^i)$ is the four vector transformation, ξ^0 is arbitrary scalar function[5] and $\bar{\xi}^i$ is divergence-free three vector[6]. Using (2.41) and the scalar transformation law and the fact that transformation change don't affect backgrounds (i.e.,$\phi(t)$) , we define metric transformation as follows

$$\delta g_{\mu\nu}(x) \to \delta\tilde{g}_{\mu\nu}(x) = \delta g_{\mu\nu} - (\nabla_\mu \xi_\nu + \nabla_\nu \xi_\mu) \tag{2.43}$$

Where $\xi_\nu = g_{\nu\sigma}\xi^\sigma$ and the covariant derivative denote by ∇_μ. The above expression shows that perturbations are not invariant under transformation coordinate system. Now if we perform the coordinate change of the perturbed line element Eq. (2.24)

$$\begin{aligned} ds^2 &= a^2(\tilde{\eta})\{-(1+2\tilde{\phi})d\tilde{\eta}^2 + 2(\tilde{B}_{|i} - \tilde{S}_i)d\tilde{x}^i d\tilde{\eta} \\ &\quad + [(1-2\tilde{\psi})\delta_{ij} + 2\tilde{E}_{|ij} + 2\tilde{F}_{(i|j)} + \tilde{h}_{ij}]d\tilde{x}^i d\tilde{x}^j \end{aligned} \tag{2.44}$$

From this we can write the gauge transformation of several metric perturbation of (scalar, vector and tensor functions)

[5] determines the separation of the const-η hypersurfaces - *time shift*
[6] *space shift* -selects the spatial coordinate with in the hypersurfaces

The *scalar functions* (ϕ, ψ, B, E)

$$\tilde{\phi} = \phi - \mathcal{H}\xi^0 - \xi^{0'} \tag{2.45}$$
$$\tilde{\psi} = \psi + \mathcal{H}\xi^0 \tag{2.46}$$
$$\tilde{B} = B + \xi^0 - \xi' \tag{2.47}$$
$$\tilde{E} = E - \xi \tag{2.48}$$

The *vector functions* (F, S)

$$\tilde{F}_i = F_i - \bar{\xi}_i \tag{2.49}$$
$$\tilde{S}_i = S_i + \bar{\xi}_i' \tag{2.50}$$

The *tensor function* (h_{ij}) is not affected by the gauge transformations. In this thesis, our work is within *conformal Newtonian gauge*, also known as *longitudinal gauge* which is defined by $\tilde{B} = 0 = \tilde{E}$. Theres are several gauge choices such as the frequently used synchronous gauge must be such that $\delta\tilde{g}_{0\mu}$, which lead to $\tilde{\phi} = 0 = \tilde{B}$. And the gauge-invariant, which was firstly introduced by Bardeen based on the two potentials Φ and Ψ explicitly denoted by [21]

$$\Phi = \phi + \mathcal{H}(B - E') + (B - E')' \tag{2.51}$$
$$\Psi = \psi - \mathcal{H}(B - E') \tag{2.52}$$

From the above expressions we can conclude that the gauge-invariant variables Φ and Ψ is consistence with the corresponding diagonal metric perturbations ϕ and ψ in conformal Newtonian gauge.

2.2.4 The geodesic equation

Geodesic is described by a curve if it fundamentals the distance between two fixed points as shown in Fig. (2.2), in this case we assume that the curve is described by the well know relation $x^\alpha(\lambda)$, Here λ being a random parameter. Suppose that every point on the curve from P to R is deformed , then in GR one can express the distance between P and R along the curve to be defined as

$$l \equiv \int_P^R \sqrt{\pm g_{\alpha\beta} \frac{dx^\alpha}{d\lambda} \frac{dx^\beta}{d\lambda}} d\lambda \tag{2.53}$$

Assuming that our path is non null from point P to R. Where positive or negative sign is hand picked if the path is space-like or time-like respectively. It is clear that under the reparametrization of the path the distance is invariant, this means that the random parameter λ implies $\frac{d\lambda(\lambda)}{d\lambda}$.

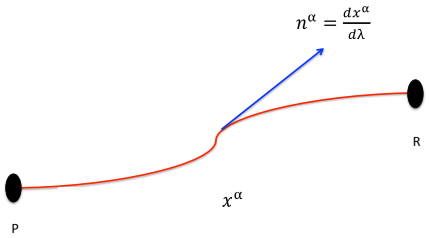

Fig. 2.2 Arbitrary path x^α from point P to R with the tangent vector n^α

Furthermore, the distance l can be simplified by substituting the Lagrangian

$$\mathcal{L}\left(\frac{dx^\alpha}{d\lambda}, x^\alpha\right) = \left(\pm g_{\alpha\beta}\frac{dx^\alpha}{d\lambda}\frac{dx^\beta}{d\lambda}\right)^{\frac{1}{2}}$$

This need to be plugged into the Euler-Lagrange equation then we arrive at

$$\frac{d}{d\lambda}\left[\frac{\partial\mathcal{L}}{\partial(\frac{dx^\alpha}{d\lambda})}\right] - \frac{\partial\mathcal{L}}{\partial x^\alpha} \equiv 0 \tag{2.54}$$

The differential equation above shows that $x^\alpha(\lambda)$ must satisfy the following

$$\frac{d^2x^\alpha}{d\lambda^2} + \Gamma^\alpha_{\beta\mu}\frac{dx^\beta}{d\lambda}\frac{dx^\mu}{d\lambda} = \kappa(\lambda)\frac{dx^\alpha}{d\lambda}, \qquad \text{(arbitrary parameter)} \tag{2.55}$$

Where $\kappa(\lambda) = \frac{d\mathcal{L}}{\mathcal{L}d\lambda}$, certainly it is of importance if one choose the proper distance s parameter of the geodesics is space-like, where $ds^2 = g_{\alpha\beta}dx^\alpha dx^\beta$ [7]. Then we have Lagrangian to be a constant and this implies that $\kappa = 0$. Thus, we can express the geodesic equation by (see [95, 176, 214] for more details)

$$\frac{d^2x^\alpha}{d\lambda^2} + \Gamma^\alpha_{\beta\mu}\frac{dx^\beta}{d\lambda}\frac{dx^\mu}{d\lambda} = 0, \qquad \text{(affine parameter)} \tag{2.56}$$

[7] as for proper time τ of the geodesics is time-like, where $ds^2 = -g_{\alpha\beta}dx^\alpha dx^\beta$

Where $\Gamma^{\alpha}_{\beta\mu}$ is defined by (2.8) and with $\frac{dx^{\alpha}}{d\lambda}$ being the tangent four-velocity along $x^{\alpha}(\lambda)$

2.2.4.1 Photon geodesic equation

In this subsection, vigorously give an explanation and some of null geodesic condition, that is when the path given by Fig. (2.2) is null, then the distance between point P and point R along a geodesic x^{α} can be given in terms of the tangent vectors which can be formulated by

$$d\eta^2 = -n^{\alpha}n_{\alpha}d\lambda^2, \qquad ds^2 = n^{\alpha}n_{\alpha}d\lambda^2 \tag{2.57}$$

The two equation respectively denote time-like geodesic and space-like geodesic, now as for null to be carried out both proper time and distance should be zeros ($d\tau = 0 = ds$) then one get to the following

$$n^{\alpha}n_{\alpha} = 0 \tag{2.58}$$

The above hold for any parametrization of choice. Null geodesic is also known as photon geodesic since it describe how a massless photon travel in the gravitational field. focusing on the killing vectors, since the killing vectors are useful to evaluate the constant related to the movement of photons along the geodesics. consider that n^{α} to affinely parametrized by λ then the following yields

$$\begin{aligned} \frac{d}{d\lambda}(n^{\alpha}k_{\alpha}) &\equiv (n^{\alpha}k_{\alpha})_{;\beta}\, n^{\beta} \\ &\equiv n^{\alpha}_{;\beta}n^{\beta}k_{\alpha} + k_{\alpha;\beta}n^{\alpha}n^{\beta} \\ &\equiv 0 \end{aligned} \tag{2.59}$$

Throughout this thesis we define the covariant differentiation as $A^{\alpha}_{;\beta} \equiv \nabla_{\beta}A^{\alpha} \equiv D_{\beta}A^{\alpha}$. In the above equation k_{α} is the killing vector , please note that due to morality of geodesic equation the first term vanishes and because of the antisymmetry tensor of the killing vector and the symmetry of the $n^{\alpha}n^{\beta}$ then the second term also disappear.

2.2.4.2 Perturbed geodesics

Adopting work by [96, 214] which is in conformal transformation regime, now we can write the metric which is given by

$$d\tilde{s}^2 = a^2 ds^2 \tag{2.60}$$

From the above transformation one can introduce some of the important perturbation

$$\tilde{g}_{\alpha\beta} \equiv a^2(\bar{g}_{\alpha\beta} + \delta g_{\alpha\beta}), \qquad \bar{g}_{00} = -1, \qquad \bar{g}_{0j} = \bar{g}_{i0} = 0, \qquad \bar{g}_{ij} = \delta_{ij} \tag{2.61}$$

Considering that $n^\alpha = \frac{dx^\alpha}{d\lambda}$, and $\tilde{n}^\alpha = \frac{d\tilde{x}^\alpha}{d\tilde{\lambda}}$, notice that we choose

$$\tilde{\lambda} \equiv a^2\lambda, \qquad \tilde{n}^\alpha \equiv a^2 n^\alpha \tag{2.62}$$

Then the geodesic equation for the perturbed metric reads

$$ds^2 = (g_{\alpha\beta} + \gamma_{\alpha\beta})dx^\alpha dx^\beta \tag{2.63}$$

We can then write

$$\frac{d\delta n^\mu}{d\lambda} = -\delta\Gamma^\mu_{\alpha\beta} n^\alpha n^\beta \tag{2.64}$$

Since our work of frame is based on FLRW perturbed Universe, one can define the following

$$n^\alpha \equiv \bar{n}^\alpha + \delta n^\alpha, \qquad \Gamma^\mu_{\alpha\beta} \equiv \bar{\Gamma}^\mu_{\alpha\beta} + \delta\Gamma^\mu_{\alpha\beta} \tag{2.65}$$

Making use of above very useful information one arrive at the perturbed geodesic equation which reads

$$\frac{d\delta n^\mu}{d\lambda} \equiv \gamma_{\alpha\mu|\beta} n^\beta n^\alpha - \frac{1}{2}\dot{\gamma}_{\alpha\beta} n^\beta n^\alpha \tag{2.66}$$

Here $\gamma_{\alpha\mu|\alpha} n^\alpha n^\alpha = \frac{d}{d\lambda}(\gamma_{\alpha\mu} n^\alpha)$, integrating the above expression the perturbed geodesic equation becomes (see [214] for details)

$$\delta n^\mu \Big|_P^R \equiv \left[\gamma_{\mu\nu} + \gamma_{\nu\beta} n^\beta\right]_P^R - \frac{1}{2}\int_P^R \dot{\gamma}_{\alpha\beta} n^\beta n^\alpha \tag{2.67}$$

2.2.5 Einstein field equations

In this section, we discuss the Einstein dynamic equations in conformal Newtonian gauge, re-introducing Einstein equation Eq. (2.19) which leads to 2-scalar, 1-vector and 1-tensor perturbation equations (see [95, 105, 151, 176, 188, 214] for detailed review), to obtain this perturbation equations we firstly decompose Eq. (2.19) into background ($\bar{G}_{\mu\nu}$) and perturbation ($\delta G_{\mu\nu}$) parts, the components of background Einstein-tensor

are given as

$$\bar{G}_{00} = 3(\mathcal{H}^2 + K), \quad \bar{G}_{0i} = 0, \quad \bar{G}_{ij} = \delta_{ij}(\mathcal{H}^2 + 2\mathcal{H}' + K) \tag{2.68}$$

Now using Eq. (2.30) together with Eq. (2.19) one get the background Friedmann and acceleration equations respectively given by

$$\mathcal{H}^2 = \frac{8\pi G a^2}{3}\bar{\rho} - K \quad \text{and} \quad \mathcal{H}' = -\frac{4\pi G a^2}{3}(\bar{\rho} + 3\bar{p}) \tag{2.69}$$

In the subsubsection. (2.2.5.1) to follow, we follow similar set of steps to obtain the (2-scalar, 1-vector, 1-tensor) perturbations.

2.2.5.1 Scalar perturbations

Here we give the scalar perturbation in perfect fluid, again considering the Eq. (2.19) the perturbed Einstein-tensor components yields

$$\begin{aligned}
\delta G_{00} &= 2[\nabla^2\Psi - 3\mathcal{H}(\mathcal{H}\Phi + \Psi') + 3K\Psi] && (2.70)\\
\delta G_{0i} &= 2(\Psi + \mathcal{H}\Phi)_{|i} && (2.71)\\
\delta G_{ij} &= 2\left[\Psi'' + 2\mathcal{H}\Psi' + \mathcal{H}\Phi' + (\mathcal{H}^2 + 2\mathcal{H}')\Phi - K\Psi - \frac{1}{2}\nabla^2\mathcal{D}\right]\delta_{ij} + \mathcal{D}_{|i|j} && (2.72)
\end{aligned}$$

Where $\mathcal{D}$ is defined by $\mathcal{D} = -\Phi + \Psi$. Note that in this case since B and E are zero this lead to $\sigma = 0$. The above expressions provide the following perturbed Einstein equations

1. Energy from Eq. (2.70) and momentum from Eq. (2.71) constraints respectively given by

$$\begin{aligned}
-3\mathcal{H}(\Psi' + \mathcal{H}\Phi) + (\nabla^2 + 3K)\Psi &= 4\pi a^2\delta\rho && (2.73)\\
\Psi' + \mathcal{H}\Phi &= -4\pi a^2(\bar{\rho} + \bar{p})v && (2.74)
\end{aligned}$$

2. Evolution equations trace from Eq. (2.72) by considering the case where $(i \neq j)$ and trace-free from Eq. (2.72) by considering the case where $(i = j)$, respectively given as

$$\begin{aligned}
\Psi - \Phi &= 8\pi G a^2\Pi && (2.75)\\
\Psi'' + 2\mathcal{H}\Psi' + \mathcal{H}\Phi' + (\mathcal{H}^2 + 2\mathcal{H}')\Phi - K\Psi &= 4\pi G a^2\left(\delta p + \frac{2}{3}\nabla^2\Pi\right) && (2.76)
\end{aligned}$$

2.2.5.2 Vector perturbations

In this subsection, we lay-out the Einstein evolution equations by considering the Friedmann metric described by the line element

$$ds^2 = a^2(\eta)[d\eta^2 + 2S_i dx^i d\eta - (\delta_{ij} - F_{i,j} - F_{j,i})]dx^i dx^j \tag{2.77}$$

Then following similar steps as subsection. 2.2.5.1, from component $0i$ we obtain the momentum constraint equation given by

$$(2K + \nabla^2)(F_i' + S_i) = -16\pi G a^2 \delta q_i \tag{2.78}$$

Relating the vector shear perturbation to the vector part of the three momentum

$$q_i = (\bar{\rho} + \bar{p})(v_i - S_i) \tag{2.79}$$

From component ij Einstein equation yields

$$q_i' + 4\mathcal{H}q_i = (\nabla^2 + 2K)\pi_i \tag{2.80}$$

This expression is equivalent to Eq. (2.40). Due to the fact that there is no vector source in Eqs. (2.78) and (2.79) means all components have to be equated to zero, these means that S_i and F_i vanishes [151, 176, 229]. We conclude that in the absence of the source of viscosity the can be any vector perturbations.

2.2.5.3 Tensor perturbations

lets look at the case of the tensor perturbations. Following the same steps as previous section the components of the perturbed Einstein tensor yields

$$\delta G_{00} = 0 = \delta G_{0i}, \quad \delta G_{ij} = -\frac{1}{2}\left(h_{ij}'' + 3\mathcal{H}h_{ij}' - \frac{1}{a^2}\nabla^2 h_{ij}\right) \tag{2.81}$$

Remainder that h_{ij} s a symmetric, transverse and traceless tensor, now the transverse, trace-free part of the Einstein evolution equations yields a simple wave equation

$$h_{ij}'' + 2\mathcal{H}h_{ij}'(2K - \nabla^2)h_{ij} = 16\pi G a^2 \pi_{ij} \tag{2.82}$$

where ${}^{(tensor)}\pi$ is the transverse and trace-free part of the anisotropic stress. Tensor metric perturbations are not subject to constraint equations and describe the free part of the gravitational field.

2.2.6 Perturbed generalized fluids

In this subsection, we look into multi-component interactions of fluids, which can be considered as an extend of subsections provided above (all this subsections where based on a perfect fluid). In this case each fluid describe different properties (i.e.,matter, DE..). Note that from now on we assume flat Universe.(comprehensive review is given by [95])

2.2.6.1 Multi-component backgrounds

The background energy density $\bar{\rho}_A$ and background background pressure $\bar{p}_A$ (A-include all species such as baryonic matter and dark energy) are respectively given by

$$\bar{\rho}_A = \sum_A \bar{\rho}_A \quad \text{and} \quad \bar{p}_A = \sum_A \bar{p}_A \tag{2.83}$$

The background conservation equation for fluid A relating energy density and pressure is given as (equivalent to equation Eq.(2.36))

$$\bar{\rho}'_A + 3\mathcal{H}(1+w_A)\bar{\rho}_A = 0 \tag{2.84}$$

Here $w_A = \frac{\bar{p}_A}{\bar{\rho}_A}$ is the equation of state parameter of A, and the evolution of the equation of state parameter is given by

$$w'_A = -3\mathcal{H}(1+w_A)(c^2_{aA} - w_A) \tag{2.85}$$

Where adiabatic sound speed of A is defined by $c^2_{aA} = \frac{\bar{p}'_A}{\bar{\rho}'_A}$, now the background acceleration given previously by Eq. (2.69) in multicomponent fluid becomes,

$$\mathcal{H}' = -\frac{\mathcal{H}^2}{2}(1+3w) \tag{2.86}$$

With the total equation of state parameter expressed in term of the energy density parameter Ω_A denoted by

$$w = \sum_A \Omega_A w_A \quad \text{with} \quad \Omega_A = \frac{\bar{\rho}_A}{\bar{\rho}} \tag{2.87}$$

At which energy density parameter evolves as follows

$$\Omega'_A = \left(\frac{a^2\bar{\rho}}{3\mathcal{H}^2M^2}\right)' \equiv -3\mathcal{H}(w_A - w)\Omega_A \tag{2.88}$$

The application of this multi-component backgrounds will be put into action later on.

2.2.6.2 Multi-component perturbations

The perturbed Einstein equations given in subsection. 2.2.5 in gauge-invariant (for various species A), in *scalar mode* : Eq. (2.73)-(2.75), becomes

$$\begin{aligned}
\nabla^2\Psi - 3\mathcal{H}(\mathcal{H}\Phi + \Psi') &= \frac{3}{2}\mathcal{H}^2\sum_A \Omega_A\delta_A && (2.89)\\
\Psi' + \mathcal{H}\Phi &= -\frac{3}{2}\mathcal{H}^2\sum_A (1+w_A)V_A && (2.90)\\
\Psi - \Phi &= 8\pi G a^2\Pi_A && (2.91)\\
& && (2.92)
\end{aligned}$$

Where $\delta_A \equiv \frac{\delta\rho A}{\bar{\rho}_A}$ and we have used the gauge-invariant velocity potential $V_A \equiv v_A$. Lastly, perturbed Einstein equation Eq. (2.76) in multi-fluid scenario becomes

$$\Psi'' + (2+3c_a^2)\mathcal{H}\Psi + \mathcal{H}\Psi' + \mathcal{H}\Phi + [2\mathcal{H} + (1+3c_a^2)\mathcal{H}^2]\Phi = \frac{3}{2}\mathcal{H}^2\left(c_s^2\Delta + \frac{2}{3}\nabla^2\Pi_A\right) \tag{2.93}$$

We define the parameters c_s^2, c_a^2 and Δ_A which represents the totals, respectively denoted by

$$c_s^2 = \sum_A \frac{\Delta_A}{\Delta}\Omega_A c_{sA}^2, \quad c_s^2 = \sum_A \frac{(1+w_A)}{1+w}\Omega_A c_{aA}^2, \quad \Delta = \sum_A \Omega_A\Delta_A \tag{2.94}$$

The advantage of using the gauge invariant V_A, Δ_A, Ψ and Φ is that they remove large-scale unphysical artifacts that might arise from choice of gauge. (see thorough review [48, 95, 172]).
In *vector mode* : Einstein evolution equation Eq. (2.80) with respect to the various species A is given by

$$q'_{Ai} + 4\mathcal{H}q_{Ai} = \nabla^2\pi_{Ai} \tag{2.95}$$

Where $q_{Ai} = (\bar{\rho}_A + \bar{p}_A)\mathbf{V}_{Ai}$, with $\mathbf{V}_{Ai} \equiv V_{Ai} - S_{Ai}$ is being the gauge-invariant vector velocity perturbation and $\pi_{Ai} \equiv \pi_{(A)i}$ is the anisotropic stress of the species A. In *tensor mode* : Einstein evolution equation Eq. (2.82) with respect to the various species A is given by

$$h''_{ij} - 2\mathcal{H}h'_{ij}\nabla^2 h_{ij} = 16\pi G a^2 \pi_{Aij} \tag{2.96}$$

where ${}^{(tensor)}\pi_{Aij}$ is the anisotropic stress perturbation for the tensor mode of species A,defined as

$${}^{(tensor)}\pi_{Aij} = \sum_A {}^{(tensor)}\pi_{(A)ij} \tag{2.97}$$

2.2.7 The standard Model

In this section we provide a short introduction to concordance model, in this model the Universe is assumed to be Λ and cold dark matter (CDM) dominated hence the name ΛCDM, In this model dark energy vacuum energy is static or at equilibrium, the constant Λ determine the density of vacuum energy, this is called cosmological constant. In order to construct a spatially finite static Universe, Einstein [100, 102] added a cosmic term with a positive cosmological constant Λ to his primary field equation to modify it into something like

$$G_{\mu\nu} \equiv -\Lambda g_{\mu\nu} + 8\pi G T_{\mu\nu} \tag{2.98}$$

where $g_{\mu\nu}$ being the spacetime metric, Meanwhile, after Hubble have discovered the expansion of the Universe, Einstein withdrew the Λ term given in above Eq. (2.98). It is vastly believed that Einstein introduced the cosmological constant into his field equation as a repulsive energy that fills "empty" space to prevent the Universe from collapsing by the gravitational pull of the matter (see [101, 102, 114, 156, 200, 215] for comprehensive details).

2.2.7.1 The background equations

This section is a follow up of chapter. 2, and its worth noting that throughout this thesis we work in conformal Newtonian gauge, now the perturbed metric is given by

$$ds^2 = a^2(\eta)\Big[-(1+2\Phi)d\eta^2 + (1-2\Phi)d\mathbf{x}^2\Big] \tag{2.99}$$

note that in ΛCDM $\Phi \equiv \Psi$, where Ψ and Φ being the two Bardeen potentials. After some algebra from the (00) and (ii) components of the Einstein equation the comoving Hubble parameter and its evolution equation are as follows

$$\mathcal{H}^2 = \frac{8\pi G}{3} a^2 \bar{\rho}_m + \frac{\Lambda}{3} a^2 \tag{2.100}$$

$$3\mathcal{H}^2 + 2\mathcal{H}' = -8\pi G a^2 \bar{\rho}_m + a^2 \Lambda \tag{2.101}$$

We make a note that for non-relativistic matter, $\bar{P}_m = 0$, Λ cosmological constant corresponds to $\bar{P}_\Lambda = -\bar{\rho}_\Lambda$ which will give the expected constant. The equation of state parameter for both matter and Λ are as denoted by $w_m = 0$ and $w_\Lambda = -1$. we can rewrite Eq. (2.100) is the following simple form

$$\Omega_m + \Omega_\Lambda = 1 \tag{2.102}$$

Where Ω_m is the matter background energy density parameters and Ω_Λ is denoted by Λ background energy density parameters, which are defined as follows

$$\Omega_m \equiv \frac{8\pi G a^2 \bar{\rho}_m}{3\mathcal{H}^2}, \qquad \Omega_\Lambda \equiv \frac{\Lambda a^2}{3\mathcal{H}^2} \tag{2.103}$$

The evolution expression for comoving Hubble parameter can also be written in the following form

$$\mathcal{H}' = \frac{3}{2}\mathcal{H}^2 \left(\Omega_\Lambda - \frac{1}{3} \right) \tag{2.104}$$

2.2.7.2 The perturbation equations

In this subsection we provide the details on how velocity, density gauge invariant, Potential velocity and Bardeen potentials $\{\Delta_A, V_A \Psi, \Phi\}$ evolves, we once again considering the line element in Newtonian gauge given by Eq. (2.99), to obtain the Poisson equation which reads

$$-k^2 \Phi = 4\pi G a^2 \bar{\rho}_m \Delta_m. \tag{2.105}$$

Here Δ_m is defined as the gauge invariant comoving density perturbation denoted by

$$\Delta_m = \delta_m + \frac{3\mathcal{H}v}{k}. \tag{2.106}$$

Making use of above information, the matter perturbations for potential velocity and density reads

$$v'_m = -\mathcal{H}v_m + k\Psi \tag{2.107}$$

$$\delta'_m = -kv_m + 3\Phi' \tag{2.108}$$

Finally the two Bardeen potentials evolve by as follows

$$\Phi' = -\mathcal{H}\Phi + \frac{3}{2}\mathcal{H}^2\Omega_m v_m, \qquad \Psi' = \Phi' \tag{2.109}$$

As we can see, from above equations involves matter but not Λ, by the definition there are no perturbation for Λ , this mean potential velocity and densities vanishes that is $\Delta_\Lambda = \delta_\Lambda = V_\Lambda = 0$.

2.2.7.3 The linear growth rate

In the linear cold matter perturbations growth rate is spatial scale dependence [131, 199] provided an explicit expression of growing perturbation's magnitude. We can also extract out growth rate from evolution equations provide above, with some algebra we get

$$v_m(z, \mathbf{k}) = \frac{2}{3\Omega_m}\frac{k}{H_0^2} f(z) D_1(a) T(k) \Phi_i(\mathbf{k}) \tag{2.110}$$

Where $f(z)$ is the growth rate, which is the quantities depend not directly on Equation given by [131], but depend on the logarithmic derivative which yields

$$f(z) \equiv \frac{\partial \ln D_1}{\partial \ln a} \tag{2.111}$$

In [157] come up with a simple approximation which is a perfect fit to the logarithmic derivative given by

$$f(z) \approx \left[\frac{\Omega_m(1+z)^3}{\Omega_m(1+z) - (\Omega_m + \Omega_\Lambda - 1)(1+z)^2 + \Omega_\Lambda}\right]^{\frac{4}{7}} \tag{2.112}$$

Some of the useful conditions of concordance model :
we have $D_m(a,k) = D_\Psi(a,k) = D_\Phi(a,k) = D_1(a)$, $D_{v_m}(a,k) = \frac{\partial D_1(a)}{\partial \eta}$, $Dv_\Lambda(a,k) = 0$
As for growth rate $f_m(a,k) = f(a)$, in matter dominated Universe we have $D_1(a) = a$ this implies that $f(a) = 1$, which can be vindicated by Eq. (2.111)

2.3 Weak gravitational lensing basics

2.3.1 Light deflection

The coming about of gravitational lensing occurrence could be predicted by Einstein's GR. Well in GR theory the spacetime geometry is mostly perturbed by very large objects, this allow the light which voyage on geodesics appear to be curved in three dimensional space [22, 61, 148, 182, 191, 195, 203, 212, 213, 219]. Suppose that the observer is looking at a distant object, the original source will appear in multiple position from the observer's prospective, this mean that the observer is no longer symmetric line of sight direction of the source this is due to the direction of the deflected light path converging. Thus, from observer's view there is this magnification and distortion of the image since the image get transformed either the size get bigger nor diagonal tilt.

In a bend spacetime the light propagation is regulated by non linear field GR equations, this equations are not a cup of tea to solve. However, in modern physics gravitational lensing only involve objects with very small peculiar velocity and weak gravitational potential these holds the following conditions respectively $v \ll c$ and $|\Phi| \ll c^2$. Lets make a note that her v is peculiar velocity, c is the speed of light and Φ being the Newtonian gravitational potential. What can we extract from this conditions? Easy, The geometry of perturbed spacetime which is described by estimation of the Minkowski metric, the metric provide the ease for us to explain the effect of the local perturbation in terms of effective index (see [195]) this can be defined as follows

$$n \equiv 1 - \frac{2\Phi}{c} \equiv 1 + \frac{2|\Phi|}{c^2} \tag{2.113}$$

As if observing the light ray being refracted through a prism the gravitational field act as if it was a refracting medium. the amount at which the deflection angle of light rays by the gravitational potential is defined as follows

$$\hat{\boldsymbol{\alpha}} \equiv -\int \nabla_{\perp} n dl \equiv \frac{2}{c^2} \int \nabla_{\perp} \Phi dl \tag{2.114}$$

Here $\hat{\boldsymbol{\alpha}}$ being the deflection angle from the point mass. Lets consider coordinate system authorize us to work in xy-plane at which the lens and the source lie on. We can rewrite the above equation as

$$\hat{\boldsymbol{\alpha}} \equiv -\int \nabla_{\perp} \Phi dz \equiv \frac{4GM}{\xi c^2} \tag{2.115}$$

Where ξ is the impact parameter, which is orthogonal to the direction of the propagation. M in this context is the point mass.

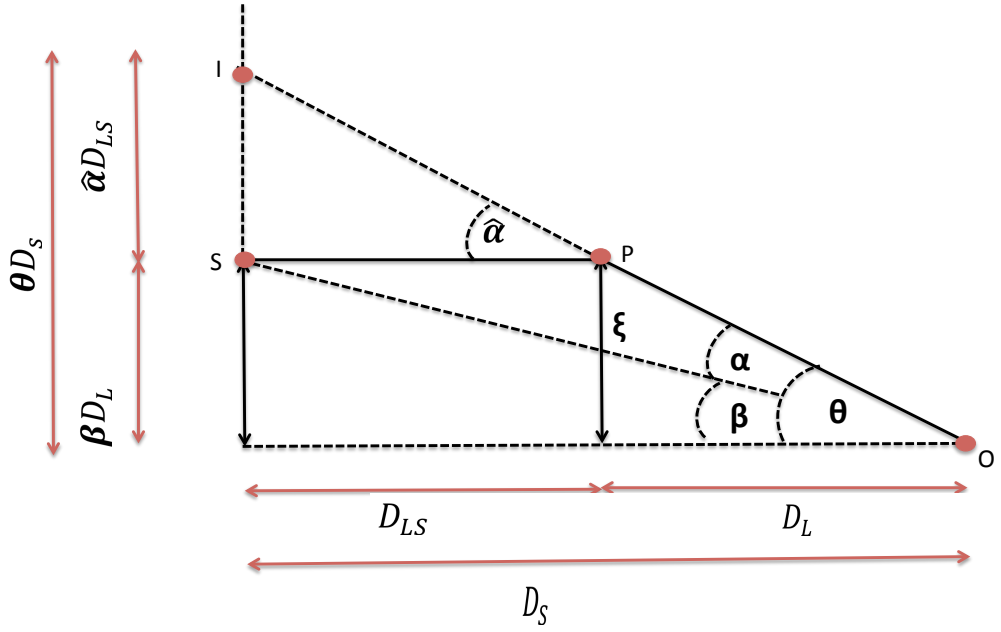

Fig. 2.3 Schematic showing the basic gravitational lensing system. At which light ray travels from the source at point S to the observer at point O, this passes through the lens at transverse distance denoted by $\boldsymbol{\xi}$

2.3.2 Thin screen approximation and Lens equation

Generally the distance between the observer's lens and the source is normally greater than the physical size of the lens, this is sustained even for galaxy clusters. In thin screen estimation lens is diminished to a plane perpendicular to the line of sight, these is where the distribution of mass is projected. we can formulate this as follows

$$\sum \boldsymbol{\xi} \equiv \int \rho(z, \boldsymbol{\xi}) dz \tag{2.116}$$

Here $\boldsymbol{\xi}$ is the 2-dimensional vector. Angular deflection can be rewritten as

$$\hat{\boldsymbol{\alpha}} \equiv \frac{4G}{c^2} \int \int \frac{\boldsymbol{\xi} - \boldsymbol{\xi}'}{|\boldsymbol{\xi} - \boldsymbol{\xi}'|^2} \sum \boldsymbol{\xi}' d^2\xi' \tag{2.117}$$

From Fig. (2.3) we get the following relation

$$\hat{\boldsymbol{\alpha}} D_{LS} \equiv \boldsymbol{\alpha} D_S, \qquad \boldsymbol{\theta} D_S \equiv \boldsymbol{\alpha} D_{LS} + \boldsymbol{\beta} \tag{2.118}$$

Making use of these relation we arrive at

$$\boldsymbol{\beta} \equiv \boldsymbol{\theta} - \boldsymbol{\alpha}(\boldsymbol{\theta}) \equiv \boldsymbol{\theta} - \hat{\boldsymbol{\alpha}} \frac{D_{LS}}{D_S} \tag{2.119}$$

This is so called Lens equation, this lensing equation is a vector equation. $\boldsymbol{\theta}$,$\boldsymbol{\alpha}$ and $\boldsymbol{\beta}$

2.3.3 Lensing potential

In this section we evaluate the lensing potential, adopting the following

$$\boldsymbol{\xi} = D_L \boldsymbol{\theta}, \qquad \hat{\boldsymbol{\alpha}} = \frac{4G}{c^2} \int\int \frac{\boldsymbol{\xi} - \boldsymbol{\xi}'}{|\boldsymbol{\xi} - \boldsymbol{\xi}'|^2} \sum \boldsymbol{\xi}' d^2\xi' \tag{2.120}$$

this two expressions take us to

$$\hat{\boldsymbol{\alpha}} = \frac{4G}{c^2} \int\int \frac{\boldsymbol{\theta} - \boldsymbol{\theta}'}{|\boldsymbol{\theta} - \boldsymbol{\theta}'|^2} \sum \boldsymbol{\theta}' d^2\theta' \tag{2.121}$$

We also define the following useful equations

$$\kappa(\boldsymbol{\theta}) \equiv \frac{\sum \boldsymbol{\theta}}{\sum_c}, \qquad \frac{1}{\sum_c} \equiv \frac{1}{\frac{c^2}{4\pi G} \frac{D_S}{D_L D_{LS}}} \tag{2.122}$$

the above equations are respectively convergence and the critical surface mass of density. With some algebra this deliver us to new equation for angle deflection

$$\hat{\boldsymbol{\alpha}} = \int\int \frac{\kappa(\boldsymbol{\theta})}{\pi} \frac{\boldsymbol{\theta} - \boldsymbol{\theta}'}{|\boldsymbol{\theta} - \boldsymbol{\theta}'|^2} d^2\theta' \tag{2.123}$$

The lensing equation should obey the following conditions firstly the gradient of the potential must be as given by

$$\nabla_\theta \Psi = \boldsymbol{\alpha} \tag{2.124}$$

secondly the Laplacian of the potential must be as given by

$$\nabla_\theta^2 \equiv 2\kappa(\boldsymbol{\theta}) \tag{2.125}$$

We finally get to the deflection potential which reads

$$\Psi(\boldsymbol{\theta}) \equiv \int\int \frac{1}{\pi}\kappa(\boldsymbol{\theta}) \ln|\boldsymbol{\theta} - \boldsymbol{\theta}'| d^2\theta' \tag{2.126}$$

2.3.4 Magnification and Distortions of the image

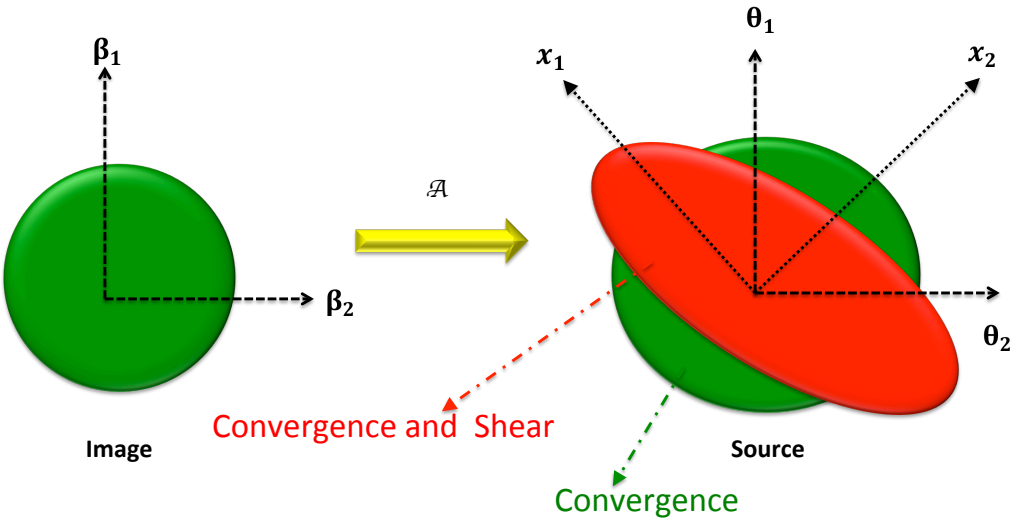

Fig. 2.4 Schematic showing the geometrical effect of the transformation of $\boldsymbol{\beta} = (\boldsymbol{\beta}_1, \boldsymbol{\beta}_2)$ to $\boldsymbol{\theta} = (\boldsymbol{\theta}_1, \boldsymbol{\theta}_2)$ initiated by the matrix $\mathcal{A}$

Since this concept is been introduced in previous subsection, so we will give a brief explanation of this concept as possible. The shape of the source image being distorted introduces the features of lensing, but what is the influence of lensing to the source image, lensing takes rays from position $\boldsymbol{\theta}$ and map it out to position to $\boldsymbol{\beta}$. Lets now put this into a tensor formula

$$A_{ij} \equiv \frac{\partial \boldsymbol{\beta}}{\partial \boldsymbol{\theta}} \equiv \delta_{ij} - \Psi_{ij} \tag{2.127}$$

We can rewrite the lensing potential as

$$\Psi_{ij} \equiv \frac{\partial^2 \Psi}{\partial \theta^i \partial \theta^j} \tag{2.128}$$

With the inverse of tensor A_{ij} defined by

$$A_{ij}^{-1} \equiv \frac{\partial \boldsymbol{\theta}}{\partial \boldsymbol{\beta}} \equiv M_{ij} \tag{2.129}$$

Here M_{ij} is magnification tensor, clearly Lensing distort $\boldsymbol{\beta}$ into $\boldsymbol{\theta}$. Now the magnification of the source can be evaluated by taking the determinant or Jacobean transformation of tensor M which reads

$$\mu \equiv \left| \frac{1}{A} \right| \equiv |M| \tag{2.130}$$

In addition, beneath lensing here is what could be picked up, the size and the brightness of the source enlarge by a factor of magnification μ remains the constant. The components of Hessian matrix, narrate the distortion from lensing by merging shear effect and convergence effect. shear $\gamma = (\gamma_1, \gamma_2)$ which add to to the distortion into the ellipse. Note that the components of shear is given by

$$\gamma_1 \equiv \frac{1}{2}(\Psi_{11} - \Psi_{22}), \qquad \gamma_2 \equiv \Psi_{12} \equiv \Psi_{21} \tag{2.131}$$

As defined before convergence is given by

$$\kappa \equiv \frac{1}{2}\nabla^2 \Psi \equiv \frac{1}{2}(\Psi_{11} + \Psi_{22}), \tag{2.132}$$

Making use of information above we can formulate magnification and tensor A as follows

$$\mu \equiv \frac{1}{[(1-\kappa)^2 - \gamma^2]} \tag{2.133}$$

And the tensor matrix reads

$$A = \begin{pmatrix} 1-\kappa-\gamma_1 & -\gamma_2 \\ -\gamma_2 & 1-\kappa+\gamma_1 \end{pmatrix} \equiv (1-\kappa) \begin{pmatrix} 1 & 0 \\ 0 & 1 \end{pmatrix} - \gamma \begin{pmatrix} \cos(2\boldsymbol{\theta}) & \sin(2\boldsymbol{\theta}) \\ \sin(2\boldsymbol{\theta}) & -\cos(2\boldsymbol{\theta}) \end{pmatrix} \tag{2.134}$$

Now the magnification Eq. (2.133) we get eigenvalues we can use this to measure the amplification in the tangential also in the radial direction which we can denote by

$$\mu_{tan} \equiv \frac{1}{1-\kappa-\gamma} \tag{2.135}$$

$$\mu_{rad} \equiv \frac{1}{1-\kappa+\gamma} \tag{2.136}$$

In a concept of lensing this two conditions describes two curves namely radial and tangential.

Chapter 3

Large scale structure

3.1 Preliminary

Large scale structure is described as the inhomogeneity or as the structure of the Universe on scales larger than that of a galaxy. In general LSS strive to unravel the unknowns of our Universe. Cosmologists tried to discover how massive matter observed in form of large objects such as galaxies and galaxy clusters and voids. But What does early time observations tell us? well they sort of suggest that while galaxies show a some tendency to cluster in some form of a group on a small scales this is scale of about less or approximately 30 Mpc.h^{-1}, Now expressed statistically by the galaxy correlation function or power spectra , most of the massive matter in the Universe is distributed randomly on large scales which is greater or approximately 30 Mpc.h^{-1}. This kind of image of a relatively smooth out universal mystery has been changing over time. Nevertheless, in recent years as new observational data have began disclosing a Universe with extensive structure and motion on very large scales of approximately 150 Mpc.h^{-1} what is known as BAO scale if not more. Now what can we get extract from this observations? the new information from data on the LSS have led to major changes in existing theoretical ideas on how galaxies and LSS might have been formed. Many models in the past have proven inadequate to explain the new observations, mean while some new candidate models have been suggested and worked out in various degrees of detail. But Still, regardless of the great effort and many ideas, no single theory for the formation of galaxies and LSS can draw some conclusions that equivalent all the observations. Since evolution of structure with time is very slow, this makes LSS fundamental to our understanding of the Universe. Moreover, LSS observation at this current epoch are cosmic relics of conditions that existed in the early epoch of the Universe, How does the relics work? this keeps track of the history of galaxies

and how the structure is formed and evolves [18, 95]. Shifting our focus to the well known principle of the modern physics that the Universe is isotropic and homogeneous, our large scale objects observations present us with the structure of the Universe show some inhomogeneities as far as we know. If we go to very large scale we see some symmetries with the distribution of CMB on large scale this links to the isotropic part of the above sentence, as for homogeneous the definitive explanation is unclear.

We structure this chapter as follows—in section. 3.2 we the small review on the inflation (initial conditions) in large scale structure. The small introduction on how linear fluctuations evolves in large-scale is show in section. 3.3. In section. 3.4 we discuss the large-scale correlation function and its Fourier transform power spectra. We discuss the large-scale transfer function in section. 3.5. In section. 3.6 we review the real and redshift space objects in large-scale structure and we discuss the large-scale bias in section. 3.7.

3.2 Initial conditions

How did it all undertake? Even though this question has doubtlessly persisted to come up for as long as humans exited on Earth, the answer still eludes us, Cosmic Inflation is the perfect candidate to explain this, which was first proposed in 1980 by the American physicist Alan Guth [124]. Guth's theory has been vastly dominant, even if he could not find a way to end inflation so that large scale objects (such as galaxies, clusters and voids) to form, and he considered the theory a failure because of this. There have been many other purifications and alterations since Guth's original model, such as the "inflationary model" of Russian physicist Andrei Linde [111, 152, 169]. This model hypothesized a slow breaking of symmetry, and the creation of many "bubble Universes". A later proposal by Linde, known as the "chaotic inflationary model", believed that the repulsive antigravity effect was caused by a "spin-0 field" rather than any kind of phase transition as Guth had thought.
Linde's work, has also given rise to the idea of "eternal inflation", where the inflation as a whole actually never stops, but small restricted energy dismiss within the overall energy field - almost like sparks of static electricity, but on on a cosmic scale - create small points of matter in the form of tiny particles. Such a process may represent the birth of a new Universe, such as our own. Beginning in this way with what we have called a Big Bang, this new Universe then itself proceeds to expand, although at a much slower rate than the continuing inflation outside of it. The rest of space outside of that Universe is still full of undischarged energy, still expanding at enormous speed,

and new Universes, new Big Bangs, are occurring all the time.
In incorporation cosmic inflation is a strong mechanism for generating primordial perturbations over the smooth Universe, inflation give the a say that quantum-mechanical perturbations in the early Universe are first produced when the relevant scales are casually connected [87]. Then these scales are whisked outside the horizon by inflation, only to re-enter much later to serve as initial conditions for growth of structure and anisotropy in the Universe. The are best described in terms of the Fourier mode, considering for example gravitational potential in Fourier mode reads.

$$\Psi(\mathbf{x},a)=\int\frac{d^3k}{(2\pi)^3}e^{-i\mathbf{k}\cdot\mathbf{x}}\Psi(\mathbf{k},a)\qquad\Psi(\mathbf{k},a)=\int d^3x e^{i\mathbf{k}\cdot\mathbf{x}}\Psi(\mathbf{x},a)\tag{3.1}$$

Here wavevector $\mathbf{k}$ it the Fourier position vector and $\mathbf{x}$ is the real space position vector, then the primordial spectrum given by the expectation value of Fourier-space pairs of the primordial potential Ψ_i yields

$$\langle\Psi_i(\mathbf{k})\cdot\Psi_i^*(\mathbf{k}')\rangle=(2\pi)^3\delta_D(\mathbf{k}-\mathbf{k}')P_{\Psi_i}(k)\tag{3.2}$$

Its worth noting that the norm of the two vectors position are; $k=|\mathbf{k}|$ and $x=|\mathbf{x}|$, δ_D is Dirac delta function enforcing the independence of the different mode, throughout this thesis asterisk denotes complex conjugate. The spectrum is given by $k^3P_{\Psi_i}(k)$ is a constant is called a scale free spectrum. Scale free spectrum is dubbed as Harrison-Zel'dovich-Peeples spectrum [196], credit to the geniuses who first proposed that these is the appropriate distribution for the initial conditions. quantifying the deviations from scale invariance, it is recommended to write the primordial power spectra as follows,

$$P_{\Psi_i}(k)\equiv\frac{50\pi^2}{9k^3}\left(\frac{k}{H_0}\right)^{n_s-1}\delta_H^2\left(\frac{\Omega_m}{D_1(a)}\right)^2\equiv\frac{A}{k^3}\left(\frac{k}{k_\lambda}\right)^{n_s-1}\tag{3.3}$$

Where n_s is the scalar spectral index , most models also predict approximately scale-invariant seed fluctuations ($n_s\approx1$) this can be seen in Fig. 3.1 , in good agreement with the measurement $n_s=0.98\pm0.03$ [232]. However, data are now getting sensitive enough to look for small departures from "vanilla" (scale-invariant, scalar, adiabatic and Gaussian) fluctuations, at least one of which is expected for essentially all published inflation models, so it is important and timely to work out the detailed predictions of competing models.

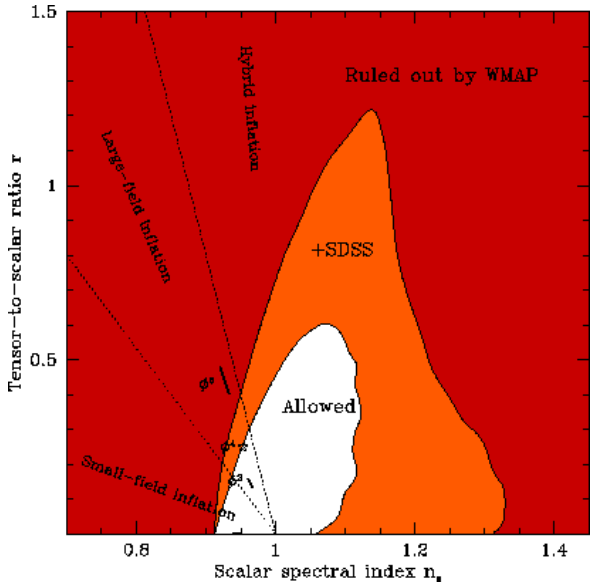

Fig. 3.1 Constraints and predictions in the $n_s - r$ plane show that observations are now finally starting to bump up against inflation theory in an interesting way. The nested shaded regions are ruled out at 95% confidence from WMAP CMB observations alone [201], when adding SDSS galaxy clustering information [232] and when also adding SDSS Lyman α Forest information [225].

3.3 How Linear fluctuations evolves

In the late structure of our Universe, prior to what we refers to as DE, we have the dark and baryonic matter in which components are perfectly described by a pressureless perfect fluid $P_m = 0 = \delta P$, then given that matter is pressureless, we have that the sound speeds are $c_s^2 = c_{sm}^2$, with the equation of state parameter ($w_m = 0$), this is with no anisotropic stress. If we shift or focuses our work in the space of Fourier and also transforming to the longitudinal gauge, In terms of the scale factor and using Friedmann's equations we can write growth as

$$a^2 \frac{\partial^2 \Delta_m}{da^2} + \left(\Omega_\Lambda(a) - \frac{\Omega_m(a)}{2} + 2 \right) a \frac{\partial \Delta_m}{\partial a} - \frac{3}{2} \Omega(a) \Delta_m = 0 \tag{3.4}$$

where parameters $\Omega_\Lambda(a)$ together with $\Omega_m(a)$ are both scale factor (see [202] for detailed derivation). Then linear growth rate yields

$$f_m(a) = \frac{\partial \ln \Delta_m}{\partial \ln a} \equiv \frac{\partial \ln D_m^+}{\partial \ln a} \tag{3.5}$$

Lets review some of the modern cosmology models that where carried out in the past, this is very powerful methods that where rigorously worked,

- For a CDM and Λ dominated Universe , $\Omega_\Lambda(a) < 1$ and $0 < \Omega_\Lambda(a) < 1$ the Hubble parameter decay mode can be expressed as follows

$$D_1^- \propto H(a) \equiv \frac{\mathcal{H}(a)}{a}, \quad \mathcal{H} = aH \tag{3.6}$$

$$H(a) = \sqrt{\Omega_{m0}a^{-3} + (1 - \Omega_{\Lambda 0} - \Omega_{m0})a^{-2} + \Omega_{\Lambda 0}}, \tag{3.7}$$

  Where $\mathcal{H}$ being the comoving Hubble parameter. Using this particular solution and the variation of parameters method, the other solution is found to be [31, 56, 131]

$$D_1^+ \propto \mathcal{H}^2(a) \int_0^a \frac{da'}{\mathcal{H}'^3} \tag{3.8}$$

  Then growth rate approximation given by [157]

$$f(\Omega_m, \Omega_\Lambda) \approx \left[\frac{\Omega_{m0}(1+z)^3}{\Omega_{m0}(1+z) - (\Omega_{m0} + \Omega_{\Lambda 0} - 1)(1+z)^2 + \Omega_{\Lambda 0}} \right]^{\frac{3}{5}} \tag{3.9}$$

  A similar approximation was carried out by [56, 168]

$$f(\Omega_m, \Omega_\Lambda) \approx \left[\frac{\Omega_{m0}(1+z)^3}{\Omega_{m0}(1+z) - (\Omega_{m0} + \Omega_{\Lambda 0} - 1)(1+z)^2 + \Omega_{\Lambda 0}} \right]^{\frac{4}{7}} \tag{3.10}$$

  Now For flat Universe, $\Omega_m + \Omega_\Lambda = 1$, we have [31, 52]

$$f(\Omega_m, \Omega_\Lambda) \approx \Omega_m^{\frac{5}{9}} \tag{3.11}$$

- For the Universe with an open cold dark matter model (OCDM) dominated ,we set the following cosmological parameters $\Omega_m(a) < 1$ & $\Omega_\Lambda = 0$ the solution for this was provided by [122] which read

$$D_1^+ \equiv 1 + \frac{3}{x} + 3\frac{(1+x)^{0.5}}{x^{\frac{3}{2}}} \ln\left[(1+x)^{0.5} - x^{0.5} \right], \tag{3.12}$$

$$D_1^- \equiv \frac{(1+x)^{0.5}}{x^{1.5}}, \quad x \equiv a\left(\frac{1}{\Omega_{m0}} - 1 \right) \tag{3.13}$$

- For Universe with a standard cold dark matter (SCDM) dominated, i.e. a particular case of an Einstein-de Sitter Universe [194] (Einstein & de Sitter, 1932) where dark matter is cold, the cosmological parameters are time independent : $\Omega_m(a) = 1$ and $\Omega_\Lambda(a) = 0$. The following solutions yields

$$D_1^+ \propto a, \qquad D_1^- \propto a^{-1.5}, \qquad f(\Omega_m, \Omega_\Lambda) \equiv 1 \tag{3.14}$$

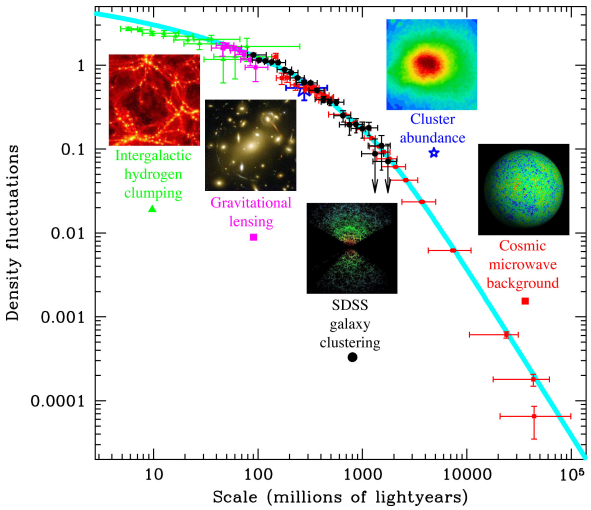

Fig. 3.2 The new SDSS results (black dots) are the most accurate measurements to date of how the density of the Universe fluctuates from place to place on scales of millions of lightyears. These and other cosmological measurements agree with the theoretical prediction (blue curve) for a Universe composed of 5% atoms, 25% dark matter and 70% dark energy. The larger the scales we average over, the more uniform the Universe appears

3.4 Fourier decay of the density field

3.4.1 The Correlation functions

The correlation functions of fields are expectation values of products of fields at different spatial points.the correlation function is the measure of the average probability that a randomly selected galaxy will lie within some separation distance d of another galaxy. From [62] the case of a random field, the two-point correlation function will measure the product of the probability density function evaluated at two different points in the

field, using the expectation value integral

$$\xi(d) = \langle \delta(\mathbf{x}) \cdot \delta(\mathbf{x}+\mathbf{r}) \rangle \tag{3.15}$$

Due to statistical homogeneity and isotropic the above depends only on norm of $\mathbf{r}$. The density contrast $\delta\mathbf{x}$ in Fourier transform convention reads

$$\delta\mathbf{x} = \int d^3\mathbf{k} \cdot \delta(\mathbf{k}) \cdot e^{i\mathbf{k}\cdot\mathbf{x}} \tag{3.16}$$

Where the quantities $\delta(\mathbf{k})$ are the complex variables, since its also real it follows that

$$\delta(\mathbf{k}) = \delta^*(-\mathbf{k}) \tag{3.17}$$

The density field is therefore determined entirely by the statistical properties of the random variable $\delta(\mathbf{k})$. We can compute the correlation function in Fourier space

$$\langle \delta(\mathbf{k}) \cdot \delta^*(\mathbf{k}') \rangle = \frac{1}{(2\pi)^6} \int d^3\mathbf{x} \cdot d^3\mathbf{r} \langle \delta(\mathbf{x}) \cdot \delta(\mathbf{x}+\mathbf{r}) \rangle e^{[-i(\mathbf{k}+\mathbf{k}')\cdot\mathbf{x} - i\mathbf{k}'\cdot\mathbf{r}]} \tag{3.18}$$

which is the same as,

$$\begin{aligned} \langle \delta(\mathbf{k}) \cdot \delta^*(\mathbf{k}') \rangle &\equiv \frac{1}{(2\pi)^6} \int d^3\mathbf{x} \cdot d^3\mathbf{r} \cdot \xi(d) e^{[-i(\mathbf{k}+\mathbf{k}')\cdot\mathbf{x} - i\mathbf{k}'\cdot\mathbf{r}]} \\ &\equiv \frac{\delta_D(\mathbf{k}+\mathbf{k}')}{(2\pi)^3} \int d^3\mathbf{r} \cdot \xi(d) e^{(\mathbf{k}\cdot\mathbf{r}} \\ &\equiv \delta_D(\mathbf{k}+\mathbf{k}') P(k) \end{aligned} \tag{3.19}$$

Where $P(k)$ is by definition the density power spectrum. The inverse relation between two-point correlation function and power spectrum thus reads

$$\xi(d) = \int d^3\mathbf{k} \cdot P(k) e^{i\mathbf{k}\cdot\mathbf{r}} \tag{3.20}$$

This leads us to the next subsection. 3.4.2

3.4.2 The Power spectra

As noted in section.3.4.1 that the power spectrum is the Fourier transform of the correlation function. The term "power" comes from the fact that if the function you are evaluating is the variance of a voltage signal , than the power spectrum will be proportional to the electrical power of the signal. In the case of a homogeneous and

isotropic random field, the power spectrum $P(k)$ is implicitly defined as follows

$$\langle \delta(\mathbf{k}) \cdot \delta^*(\mathbf{k}') \rangle \equiv (2\pi)^3 \delta_D(\mathbf{k}+\mathbf{k}') P(k) \equiv \frac{k^3}{2\pi^3} P(k) \tag{3.21}$$

therefore we can write the power spectrum as,

$$P(k) = \frac{1}{(2\pi)^3} \int d^3\mathbf{x} \cdot \xi(d) e^{i\mathbf{k}\cdot\mathbf{r}} \tag{3.22}$$

Its easy to note that Eq. (3.20)) and (3.22) they are two conventions which differ by a factor of $(2\pi)^3$. The Primordial shape of the power spectrum comes from the inflationary scenario for the very early Universe (more details can be obtained from [124, 125])

3.5 Transfer function

Early Universe perturbations of modern cosmology is composed of this following schemes see Fig. 3.3, inflation scheme, this regime was introduced to sort out the flatness and horizon problems. These epoch deals with wavelengths longer than the horizon. Inflation is also powerful in our understanding of cause mechanism for large scale structure in the Universe's origin. After the end of inflation scheme of the Universe invaded the radiation-dominated epoch during which light elements such as helium and deuterium were formed. These epoch sort out the intermediate wavelengths that are within the horizon. Finally we have matter dominated epoch, this is where large scale objects (galaxies, clusters) are formed. These epoch deals with wavelengths longer than the horizon. After the Universe enters the matter-dominated epoch, the magnitude of approaches a constant value. Thus we have shown that the evolution of the gravitational potential Ψ depends strongly on the scales of perturbations. In order to describe its evolution for each wavenumber (k) during the epoch of transfer or rather transfer epoch we have the following

$$T(k) \equiv \frac{\Psi_d(a,k)}{\Psi(a,k)} \tag{3.23}$$

Here $\Psi(a,k)$ being the large-scale solution which reduced by $\frac{9}{10}$ if compared with initial value ,the the above expression simplify to

$$T(k) \equiv \frac{9}{10} \frac{\Psi_d(a,k)}{\Psi_i(a,k)} \tag{3.24}$$

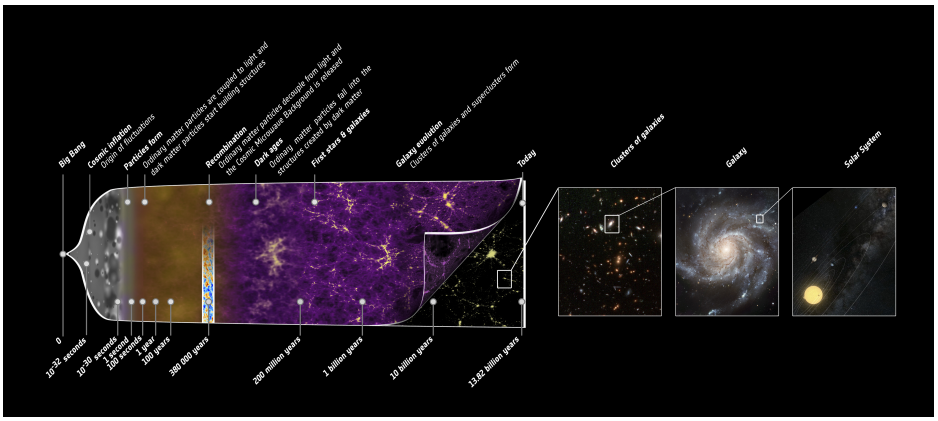

Fig. 3.3 The diagram showing the structure of the Universe from early epoch to late epoch. Credit to Planck collaborators

Note that $\Psi_d(a,k) = \Psi(a_d,k)$ and $\Psi_i(a,k) = \Psi(a_i,k)$. Also this happens just after the matter-dominated which is at equality this is where $(a = a_{eq})$ i.e for late times $(a \gg a_{eq})$

In general, the transfer function has to be derived numerically by integrating the equations for each k mode. A popular fit has been given by Bardeen, Bond, Kaiser, and Szalay (BBKS)[1]

$$T(x) \equiv \frac{\ln(1+0.171x)}{0.171x}[1+0.284x+(1.181x)^2+(0.399x)^3+(0.490x)^4]^{-\frac{1}{4}} \quad (3.25)$$

$$T(x) \equiv \frac{\ln(1+2.34x)}{2.34x}[1+3.89x+(16.1x)^2+(5.46x)^3+(6.71x)^4]^{-\frac{1}{4}} \quad (3.26)$$

$$T(x) \equiv e^{-3.9x-2.1x^2} \quad (3.27)$$

$$T(x) \equiv (5.6x)^2\left\{1+\left[15x+(0.9x)\frac{3}{2}+(5.6x)^2\right]^{1.24}\right\} \quad (3.28)$$

Where $x = \frac{k}{k_{eq}}$. On large scales characterized by the condition $x = \frac{k}{k_{eq}} \ll 1$ the BBKS transfer function reduces to $T(x) \approx 1$, which give us this following $\Psi = \frac{9}{10}\Psi_i(a,k)$ as expected. On small scales with $x = \frac{k}{k_{eq}} \gg 1$the transfer function has a wavenumber dependence $T(k) \propto \frac{(Ink)}{k^2}$, which means that the gravitational potential is suppressed for increasing k The scenario with this transfer function fits is as follows: Eqs. (3.25) & (3.26) - Adiabatic CDM; Eq. (3.27) - Adiabatic massive neutrinos Eqs. (3.25) & (3.26) - massive, Eq. (3.27) - massless; Eq. (3.28) Isocurvature CDM; these expressions come from [21].

[1]In Fig. 3.4 We've shown the behavior of the given by [103] and compare it with the BBKS fitting given above

If we consider $a > a_{eq}$ the gravitational potential remains constant during the matter epoch at least in standard GR, but after the Universe has entered the epoch of cosmic acceleration is expected to vary. In order to quantify this, we introduce the suppressed growth function $\frac{D(a)}{a}$ which yields

$$\frac{\Psi(a)}{\Psi_{eq}} = \frac{D(a)}{a} \tag{3.29}$$

Assembling information in our hands we find that the gravitational potential today is given by

$$\Psi(a,k) = \frac{9}{10}\Psi_i(a_i,k)T(k)D(a_0) \tag{3.30}$$

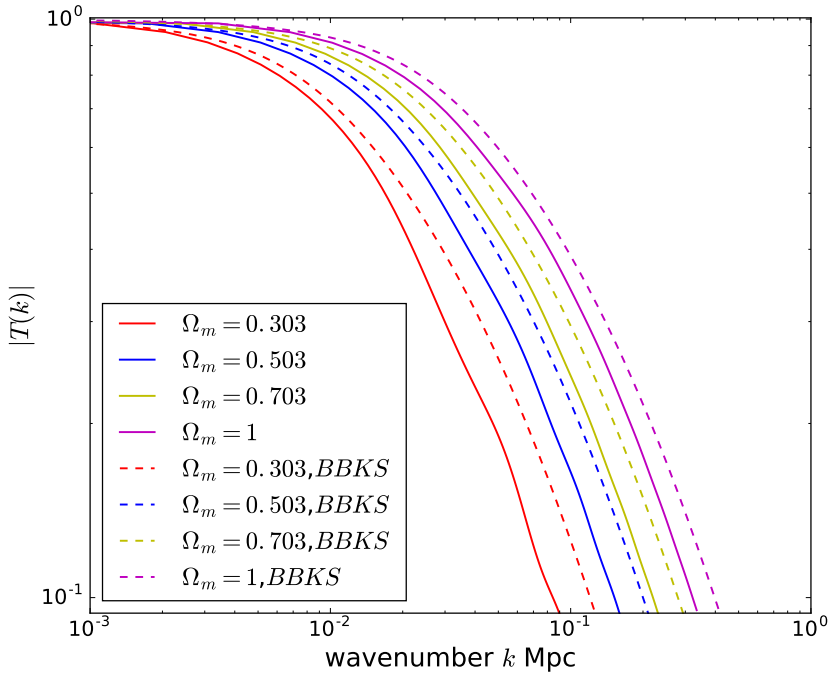

Fig. 3.4 Schematic showing the behavior of transfer function (solid line) together with its best fit that is BBKS (broken line) for various matter energy parameter Ω_m

3.6 Real and Redshift space Clustering

Evaluation of far away objects distances require the objects observed redshift caused by expansion of the Universe , nevertheless they also include contributions from the peculiar motion of the objects, this is in the local rest frame, thus we can say, the distances approximated from redshift does not match the accurate distance and this are set to be measured in redshift space (see Fig. 3.5 for apparent and actual objects). The measure in real space, holds if the accurate position of the objects were well known, Therefore, peculiar motions will introduce distortions in the measured clustering pattern .

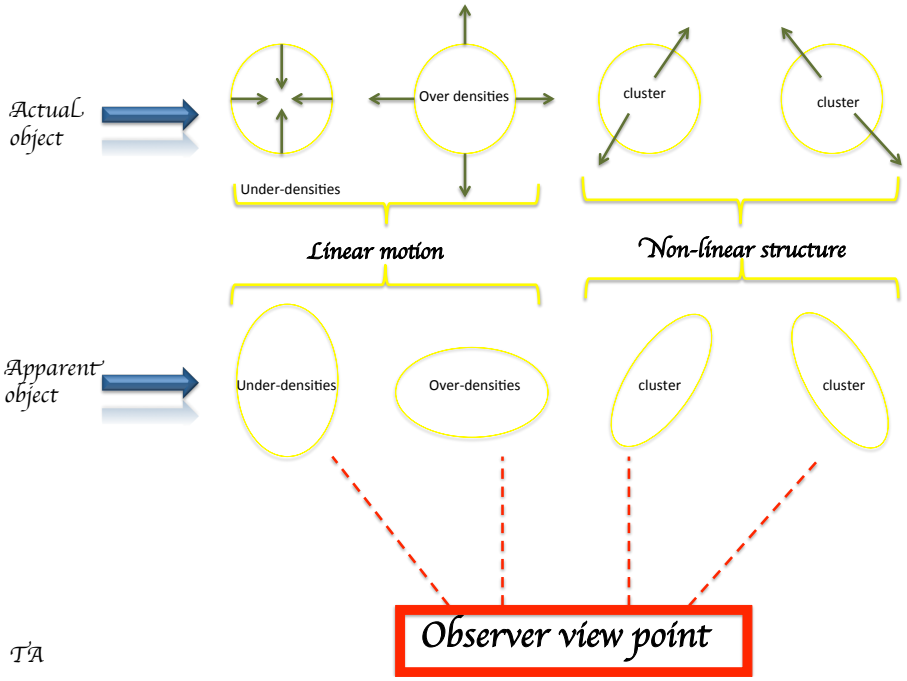

Fig. 3.5 The schematically diagram showing the difference between real space and redshift space.

3.6.1 Redshift space distortion

The estimation of large scale objects are estimated from different redshifts, well these redshifts are caused by both motions within a comoving frame and Hubble expansion known as peculiar velocity this description can be put in to expression as

$$\mathbf{s}(\mathbf{r}) \equiv \mathbf{r} - v_r(r)\frac{\mathbf{r}}{r} \equiv \mathbf{r} + \frac{a}{H(z)}v_r\mathbf{r} + l.e.o.m \tag{3.31}$$

Here l.e.o.m this abbreviated by linearized equation of motion that it is negative of the multiple of growth rate and density contrast, Where **r** is the real space position of the away from observer at the origin , **s** is the redshift space position of the galaxy and v_r is the radial component of the peculiar velocity. Furthermore, measuring the clustering of distant objects (such as galaxies, clusters) does not supply a direct determination of galaxies/clusters real spatial distribution of the underlying Dark matter DM. The distances are distorted by two different distortions namely (i) dynamical distortion and (ii) geometrical distortion, in case incorrect cosmology is been used to convert the observed redshift into distance. This two are rigorously explained in the next two subsections

3.6.1.1 Dynamical distortion

dynamical redshift space distortions is basically composed of two mechanisms . While growth of structure through gravity, the collapsing inwards of objects to higher density regions contributes to the measured redshifts. If these are presumed to be uniquely requires to the Hubble flow, than the large-scale distribution will appear flatter, or thinner, along the line of sight, thus "distorting" the clustering signal. At very smaller scales, the arbitrary peculiar motions of the objects will also contribute to the measured redshifts, and hence distort the measured clustering signal for close pairs of objects. If the distribution of distant objects has, on the mean, a spherically symmetric clustering pattern in real space, but large velocity dispersion, then the clustering signal measured in redshift space will be grease along the line-of-sight. These features are often referred to as "fingers-of-God", and are commonly observed as elongated structures in radial wedge plots of distant galaxy surveys, such as the 2dFGRS (e.g. Hawkins et al., 2003). As shown by [148, 199], the large scale coherent collapsing inwards can be used to probe the clustering of the underlying DM clustering and the matter content of the Universe. This inwards collapsing could be parameterized by comparing the large-scale clustering in real and redshift space. In terms of the power-spectrum:

$$P_g(k_s) = P_g(k_r)(1+\beta\mu^2)^2 \tag{3.32}$$

where the subscripts r and s refer to the real and redshift space measurements, respectively. here μ is the cosine between the velocity vector and the line of sight, and β is correlating the observed large-scale inwards collapse to the clustering of the (invisible) DM. The equation above can be written in terms of correlation functions

(see Kaiser, 1987 for more details):

$$\xi_g(s) \equiv \xi_g(r)\left(1+\frac{2}{3}\beta+\frac{1}{5}\beta^2\right) \tag{3.33}$$

Where β can be expressed in term of matter distribution which yields

$$\beta \equiv \frac{f_m(z)}{b} \tag{3.34}$$

Here, b is the bias, which provide correlation between the luminous matter clustering and the underlying DM $\left(b^2 = \frac{\xi_g}{\xi_{mass}}\right)$ This association means intrinsically that luminous objects are biased tracers of the underlying mass distribution, which dominates the overall dynamics due to gravitational effects. However, it has been found that galaxy clustering is a function of galaxy properties, such as morphology type luminosity. Therefore, the true bias will also depend on the physics of galaxy formation, interactions and feedback mechanisms, which are still not so well understood [199]. Growth of structure as a function of the cosmological parameter, in the case of a flat Universe can be approximated to [157]

$$f \equiv \frac{\partial \ln \delta}{\partial \ln a} \approx \Omega_m^{0.6}(z) + \frac{1}{70}\left(1-\frac{1}{2}\Omega_m(z)(1+\Omega_m(z))\right) \tag{3.35}$$

The approximation is normally expressed as follows

$$f \approx \Omega_m^{0.6}(a) \tag{3.36}$$

The formalism for redshift space to real space mapping of the large-scale structure distribution is hardly unique. From Whilst Kaiser et al 1987 related the real and redshift space correlation functions through Eq. ((3.33)), [199] uses the simpler form $\xi_g(s) = \xi_g(r)(1+1.5\beta)$; [132] have used a spherical harmonic approach to relate the redshift space to real space clustering measurements. More recently the modeling of dynamical distortions has been developed under the halo occupation distribution framework and non-linearities and scale depending on parameterizations of the velocity dispersion. Furthermore , more recently the mapping of DM from real space to redshift space [253], Their mapping formula is intrinsically non-linear, which is complicated by the higher order polynomials due to indefinite cross correlations between the density and velocity fields, and the Finger-of-God effect due to the randomness of the peculiar velocity field.

3.6.1.2 Geometrical distortion

In this section we provide a short introduction on Alcock and Paczynski (see for more details [5]) and the volume effect, more detailed description of the AP effect has been provided in [164]. As shown from [5] if one assumes a wrong cosmology, underlying cosmology of the Universe to convert redshifts into distances, the effect on separations along the line of sight differs from that affecting the separation in the sky direction. As a consequence, the clustering signal might appear elongated (or squashed) in the redshift direction. As shown by Alcock ,these geometric distortions can be a robust cosmological test. Suppose that we are probing the shape and volume of an object in the Universe. We measure its redshift span Δz and angular size $\Delta\theta$, then compute its sizes in the radial and transverse directions from the relations of

$$\Delta r_{\parallel} = \frac{c\Delta z}{H(z)}, \qquad \Delta r_{\perp} = (1+z) D_A \Delta\theta \tag{3.37}$$

where H is the Hubble parameter, DA is the angular diameter distance (Its behavior is shown by Fig. 3.6). In the particular case of a flat Universe with constant dark energy EoS, they take the forms of

$$D_A(z) = \frac{1}{1+z} r(z) = \frac{1}{1+z} \int_0^z \frac{dz'}{H(z')} = \frac{1}{1+z} \int_0^z \frac{dz'}{H_0 \sqrt{\Omega_m a^{-3} + (1-\Omega_m) a^{-3(1+w)}}} \tag{3.38}$$

Where H_0 is the current Hubble parameter, $a(z)$ is the scale factor and $r(z)$ is the comoving distance, we adopt the formalization [165].The degree of variations in shape and volume can be described by the following quantities. where "true" and "wrong" denote the values of quantities in the true cosmology and wrongly assumed cosmology.

$$\frac{[\Delta r_{\parallel}(\Delta r_{\perp})]_{wrong}}{[\Delta r_{\parallel}(\Delta r_{\perp})]_{true}} = \frac{[D_A(z)H(z)]_{true}}{[D_A(z)H(z)]_{wrong}} \tag{3.39}$$

$$\frac{[\Delta r_{\parallel}(\Delta r_{\perp})^2]_{wrong}}{[\Delta r_{\parallel}(\Delta r_{\perp})^2]_{true}} = \frac{[D_A^2(z)/H(z)]_{wrong}}{[D_A^2(z)/H(z)]_{true}} = \frac{V_{wrong}}{V_{true}} \tag{3.40}$$

3.7 Large-scale structure bias

The correspondence between luminous matter and tracers dubbed as "bias", configure a vital information in the interpretation of the observed large scale structure. The reason

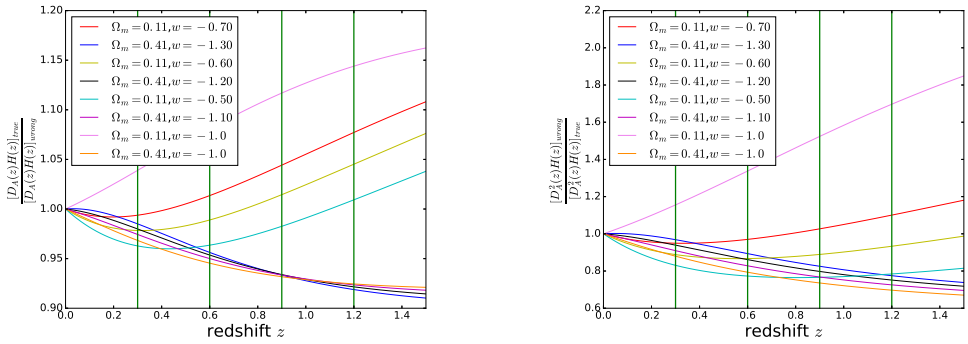

Fig. 3.6 The behavior of two effects given by equations Eq. (3.39) and (3.40) which depends on redshift in two wrongly assumed cosmology i.e $\Omega_m = 0.41$, $w = -1.3, -1.2, -1.1, -1$ and $\Omega_m = 0.11$, $w = -0.7, -0.6, -0.5, -1$, as for the truly assumed cosmology we set the following $\Omega_m = 0.26$,$w = -1$.

being, the observed distribution of galaxies, quasars, and clusters of galaxies (see [228] for details), the large-scale structure of the Universe. These tracers can be observed out to cosmological distances, and thus can be used to contemplate remarkable amount of the observable Universe. If we understand the correspondence distribution of tracers to the underlying distribution of matter, we can access a significant amount of information on the composition of the Universe, properties of dark matter, dark energy and gravity, as well as the nature of the process that produced the initial source of structure. In the next subsections of the thesis we focus on two well known counter-parts of bias which is magnification bias and galaxy bias

3.7.1 magnification bias

In brief , Turner et al 1984 gave a description that bias is caused by gravitational lensing this is happen by modulation the of the apparent surface density of the galaxies on the the sky or space, though the two participating effects. Lets get this out of the way , lensing can be magnified or demagnified individual source/origin galaxies from the background this causes the increase nor decrease of the their flux. Weak lensing (WL) surveys for a flux limited, some how otherwise eliminated the faint galaxies can therefore make it into (or drop out of) the sample because of this demagnification. Also a indistinguishable, scenario demagnification petitions to the portion of the sky around the galaxy, geometrically diluting or enhancing the apparent surface density of galaxies in this region. These effects mentioned above counteract each other, and the net bias strongly depends on the slope of the intrinsic unlensed galaxy luminosity function at the survey flux limit. In addition to these effects, lensing can increase or

decrease the apparent angular size of spatially resolved individual galaxies. If either the survey selection, or a derived statistic such as weak lensing shear, depends on the apparent size, then this can introduce an additional size bias [170]. Now lets consider a simple ansatz, with fixed time then the relation between density contrast large scale objects and matter distribution

$$\begin{aligned} \delta_g &\equiv n_g(\mathbf{x}) - \bar{n}_g \\ &= b \cdot \delta(\mathbf{x}) \\ &\equiv b\left(\frac{\rho_m(\mathbf{x})}{\bar{\rho}_m} - 1\right) \end{aligned} \tag{3.41}$$

Here b parameter being what we refer to as bias , while $\bar{n}_g$ denotes the mean galaxy comoving number density and $\bar{\rho}_m$ being the background matter comoving density. In addition two point correlation of large scale objects is enhanced by a factor of about the square of bias over matter two point correlation. If we allow for clusters to have a larger bias parameter than galaxies, their different observed correlation functions can be explained. Making use information provided in Chapter. 2 and some algebra we can work out the the relation between gauge invariant and galaxy bias which yields

$$\Delta_g = b \cdot \Delta_m \tag{3.42}$$

This holds for all linear scales.

Chapter 4

Effective field theory

In the past various alternative models to the so-called standard model of cosmology has been carried out, however the most interesting and rather simple approach have been recently introduced to be the scalar field (see [146] for more comprehensive details). This could be considered either as modification of gravity or as the contribution of dark energy with incorporates a single scalar degree of freedom[1] dubbed effective field theory EFT [28, 42, 67, 116, 119, 123, 141, 171, 197, 206, 233] or unified dark energy. Furthermore, mainly the motive of modification of gravity MG or DE is to identify the source of the late-time acceleration expansion of the Universe [42, 67]. There are couple of assets in making use of EFT or UDE framework i.e providing a more general view point of models such as Horndeski theories and beyond [116]. Another advantage is that we can easily compare or relate EFT with current observational constraints. One needs to keep in mind that commonly if we add an extra scalar field this will results in a spatially homogenous and isotropic background solution or value which solely depends on time. Moreover, the spatially homogenous and isotropic background of our Universe at low energies perturbation around it will typically be explained by this additional scalar[2].

This chapter is organized as follows—After descibing the unitary gauge, we provide the background actions or Lagrangians and perturbations around them in section. 4.1. In section. 4.2, we give a small overview of unified dark energy (UDE) or Effective field theory (EFT).

[1]This is much simpler modification since we consider only one additional degree of freedom, there are more complex cases such as bimetric gravity [127] and massive gravity [77] i.e. for this complicated scenarios one can recover a single fdegree of freedom by applying some specific conditions.

[2]This apply without regarding any basics of the the theory.

4.1 Unitary gauge

In this gauge the time coordinate is picked keeping in mind the end goal to assimilate the scalar field perturbations in the metric $g_{\mu\nu}$, this brought together treatment lessens to finding a summed up action which composed of geometric operators that are gauge-invariant under time-dependent spatial diffeomorphisms with free time-dependent coefficients [172]. Specifically we mean that under all time and space diffeomorphisms the scalar field ϕ is considered to be invariant but its perturbation $\delta\phi$ is not gauge-invariant. Furthermore, this is only gauge-invariant under spatial diffeomorphisms in which under the time diffeomorphisms one can perform the following transform [9, 63, 69]

$$t \to t + \bar{\xi}(t,\vec{x}), \quad \delta\phi \to \delta\phi + \dot{\bar{\phi}}(t)\bar{\xi} \tag{4.1}$$

This choice of the time coordinate is known to be the *unitary gauge* or *torus gauge*. The unitary gauge is such that we have

$$\phi(t,\vec{x}) = \bar{\phi}(t) + \delta\phi(t,\vec{x}) = \bar{\phi}(t) \tag{4.2}$$

Here we need to make a note that the perturbation $\delta\phi$ in above expression did not just vanish - it just became constituent of the metric perturbations. For example the standard kinetic term $X \equiv \nabla_\mu\phi\nabla^\mu\phi = g^{00}\dot{\bar{\phi}}^2 = -\dot{\bar{\phi}}^2/N^2$ in a way that operators partake in the expansion of perturbation given as $\delta g^{00} = 1 + g^{00}$.

4.1.1 Background fluctuations

In this subsection we outline the relevant background equations, specifically the two Friedmann equations [3, 10–12, 25, 27–29, 34–39, 41, 42, 51, 54, 63, 64, 67, 69, 71–73, 75, 78–81, 88, 106, 107, 115–119, 123, 155, 158, 162, 184, 186, 187, 192, 197, 243, 246–248, 254] (which we will be obtained from total homogeneous $\bar{S} = \bar{S}_g + \bar{S}_m$). We consider a spatially flat FLRW space metric, given by

$$ds^2 = -\bar{N}^2dt^2 + a^2(t)\delta_{ij}dx^idx^j \tag{4.3}$$

Adopting Eq. (2.13) the linear variation background of the homogeneous action $\bar{S}_g$ together with the matter minimally coupled to the metric $g_{\mu\nu}$ given with respect to

the lapse N and the scale factor a. In the FLRW Universe yields

$$\begin{aligned}\delta\bar{S}=\delta\bar{S}_g+\delta\bar{S}_m &= \int d^4x\bar{N}a^3\left[\left(\frac{\bar{\mathcal{L}}}{\bar{N}}+\bar{\mathcal{L}}_N-\frac{3H\bar{\mathcal{F}}}{\bar{N}}\right)\delta\bar{N}+3\bar{N}\left(\bar{\mathcal{L}}-3H\bar{\mathcal{F}}\right)\frac{\delta a}{a}\right]\\ &+ \int d^4x\bar{N}a^3\left(-\bar{\rho}_m\frac{\delta\bar{N}}{\bar{N}}+3\bar{p}_m\frac{\delta a}{a}\right)\end{aligned} \tag{4.4}$$

Where homogeneous Lagrangian as a function of lapse, scale and physical time reads $\bar{\mathcal{L}}=\mathcal{L}\Big[K_{ij}=H\delta_{ij}, R_{ij}=0, N=\bar{N}(t)\Big]$, it can be shown that the intrinsic curvature tensor of the constant time $\sum_t$ hypersurfaces vanishes ($R_{ij}=0$) and the components of the extrinsic curvature tensor are given $K_{ij}=\frac{\dot{a}}{\bar{N}a}g_{ij}$. Moreover, the homogeneous background partial derivative is given with respect to lapse $\bar{\mathcal{L}}_N=\frac{\partial\mathcal{L}}{\partial N}$, and finally we also introduced the coefficient $\bar{\mathcal{F}}\bar{g}_{ij}=\frac{\partial\mathcal{L}}{\partial K_{ij}}$. Making use of $\sqrt{-g}=a^3\bar{N}$ with some algebra the Friedmann equations are given as follows

$$\bar{\mathcal{L}}+\bar{N}\bar{\mathcal{L}}_N-3H\bar{\mathcal{F}}=\bar{\rho}_m \tag{4.5}$$

$$\bar{\mathcal{L}}-3H\bar{\mathcal{F}}-\frac{\dot{\bar{\mathcal{F}}}}{\bar{N}}=\bar{p}_m \tag{4.6}$$

The matter background energy density and background pressure are related by

$$\frac{\dot{\bar{\mathcal{F}}}}{\bar{N}}+\bar{N}\bar{\mathcal{L}}_N=(1+w_m)\bar{\rho}_m \tag{4.7}$$

4.1.2 Perturbation fluctuations

The perturbed evolution equations encompassing the FLRW background solution are based on the incorporation of the following perturbative quantities; $\delta N\equiv N-\bar{N}$, $\delta K_{ij}\equiv K_{ij}-\frac{\dot{a}}{\bar{N}a}g_{ij}$, $\delta R_{ij}=R_{ij}$. We use this to expand the Lagrangian $\mathcal{L}$ in Eq. (2.13) to the second order. As for the quadratic action, we only consider the perturbations of $\sqrt{-g}$ at first order. Hence, using $\delta\sqrt{-g}=\delta\sqrt{h}+a^3\delta N$ in the ADM decomposition the quadratic Lagrangian for perturbations is given by

$$\begin{aligned}\mathcal{L}_2 &= \bar{N}\mathcal{G}\,\delta_1 R\delta\sqrt{h}+a^3\left(\bar{\mathcal{L}}_N+\frac{1}{2}\bar{N}\bar{\mathcal{L}}_{NN}\right)\delta N^2\\ &+ \bar{N}a^3\Big[\mathcal{G}\delta_2 R+\frac{1}{2}\hat{\mathcal{A}}_K\delta K^2+\mathcal{B}\delta K\delta N+\hat{\mathcal{C}}\,\delta K\delta R+\mathcal{C}\delta K_{ij}\delta R^{ij}\\ &+ \mathcal{A}_K\delta K_{ij}\delta K^{ij}+\mathcal{A}_R\delta R_{ij}\delta R^{ij}+\frac{1}{2}\hat{\mathcal{A}}_R\delta R^2+\left(\frac{\mathcal{G}}{\bar{N}}+\mathcal{B}_R\right)\delta N\delta R\Big]+...,\end{aligned} \tag{4.8}$$

Where coefficients $\hat{\mathcal{A}}_K$, $\mathcal{A}_K$, $\mathcal{B}$, $\mathcal{B}_R$, $\mathcal{A}_R$, $\mathcal{G}$, $\hat{\mathcal{A}}_R$ and $\hat{\mathcal{C}}$ are defined by (note that the lower index of $\mathcal{L}$ denotes the partial derivative with respect to specified scalar quantity i.e ., $\mathcal{L}_R = \frac{\partial \mathcal{L}}{\partial R}$) see [GLPV] for detailed review

$$\hat{\mathcal{A}}_K = 4H^2\mathcal{L}_{SS} + 4H\mathcal{L}_{SK} + \mathcal{L}_{KK}, \quad \mathcal{A}_K = \mathcal{L}_S, \quad \mathcal{B} = 2H\mathcal{L}_{SN} + \mathcal{L}_{KN} \tag{4.9}$$

$$\mathcal{B}_R = \mathcal{L}_{NR}, \quad \mathcal{A}_R = \mathcal{L}_Z, \quad \mathcal{G} = \mathcal{L}_R, \quad \hat{\mathcal{L}}_R = \mathcal{L}_{RR} \quad \hat{\mathcal{C}} = 2H\mathcal{L}_{SR} + \mathcal{L}_{KR} \tag{4.10}$$

Where we considered the geometric scalar quantities; $S \equiv K_{ij}K^{ij}$, $Z \equiv R_{ij}K^{ij}$ and $U \equiv R_{ij}K^{ij}$. Now re-introducing $\delta K_{ij}\delta R^{ij}$ in a different form as shown in ref. Gleyzes et al. [116] the quadratic Lagrangian Eq. (4.8) simplifies to

$$\begin{aligned}
\mathcal{L}_2^{(new)} &= \bar{N}\mathcal{G}^*\delta_1 R\delta\sqrt{h} + a^3\left(\bar{\mathcal{L}}_N + \frac{1}{2}\bar{N}\bar{\mathcal{L}}_{NN}\right)\delta N^2 \\
&+ \bar{N}a^3\Big[\mathcal{G}^*\delta_2 R + \frac{1}{2}\hat{\mathcal{A}}_K\delta K^2 + \mathcal{B}\delta K\delta N + \mathcal{C}^*\delta K\delta R \\
&+ \mathcal{A}_K\delta K_{ij}\delta K^{ij} + \mathcal{A}_R\delta R_{ij}\delta R^{ij} + \frac{1}{2}\hat{\mathcal{A}}_R\delta R^2 + \left(\frac{\mathcal{G}^*}{\bar{N}} + \mathcal{B}_R^*\right)\delta N\delta R\Big] + .
\end{aligned} \tag{4.11}$$

Where the coefficients are renormalized by

$$\mathcal{G}^* = \mathcal{G} + \frac{\dot{\mathcal{C}}}{2\bar{N}} + H\mathcal{C}, \quad \mathcal{C}^* = \hat{\mathcal{C}} + \frac{\mathcal{C}}{2}, \quad \mathcal{B}_R^* = \mathcal{B}_R + \frac{\dot{\mathcal{C}}}{2\bar{N}^2} \tag{4.12}$$

Similarly to the previous section, we look into the behavior of the scalar, vector and tensor modes in the general quadratic Lagrangian Eq. (4.11), at linear order,

Scalar mode: We begin by making a remark that the following linear perturbations equations of motions are of 2-order under the conditions

$$\hat{\mathcal{A}}_K + 2\mathcal{A}_K = 0, \quad \mathcal{C}^* = 0, \quad 4\hat{\mathcal{A}}_R + 3\mathcal{A}_R = 0 \tag{4.13}$$

Adopting the relations;

$$\delta\sqrt{h} = 3a^3\zeta, \quad \delta R_{ij} = -(\delta_{ij}\partial^2\zeta + \partial_i\partial_j\zeta), \quad \delta_1 R = -4a^{-2}\partial^2\zeta \tag{4.14}$$

$$\delta_2 R = -2a^{-2}[(\partial\zeta)^2 - 4\zeta\partial^2\zeta], \quad \delta K_{ij} = (\dot{\zeta} - H\delta N)\delta_{ij} - \delta^{ik}(\partial_k N_j + \partial_j N_k) \tag{4.15}$$

$$\delta K = 3(\dot{\zeta} - H\delta N) - \partial^2\frac{\phi}{a^2} \tag{4.16}$$

Applying this into the Lagrangian we get the extended new Lagrangian (represented as a function of δN, ψ and ζ), which doesn't depend on the derivatives of the shift and lapse. Furthermore, varying the new Lagrangian with respect to δN and ψ results in

momentum and Hamiltonian constraints with some algebra the momentum constraint becomes

$$\delta N = \frac{\dot{\zeta}}{H(1+\alpha_B)} \tag{4.17}$$

Where we introduced the normalized parameter $\alpha_B \equiv \frac{\mathcal{B}}{4H\mathcal{A}_K}$. Thus, blending in all the formation given above the quadratic action with respect to ζ yields

$$\begin{aligned} S &= \int d^4x \left(\frac{a^3}{2}\right)\left\{\frac{M^2\alpha}{(1+\alpha_B)^2}\dot{\zeta}^2 + \left[1+\alpha_T - \frac{1+\alpha_H}{1+\alpha_B}\left(1+\alpha_M - \frac{\dot{H}}{H^2}\right)\right.\right. \\ &- \left.\left.\frac{d}{Hdt}\left(\frac{1+\alpha_H}{1+\alpha_B}\right)\right]\frac{(\partial_i\zeta)^2}{a^2} + \frac{M^4}{4}(1+\alpha_T)\frac{(\partial_k\gamma_{ij})^2}{a^2}\right\} \end{aligned} \tag{4.18}$$

Where we have introduced the normalized functions which depends to time given as

$$\alpha_H = \frac{\mathcal{G}^* + \mathcal{B}_R^*}{\mathcal{A}_K} - 1, \quad \alpha_K = \frac{2\bar{\mathcal{L}}_N + \bar{\mathcal{L}}_{NN}}{2H^2\mathcal{A}_K}, \quad \alpha = \alpha_K + \alpha_B^2 \tag{4.19}$$

Parameters α_M and α_T originate from vector and tensor modes which we will describe below. The evolution of squared sound speed can be obtained by evaluating the ratio of the two terms inside the square bracket of the action given above involving matter can be denoted as follows

$$\begin{aligned} c_s^2 &= \frac{-2(1+\alpha_B)^2}{\alpha}\left[1+\alpha_T - \frac{1+\alpha_H}{1+\alpha_B}\left(1+\alpha_M - \frac{\dot{H}}{H^2}\right) - \frac{d}{Hdt}\left(\frac{1+\alpha_H}{1+\alpha_B}\right)\right] \\ &- \frac{(1+\alpha_H)^2}{\alpha}\frac{\bar{\rho}_m + \bar{p}_m}{M^2H^2} \end{aligned} \tag{4.20}$$

In order to avoid the instabilities we require the kinetic coefficient to be positive $\alpha = \alpha_K + 6\alpha_B^2 > 0$

Vector mode: Are given in a parametric form $N_i = N_V^i$ (known as the transverse components of the shift vector) their partial derivatives are zero $\partial_i N_V^i$ exploiting this in a quadratic action for vector modes we get the transverse part of the momentum constraint outputs $\frac{\nabla^2}{2}N_i^V = \frac{a^2}{M^2}T_{0i}$ which is the transverse projection of the matter stress-energy flux.

Tensor mode: In unitary gauge, we define the evolution equation for tensor mode which correspond to Eq. (2.82) to be expressed by

$$\ddot{h}_{ij} + (3+\alpha_M)H\dot{h}_{ij} - (1+\alpha_T)\frac{\nabla^2}{a^2}h_{ij} = \frac{2}{M^2}^{(tensor)}\left(T_{ij} - \frac{1}{3}T\delta_{ij}\right) \tag{4.21}$$

In this case the transverse-traceless projection of the anisotropic matter stress-tensor is denoted by ${}^{(tensor)}\left(T_{ij}-\frac{1}{3}T\delta_{ij}\right)$, the square of the graviton propagation speed is given by

$$c_T^2 \equiv 1+\alpha_T = \frac{\mathcal{G}^*}{\mathcal{A}_K} \tag{4.22}$$

And we also introduced the dimensionless mass evolution rate function $\alpha_M \equiv \frac{1}{H}\frac{t}{dt}\ln M^2$. Combining all information provided above the generalized action form of Eq. (4.11) which obeys Eq. (4.13) conditions, evaluated at second order can be express in term of five-free background equations ($\alpha_B, \alpha_H, \alpha_K, \alpha_M$ and α_T which we will describe below) as follows

$$\begin{aligned} S &= \int d^4x\, a^3 \frac{M^2}{2}\Bigg[\delta K_{ij}\delta K^{ij} - \delta K^2 + (1+\alpha_T)\left(R\frac{\delta\sqrt{h}}{a^3} - \delta_2 R\right) \\ &+ \alpha_K H^2 \delta N^2 + 4\alpha_B H \delta K \delta N + (1+\alpha_H) R \delta N\Bigg] \end{aligned} \tag{4.23}$$

Where perturbations evaluated at second order are denoted by δ_2

4.2 Unified Dark-Energy

The effective field theory EFT [42, 63, 123] issues a efficient approach to parametrize our ignorance about fundamental physics, without any commitment to a specific model. In unitary gauge, the action given by Eq. (4.23) in conformal time can be re-written as follows

$$\begin{aligned} S &= \frac{1}{2\kappa^2}\int d^4x\sqrt{-g}\Bigg\{[1+\Omega(\eta)]\,{}^{(4)}R + 2\Lambda(\eta) - a^2 c(\eta)\delta g^{00} + M_2^4(\eta)(a^2\delta g^{00})^2 \\ &- a^2\bar{M}_1^3(\eta)\delta g^{00}\delta K^{\mu}{}_{\mu} - \bar{M}_2^2(\eta)(\delta K^{\mu}{}_{\mu})^2 - \bar{M}_3^2(\eta)\delta K^{\mu}{}_{\nu}\delta K^{\nu}{}_{\mu} + a^2\hat{M}^2(\eta)\delta g^{00}\delta R \\ &+ m_2^2(\eta)(g^{\mu\nu}+n^\mu n^\nu)\partial_\mu(a^2 g^{00})\partial_\nu(a^2 g^{00})\Bigg\} + S_m[\psi_m, g_{\mu\nu}] \end{aligned} \tag{4.24}$$

Here $\kappa^2 \equiv 8\pi G = M_{\rm pl}^{-2}$ is the bare reduced Planck mass, with gravitational constant G and S_m is the matter part of the action[3]. Its easy to see that the action in Eq. (4.24) is dependent on functions $(\Omega, c, \Lambda, M_2^4, \bar{M}_1^3, \bar{M}_2^4, \bar{M}_3^2, \hat{M}^2, m_2^2)$ and all this functions depends on time. Moreover, this provide a complete way to characterize the linear

[3]matter - include fluids components such as, baryons, neutrinos, radiation and dark matter

perturbations and background evolution of sizeable class of scalar-tensor theories. A particular sub-class are Horndeski theories which in recent years have attracted sizable amount of attention, which include several theories of interest i.e., Quintessence [207, 245], k-essence [10, 12], Brans-Dicke models [53], covariant galileons [78, 79], Gauss-Bonnet couplings [107, 181] and $f(R)$ and $f(G)$ gravity [58, 59]. However, in this work we consider the formalization developed by [28] describing the background contributions and linear perturbation theory that corresponds to Horndeski theories. In this formalism, the linear perturbations are determined by the background contribution UDE energy-density parameter and five dimensionless functions of time - this certainly holds distinct physical properties of the UDE.

- **The Kineticity** α_K : This characterize the kinetic energy of the scalar field which instantly can be extracted out from the action. Moreover, in large scale this results into a clustering of the dark energy component.

- **The Braiding** α_B : In small scales, influenced by the mixology of the interaction of the metric and scalar field of the kinetic contributions of the fields results into clustering of dark energy components.

- **(effective) mass evolution-rate parameter** α_M : Characterize the evolution gravitational coupling which yields the relation between the two Bardeen potentials Φ and Ψ dubbed as gravitational slip. The parameter is expressed by

$$\alpha_M = \frac{d\ln M^2}{d\ln a} \equiv \frac{2M'}{\mathcal{H}M} \tag{4.25}$$

  governing the rate of evolution of M - effective Planck mass from action in Eq. (4.24) is denoted by $M^2 = \kappa^{-2}(\Omega + \bar{M}_2^2)$

- **Tensor speed excess** α_T : In context of clustering of the dark energy component this provide the deviation of the gravitational wave speed and the speed of light contributing in the form of effective anisotropic stress.

- **Beyond-Horndeski parameter** α_H : On small scales clustering of dark energy and the effective anisotropic stress are influenced by by velocity fields and the evolution rate of the Bardeen potentials.

This parameters α_i are related to EFT functions through the following relation :

$$\alpha_K = \frac{c+4M_2^4}{\mathcal{H}^2(\Omega+\bar{M}_2^2)}, \quad \alpha_B = \frac{\mathcal{H}\Omega' + \bar{M}_2^3}{2\mathcal{H}(\Omega+\bar{M}_2^2)}, \quad \alpha_M = \frac{\Omega' + (\bar{M}_2^2)'}{\Omega+\bar{M}_2^2} \tag{4.26}$$

$$\alpha_T = -\frac{\bar{M}_2^2}{\Omega+\bar{M}_2^2}, \qquad \alpha_H = \frac{\hat{M}^2+\bar{M}_2^2}{\Omega+\bar{M}_2^2} \tag{4.27}$$

It is conceivable to consider MG not founded on a particular Lagrangian by determining a parameterization of the expansion of a FLRW background and the free-functions α_i. One can give a general parametrization relating the UDE energy-density parameter and the five free-function (this was firstly proposed by [28]) as follows

$$\alpha_i = \Omega_x \alpha_{i0} \equiv (1-\Omega_m)\alpha_{i0}, \quad \alpha_{i0} = \text{constant} \tag{4.28}$$

It's worth mentioning the early-universe modification of gravity is not encompassed, due to proportionality of UDE energy-density to the free-functions. Moreover, this ensures that there is no alterations on high-redshift phenomenons such as cosmic microwave background. We also make a note that If one set all free-function α_i to zero we recover GR.

Chapter 5

Probing beyond-Horndeski gravity on horizon scales

In this topic we explore the well-grounded models of DE—given a lack of fundamental understand of the DE, the alternative might be the an idea that DE is not real, with the exception that the relative weakening of gravity at late-time is the key factor for the acceleration[1]. In particular, we look into the so-called 'Horndeski theories' and their extensions dubbed 'beyond-Horndeski gravity', as the satisfactory alternative to concordance model Λ. The beyond-Horndeski gravity are characterized by the scalar field ϕ—which introduces the degree of freedom in addition to the GR tensor modes—which could result by minimizing the symmetry of the theories. This have recently gained exponential interest; e.g. of this method is the effective field theory of inflation EFT and unified dark energy UDE [19, 60, 68, 70, 85, 108, 134, 143, 149, 190, 198, 216, 218] presented in chapter. 4. Furthermore, the UDE paradigm is constructed from beyond the scope of the Horndeski theory, now suppose that UDE model seeks to combine—in a single description—a broad spectrum of the well-grounded existing models, such as the quintessence, k-essence [10, 76] models, the scalar-tensor theories and their Horndeski extensions; the $f(R)$ gravity and the Horava-Lifshitz theories [37, 38, 137], respectively[2]. This method provide the unified framework of cosmological perturbations about a FLRW Universe, at linear order. Most importantly however, the description of the EFT or UDE provides a means for a generalized approach to confront theoretical ideas with observations; the cosmological parameters of the given

[1] The breakdown of general relativity in the infrared—hence, one needs to do some modifications to general relativity GR

[2] In subsections to follow we provide the explicit Lagrangian examples of most of this theories

UDE may be probed and the implication for various models is thus inferred, rather than probing the individual models.

Moreover, the next generation of cosmological survey on very large scale structure—will extent to very large redshifts—which will also cover a sizable cosmic scale, to nearly and beyond the Hubble horizon, this could potentially provide the best information on the nature of modification of gravity and dark energy—thus this will be used as a powerful tool to test GR. Nevertheless, for this to be carried out one needs to consider correction for relativistic effects which surface naturally in the overdensity of galaxies and convergence [15, 20, 23, 45, 46, 48, 50, 62, 89–92, 94, 97, 208] in the redshift space. In the past, up-until recently, the relativistic effects where ignored or disregarded—however the relativistic effects become more significant on the same reshifts and scales which will be the reach of the next generation of cosmological surveys. Therefore on large scale evaluation of the relativistic corrections and their imprint will be very important in future.

We start by a concise review of the scalar-tensor descriptive of the interacting dark energy in section. 5.1. In section. 5.2, we introduced the unified dark energy background and perturbations. The full relativistic expressions of galaxy number count and convergence are given in section. 5.3. In section. 5.4, we provide two ways to compute the power spectrum in beyond-Horndeski theories. In section. 5.5, we numerically test UDE background and perturbations evolution equations. Finally we conclude in section. 5.6.

5.1 Scalar-tensor descriptive of the interacting DE

In this section we outline few among several scalar-tensor theories which have been vigorously studied in the past—in the context of DE—here we provide their explicit standard action and reformulate this into general form shown by (2.13). In order for us to focus at the coupling of the scalar field, we need to recall the action for GR paradigm in ADM formalism which we denoted by (2.14).

5.1.1 Quintessence and k-essence models

Lets start by making available the expression for the energy-momentum tensor associated to the canonical scalar field which is given by,

$$T_{\mu\nu} = \nabla_\mu\phi\nabla_\nu\phi - \frac{1}{2}[g_{\mu\nu}g^{\rho\sigma}\nabla_\rho\phi\nabla_\sigma\phi + 2g_{\mu\nu}V(\phi)] \tag{5.1}$$

Where $V(\phi)$ is the potential which depends on scalar field. It's direct and easy to compute the action that will result in the energy-momentum tensor given in (5.1). In classical mechanics the canonical Lagrangian can be rewritten the context of the classical field theory [57] by,

$$\mathcal{L} = \frac{1}{2}\dot{\phi}^2 - \frac{1}{2}[\partial_\mu\phi\partial_\nu\phi + 2V(\phi)] \tag{5.2}$$

The above expression describes different energies, i.e., The first term coincides with kinetic energy and the terms inside the square brackets corresponds to the gradient energy plus customary potential energy respectively. Furthermore, we can rewrite the Lagrangian density as follows[3]

$$\mathcal{L} = \frac{1}{2}[g^{\mu\nu}\partial_\mu\phi\partial_\nu\phi + 2V(\phi)] \tag{5.3}$$

Henceforth, the initial scalar field action becomes,

$$S_Q = -\int d^4x\sqrt{-g}\frac{1}{2}[g^{\mu\nu}\partial_\mu\phi\partial_\nu\phi + 2V(\phi)] \tag{5.4}$$

Thus, after some algebra in ADM formalism the action yields,

$$\mathcal{L} = \mathcal{L}_{EH}(t,N) + \mathcal{L}_Q(t,N), \quad \mathcal{L}_Q(t,N) = \frac{\phi^2}{2N^2} - V(\phi(t)) \tag{5.5}$$

In the case of non-canonical kinetic energy terms,*k-essence* theories (for comprehensive description see [11, 12, 112, 119, 193]) by expressing the Lagrangian $P(X,\phi)$—in ADM formalism—can be obtained by following the similar set of steps as above which eventually yield,

$$\mathcal{L}_{k-essence}(t,N) = P\left[-\frac{\dot{\phi}^2}{2N^2}, \phi\right] \tag{5.6}$$

Note that here initially we considered the action,

$$S_{k-essence} = \int d^4x\sqrt{-g}P(X,\phi), \quad \text{with}, \quad X = \frac{1}{2}g^{\mu\nu}\partial_\mu\phi\partial_\nu\phi \tag{5.7}$$

Here we denote P as an arbitrary function which depends on both X and ϕ

[3]Note that we have considered the fact that the Minkowski metric $\eta_{\mu\nu}$ is diagonal—$\eta_{\mu\nu}$=diagonal(-1,1,1,1)—the local frame was constructed in addition to this.

5.1.2 $f(^4R)$gravity

In this subsection we describe the action and Lagrangian density of nonlinear $f(^4R)$ gravitational models which we will use hereinafter to reproduce known equations. Starting from the action[75, 99],

$$S_{f(R)} = \int d^4x\sqrt{-g}f(^4R) \tag{5.8}$$

We then define the following; $f(^4R) = f(\phi) - f_\phi(\phi)(-^4R+\phi) \equiv f(R)$, making use of Eq. (5.8) with some algebra we get the following Lagrangian

$$\mathcal{L}_{f(R)} = f(\phi) + f_\phi(\phi)(^4R-\phi) \tag{5.9}$$

The above Lagrangian is equivalent to $f(^4R)$ Lagrangian. Henceforth, to avoid confusion/s in the notation, subscript Φ and X[4] denotes the derivatives with respect to ϕ and X respectively[5] Provided the property from [119](which state that $f(^4R^4R) \neq 0$) and making use of the Gauss-Codazzi expression given in section. 2.1 by Eq. 2.12 we can rewrite the above Lagrangian in ADM formalism as follows

$$\mathcal{L}_{f(R)} = f_\phi(R + K_{\mu\nu}K^{\mu\nu} - K^2) + 2f_{\phi\phi}K\sqrt{-X} + f(\phi) - \phi f_\phi \tag{5.10}$$

5.1.3 Horndeski gravity

In 1974 [138], Horndeski provided a derivation of the action of a large class of scalar-tensor theories with second-order equations of motion, proven to be equivalent to generalized Galileons [80, 150]—the importance of this being that it encompass all DE or MG theories sub-classes we introduced above.Then the Horndeski Lagrangian is given as

$$\mathcal{L}_H = \mathcal{L}_2 + \mathcal{L}_3 + \mathcal{L}_4 + \mathcal{L}_5 \tag{5.11}$$

[4]This will be useful in the very next subsection

[5]For example, $f_\phi \equiv \frac{\partial f}{\partial \phi}$ and $f_X \equiv \frac{\partial f}{\partial X}$

Where arbitrary linear Lagrangian $\mathcal{L}_n$ are given by

$$\begin{aligned}
\mathcal{L}_2 &= G_2(\phi, X) \\
\mathcal{L}_3 &= G_3(\phi, X)\Box\phi \\
\mathcal{L}_4 &= G_4(\phi, X)^4 R + \partial_X G_4(\phi, X)\delta^{\mu\nu}_{\alpha\beta}\nabla^\alpha_\mu\phi\nabla^\beta_\nu\phi \\
\mathcal{L}_5 &= G_5(\phi, X)G_{\mu\nu}\nabla^{\mu\nu}\phi - \frac{1}{6}\partial_X G_5(\phi, X)\delta^{\mu\nu\rho}_{\alpha\beta\gamma}\nabla^\alpha_\mu\phi\nabla^\beta_\nu\phi\nabla^\gamma_\rho\phi
\end{aligned} \tag{5.12}$$

Where $X = -\frac{1}{2}(\nabla\phi)^2$ and $G_i(\phi, X)$ are arbitrary function and we need to add to this that $\delta^{\mu\nu}_{\alpha\beta} = 2!\delta^\mu_{[\alpha}\delta^\nu_{\beta]}$ and $\delta^{\mu\nu\rho}_{\alpha\beta\gamma} = 3!\delta^\mu_{[\alpha}\delta^\nu_\beta\delta^\rho_{\gamma]}$. Thus, in ADM formalism the Horndeski Lagrangian $\mathcal{L}_H$ reads

$$\mathcal{L}_{H,A} = \mathcal{L}_{2,A} + \mathcal{L}_{3,A} + \mathcal{L}_{4,A} + \mathcal{L}_{5,A} \tag{5.13}$$

Where $\mathcal{L}_{n,A}$ are defined as follows

$$\begin{aligned}
\mathcal{L}_{2,A} &= M_2(\phi, X) \\
\mathcal{L}_{3,A} &= M_3(\phi, X)K \\
\mathcal{L}_{4,A} &= M_4(\phi, X)R + (2X\partial_X M_4 - M_4)(K^2 - K_{\mu\nu}K^{\mu\nu}) \\
\mathcal{L}_{5,A} &= M_5(\phi, X)G_{\mu\nu}K^{\mu\nu} - \frac{1}{3}X\partial_X M_5(K^3 - KK_{\mu\nu}K^{\mu\nu} + 2K_{\mu\nu}K^{\mu\alpha}K^\nu_\alpha)
\end{aligned} \tag{5.14}$$

Where functions M_n are given by

$$M_2 = G_2 - \sqrt{-X}\int\frac{\partial_\phi G_3}{2\sqrt{-x}}dX, \quad M_3 = -\int\partial_X G_3\sqrt{-X}dX - 2\sqrt{-X}\partial_\phi G_4 \tag{5.15}$$

$$M_4 = G_4 + \sqrt{-X}\int\frac{\partial_\phi G_5}{4\sqrt{-X}}dX, \quad M_5 = -\int\partial_X G_5\sqrt{-X}dX \tag{5.16}$$

The detailed derivation of this work is comprehensive given by [116].

5.1.4 Beyond-Horndeski gravity

In general higher-derivative theories have extra degree of freedom and usually plagued by instabilities—Horndeski theories[6]—suppress ghost-like instabilities also known as Ostrogradski's instability by requiring second-order Euler-Lagrange equations which can be obtained from the Lagrangian density given above. However, for some reasons it is conceivable to extend the Horndeski Lagrangians presented above without encountering

[6]This does not introduce any new degree of freedom, but not necessarily stable.

ghost-like Ostrogradski instabilities. In ADM formalism, the beyond-Horndeski theory provided by [118] the actions reads

$$S_{BH} = \int d^4x\sqrt{-g}(\mathcal{L}_2+\mathcal{L}_3+\mathcal{L}_4+\mathcal{L}_5) \tag{5.17}$$

Where

$$\begin{aligned}
\mathcal{L}_2 &= A_2(t,N) \\
\mathcal{L}_3 &= A_3(t,N)K \\
\mathcal{L}_4 &= A_4(t,N)(K^2-K^{\mu\nu}K_{\mu\nu})+B_4(t,N)R \\
\mathcal{L}_5 &= A_5(t,N)(K^3-3KK^{\mu\nu}K_{\mu\nu}+2K^{\mu\alpha}K_{\mu\nu}K^{\nu}_{\alpha})+B_5(t,N)K^{\mu\nu}\left(R_{\mu\nu}-\frac{1}{2}h_{\mu\nu}R\right)
\end{aligned} \tag{5.18}$$

Where A_n and B_n (n=2,3,4,5) are arbitrary functions that depends on t and N

5.2 The Unified Dark Energy Model

As proposed by Gleyzes et al. [119] in this section we provide the UDE model; Our equations are rewritten in conformal coordinates—assuming a late-time universe dominated by matter and UDE only—the subsections below are supplementary to work introduced in subsection. 2.2.6.

5.2.1 The background equations

In this subsection we provide the gravitational field equations for background. We begin by defining the UDE energy density and pressure, respectively as follows

$$\bar{\rho}_x \equiv 3a^{-2}M^2\mathcal{H}^2-\bar{\rho}_m, \quad \bar{p}_x \equiv -\frac{M^2}{a^2}(2\mathcal{H}'+\mathcal{H}^2)-\bar{p}_m \tag{5.19}$$

With M is an effective Planck mass; a prime denote derivatives with respect to conformal time (with $A=m,x$), $\mathcal{H}=a'/a$ is the comoving Hubble parameter . Matter and UDE energy density conservation equations are given by

$$\bar{\rho}'_m+3\mathcal{H}(1+w_m)\bar{\rho}_m=0, \quad \bar{\rho}'_x+3\mathcal{H}(1+w_{x,\text{eff}})\bar{\rho}_x=0 \tag{5.20}$$

Where $w_A = \bar{p}/\bar{\rho}_A$ is the equation of state parameter of A, $\Omega_A = \bar{\rho}_x/\bar{\rho}$ is the energy density parameter, with $\bar{\rho}$ being the total background energy density and with

$$w_{x,\text{eff}} = w_x - \frac{\alpha_M}{(3\Omega_x)} \tag{5.21}$$

Describing an effective UDE equation of state parameter; where $\alpha_M \equiv 2M'/(\mathcal{H}M)$ is the mass evolution rate parameter. We also have the pressure conservation equation which is given by

$$\bar{p}'_x = -\bar{p}'_m - 3a^{-2}M^2\mathcal{H}^3[(1+w)(3c_a^2 - \alpha_M) + \alpha_M] \tag{5.22}$$

Where w is the total equation of state parameter and c_a^2 is the total (squared) adiabatic sound speed which are respectively given by

$$w = \sum_A \Omega_A w_A, \quad c_a^2 = \frac{1}{1+w}\sum_A \Omega_A(1+w_A)c_{aA}^2 \tag{5.23}$$

Moreover, the evolution of UDE equation of state parameter is then given by

$$w'_x = -3\mathcal{H}(1+w_{x,\text{eff}})(c_{ax}^2 - w_x) \tag{5.24}$$

with $c_{aA}^2 \equiv \bar{p}'_A/\bar{\rho}'_A$ is the square of the adiabatic sound speed, its easy to show that if we set $A = x$, and divide Eq. (5.22) by Eq. (5.20) then the following definition yields

$$c_{ax}^2 = s_m + \frac{\alpha_M + (1+w)(3c_a^2 - \alpha_M)}{3\Omega_x(1+w_{x,\text{eff}})} \tag{5.25}$$

Where we denote the parameter $s_m \equiv \bar{p}'_m/\bar{\rho}'_x$

5.2.2 The perturbations equations

In this subsection we outline the applicable perturbations equations—we provide the specific constraints and the evolution equations. Here we adopt the perturbed FLRW metric Eq. (2.99) and the effective Poisson equation is given by

$$\nabla^2\Phi = \frac{3}{2}\mathcal{H}^2(\sum_A \Omega_A\Delta_A - \alpha_M\mathcal{H}V_A), \qquad \Delta_A = \delta_A + \frac{\bar{\rho}'_A}{\bar{\rho}_A} \tag{5.26}$$

Where $\delta_A = \delta\rho_A/\bar{\rho}_A$ is the energy density contrast for A, with V_A being the gauge-invariant comoving velocity potential and Δ_A is the comoving energy density[7]. The spatial metric potential evolves as follows

$$\Phi - \mathcal{H}\Psi = -\frac{3}{2}\mathcal{H}^2 \sum_A \Omega_A \frac{q_A}{\bar{\rho}_A}, \quad q_A = (\bar{\rho}_A + \bar{p}_A)V_A \tag{5.27}$$

Here $q_A = a^{-1}q_A^{phys}$ is the comoving momentum density for species A; the superscript *phys* (henceforth) denotes the physical component—as given by [119] i.e. defined with respect to physical time. The metric potentials are constraint by

$$\Phi + \Psi = 3\mathcal{H}^2 \sum_A \Omega_A \frac{\sigma_A}{\bar{\rho}_A} \tag{5.28}$$

Where σ_A is the comoving anisotropic stress potential for species A.

The perturbed energy-momentum tensor for multiple components is given by

$$\delta T_A^{\mu\nu} = (\delta\rho_A + \delta p_A)\bar{u}_A^\mu \bar{u}_A^\nu + (\bar{\rho}_A + \bar{p}_A)(\delta u_A^\mu \bar{u}_A^\nu + \bar{u}_A^\mu \delta u_A^\nu) + \delta p_A g^{\mu\nu} + \bar{p}_A g^{\mu\nu} \tag{5.29}$$

Where we define the 4-velocity as (shown by [94]) $u_A^\mu = a^{-1}(1-\Phi, \partial^i V_A)$ and with $\delta p_A, \delta g^{\mu\nu}$ and δu_A^μ are perturbed pressure, metric tensor and 4-velocity, respectively. The leads to the energy-momentum conservation to be

$$\sum_A T^{\mu\nu}_{,\mu} = 0 = \delta T^{\mu\nu}_{,\mu} \tag{5.30}$$

Therefore, given Eq. (5.30) the matter comoving velocity potential and comoving density, respectively, evolve in time according to the equations given by

$$V_m' + \mathcal{H}V_m = \frac{2k^2\sigma_m}{3(1+w_m)\bar{\rho}_m} - \frac{c_{sm}^2}{1+w_m}\Delta_m + \Psi \tag{5.31}$$

$$\begin{aligned} \Delta_m' - 3w_m\mathcal{H}\Delta_m &= \frac{9}{2}\mathcal{H}^2(1+w_m)\sum_A (1+w_A)(V_m - V_A) \\ &+ (1+w_m)k^2 V_m - 2\mathcal{H}k^2\frac{\sigma_m}{\bar{\rho}_m} \end{aligned} \tag{5.32}$$

[7]Note that we take care to use the gauge-invariant comoving density Δ_A, in order to simplify Poisson equation and to define bias properly; moreover this helps avoid any large-scale unphysical artefacts, see e.g. [82].)

where c_{sm}^2 is the matter physical sound speed. Similarly, the UDE comoving velocity potential evolves by

$$\begin{aligned} V_x' + \mathcal{H}V_x &= \frac{2k^2\sigma_x}{3(1+w_x)\bar{\rho}_x} - \frac{c_{sx}^2}{1+w_x}\Delta_x + \Psi \\ &- \frac{\alpha_M \mathcal{H}}{\Omega_x(1+w_x)}\left[V_x - \sum_A \Omega_A(1+w_A)V_A\right] \end{aligned} \tag{5.33}$$

Here we denote c_{sx}^2 is the UDE physical sound speed, given by [28, 117–119, 171]

$$\begin{aligned} c_{sx}^2 &= -2\frac{(1+\alpha_B)^2}{\alpha}\left[1+\alpha_T - \frac{1+\alpha_H}{1+\alpha_B}\left(2+\alpha_M - \frac{\mathcal{H}'}{\mathcal{H}^2}\right) - \frac{1}{\mathcal{H}}\left(\frac{1+\alpha_H}{1+\alpha_B}\right)'\right] \\ &+ \frac{(1+\alpha_H)^2}{\alpha}\frac{\bar{\rho}_m + \bar{p}_m}{a^{-2}M^2\mathcal{H}^2} \end{aligned} \tag{5.34}$$

Where the various α_i are provided in chapter. 4 (see [28, 117–119, 171, 217] for more details)

The evolution of UDE comoving density given by

$$\begin{aligned} \Delta_x' - 3w_x\mathcal{H}\Delta_x &= \frac{9}{2}\mathcal{H}^2(1+w_x)\sum_A(1+w_A)(V_x - V_A) + (1+w_x)k^2V_m - 2\mathcal{H}k^2\frac{\sigma_x}{\bar{\rho}_x} \\ &+ \frac{\alpha_M\mathcal{H}}{\Omega_x}\left\{V_x' - \Delta_x + \left[\frac{\alpha_M'}{\alpha_M} - \frac{1}{2}(1+9w-2\alpha_M)\mathcal{H}\right]V_x\right. \\ &+ \left.\sum_A \Omega_A\left[\Delta_A - \frac{\bar{\rho}_A'}{\bar{\rho}_A}V_A - 3\mathcal{H}(1+w_A)V_A\right]\right\} \end{aligned} \tag{5.35}$$

Considering the fine work by [216, 217], then we can write the relation between the parameter α_B dubbed kinetic braiding, beyond-Horndeski parameter α_H and the tensor speed alteration (measuring the difference between the speed $c_T^2 = 1+\alpha_T > 0$ of gravitational waves and speed of light.) as follows

$$\alpha_B = \alpha_H\left(1 - 5\frac{\Upsilon_2}{\Upsilon_1}\right), \qquad c_T^2 = \frac{4\alpha_H^2 + (1+\alpha_H)\Upsilon_1}{(1+\alpha_B)\Upsilon_1} \equiv 1+\alpha_T \tag{5.36}$$

where cosmological constraints are placed on the parameter governing deviations from Newton's law, $\Upsilon_1 = -0.11^{+0.93}_{-0.67}$, and the parameter governing light bending, $\Upsilon_2 = -0.22^{+1.22}_{-1.19}$. Clearly we see that, if $\alpha_H = 0$, then $\alpha_B = 0$ and $c_T^2 = 1$; thus implying that the we recover Horndeski gravity when $\alpha_H = 0$—as well as general relativity—restricts gravitational waves to propagate with the speed of light. However,

in beyond-Horndeski gravity ($\alpha_H \neq 0$), the gravitational waves can propagate either faster ($\alpha_T > 0$) or slower ($\alpha_T < 0$) than light.

In addition, we also reintroduce the following expression

$$\alpha_i = \alpha_{i0}\Omega_x \tag{5.37}$$

This tells us that the free parameters are directly proportional to UDE energy density with some constant. Thus, equations (5.19)–(5.37) establish the applicable background and perturbations equations. By comparing the given equations in this section with the work by e.g. [94], we see that the UDE essentially corresponds to an interacting DE scenario in which the total energy-momentum tensor is not conserved (there are no α_M terms in all the matter evolution equations, unlike those for UDE; thus α_M induces a self, non-conservative interaction in UDE). The procedure as to how we strictly obtained the above evolution's is detailed in Appendix. D.

5.3 The relativistic effect in galaxy number count and convergence

In order to adequately account for the pure number counts surveys, perfumed at a fixed luminosity which is cut-off within a varying volume, the observed overdensity [48, 62, 144, 145, 174, 249, 250]—incorporating all relativistic effects/corrections—along the direction of observation $\hat{\mathbf{n}}$ (where $\hat{\mathbf{n}}$ is the direction at which the photon is propagating) at redshift z is given by

$$\Delta(z,\hat{\mathbf{n}}) = \Delta^{\mathrm{st}}(z,\hat{\mathbf{n}}) + \Delta^{\mathrm{v}}(z,\hat{\mathbf{n}}) + \Delta^{\mathrm{g}}(z,\hat{\mathbf{n}}) + \Delta^{\mathrm{SW}}(z,\hat{\mathbf{n}}) + \Delta^{\mathrm{td}}(z,\hat{\mathbf{n}}) + \Delta^{\mathrm{ISW}}(z,\hat{\mathbf{n}}) \tag{5.38}$$

Where the terms $\Delta^i(z,\hat{\mathbf{n}})$ are defined as follows

$$\Delta^{\rm st}(z,\hat{\mathbf{n}}) = b\cdot\Delta_m - \frac{1}{\mathcal{H}}\partial_r(\mathbf{V}\cdot\hat{\mathbf{n}}) \tag{5.39}$$

$$\Delta^{\rm v}(z,\hat{\mathbf{n}}) = \frac{1}{\mathcal{H}}\mathbf{V}'\cdot\hat{\mathbf{n}} - \left(\frac{\mathcal{H}'}{\mathcal{H}^2}+\frac{2}{r_s\mathcal{H}}-1\right)\mathbf{V}\cdot\hat{\mathbf{n}} + \frac{1}{\mathcal{H}}\partial_r\Psi \tag{5.40}$$

$$\Delta^{\rm g}(z,\hat{\mathbf{n}}) = -\frac{1}{r_s}\int_0^{r_s} dr\frac{r_s-r}{r}\nabla_\perp^2(\Phi+\Psi) \tag{5.41}$$

$$\Delta^{\rm SW}(z,\hat{\mathbf{n}}) = \left(1+\frac{\mathcal{H}'}{\mathcal{H}^2}+\frac{2}{r_s\mathcal{H}}\right)\Psi - 2\Phi + \frac{1}{\mathcal{H}}\Phi' - 3\mathcal{H}V \tag{5.42}$$

$$\Delta^{\rm td}(z,\hat{\mathbf{n}}) = \frac{1}{r_s}\int_0^{r_s} dr(\Phi+\Psi) \tag{5.43}$$

$$\Delta^{\rm ISW}(z,\hat{\mathbf{n}}) = \left(\frac{\mathcal{H}'}{\mathcal{H}^2}+\frac{2}{r_s\mathcal{H}}\right)\int_0^{r_s}(\Phi'+\Psi') \tag{5.44}$$

Where Δ_m and $\mathbf{V}$ are defined as the gauge invariant comoving density and velocity potential,respectively—This density is the one utilized in Poisson equation [32, 238] and it can be related to galaxy comoving density via the linear galaxy bias b (see [54, 82] which is given by $\Delta_g = b\Delta_m$). Furthermore, the line-of-sight component of the peculiar velocity is denoted by $\mathbf{V}\cdot\hat{\mathbf{n}}$ (which in Fourier space it yields $-i\mathbf{k}V(z,k)\cdot\hat{\mathbf{n}}$). Moving on, $r_s = r(z_s)$ is the background comoving radial distance at source redshift z_s and $\nabla_\perp^2 = r^2(\nabla^2 - \partial_r^2 - 2r^{-1}\partial_r)$ is the angular part of the Laplacian. Throughout this thesis we've neglected magnification and evolution of bias ($s = 0 = f_{evol}$).

The first contribution is the sum of density and redshift distortion dubbed as standard contribution $\Delta^{\rm st}(z,\hat{\mathbf{n}})$, second contribution is Doppler lensing $\Delta^{\rm v}(z,\hat{\mathbf{n}})$ and the third contribution is gravitational lensing $\Delta^{\rm g}(z,\hat{\mathbf{n}})$. The last three contribution are directly dependent on the two Bardeen potentials Φ and Ψ they know as Sachs-Wolfe effect $\Delta^{\rm SW}(z,\hat{\mathbf{n}})$, Integrated Sachs-Wolfe effect $\Delta^{\rm ISW}(z,\hat{\mathbf{n}})$ and Shapiro time-delay $\Delta^{\rm td}(z,\hat{\mathbf{n}})$. While standard contribution terms are proportional to Bardeen potentials. Standard contributions are suppressed by $(\frac{\mathcal{H}}{k})^2$ in Fourier space and gravitational lensing term and Doppler lensing terms are suppressed by $(\frac{\mathcal{H}}{k})$. The standard contribution terms, gravitational lensing term and Doppler lensing terms they are not important in scales much smaller than the horizon ($k \gg \mathcal{H}$), but they are much more important on large scale. In addition, the slope of gravitational potential is proportional to velocity terms shown in Table. 5.1, they both suppressed by $(\frac{\mathcal{H}}{k})$. This term has precise order of magnitude as the velocity terms, this mainly due to the slope of Ψ. In gravitational

Quantity	Eq	Contribution	Scale	b dependence
$\Delta^{\rm st}(z,\hat{\mathbf{n}})$	(5.39)	Intrinsic clustering + RSD	$\left(\frac{k}{\mathcal{H}}\right)^2\Psi$	b
$\Delta^{\rm v}(z,\hat{\mathbf{n}})$, $\kappa^{\rm v}(z,\hat{\mathbf{n}})$	(5.40),(5.48)	Doppler lensing	$\left(\frac{k}{\mathcal{H}}\right)\Psi$	-
$\Delta^{\rm g}(z,\hat{\mathbf{n}})$, $\kappa^{\rm g}(z,\hat{\mathbf{n}})$	(5.41),(5.49)	Gravitational lensing	$\left(\frac{k}{\mathcal{H}}\right)\Psi$	-
$\Delta^{\rm SW}(z,\hat{\mathbf{n}})$, $\kappa^{\rm SW}(z,\hat{\mathbf{n}})$	(5.42),(5.50)	Sachs Wolfe	Ψ	-
$\Delta^{\rm td}(z,\hat{\mathbf{n}})$, $\kappa^{\rm td}(z,\hat{\mathbf{n}})$	(5.43),(5.51)	Shapiro time-delay	Ψ	-
$\Delta^{\rm ISW}(z,\hat{\mathbf{n}})$, $\kappa^{\rm ISW}(z,\hat{\mathbf{n}})$	(5.44),(5.52)	Integrated Sachs Wolfe	Ψ	-

Table 5.1 Summary of relativistic effects and their dependence on scale and bias—which contribute on both galaxy overdensity and convergence.

theories that obey Euler equation (galaxies follows the geodesics)

$$\partial_r\Psi + \mathbf{V}'\cdot\hat{\mathbf{n}} + \mathcal{H}\mathbf{V}\cdot\hat{\mathbf{n}} = 0 \tag{5.45}$$

The expression for $\Delta^{\rm v}(z,\hat{\mathbf{n}})$ in eq. (5.40) simplifies to

$$\Delta^{\rm v}(z,\hat{\mathbf{n}}) = -\left(\frac{\mathcal{H}'}{\mathcal{H}^2} + \frac{2}{\bar{r}_s\mathcal{H}}\right)\mathbf{V}\cdot\hat{\mathbf{n}} \tag{5.46}$$

All terms integrated along the line of sight are negligible on small scale. The relativistic effects also affects convergence, this involve The standard gravitational lensing term, Doppler lensing term, the integrated Sachs-Wolfe, Shapiro time-delay and the Sachs-Wolfe, the full expression can be obtained from [16, 30, 44].

$$\kappa(z,\hat{\mathbf{n}}) = \kappa^{\rm v}(z,\hat{\mathbf{n}}) + \kappa^{\rm g}(z,\hat{\mathbf{n}}) + \kappa^{\rm td}(z,\hat{\mathbf{n}}) + \kappa^{\rm ISW}(z,\hat{\mathbf{n}}) + \kappa^{\rm SW}(z,\hat{\mathbf{n}}) \tag{5.47}$$

Where the terms $\kappa^i(z,\hat{\mathbf{n}})$ are defined as follows

$$\kappa^{\rm v}(z,\hat{\mathbf{n}}) = \left(1-\frac{1}{r_s\mathcal{H}}\right)\mathbf{V}\cdot\hat{\mathbf{n}} \tag{5.48}$$

$$\kappa^{\rm g}(z,\hat{\mathbf{n}}) = \frac{1}{2r_s}\int_0^{\bar{r}_s} dr\frac{r_s-r}{\bar{r}}\nabla_\perp^2(\Phi+\Psi) \tag{5.49}$$

$$\kappa^{\rm SW}(z,\hat{\mathbf{n}}) = \left(2-\frac{1}{r_s\mathcal{H}}\right)\Psi \tag{5.50}$$

$$\kappa^{\rm td}(z,\hat{\mathbf{n}}) = -\frac{2}{r_s}\int_0^{r_s} dr\Psi \tag{5.51}$$

$$\kappa^{\rm ISW}(z,\hat{\mathbf{n}}) = \left(1-\frac{1}{r_s\mathcal{H}}\right)\int_0^{r_s} dr(\Phi'+\Psi') \tag{5.52}$$

If the galaxy and observer are moving respectively, the galaxy appears further away or closer in redshift space, this reflect Doppler term $\kappa^{\rm v}(z,\hat{\mathbf{n}})$. To firmly decide whether the galaxy demagnified or magnified is determined by the sign of this contribution which depends on the direction of velocities and the prefactor sign. Gravitational lensing term shows how overdense regions situated between the galaxy and the observer magnify the galaxy and change consequently its size and its luminosity. We need to make a note that convergence is not observable on its own in the relativistic scenario, since its gauge dependent quantity (see [48] for more comprehensive details).

5.4 Correlation function in beyond-Horndeski

In this section we evaluate modification of gravity or DE in the context of the beyond-Horndeski theories by altering the observed overdesity and convergence power spectrum; accounting for all relativistic contributions. In particular, we look into two well grounded statistical measurements that are suitable for large scale regime; the angular power spectrum and two point correlation function (2PCF)—note that in subsection. 5.4.2 we only consider the cross-correlation of dominant contributions. In particular, we compute the quantity $\xi^{\Delta^{\rm st}\kappa^{\rm v}}$—which is the cross-correlation between the number-count and convergence.

5.4.1 The number count-convergence angular power spectra

We consider the observed number-count overdensity (5.38), for galaxy surveys; we expand the number-count overdnesity in spherical multipoles, given by

$$\Delta(z,\hat{\mathbf{n}}) = \sum_{lm} a_{lm}(z) Y_{lm}(\hat{\mathbf{n}}), \quad a_{lm}(z) = \int d\Omega_{\hat{\mathbf{n}}} Y^*_{lm}(\hat{\mathbf{n}}) \Delta(z,\hat{\mathbf{n}}) \tag{5.53}$$

where Y_{lm} are the spherical harmonics and a_{lm} are the multipole expansion coefficients, with the star or asterisk denoting complex conjugation. We compute the angular power spectrum observed at a source redshift z_s by

$$C_l = \langle a_{lm}(z_s) a_{lm}(z'_s) \rangle \tag{5.54}$$

Note that the primes on redshift refer to the object where the number-count is estimated. Henceforth, we will embrace the following convention—at which the density, velocity and two Bardeen's potentials are decomposed by

$$\Delta_m(z,\hat{\mathbf{n}}) = \int \frac{d^3\mathbf{k}}{(2\pi)^3} e^{-i\mathbf{k}\cdot\mathbf{x}} \Delta_m(z,\mathbf{k}), \tag{5.55}$$

$$\Psi(z,\hat{\mathbf{n}}) = \int \frac{d^3\mathbf{k}}{(2\pi)^3} e^{-i\mathbf{k}\cdot\mathbf{x}} \Psi(z,\mathbf{k}), \tag{5.56}$$

$$\mathbf{V}(z,\hat{\mathbf{n}})\cdot\hat{\mathbf{n}} = \int \frac{d^3\mathbf{k}}{(2\pi)^3} e^{-i\mathbf{k}\cdot\mathbf{x}} iV(z,\mathbf{k})(\mathbf{k}\cdot\hat{\mathbf{n}}), \tag{5.57}$$

$$\partial_r(\mathbf{V}(z,\hat{\mathbf{n}})\cdot\hat{\mathbf{n}}) = \int \frac{d^3\mathbf{k}}{(2\pi)^3} e^{-i\mathbf{k}\cdot\mathbf{x}} V(z,\mathbf{k})(\mathbf{k}\cdot\hat{\mathbf{n}})^2. \tag{5.58}$$

Where the density velocity and Bardeen's potential are related as follows

$$\Delta_m(z,\mathbf{k}) = \tilde{\Delta}_m(z,k) T(k) \Psi(\mathbf{k}), \tag{5.59}$$

$$V_m(z,\mathbf{k}) = \tilde{V}_m(z,k) T(k) \Psi(\mathbf{k}), \tag{5.60}$$

$$\Psi(z,\mathbf{k}) = \tilde{\Psi}(z,k) T(k) \Psi(\mathbf{k}). \tag{5.61}$$

We also define the initial power spectrum as follows

$$\langle \Psi(\mathbf{k}) \Psi^*(\mathbf{k}') \rangle = (2\pi)^3 \delta(\mathbf{k}+\mathbf{k}') P_{\Psi_{\rm i}}(k) \tag{5.62}$$

Applying equations. (5.55)—(5.62) into (5.54) with some algebra the total angular power spectrum yields [46, 48]

$$C_l^{\Delta\Delta}(z_s,z_s') = \frac{4}{\pi^2}\left(\frac{43}{50}\right)^2 \int dk k^2 T^2(k) P_{\Psi_\mathrm{i}}(k) |\Delta_l(z_s,k)\Delta_l(z_s',k)| \tag{5.63}$$

Where $T(k)$ is the linear transfer function that dependent on time and with

$$\begin{aligned}
\Delta_l(z_s,k) &= b(z_s)\tilde{\Delta}_m(z_s,k) - \frac{1}{\mathcal{H}}\tilde{V}_m(z_s,k) j_l''(kr_s) + \frac{1}{\mathcal{H}}\tilde{\Psi}'(z_s,k) j_l(z_s,k) \\
&- 3\mathcal{H}\tilde{V}_m(z_s,k) j_l(z_s,k) - \left(-1 - \frac{\mathcal{H}'}{\mathcal{H}^2} - \frac{2}{r_s\mathcal{H}}\right) j_l(kr_s)\tilde{\Phi}(z_s,k) \\
&- 2\tilde{\Psi}(z_s,k) j_l(z_s,k) + \int_0^{r_s} dr j_l(kr)\left[2 + \frac{r_s - r}{r} l(1+l)\right](\tilde{\Phi}+\tilde{\Psi})(z,k) \\
&+ \left(\frac{\mathcal{H}'}{\mathcal{H}^2} + \frac{2}{r_s\mathcal{H}}\right)\left[\tilde{V}(z_s,k) j_l'(kr_s) + \int_0^{r_s} dr j_l(kr)(\tilde{\Phi}+\tilde{\Psi})(z,k)\right]
\end{aligned} \tag{5.64}$$

Where j_l denote the spherical Bessel function of order l, then $j_l'(x) = \partial j_l(x)/\partial x$—where we define the argument $x = kr$; a tilde denotes division by the gravitational potential at the epoch of photon-matter decoupling by this we mean for a given parameter X this holds $\tilde{X}(z,k) \equiv X(z,k)/\Phi_d(k)$ and the gravitational potential at decoupling is then defined by

$$\Psi_d(k) = \left(\frac{43}{50}\right)\Psi_\mathrm{i}(k) T(k) \tag{5.65}$$

Here Ψ_p is the primordial gravitational potential; $\tilde{X}$ measures the growth function of the associated parameter. In a similar fashion as above one can evaluate the convergence angular power spectrum to result in

$$C_l^{\kappa\kappa}(z_s,z_s') = \frac{4}{\pi^2}\left(\frac{43}{50}\right)^2 \int dk k^2 T^2(k) P_{\Psi_\mathrm{i}} |\kappa_l(z_s,k)\kappa_l(z_s',k)| \tag{5.66}$$

With

$$\begin{aligned}
\kappa_l(z_s,k) &= \frac{1}{r_s}\int_0^{r_s} dr j_l(kr)\left[2\tilde{\Psi} + \frac{r_s - r}{2r} l(1+l)(\tilde{\Phi}+\tilde{\Psi})(z,k)\right] \\
&- \left(1 - \frac{1}{r_s\mathcal{H}}\right) j_l'(kr_s) V_m(z_s,k) + \left(2 - \frac{1}{r_s\mathcal{H}}\right)\tilde{\Phi}(z_s,k) j_l(kr_s) \\
&+ \left(1 - \frac{1}{r_s\mathcal{H}}\right)\int_0^{r_s} dr j_l(kr)(\tilde{\Phi}'+\tilde{\Psi}')(z,k)
\end{aligned} \tag{5.67}$$

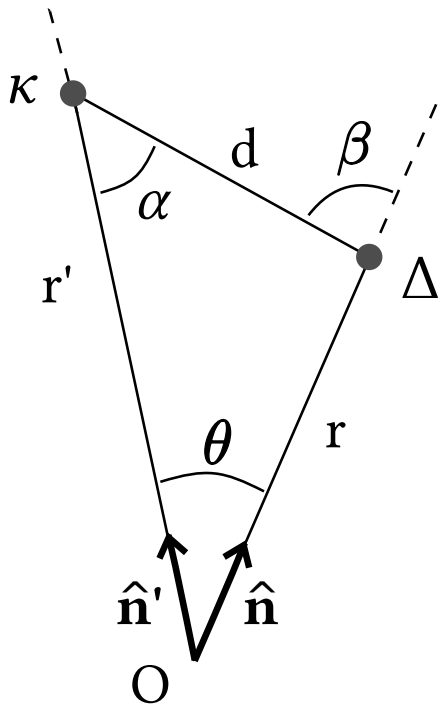

Fig. 5.1 The useful definitions and geometry set-up used in our evaluations. (credit to: C. Bonvin.)

For the record, we need to point out that the leading factor (43/50)—in equations. (5.63),(5.65) and (5.66) differ from the usual factor of (9/10)[87, 92, 94, 95] because in aforementioned references they've assumed that $\Phi = \Psi$—dropping this approximation we get (43/50).

5.4.2 Two point correlation function

Here we describe the another statistic measurement suitable for large scale regime—Doppler lensing; which can be measured with the next generation of cosmological surveys. Let's begin by correlating the observed overdensity with an approximate of the convergence—along the direction $\hat{\mathbf{n}}$ with redshift z, which we can quantify by

$$\xi(z, \hat{\mathbf{n}}) = \langle \Delta(z, \hat{\mathbf{n}}) \kappa(z', \hat{\mathbf{n}}') \rangle \tag{5.68}$$

The correlation function ξ consists of hierarchy multipoles around the observed overdensity—due to the coupling between contributions terms such as density, velocity, lensing, Sachs-Wolfe SW and Integrated Sachs-Wolfe ISW (most of these contributions can be dropped out on redshift approximately to one)[48, 62, 250].

At linear order, the galaxy number count is dominated by standard contribution term given by (5.40), at which gravitational lensing and relativistic effects to galaxy number count are sub-dominant and hence can be dropped off on low redshifts; they become significant on high redshifts. For convergence we consider the Doppler contributions (5.48) to be the dominant, even though gravitational lensing contributions are also significant but, for the same reasons mentioned above they are important on high redshifts. The optimal estimator for a realistic survey we consider an expression given by Bonvin et al. [47]

$$\xi_{\rm dip}(d) = a_N \sum \Delta_i \kappa_i \cos\beta_{ij} \delta_k(d_{ij} - d), \tag{5.69}$$

$$\xi_{\rm oct}(d) = b_N \sum \Delta_i \kappa_i P_3(\cos\beta_{ij}) \delta_k(d_{ij} - d). \tag{5.70}$$

The normalization factors are denoted by a_N and b_N and the sum is pair of pixels in the survey separated by a physical distance d_{ij}, with the angle β_{ij} is the angle at Δ_i between the line-of-sight angle $\hat{\mathbf{n}}$ and the direction vector κ_i all this is shown in Fig. 5.1. In unified dark energy context, the relation between between the velocity potential and the gravitational potential and the matter gauge-invariant comoving density is typically modified. This relation, arise from the energy conservation equation for the velocity, it thus a critical test of GR on cosmological scales, and certainly one which Doppler dipole will be particularly sensitive to.

5.4.2.1 Multipole expansions

We consider the cross-correlation of the observed number count-convergence, for galaxy survey; we expand this quantity in Fourier space which yields[8]

$$\begin{aligned} \xi^{\Delta^{\rm st}\kappa^{\rm v}} &= \left(1 - \frac{1}{r(z_s')\mathcal{H}(z_s')}\right) \int \frac{d^3\mathbf{k}}{(2\pi)^3} e^{-i\mathbf{k}\cdot\mathbf{x}} \tilde{V}_m(z_s', k)(\mathbf{k}\cdot\hat{\mathbf{n}}') T^2(k) P_{\Psi_{\rm i}}(k) \\ &\times \left(b(z)\tilde{\Delta}_m(z_s, k) - \frac{1}{\mathcal{H}} \tilde{V}_m(z_s, k)(\mathbf{k}\cdot\hat{\mathbf{n}})^2\right) \end{aligned} \tag{5.71}$$

Here the cross-correlation above is expressed in-terms of (z_s, z_s', θ), where z_s is the redshift of the source z_s and θ being the between $\hat{\mathbf{n}}$ and $\hat{\mathbf{n}}'$. Following [47] formalism the cross-correlation can be re-expressed in a form (r, d, β), where d denotes the comoving distance between the galaxies and the orientation of the pair with respect to line-of-sight is denoted by β (this is shown in Fig. 5.1). Then we expand the cross-correlation in

[8]Henceforth in the thesis we assume the metric convention to take the form $ds^2 = a^{-2}[-(1+2\Psi)d\eta^2 + (1+2\Phi)d\mathbf{x}^2]$ and the Fourier convention $f(x,\eta) = (2\pi)^{-3}\int d^3\mathbf{k} e^{i\mathbf{k}\cdot\mathbf{x}} f(\mathbf{k},\eta)$

spherical multipoles (see also appendix B of [50] for comprehensive derivation), given by

$$\begin{aligned}\xi^{\Delta^{\rm st}\kappa^{\rm v}} &= \frac{1}{2\pi^2}\left(1-\frac{1}{r(z_s')\mathcal{H}(z_s')}\right)\Bigg[\cos\beta\left(\frac{1}{15}\nu_1+\lambda_1-\frac{1}{10}\nu_3\right)\\ &+ \frac{1}{5}\cos\alpha\cos\beta\left(\nu_1-\frac{3}{2}\nu_3\right)+\frac{1}{5}\sin\alpha\sin\beta\left(\nu_1+\nu_3\right)\Bigg] \end{aligned} \tag{5.72}$$

With the parameters λ_l and ν_l with $l=1,3$ are respectively given by

$$\begin{aligned}\lambda_l(r,d,\beta) &= \int dk k^2 j_l(kd)\tilde{V}_m(z_s',k)T^2(k)P_{\Psi_{\rm p}}(k)\\ &\times \left[b\tilde{\Delta}_m(z_s,k)-\frac{1}{3\mathcal{H}}\tilde{V}_m(z_s,k)\right] \end{aligned} \tag{5.73}$$

$$\nu_l(r,d,\beta) = \int dk k^2 j_l(kd)\frac{1}{\mathcal{H}}\tilde{V}_m(z_s',k)\tilde{V}_m(z_s,k)T^2(k)P_{\Psi_{\rm p}}(k) \tag{5.74}$$

For us to to able to plug-out the signal for dipole and octupole from the cross-correlation, given by (5.71) we express the comoving distance $r(z_s')$, the redshift z_s' and the angle α in-terms of (r,d,β) for example in distant-observer approximation regime (regime at which $d/r \ll 1$) Taylor expansion around r leads to $\mathcal{H}(z')=\mathcal{H}(r')=\mathcal{H}(r)+\mathcal{O}(d/r)$. And we also weight the cross-correlation by their appropriate Legendre polynomials $P_1(\cos\beta)$ and $P_3(\cos\beta)$; respectively denotes dipole and an octupole which can easily be computed by multiplying the cross-correlation with $\cos\beta$ and integrating over β. Therefore, in flat-sky approximation, the cross-correlation works out to become

$$\xi^{\Delta^{\rm st}\kappa^{\rm v}} = \frac{1}{2\pi^2}\left(1-\frac{1}{r_s\mathcal{H}}\right)\left[\left(\lambda_1-\frac{4}{15}\nu_1\right)P_1(\cos\beta)-\frac{2}{3}\nu_3 P_3(\cos\beta)\right] \tag{5.75}$$

Notice that by considering the approximations pointed-out above the evolution for $z_s', r(z_s')$ and $\tilde{V}_m(z_s',k)$ encompassed in Eq. (5.72), (5.73) and (5.74) simplify to becomes $(z_s, r(z_s), \tilde{V}_m(z_s,k))$ in Eq. (5.75).

5.5 Probing background-perturbation evolution of the UDE

In this section we explore the inherent features of the UDE model—by studying the behavior of the background parameter. We considering the parameters α_M, α_K and α_H, accordingly. We adopt current epoch cosmological parameter given by

α_H	Υ_1	Υ_2	α_B	α_T	α_K	α_{M0}	$w_{x,\text{eff}}$	w_x
0.05	0.8	-0.5	0.45	0	0	0.3	-1	-0.9
0.05	0.8	-0.5	0.45	0	0	0.5	-1	-0.83
0.05	0.8	-0.5	0.45	0	0	0.7	-1	-0.77
0.05	0.8	-0.5	0.45	0	0	0.85	-1	-0.72
0.05	0.8	-0.5	0.45	0	0	0.3	-1	-0.9
0.05	0.8	-0.5	0.45	0	0.1	0.3	-1	-0.9
0.05	0.8	-0.5	0.45	0	0.3	0.3	-1	-0.9
0.05	0.8	-0.5	0.45	0	0.6	0.3	-1	- 0.9

Table 5.2 The beyond-Horndeski gravity five free-parameters constraints (5.37), by making use of the XMM Cluster Survey and CFHLenS (see for more details [217] and [216]). Reader should note that for gravitational wave speed c_T^2 we've adopted the recently introduced aLIGO (advanced Laser Interferometer Gravitational Observatory) constraints—this leads to the chosen value of α_T (see also [19]).

Planck 2018 [4]. In particular, we utilize the matter density parameter $\Omega_{m0} = 0.307$ and with dimensionless Hubble constant $h = 0.679$—which is consistent with $H_0 = 2.3 \times 10^{-4}\, h/\text{Mpc}$.

5.5.1 Exploring the UDE properties

It's important to examine consistency of UDE or effective modification with the standard cosmological concordance model; if we set all free parameters α_i are equal to zero, we recover ΛCDM—provided that $M^2 = 1$ and $H = H_\Lambda = \sqrt{H_0^2(\Omega_m a^{-3} - (1-\Omega_m)}$. Hereinafter we presume pressureless matter, i.e., $\bar{p}_m = 0 = \delta p_m$—with the matter equation of state parameter $w_m = \bar{p}_m/\bar{\rho}_m = 0 = \sigma_m$ and the matter (squared) sound speed $c_{sm}^2 = 0$, we also choose Newton-law-deviation parameter to be $\Upsilon_1 = 0.8$, and light-bending parameter $\Upsilon_2 = -0.5$, this are used throughout our numerical computations.

The significance modified gravity theories or UDE background parameters are shown in Fig. 5.2—which we shown by varying parameter α_{M0}, and α_K, accordingly. In (top left panel) the scheme represents the behavior of the energy density Ω_x and *effective* mass evolution rate parameter α_M, which act as a driving factor for the UDE evolution. We see that at early times $z \gtrsim 3$ (which corresponds to scale factor of about $a \lesssim 0.25$), the beyond-Horndeski gravity theories and GR appears to be identical

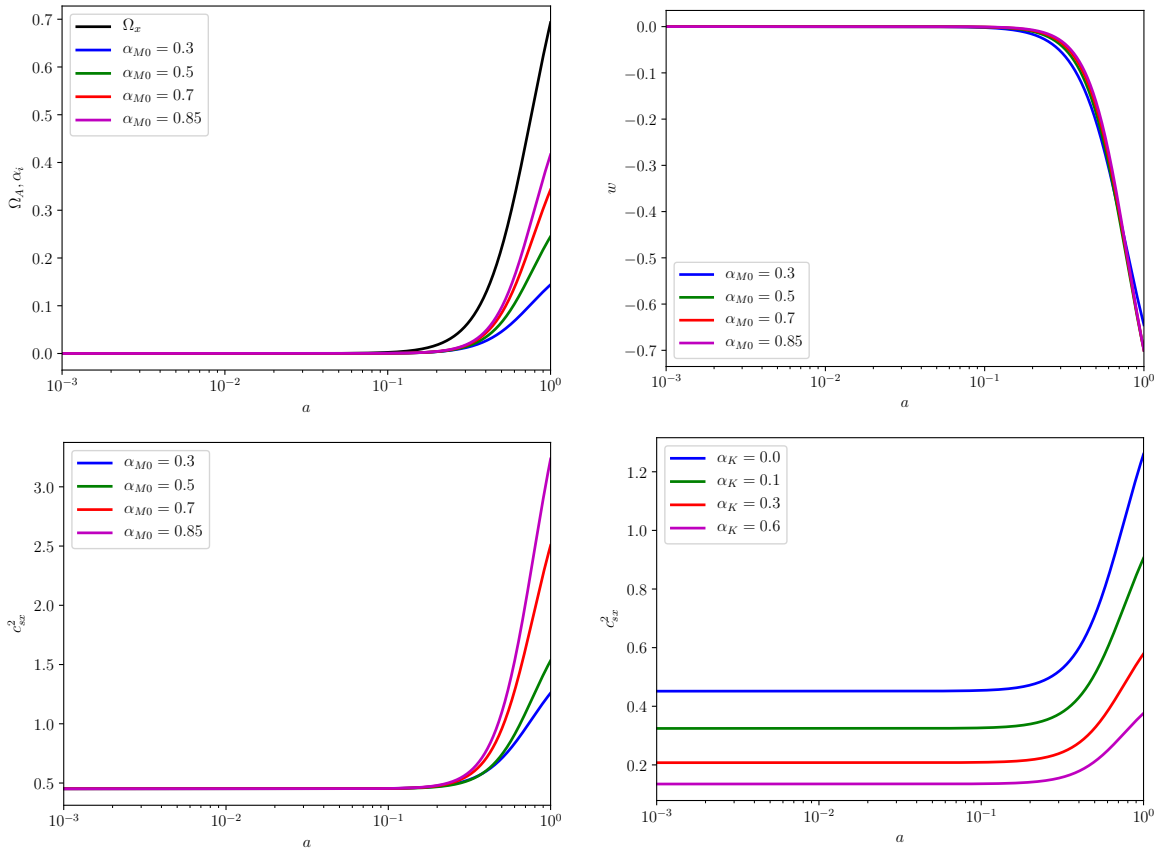

Fig. 5.2 *Top left panel*: The plots of the mass evolution-rate parameter, given by Eq. (5.37) and UDE energy density—with respect to scale factor, for various values of the proportionality constant α_{M0} which are given in Table. 5.2. *Top right panel*: we show the evolution of the total equation of state parameter, given by Eq. (5.23) as a function of scale factor—for different values of constant $\alpha_{M0} = 0.3, 0.5, 0.7, 0.85$. *Bottom panel*: we show the behavior of the square of the physical sound speed, given by Eq. (5.34) as function of scale factor, *left panel*: we considered $\alpha_{M0} = 0.3, 0.5, 0.7, 0.85$ with remaining free-parameters fixed, *right panel*: we considered various kineticity parameter $\alpha_K = 0, 0.1, 0.3, 0.3$ with rest of the free-parameters kept constant (see Table. 5.2).

in the background in these epochs—by this we mean that lessen to GR specifically $\Omega_x \simeq 0$ and $\alpha_M \simeq 0$; This mimics ΛCDM, where $w_{x,\text{eff}} = -1 = w_x$. On the other hand, at late times $z < 3$ there is a sudden incompatible separation of beyond-Horndeski gravity from GR ($\alpha_M, \Omega_x > 0$); this indicates the beyond-Horndeski gravity background gradually deviates from ΛCDM, with UDE equation of state parameter satisfying this condition $w_x \neq -1$. Therefore, since we have $\alpha_M \propto \Omega_x$, we focus only on the behavior of α_M which might be very useful for the reduction of the well established cosmological

constant problem—particularly because at early epochs, α_M can be neglected and at late epochs it grow with time resulting in UDE of a positive evolution, with an increasing density[9].

We show in (top right panel) the plots of the total equation of state parameter, we provided by Eq. (5.23), which effectively determines the acceleration of the Universe. It's of importance to point out that, chosen value/s for w_x and α_{M0} are not certainly important provided ($w < -1/3$) which is solely the condition for the late time of the cosmic acceleration. We also see that UDE seems to track matter ($w_m = 0 = w$) from the decoupling epoch until at $a = (1+z)^{-1} \gtrsim 0.25$, when it deviates into the negative, *anti gravity* mode; however, it only begins to drive the cosmic expansion into acceleration much later, at $z \lesssim 0.036$. The fact that the cosmic acceleration sets in so late leads to the high value of w_x. Moreover, given the chosen w_x throughout the cosmic evolution history, it implies that there will be relatively more suppression of the matter perturbations in the beyond-Horndeski gravitational field compared to the standard, GR case.

In Fig. 5.2 bottom left panel, we show the plots of UDE physical sound speed c^2_{sx}, given by Eq. (5.34), for various values of $\alpha_{M0} = 0.2875, 0.85, 2, 2.5$, with fixed $\alpha_K = 0$. We note that the change in amplitude of c^2_{sx} is determined by α_K and its behavior is characterized by the evolution of α_M which can be controlled by constant α_{M0}. We see that at early epochs $z \gtrsim 3$ when $\alpha_M \simeq 0$ corresponding to $c^2_{sx} \simeq 1$, this value coincide with speculated value by standard cosmologies. Therefore, the matter perturbations in the UDE Universe have similar magnitude and evolution as those of ΛCDM. Similarly, at late epochs $z < 3$ when $\alpha_M > 0$ the following conditions holds;
(i) $c^2_{sx} \lesssim 1$ provided that $\alpha_{M0} \lesssim 1.5$ and (ii) $c^2_{sx} > 1$ given $\alpha_{M0} > 1.5$. In the former scenario, it implies that α_M causes the UDE perturbations to cluster to significant amount easily from sub-Hubble scales; thereby availing the UDE perturbations more space to suppress the matter perturbations. Conversely, in the latter scenario it implies that α_M causes the UDE perturbations to propagate with super-luminal speed such that they are unable to cluster and are hence perturbatively insignificant, up to super-Hubble scales. Note that the sound speed determines the scale beyond which the perturbations of the given DE are able to cluster to a significant amplitude; hence the bigger the sound speed, the larger the scale the DE perturbations have to exceed (and thus, the longer it takes) before they can cluster to cause any significant effect on the mater perturbations [93].

[9]Eventually, the UDE will act to drive the cosmic expansion into an acceleration, at late times $z \lesssim 0.5$.

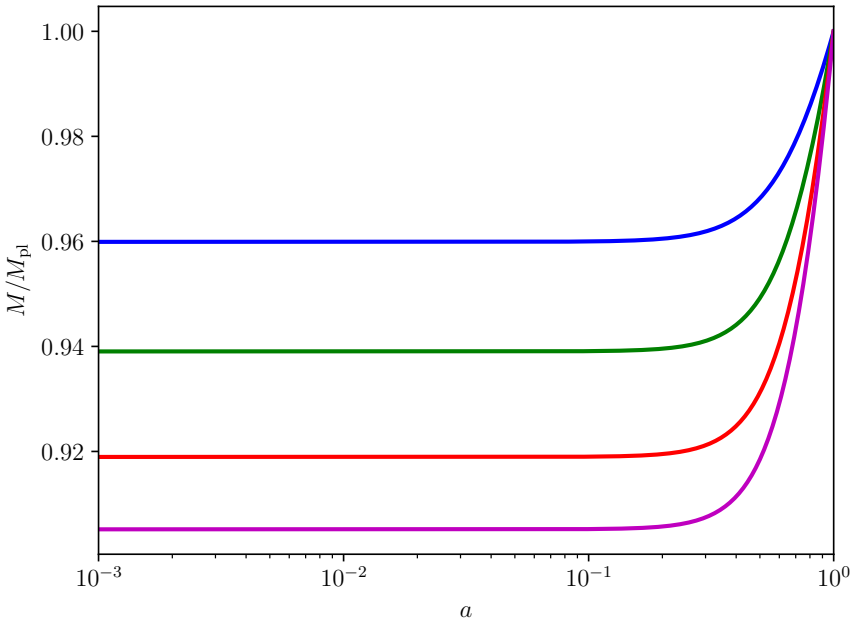

Fig. 5.3 The ratio of the effective Planck mass M to the standard Planck mass $M_{pl} = 1/(8\pi G)$ (with the Newton's gravitational constant denoted by G) plotted as function of scale factor, for various values of $\alpha_{M0} = 0.3, 0.5, 7, 0.85$ and $\alpha_K = 0$

In bottom right panel show the plots of the UDE sound speed for the values of the kineticity parameter $\alpha_K = 0, 0.1, 0.3, 0.6$ and with fixed $\alpha_{M0} = 0.2875$. We see that the various values of α_K leads to sort of constant separations in the amplitude of the UDE sound speed. We also note that an increase of kineticity α_K results in a decrease of sound speed and there is an converges at certain fixed values ($c_{sx}^2 > 0$ and $c_{sx}^2 \ll 1$), This means that, kinetic contributions will reduce the sounds horizon such that the UDE perturbations easily become substantial on sub-Hubble scales; thus eroding the growth and formation of structure—to become lower than the GR case with the fixed value of w_x. In Fig. 5.3 we show the ratio between the effective Planck mass M and standard Planck mass $M_{pl} = (8\pi G)^{-1}$ (with G being the Newton's gravitational constant) as function of scale factor, for separate values of α_{M0} given in Table. 5.2. We choose the present value for $M_0 = M_{pl}$,which put a constraint on the effective Planck mass. We see that as the amplitude of the effective Planck mass decreases with an increase of the constant α_{M0}. However, we should pointed out that, the UDE and the cosmic acceleration is not driven by the amplitude of the effective Planck mass, but by its time rate of change; governed by α_M. We have that at ($z < 1$), the larger the value of α_{M0}, the steeper the slope of M; thus, a stronger acceleration.

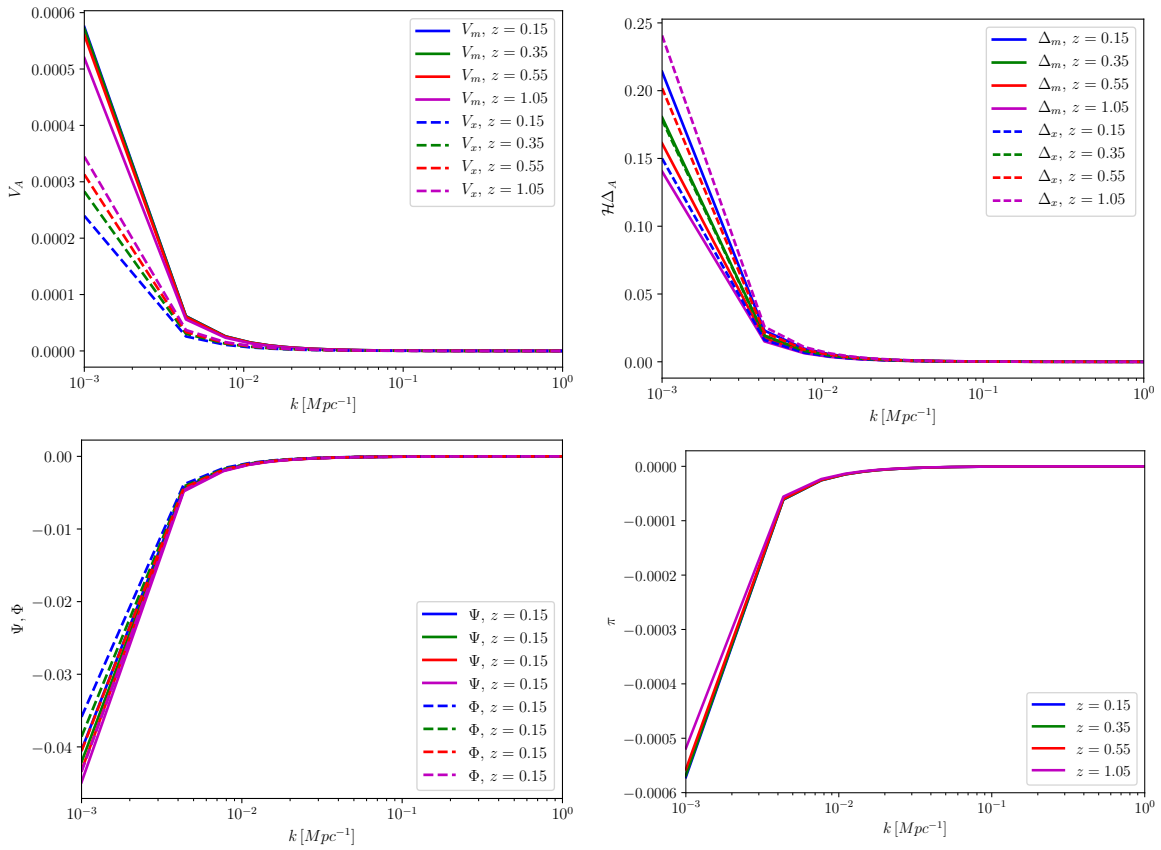

Fig. 5.4 We plot for various redshift ($z = 0.15, 0.35, 0.55, 1.05$)—with $\alpha_{M0} = 0.3$, $\alpha_H = 0.05$, $\alpha_K = 0$, $\alpha_T = 0$ and $\alpha_B = 0.45$: *Top left panel*: The UDE and matter velocity potentials, $V_x(z,k)$ (dashed lines) and $V_m(z,k)$ (solid lines) respectively. *Top right panel*: The UDE and matter comoving density, $\Delta_x(z,k)$ (dashed lines) and $\Delta_m(z,k)$ (solid lines) respectively, which we multiplied by dimensionless Hubble parameter. *Bottom left panel*: The behaviour of the two Bardeen potentials $\Psi(z,k)$ (dashed lines) and $\Phi(z,k)$ (solid lines). *Bottom right panel*: The behaviour of the scalar potential $\pi(z,k)$.

In Fig. 5.4 we illustrate the behaviour of UDE in the framework of beyond-Horndeski theories affect the perturbations by considering constant $\alpha_{M0} = 0.3$, beyond-Horndeski parameter $\alpha_H = 0.05$, kineticity $\alpha_K = 0$, tensor speed alteration $\alpha_T = 0$ and braiding $\alpha_B = 0.45$—for various redshifts. We show (top left panel) the evolution of the UDE and matter velocity potentials. We see that matter dominates the UDE on the following scale ($10^{-3} < k < 10^{-2}$)—We also see that UDE amplitude increase with an increase of redshift, now at scale $k > 10^{-2}$ UDE appears to track matter $V_x = 0$. While on the other hand the matter velocity potential magnitude decrease with an increase of redshift on scale ($10^{-3} < k < 10^{-2}$).

In top right panel, we show the of the UDE comoving density and matter comoving density which we both multiplied by dimensionless Hubble parameter (this is consistent with Fig. (1) given in [94] for clustering QCDM). Similarly to the left panel, we see that the behavior of $\mathcal{H}\Delta_x$ for given fixed values of all five-free parameters; the amplitude of $\mathcal{H}\Delta_x$ increase or decrease according to whether the value of redshift is bigger or smaller. We also see that the $\mathcal{H}\Delta_x$ at scale $k > 10^{-2}$ UDE appears to track matter $D_x = 0$.

In Fig. 5.4, bottom panel, we show the plots of the metric potentials Ψ, Φ and π. We see that all the amplitude of metric potentials appears increase with an increase of redshift—amplitude of scalar π is 10^{-3} smaller that the amplitude of the two Bardeen potentials.

5.5.2 The imprint of relativistic effects in beyond-Horndeski gravity

The evaluation of the correlation function of galaxy survey has a quite lengthy history. However, in past this quantity has usually been evaluated in terms of the distance r (see [230] for details) between the galaxies, this normally presents issues due to the fact that this depends on the cosmological parameters[10]. Moreover, recently this quantity has been reformulated to be described by the source epochs z and z' in the direction $\hat{\mathbf{n}}$ and $\hat{\mathbf{n}}'$ with angle θ between them [45, 47, 49, 84] this is best described by Fig. 5.1.

Taking into consideration the reasons above, for us to analyze the imprint of relativistic effects in beyond-Horndeski gravity in redshift space, we work directly with the two-point correlation function and standard radial angular power spectrum. Which can be related by

$$\xi(z, z', \theta) = \langle \Delta(z, \hat{\mathbf{n}}) \kappa(z, \hat{\mathbf{n}}) \rangle = \frac{1}{4\pi} \sum_{l=0}^{\infty} (2l+1) C_l(z, z') P_l(\cos\theta) \tag{5.76}$$

Here we adopt [47] formalism in order to work out the odd multipoles, which are observable. While the behavior of the C_l's will be presented in [93], the reason being that the two-point correlation functions are actually very important as they give more insides on the the radial BAO's.

In Fig. 5.5 we show the relevant UDE two-point correlation function multipole. We show (left panel) the cosmic behavior of the dipole multiplied by separation d^2, given in Eq. (5.75), as function of separation d for constants $\alpha_{M0} = 0.3$ (blue) and $\alpha_{M0} = 0.5$

[10] This cause similar problems or issues for it's Fourier transform—Power spectrum

(green) at source epoch $z = 0.15$ and with galaxy bias $b = 2$. We have that at very early epochs $d \lesssim 40$ Mpc/h the two curves are identical; however, the two curves deviates away from each other at epochs $d \gtrsim 40$ Mpc/h. We see that the amplitude of UDE dipole increase with an increase of the various values of α_{M0}. We also see that the curve ($\alpha_{M0} = 0.5$) is more dominant while curve ($\alpha_{M0} = 0.3$) is subdominant.

Also in Fig. 5.5 We show (right panel) the cosmic behavior of the dipole multiplied by separation d^2, given in Eq. (5.75), as function of separation d for constants $\alpha_{M0} = 0.3$ (blue) and $\alpha_{M0} = 0.5$ (green) at source epoch $z = 1.05$ and with galaxy bias $b = 2$. We have that the dipole have the similar behavior as the one on the left panel. In comparison, we see that left panel($z = 0.15$) remains a factor 10^{-2} greater than that of the right panel ($z = 1.05$) at all scales.

In Fig. 5.6 we show the relevant UDE two-point correlation function multipole. We show (left panel) the cosmic behavior of the octupole multiplied by separation d^2, given in Eq. (5.75), as function of separation d for constants $\alpha_{M0} = 0.3$ (blue) and $\alpha_{M0} = 0.5$ (green) at source epoch $z = 0.15$ and with galaxy bias $b = 2$. We have that at very early epochs $d \lesssim 40$ Mpc/h the two curves are identical; however, the two curves deviates away from each other at epochs $d \gtrsim 40$ Mpc/h. We see that the amplitude of UDE octupole increase with an increase of the various values of α_{M0}. We also see that the curve ($\alpha_{M0} = 0.3$) is more dominant while curve ($\alpha_{M0} = 0.5$) is subdominant.

Also in Fig. 5.6 We show (right panel) the cosmic behavior of the octupole multiplied by separation d^2, given in Eq. (5.75), as function of separation d for constants $\alpha_{M0} = 0.3$ (blue) and $\alpha_{M0} = 0.5$ (green) at source epoch $z = 1.05$ and with galaxy bias $b = 2$. We have that the octupole have the similar behavior as the one on the left panel. In comparison, we see that left panel($z = 0.15$) remains a factor 10^{-2} greater than that of the right panel ($z = 1.05$) at all scales. We also note that due to the fact the pre-factor $(1 - 1/r_s\mathcal{H})$ decreases with redshift, the Doppler/relativistic contributions varies very strongly with redshift.

In figure. 5.7 we show the deviation between GR and beyond-Horndeski model, considering dipole; for $\alpha_{M0} = 0.3$ and $\alpha_{M0} = 0.5$, at source epochs $z = 0.15$ (left panel) and $z = 1.05$ (right panel) and with a galaxy bias $b = 2$. In figure. 5.8 we show the deviation between GR and beyond-Horndeski model, considering octupole; for $\alpha_{M0} = 0.3$ and $\alpha_{M0} = 0.5$, at source epochs $z = 0.15$ (left panel) and $z = 1.05$ (right panel) and with a galaxy bias $b = 2$.

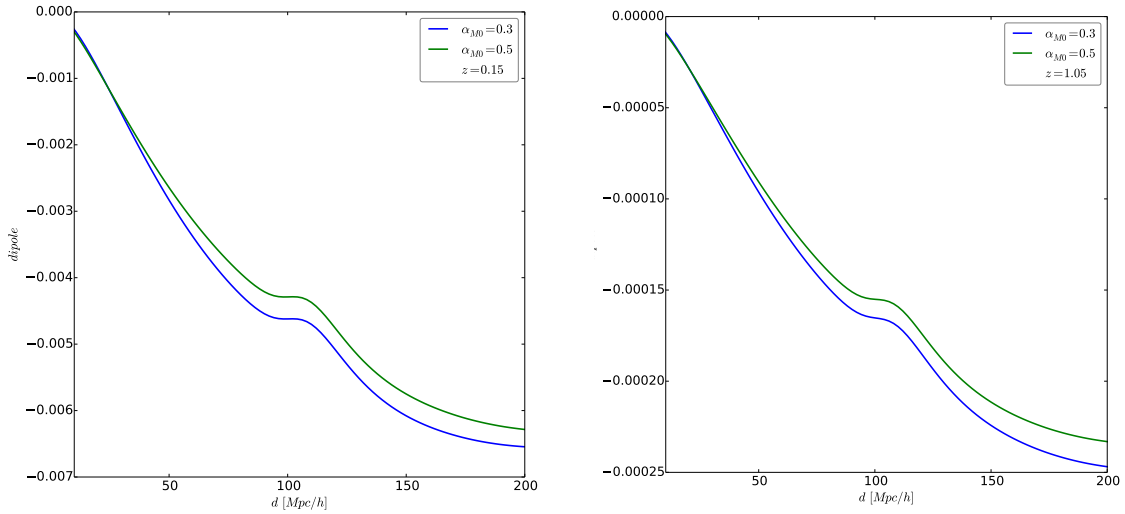

Fig. 5.5 The plots of the two-point correlation function dipole ($d^2\xi_1^{\Delta_{\rm st}\kappa_v}$): for $\alpha_{M0}=0.3$ and $\alpha_{M0}=0.5$, at source epochs $z=0.15$ (left panel) and $z=1.05$ (right panel) and with a galaxy bias $b=2$

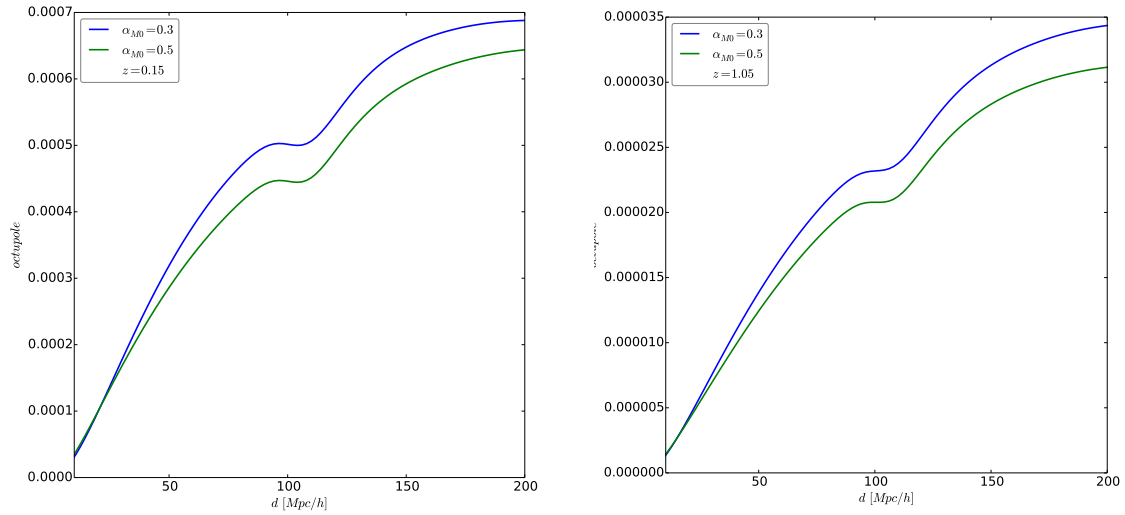

Fig. 5.6 The plots of the two-point correlation function octupole ($d^2\xi_3^{\Delta_{\rm st}\kappa_v}$): for $\alpha_{M0}=0.3$ and $\alpha_{M0}=0.5$, at source epochs $z=0.15$ (left panel) and $z=1.05$ (right panel) and with a galaxy bias $b=2$

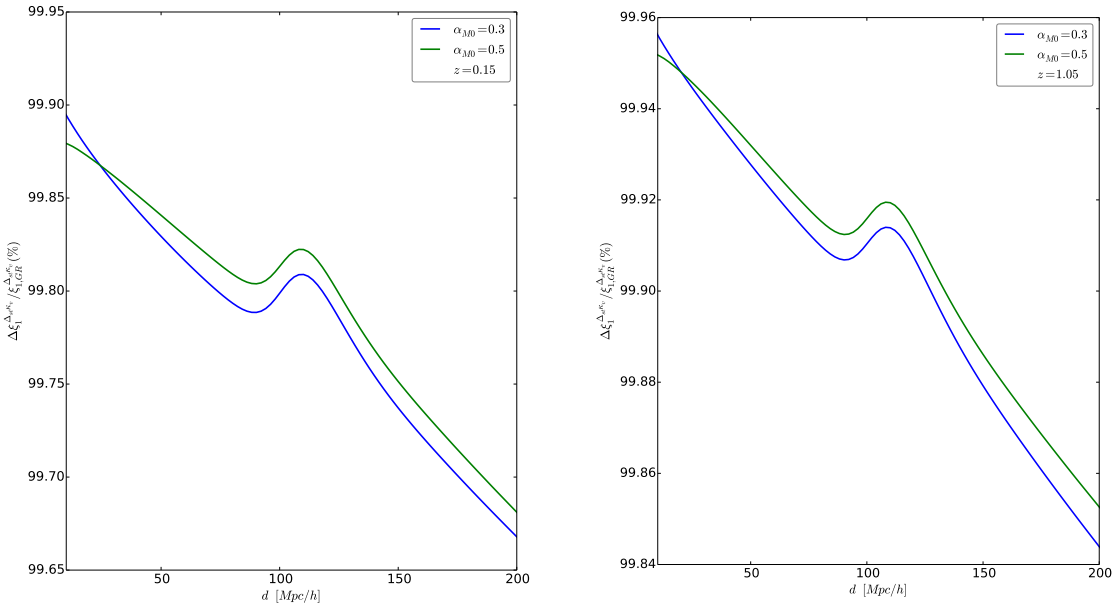

Fig. 5.7 Fractinal deviation of dipole: for $\alpha_{M0} = 0.3$ and $\alpha_{M0} = 0.5$, at source epochs $z = 0.15$ (left panel) and $z = 1.05$ (right panel) and with a galaxy bias $b = 2$

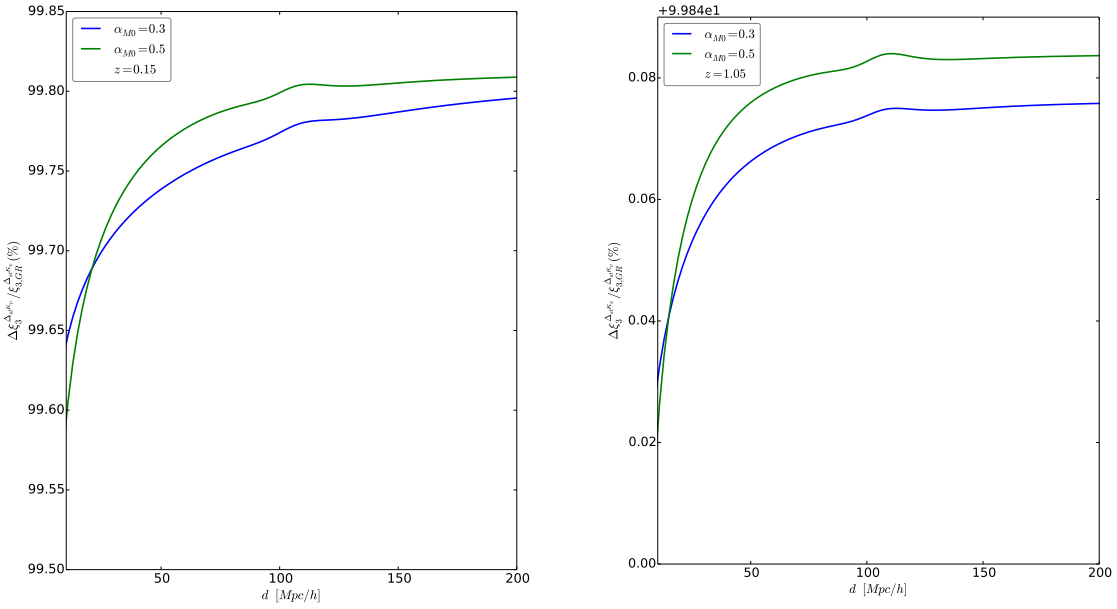

Fig. 5.8 Fractinal deviation of octupole: for $\alpha_{M0} = 0.3$ and $\alpha_{M0} = 0.5$, at source epochs $z = 0.15$ (left panel) and $z = 1.05$ (right panel) and with a galaxy bias $b = 2$

5.6 Conclusions

We have given an analytical treatment of the beyond-Horndeski gravity which has recently been reformulated in the dark energy paradigm—which has been dubbed unified dark energy; this accounts for large-scale peculiar velocity fields and the time derivatives of the metric potentials. The evolution equations of the unified dark energy appears to corresponds to non-conservation dark energy paradigms, in which the total energy-momentum tensor is not conserved.

We have reviewed the large-scale imprint of the UDE, by introducing the angular power spectrum of the galaxy number counts $C_l(z_s, z_s')$, on horizon scale; taking care to involve the full relativistic corrections in the observed overdensity. Moreover, we also computed the full-sky cross-correlation function $\xi(z_s, d, \beta)$ between galaxy number counts standard term (the combination of intrinsic clustering and RSD; this are most dominant terms of galaxy number count at low and mid redshifts) and the convergence Doppler term (this is considered the dominant term of the convergence at low and mid redshifts), in configuration space. While varying the constant proportional the running of the effective Planck mass α_{M0}. We have shown that the two-point correlation function generates the two odds multipoles dipole and octupole. We adopted the estimators of dipole and octupole, prescribed by [8, 47], and we found a good agreement in their model and our beyond-Horndeski gravity in that the octupole contribution is also about one order of magnitude smaller than that of the dipole. Thus, octupole can be neglected. We also found that the galaxy correlator at different redshifts increases the sensitivity of beyond-Horndeski gravity.

Chapter 6

Probing modified gravity signature

The investigation of different theories of gravity extend more robust explanation than that of cosmological constant Λ, this can be invigorated by the cosmic acceleration which is pointed out by the current cosmological observations. Our apprehension of gravity by probing activities have foregrounded the observational constraints and theoretical that alternates to satisfactory of GR, even though this efforts are not leading to a solid stand or the understanding of the increase of expansion of the Universe. The expansion of the Universe remains the deepest mysteries of modern physics. On large scale Einstein's general relativity is one of the possibilities due to the presence of additional degrees of freedom [64]. From [3, 154, 241] the phenomenon of cosmic acceleration, current and forthcoming cosmological observations will allow us to test gravity through many effects predicted by alternative theories using observations of the Universe's expansion and the formation of large scale structure (LSS). The non-success to elaborate or explain the technically peculiar fine-tuning needed to reunite the enormous vacuum energy this gives supplementary motivation, this is predicted by particle physics with small value of the observed cosmological constant Λ.

Underneath quasi-static regime approximation amount of studies of large scale structure formation in alternative theories have been carried out, at which the dynamics can be negligible (see [6, 74] for more details). Going beyond the usual approximation well ground on small scale is required to confront the consequences of modified gravity on scale approximate to Hubble scale radius. In [220] the above approximation has been shown to be really consistent on very small linear scales at which the dynamics have relaxed to the equilibrium values, with the regime of validity characterized by the sound horizon of the new degrees of freedom. In general the is inconsistency on ultra-large scale on quasi-static approximation and solving system of equations is of necessity, this is worked out by [42, 119, 123]. A particularly transparent application

of the UDE has been developed in the context of Horndeski's theory and beyond, the most general local, Lorentz-invariant, scalar-tensor theory described by second order equations of motion. In [119, 133] engage properties of gravity to parameterize cosmological perturbations in scalar-tensor theories.

An alternative approach is to consider an effective field theory or dark energy linear perturbations on the very crown of a Friedmann-Robertson-Walker (FRW) cosmological background. This method was introduced in [63, 69] and has been developed in the context of general dark-energy cosmologies in [39, 42, 116, 123, 205] (for more details on the review [233]). As reviewed by [28], the idea is that one writes down an action for linear perturbations containing all possible operators allowed by the symmetries of the FRW background and properties required of the underlying dark energy. These operators have arbitrary coefficients that are purely functions of time and represent the maximal freedom that is permitted in the equations of motion for perturbations. Not all these operators contribute in a distinct manner to the perturbations but they do represent the maximal freedom that one has in deforming Einstein equations according to whichever DE properties are required.

In chapter. 5 we've looked at more general case of testing modification of gravity or DE. In this chapter we focus on static-limit approximation—our work is divided into two parts. The first part; we enlarge previous work[1] by deriving the energy-momentum conservation equations and couple of modified Einstein equations or UDE equations combined whereby the scalar field fluctuations are eliminated and which assimilate beyond-Horndeski models, In our approach, we investigate the effects of UDE model on galaxy clustering, by evaluating the cross-correlation function between galaxy number count and convrgence, auto-correlation function of galaxy number count and auto-correlation of convergence. The main goal is to probe how the cosmological perturbations in the unified DE affect the clustering of galaxies on very large scales, in the presence of GR effects; whether the GR effects may be of the significance in putting constraints on DE and MG models. The second part; we consider the subclass of the first part but we only focus on the Doppler magnification effect.

[1] Work by GLPV [116, 118, 119]

6.1 Probing beyond-Horndeski theories in Quasi-static limit approximation

6.1.1 The background and perturbed equations

In this section, we choose the time dependent parameter α_i and the background gravitational field equations to take the form

$$\alpha_M = \alpha_{M0}\Omega_x, \quad \mathcal{H}^2 = \frac{8\pi G a^2}{3}(\bar{\rho}_m + \bar{\rho}_x), \quad \mathcal{H}' = -\frac{\mathcal{H}^2}{2}(1+3w), \tag{6.1}$$

With α_{M0} being the arbitrary constant, where the total equation of state parameter is $w = \sum_A \Omega_A w_A$ and the matter equation of state parameter $w_m = 0$. We also define the matter and UDE energy density parameter $\Omega_m = \frac{\bar{\rho}_m}{\bar{\rho}}$ and $\Omega_x = \frac{\bar{\rho}_x}{\bar{\rho}}$, which respectively evolves, by

$$\Omega_m' = -3\mathcal{H}\Omega_m(w_m - w + \frac{\alpha_M}{3}), \quad \Omega_x' = -3\mathcal{H}\Omega_x(w_{x,\text{eff}} - w + \frac{\alpha_M}{3}), \tag{6.2}$$

Similarly, we define UDE equation of state parameter $w_x = \frac{\bar{p}_x}{\bar{\rho}_x}$, which evolves according to eq. (5.24).

We adopt the perturbed FLRW metric in Newtonian gauge to be described by

$$ds^s = -a^2(1+2\Psi)d\eta^2 + a^2(1+2\Phi)d\vec{x}^2. \tag{6.3}$$

In the build-up of deriving the evolution equations for linear perturbations represented by Eq. (4.24) and (6.3)—we execute the time diffeomorphism $t \to t + \pi(t, \vec{x})$ (see [9, 69, 116] for more details)—which contains the fluctuations of scalar degree of freedom—applying this to the action we restore the complete 4-dimensional covariance of the action. At linear order the total matter energy-momentum tensor $T^{\mu}{}_{\nu}$ components can be disintegrated in the following expressions[2]– this leads to the Hamiltonian constraint also known as time-time component of the modified Einstein equation, then the momentum constraint or time-space component, Anisotropy constraint (traceless space-space) and the trace of the space-space component which we respectively defined in Appendix. D.2.

[2]The total matter stress-energy tensor is decomposed by

$$T^0{}_0 = -(\bar{\rho}_m + \bar{\rho}_x), \quad T^0{}_i = \partial_i q_m, \quad T^i{}_j = (\bar{p}_m + \delta p_m)\delta^i_j + (\partial^i\partial_j + \frac{1}{3}\delta^i_j\partial^2)\sigma_m$$

In order for us to derive the two modified Einstein equations we follow [28, 119] approach, this approach is very useful because it can be easily related to late time observations. Furthermore since scalar fluctuations π is not easily related to observations, here we get rid of π along with its derivatives, we also eliminate the derivatives of gravitational potential Ψ', this approach was introduced by [172]. Since our focus is mainly in beyond-Horndeski theories context at which $\alpha_H \neq 0$— this provides some extensions to the work provided by [28, 119]. For us to get rid of scalar field π and gravitational potential Ψ' we make use of Eqs. (D.9)-(D.12) and with some algebra, we obtain the the second order evolution expression for potential Φ which represents the first blended modified Einstein equation which yields

$$\Phi'' + \mathcal{R}_1\Phi' + \mathcal{R}_2\mathcal{H}\Phi - \mathcal{R}_3\mathcal{H}\Delta_m - \mathcal{R}_4\mathcal{H}^2 V_m = 0 \tag{6.4}$$

The decomposition of the function $\mathcal{R}_i$ for $(i = 1, 2, 3, 4)$ are provided in Appendix. D.3; this function are scale dependent, they also involve β_i parameters which can be found from [119], it also includes the non zero beyond-Horndeski parameter and new parameters ϵ_i which we also defined in Appendix. D.3.The second evolution equation which relate the two Bardeen potentials can be obtained by, eliminating the potential π' from Eq. (D.9) and (D.11) which will give rise to a new equation and eliminating π' from Eq. (D.10) and (D.11) which will also result in a new equation. finally eliminating π from the two new set of equation we get to

$$\Phi' + \mathcal{S}_1\mathcal{H}\Phi + \mathcal{S}_2\mathcal{H}\Psi - \mathcal{S}_3\mathcal{H}\Delta_m - \mathcal{S}_4\mathcal{H}^2 V_m = 0, \tag{6.5}$$

we've defined the decomposition of $\mathcal{S}_i(a)$ for $(i = 1, 2, 3, 4)$ in Appendix. D.3 which involve parameters such as $\tilde{\gamma}_9$ which we also defined as $\tilde{\gamma}_9 = \gamma_9 - \alpha_H\epsilon_1$ with the epsilon's (ϵ_i) are provided in Appendix. D.3. Note that the gamma's and beta's are provided by [28, 119].

We need to point out that our work is within the context of parametrized Post-Friedmann (PPF) formalism at which we parametrize the gravitational properties of UDE as an effective modification of the Poisson equation μ and the modification is the gravitational slip relating the two Bardeen potentials γ , its worth noting that this two parameter are both scale and time dependent. The two parameters are, respectively, given by

$$-k^2\Psi = 4\pi G a^2 \bar{\rho}_m \mu(a, k)\Delta_m, \tag{6.6}$$

and the slip parameter is given by

$$\Phi = \gamma(a,k)\Psi. \tag{6.7}$$

Lastly, we derive the momentum and energy conservation equations from the modified Einstein equations provided in Appendix. D.3. We start of by getting rid of Φ'' with π' from the momentum constraint and the time derivatives of the momentum constraint and the trace of the space-space component. We get the momentum conservation equation to yield

$$V_m' + \mathcal{H}V_m = -\Psi, \tag{6.8}$$

working out the energy conservation equation, we make use of all the constraint equation provide in Appendix. D.3 together with the time derivatives of momentum constraint, anisotropy constraint and Hamiltonian constraint we get the energy conservation equation

$$\Delta_m' = -k^2 V_m + 3\Phi' - 3(\mathcal{H}'V_m + \mathcal{H}\dot{V}_m), \tag{6.9}$$

We make a note that eqs. (6.4), (6.5), (6.8) and (6.9) closes the system of differential equations.

6.1.2 Velocity potential and growth in PPF

Taking into consideration the energy-momentum conservation equations given above and the modified Poisson equation, we get the following velocity potential

$$\begin{aligned} V_m &= -\left\{\left[3\left(1+\frac{\eta}{\mathcal{H}}\right) + \frac{2ak^2}{3\mathcal{H}_0^2\mu\Omega_m}\left(1-\frac{\mu'}{\mathcal{H}\mu}\right)\right]\mathcal{H}\Psi \right. \\ &+ \left.\left(3\eta + \frac{2ak^2}{3\mathcal{H}_0^2\mu\Omega_m}\right)\Psi'\right\}\frac{1}{[k^2+3(\mathcal{H}^2-\mathcal{H})]}, \end{aligned} \tag{6.10}$$

on sub-horizon scales ($k \gg \mathcal{H}$) we can use the following approximation [8]

$$V_m = -\frac{2a}{3\mathcal{H}_0^2\mu\Omega_m}\left[\left(1-\frac{\mu'}{\mathcal{H}\mu}\right)\mathcal{H}\Psi + \Psi'\right], \tag{6.11}$$

assuming that the Universe is homogeneous and isotropic, then it can be shown that under certain assumptions, the growth of matter is governed by the evolution equation

below.

$$\Delta_m'' + \left(2 + \frac{\mathcal{H}'}{\mathcal{H}^2}\right)\Delta_m' = \frac{3}{2}\Omega_m \mu(a,k)\Delta_m. \tag{6.12}$$

Using Poisson equation given in subsection. (6.2) and the fact that $\bar{\rho}_m = \frac{3\Omega_m \mathcal{H}_0^2}{8\pi G a^3}$ the density can be denoted by

$$\Delta_m(z,\mathbf{k}) = -\frac{2}{3}\left(\frac{k}{\mathcal{H}_0}\right)^2 \frac{a}{\Omega_m \mu(a,k)} T(k) g_m(z,k)\Psi(\hat{\mathbf{k}}), \tag{6.13}$$

and the velocity potential is given by

$$V_m(z,\mathbf{k}) \;=\; -\frac{2a}{3\mu\mathcal{H}_0^2\Omega_m}\left[g_m'(z,k) + g_m(z,k)\mathcal{H}\left(1 - \frac{\mu'}{\mathcal{H}\mu}\right)\right] T(k)\Psi(\hat{\mathbf{k}}). \tag{6.14}$$

Where $T(k)$ is transfer function given by [104].

6.1.3 Description of the two fiducial UDE models

In this subsection, we compose the two main models we considered throughout this paper which encompass Horndeski theory which involves the following parameters $(\alpha_B, \alpha_K, \alpha_M, \alpha_T)$ and beyond-Horndeski theory which include the following parameters $(\alpha_B, \alpha_K, \alpha_M, \alpha_T, \alpha_H)$. We adopt the following fiducial models;

1. firstly we have Horndeski model where;
   $\mathcal{M}_1 : \quad \alpha_M \neq 0, \quad \alpha_B \neq 0, \quad \alpha_K = 0 = \alpha_T,$

2. secondly we also consider beyond-Horndeski model where;
   $\mathcal{M}_2 : \quad \alpha_H \neq 0, \quad \alpha_B \neq 0, \quad \alpha_M \neq 0, \quad \alpha_K = 0 \simeq \alpha_T,$

due to strong constraints on cosmological gravity from GW170817 and GRB 170817A we apply some conditions on $\mathcal{M}_2$, by adopting the recent introduced aLIGO (advanced Laser Interferometer Gravitational Observatory) constraints on tensor speed alteration α_T parameter which measures the difference between gravitational wave speed c_T^2 and speed of light, to be approximated by (see [19] for more details)

$$|\alpha_T| \lesssim 1 \times 10^{-15}, \tag{6.15}$$

this results into the solution of α_H provided in Table. 6.1. In order for us to avoid gradient instabilities, we require the physical sound speed to be conditioned as follows

α_H	Υ_1	Υ_2	α_B	α_T	α_K	w_x
0.3	0.5	-0.3	1.2	0	0	-1

Table 6.1 Some of beyond-Horndeski gravity free-parameters and the two parameters governing the deviation of Newtown's law and light bending—by making use of the XMM Cluster Survey and CFHLenS (see for more details [217] and [216]).

$c_{sx}^2 > 0$, the tensor speed alterations, measuring the difference between the speed $c_T^2 = 1 + \alpha_T > 0$ of the gravitational wave and the speed of light and the kinetic energy and the scalar field contributions $\alpha = \alpha_K + 6\alpha_B^2 > 0$.

6.1.4 Generalized modified gravity models

In our computations, We choose the matter density parameter to $\Omega_{m0} = 0.308$ and dimensionless Hubble constant $h = 0.678$ which corresponds to Hubble constant of about ($H_0 \approx 2.3 \times 10^{-4} h.\mathrm{Mpc}^{-1}$). We also assuming pressureless matter, i.e. $\bar{P}_m = 0 = \delta P_m$, thus we have $c_{sm}^2 = 0 = \sigma_m$ and $w_m = 0$. We (from [217], the density of astrophysical objects decreases radially outwards from the centre so that if $\Upsilon_1 > 0$ implies weakening of gravity and if $\Upsilon_1 < 0$ implies weakening of gravity) choose $\Upsilon_1 = 0.5$ this correspond to weakening of gravity on cosmological scale, in the late-time Universe, We also choose $\Upsilon_2 = -0.3$.
In preparation to quasi-static limit approximation approach, we examine if our approach is consistent with ΛCDM. To do so we set all free-parameters to zero ($\alpha_i = 0$) and Hubble parameter $\mathcal{H} = \mathcal{H}_{\Lambda CDM} = H_0[\Omega_{m0} a^{-2} + (1 - \Omega_{m0}) a^{-1}]$.

6.1.4.1 Horndeski theories

Here we investigate the behavior of the running Planck mass ($\alpha_M \neq 0$) and braiding ($\alpha_B \neq 0$) parameter contributions. As described by [28], if both the running Planck mass and scalar parameter and $\alpha_H = \alpha_K = \alpha_T = 0$, this mimics $f(R)$ gravity. Where the Einstein-Hilbert action (see ref. [227, 245] for details) appendage by a term that is non-linear in Ricci scalar R and represented by $\alpha_M = f_R'/\mathcal{H}(1 + f_R) = 2\alpha_B$ with the chameleon field $f_R \equiv df/dR$. We define squared Compton wavelength in the background in the unit of the Hubble length squared which is given by

$$B = \frac{f_{RR}}{1 + f_R} \frac{R'}{\mathcal{H}^3} \left(\frac{\mathcal{H}^2}{\mathcal{H}'} - 1 \right) \tag{6.16}$$

Where $f_{RR} \equiv d^2 f/dR^2$ which is proportional to the squared Compton wavelength, where Ricci scalar is evaluated at background density. The squared Compton wavelength evaluated today is given by

$$B_0 \equiv \frac{f_{RR}}{1+f_R}\frac{R'}{\mathcal{H}^3}\left(\frac{\mathcal{H}^2}{\mathcal{H}'}-1\right)\Bigg|_{z=0} \approx 2.1\Omega_{m0}^{-0.76}|f_{R0}| \tag{6.17}$$

Exploring quasi-static approximation perturbations and comparing them to the perturbations that denote $f(R)$ gravity described by [227]. In static limit, if we make use of Eq. (6.4) and (6.5) the following expression yields

$$\alpha_M' + 2\frac{\mathcal{H}'}{\mathcal{H}^2} - \frac{\mathcal{H}''}{\mathcal{H}^3} - 1 = 0 \tag{6.18}$$

Which is equivalent to equation (Eq. (43) [227] neglecting velocities and time derivatives of Φ), with the running Planck mass being denoted by

$$\alpha_M \equiv B(\frac{\mathcal{H}^2}{\mathcal{H}'}-1). \tag{6.19}$$

Making use of the Friedmann equations given by [28, 119, 123], we find that in $f(R)$ gravity the squared physical sound speed $c_{sx}^2 = 1$. Using the information we provided above we get the expressions below for $\mu(a,k)$ and $\gamma(a,k)$

$$\mu_{\mathcal{M}_1}(a,k) = \frac{\mu_a k_{\mathcal{H}}^2 + \frac{2}{3}\alpha_M k_{\mathcal{H}}^4}{a^{-2}M^2(\mu_b + \mu_c k_{\mathcal{H}}^2 + \frac{1}{2}\alpha_M k_{\mathcal{H}}^4)}, \tag{6.20}$$

$$\gamma_{\mathcal{M}_1}(a,k) = \frac{\gamma_a + \frac{1}{3}\alpha_M k_{\mathcal{H}}^2}{\mu_a + \frac{2}{3}\alpha_M k_{\mathcal{H}}^2}. \tag{6.21}$$

Where μ_a, μ_b, μ_c and γ_a are given by Appendix. D.4.

6.1.4.2 beyond-Horndeski theories

Examining the recent introduced concept where $\alpha_H \neq 0$. In this concept we adopt ref. [217]—for our approach we set the running Planck mass parameter to evolve and depend on scale factor, kineticity is set to zero and braiding and tensor speed alterations depends on beyond-Horndeski parameter which is a non-zero. For illustrative reasons we consider the specified beyond-Horndeski parameter value given in Table. 6.1,together with UDE equation of state component $w_x = -1$.

To compute the parametrization of the gravitational significance of UDE presented as generalized modification of Poisson equation μ and the gravitational slip γ one can

make use of Eqs. (6.4) and (6.5) and by neglecting time derivatives with respect to spatial and on scales much below the sound horizon.

$$\mu_{\mathcal{M}_2}(a,k) = \frac{\mu_I k_{\mathcal{H}}^2 + \mu_{II} k_{\mathcal{H}}^4 + \mu_{III} k_{\mathcal{H}}^6}{a^{-2} M^2 (\mu_{IV} + \mu_V k_{\mathcal{H}}^2 + \mu_{VI} k_{\mathcal{H}}^4 + \mu_{VII} k_{\mathcal{H}}^6)}, \tag{6.22}$$

then the gravitational slip parameter is given by

$$\gamma_{\mathcal{M}_2}(a,k) = \frac{\gamma_I + \gamma_{II} k_{\mathcal{H}}^2 + \gamma_{III} k_{\mathcal{H}}^4}{\mu_I + \mu_{II} k_{\mathcal{H}}^2 + \mu_{III} k_{\mathcal{H}}^4}, \tag{6.23}$$

we define the time dependent coefficients μ_i and γ_i (with $i = I, II, III...$) in Appendix. D.4. In the limit $k \to \infty$

$$\mu_\infty = \frac{\mu_{III}}{M^2 \mu_{VII}}, \tag{6.24}$$

then the gravitational slip parameter is denoted by

$$\gamma_\infty = \frac{\gamma_{III}}{\mu_{III}}, \tag{6.25}$$

where the parameters $\mu_i(a)$ and $\gamma_i(a)$ are defined in Appendix. D.4. In Horndeski theories at which ($\alpha_H = 0$) the above parameters simplifies to similar expressions as [119, 220]

$$\mu = \frac{\alpha c_{sx}^2 (1+\alpha_T) + 2[\alpha_B(1+\alpha_B) + \alpha_T - \alpha_M]^2}{a^{-2} M^2 \alpha c_{sx}^2}, \tag{6.26}$$

$$\gamma = \frac{\alpha c_{sx}^2 + 2\alpha_B[\alpha_B(1+\alpha_T) + \alpha_T - \alpha_M]}{\alpha c_{sx}^2 (1+\alpha_T) + 2[\alpha_B(1+\alpha_B) + \alpha_T - \alpha_M]^2}. \tag{6.27}$$

Here we have expressed Eqs. (6.22) and (6.23) in terms of the functions α_i; remainder this are considered the extensions or more general form of context introduced in subsubsection. 6.1.4.1—we get this functions simply from derivatives of the initial ADM-Lagrangian [119].

6.1.5 Galaxy overdensity-convergence correlation functions

Executing the quasistatic-limit approximation of the modified Einstein equations Eqs. (6.4) and (6.5) and energy-momentum conservation equations (6.8) and (6.9) provide a comprehensive probe of gravity—hence one can use this to constraint UDE or EFT models on cosmological scales. We probe quasistatic-limit approximation

introduced above by evaluating the the total correlation function between the galaxy overdensity and convergence, which we construct as a combination of three main quantities; *i* the galaxy overdensity auto-correlation functions $\xi^{\Delta\Delta}$, *ii* the convergence auto-correlation functions $\xi^{\kappa\kappa}$ and *iii* the cross-correlation functions between galaxy overdensity and convergence $\xi^{\Delta\kappa}$—considering the fully relativistic contributions of the galaxy overdensity (5.38) and convergence (5.47). We are mostly interested in the following quantity

$$\begin{aligned}
\xi^{T}(z,z',\theta) &= \langle\Delta(z,\hat{\mathbf{n}})\Delta(z',\hat{\mathbf{n}}')\rangle + \langle\kappa(z,\hat{\mathbf{n}})\kappa(z',\hat{\mathbf{n}}')\rangle \\
&+ 2\langle\Delta(z,\hat{\mathbf{n}})\kappa(z',\hat{\mathbf{n}}')\rangle, \qquad (6.28)\\
&\equiv \xi^{\Delta\Delta} + \xi^{\kappa\kappa} + \xi^{\Delta\kappa} \qquad (6.29)
\end{aligned}$$

Clearly from Fig. 5.1 we observe that as a reason of statistical homogeneous together with isotropy the quantity ξ^{T} depends on the redshift of the galaxy overdensity z (due to the fact that this galaxy is closer to the observer we consider it as the brighter galaxy), also on the redshift of the convergence z' (since this galaxy is further away from the the observer we consider it as fainter galaxy) and θ denote the angle between the two galaxies. The very first term in Eq. (6.28) consist of the following contributions

$$\begin{aligned}
\xi^{\rm st}_{\Delta\Delta}(z,z',\theta) &= \langle\Delta^{\rm st}(z,\hat{\mathbf{n}})\Delta^{\rm st}(z',\hat{\mathbf{n}}')\rangle, \qquad (6.30)\\
\xi^{\rm v}_{\Delta\Delta}(z,z',\theta) &= 2\langle\Delta^{\rm st}(z,\hat{\mathbf{n}})\Delta^{\rm v}(z',\hat{\mathbf{n}}')\rangle + \langle\Delta^{\rm v}(z,\hat{\mathbf{n}})\Delta^{\rm v}(z',\hat{\mathbf{n}}')\rangle \\
&+ 2\langle\Delta^{\rm g}(z,\hat{\mathbf{n}})\Delta^{\rm v}(z',\hat{\mathbf{n}}')\rangle + 2\langle\Delta^{\rm poten}(z,\hat{\mathbf{n}})\Delta^{\rm v}(z',\hat{\mathbf{n}}')\rangle, \qquad (6.31)\\
\xi^{\rm g}_{\Delta\Delta}(z,z',\theta) &= 2\langle\Delta^{\rm st}(z,\hat{\mathbf{n}})\Delta^{\rm g}(z',\hat{\mathbf{n}}')\rangle + \langle\Delta^{\rm g}(z,\hat{\mathbf{n}})\Delta^{\rm g}(z',\hat{\mathbf{n}}')\rangle \\
&+ 2\langle\Delta^{\rm v}(z,\hat{\mathbf{n}})\Delta^{\rm g}(z',\hat{\mathbf{n}}')\rangle + 2\langle\Delta^{\rm poten}(z,\hat{\mathbf{n}})\Delta^{\rm g}(z',\hat{\mathbf{n}}')\rangle, \qquad (6.32)\\
\xi^{\rm poten}_{\Delta\Delta}(z,z',\theta) &= 2\langle\Delta^{\rm st}(z,\hat{\mathbf{n}})\Delta^{\rm poten}(z',\hat{\mathbf{n}}')\rangle + \langle\Delta^{\rm poten}(z,\hat{\mathbf{n}})\Delta^{\rm poten}(z',\hat{\mathbf{n}}')\rangle \\
&+ 2\langle\Delta^{\rm g}(z,\hat{\mathbf{n}})\Delta^{\rm poten}(z',\hat{\mathbf{n}}')\rangle + 2\langle\Delta^{\rm v}(z,\hat{\mathbf{n}})\Delta^{\rm poten}(z',\hat{\mathbf{n}}')\rangle. \qquad (6.33)
\end{aligned}$$

Note that for quantities with two different contributions such as the relation between standard and relativistic contribution should be indicated as $\Delta^{\rm st}(z',\hat{\mathbf{n}}')\Delta^{\rm v}(z,\hat{\mathbf{n}}) + \Delta^{\rm st}(z,\hat{\mathbf{n}})\Delta^{\rm v}(z',\hat{\mathbf{n}}')$ because they are asymmetric, but in above expressions we denoted this by coefficient 2 since when evaluating them they yield the same results. Also we combined dominant and subdominant contributions in order for us to see the behaviour of the total correlation function—the behavior of dominant contributions have been well studied by Camille, here we check the relevancy of the subdominant contributions. Similarly, the contributions involved in the second term and the last term of Eq. (6.28) are respectively provided in sections. C.3 and C.4.

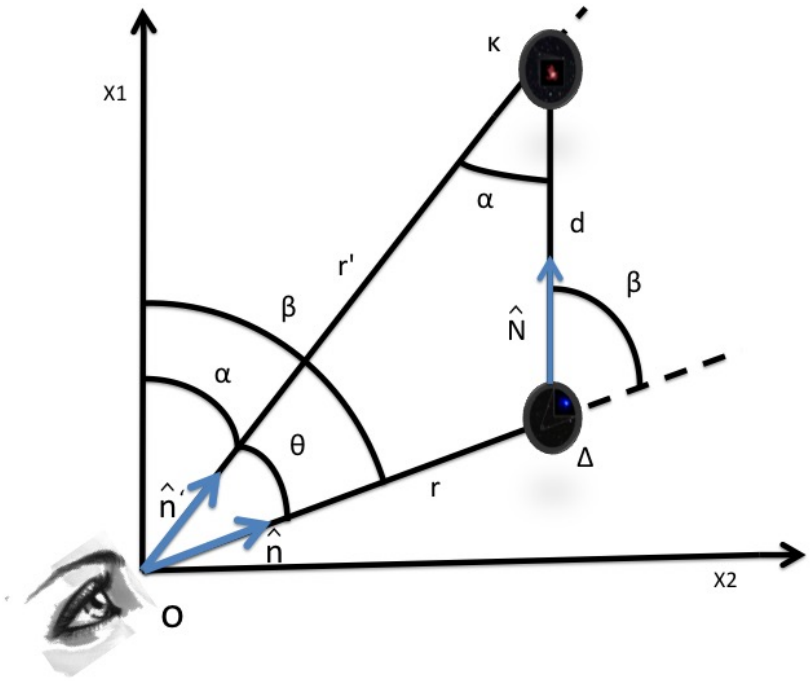

Fig. 6.1 Schematic diagram that represent the position of galaxy overdensity and convergence with respect to the observer O.

6.1.6 Standard contributions acting on $\Delta\Delta$

Lets begin by computing the standard contribution by following [8, 45, 47, 48, 50] where they introduce the coordinate system with the directions $\hat{\mathbf{n}}$, $\hat{\mathbf{n}}'$ and $\hat{\mathbf{N}}$ also $\mathbf{x}-\mathbf{x}' = d\hat{\mathbf{N}}$ which are all reconstructed to have a polar coordinate angle $\theta = \pi/2$. Additionally, they also reconstruct the azimuthal angle α and β of $\hat{\mathbf{n}}$ and $\hat{\mathbf{n}}'$, respectively (see comprehensive details from [50])(also see Fig. 6.1).

We make a note that the fully worked-out derivation of standard contribution auto-correlation function is provide in Appendix. C.2—though the next couple of subsections we will just presents the results of the correlations. Hence after some

algebra the auto-correlation function becomes

$$\begin{aligned}\xi^{st}_{\Delta\Delta} &= -\frac{8\pi^2(3\cos 2\alpha+3\cos 2\beta+2)\nu_2^3}{45}+\frac{1}{730\mathcal{H}}\Bigg(3280\pi\nu_0^2\mathcal{H}+64\Bigg\{\Bigg[\frac{5\pi}{8}\\ &+ \frac{5\pi(\cos 2\alpha\cos 2\beta+\sin 2\alpha\sin 2\beta)}{8}\Bigg]\nu_0^3+\frac{135\pi}{224}+\frac{225\pi(\cos 2\alpha+\cos 2\beta)}{224}\\ &+ \frac{25\pi(\cos 2\alpha\cos 2\beta+\sin 2\alpha\sin 2\beta)}{64}\Bigg]\nu_4^3\Bigg\}\Bigg)+\frac{1}{4}\pi\nu^3_{(I)0}+\frac{4}{3}\pi\nu^3_{(II)0}\\ &+ \frac{1}{4}\pi(1+3\cos 2\alpha)\nu^3_{(I)2}. \end{aligned} \tag{6.34}$$

Where functions $\nu^n_{(I)l}$, $\nu^3_{(II)0}$ and ν^n_l are defined as follows

$$\nu^n_l = \int dk k^n P_\nu(k,z_s,z_s')j_l(kd), \tag{6.35}$$

$$\nu^n_{(I)0} = \int dk k^n P_{\nu_I}(k,z_s,z_s')j_l(kd), \tag{6.36}$$

$$\nu^n_{(II)0} = \int dk k^n P_{\nu_{II}}(k,z_s,z_s')j_l(kd). \tag{6.37}$$

With Bessel function being denoted by j_l with $(l=0,1,3,4)$ and we define the following P_ν, P_η and P_γ in Appendix. C. We make note that Eq. (6.34) is dependent on r, r' and d, we then can rewrite the correlation function in term of r, β and d by applying the trigonometrical relationships given by [47]. To further simplify expression (6.34) we assume the flat sky approximation and by omitting the evolution between the redshift z' and z. With this information and after some algebra the standard contribution auto-correlation function yields

$$\begin{aligned}\xi^{st}_{\Delta\Delta}(r_s,d,\beta) &= \frac{32}{365\mathcal{H}}\left[\frac{5\pi}{4}\nu_0^3(d)P_0(\cos\beta)+\frac{32\pi}{35}\nu_4^3(d)P_4(\cos\beta)\right]\\ &+ 8\pi^2\nu_2^3(d)P_2(\cos\beta)+\frac{9}{2}\pi\nu_0^3(d)P_0(\cos\beta)\\ &+ \frac{\pi}{2}\nu^3_{(II)0}(d)P_0(\cos\beta)+\frac{4}{3}\pi\nu^3_{(I)0}(d)P_0(\cos\beta)\\ &+ 2\pi\nu^3_{(I)2}(d)P_2(\cos\beta). \end{aligned} \tag{6.38}$$

The standard contribution auto-correlation function Eq. (6.38) concurs with [50, 65, 66, 126, 147] at which they state that the standard contributions are strictly symmetric—consisting of monopole, quadrupole and hexadecapole, at distant observer approximation (d/r). Furthermore, this contains a dimensionless factor $(k/\mathcal{H}_0)^4$—thus this

quantity should be observable or detectable with the next generation of cosmological surveys.

6.1.7 All Doppler lensing contributions

In this subsection we calculate all Doppler lensing contributions which contribute to correlation function $\xi^{\rm v}_{\Delta\Delta}$. We follow the same methodology as shown in subsection. (6.1.6).

6.1.7.1 cross-correlation function between standard and Doppler terms

Taking into consideration the Fourier transform of the velocity and introducing the Legendre polynomial the cross-correlation function yields

$$\begin{aligned}\xi^{\text{st-v}}_{\Delta\Delta} &= \left(\frac{\mathcal{H}'(z'_s)}{\mathcal{H}^2(z'_s)}+\frac{2}{\mathcal{H}(z'_s)r(z'_s)}\right)\Bigg[-4\pi\cos\alpha\left(\nu^2_{(I)1}+\frac{6}{15}\nu^2_1-\frac{1}{10}\nu^2_3\right)\\ &- \frac{4\pi}{5}\cos\alpha\cos2\beta\left(\nu^2_1+\frac{3}{2}\nu^2_3\right)-\frac{4\pi}{5}\sin\alpha\sin2\beta\left(\nu^2_1+\nu^2_3\right)\Bigg] \qquad (6.39)\end{aligned}$$

Here we denoted the superscript (st-v) to avoid confusion in the notation, and to clearly see which terms have been correlated. Working out the expansion of the exponential factor and Fourier transform of the spherical harmonic expansion of Legendre polynomial. Then reintroducing the Legendre polynomials and adopting the assumptions given by [47] for distant observer the cross-correlation function becomes

$$\xi^{\text{st-v}}_{\Delta\Delta}(r_s,d,\beta) = \left(\frac{\mathcal{H}'}{\mathcal{H}^2}+\frac{2}{\mathcal{H}r_s}\right)\left[\left(\frac{4\pi}{3}\nu^2_1+4\pi\nu^2_{(I)1}\right)P_1(\cos\beta)-\frac{8\pi}{5}\nu^2_3P_3(\cos\beta)\right] \qquad (6.40)$$

We clearly see that the standard contributions produces the even multipoles, i.e, monopole, quadrupole, hexadecapole, this can be be seen from Eq. (6.38). While on the other hand the odd multipoles (specifically dipole and octupole) are generated by the Doppler contributions at lower order in distant observer approximation.

6.1.7.2 Doppler auto-correlation function

In this subsubsection, we compute galaxy overdensity Doppler term auto-correlation function.

$$\begin{aligned}\xi^{\text{v-v}}_{\Delta\Delta} &= \frac{2\pi}{3}\left(\frac{\mathcal{H}'}{\mathcal{H}^2}+\frac{2}{\mathcal{H}r_s}\right)\left(\frac{\mathcal{H}'(z')}{\mathcal{H}^2(z')}+\frac{2}{\mathcal{H}(z')r'_s}\right)\mathcal{H} \\ &\times \quad [2(\nu_0^1+\nu_2^1)\sin\alpha\sin\beta+2(\nu_0^1+2\nu_2^1)\cos\alpha\cos\beta] \end{aligned} \tag{6.41}$$

Working out the expansion of the exponential factor and Fourier transform of the spherical harmonic expansion of Legendre polynomial. Then reintroducing the Legendre polynomials and adopting the assumptions given by [47, 50] for distant observer the auto-correlation function becomes

$$\xi^{\text{v-v}}_{\Delta\Delta}(r_s,d,\beta) = \frac{2\pi}{3}\left(\frac{\mathcal{H}'}{\mathcal{H}^2}+\frac{2}{\mathcal{H}r_s}\right)^2\mathcal{H}\left[2\nu_0^1P_0(\cos\beta)-\frac{\nu_2^1}{2}P_2(\cos\beta)\right] \tag{6.42}$$

At distant observer approximation (d/r), we analogize Doppler auto-correlation function Eq. (6.42) to the standard auto-correlation function Eq. (6.38) and standard-Doppler contributions cross-correlation function Eq (6.40), we see that Doppler auto-correlation function is suppressed by a dimensionless factor $(\mathcal{H}_0/k)$.

6.1.7.3 cross-correlation function between lensing and Doppler terms

Here we provide the results of the cross-correlation between galaxy overdensity gravitational lensing and Doppler lensing term. Note that in this thesis we don't consider Limber approximation to evaluate any contributions which include lensing term[3]. Using the same set of steps as in previous subsubsections, in full-sky approximation the cross-correlation functions becomes

$$\begin{aligned}\xi^{\text{g-v}}_{\Delta\Delta}(r,d,\beta) &= \left(\frac{\mathcal{H}'(z'_z)}{\mathcal{H}^2(z'_s)}+\frac{2}{\mathcal{H}(z'_z)r_s(z'_s)}\right)\int\frac{d^3k}{(2\pi)^3}e^{id\mathbf{k}\cdot\hat{\mathbf{N}}}iP_1(\hat{\mathbf{k}}\cdot\hat{\mathbf{n}}) \\ &\times \quad \int_0^{r_s}dr(r_s-r)\frac{r}{r_s}\mu[1+\gamma(z_s,k)]\frac{a(z'_s)D(z_s,k)\mathcal{F}(z_s,k)}{a\mu(z'_s,k)}T^2(k). \end{aligned} \tag{6.43}$$

After some algebra, In the flat sky approximation, we express the cross-correlation between galaxy overdensity gravitational lensing and Doppler lensing term

$$\xi^{\text{g-v}}_{\Delta\Delta} = -4\pi\left(\frac{\mathcal{H}'}{\mathcal{H}^2}+\frac{2}{\mathcal{H}r_s}\right)\int_0^{r_s}dr(r_s-r)\frac{r}{r_s}\eta_1^1(d)P_1(\cos\beta). \tag{6.44}$$

[3] In work by [46, 47, 50] this approximation is being used to evaluate gravitational lensing.

Where

$$\eta_l^n = \int dk k^n P_\eta(k, z_s, z_s') j_l(kd). \tag{6.45}$$

We provide function P_η in Appendix. C.

6.1.7.4 cross-correlation function between potentials and Doppler terms

Lets now we provide the results of the cross-correlation between galaxy overdensity potentials (note that here we've combined Sachs-Wolfe, Shapiro-time delay and integrated Sachs-Wolfe terms) and Doppler lensing term. Note that in this thesis we don't consider Limber approximation to evaluate any contributions which include lensing term (note that in work by [46, 47, 50] this approximation is being used to evaluate gravitational lensing). Using the same set of steps used in previous subsubsections the of cross-correlation function becomes

$$\xi_{\Delta\Delta}^{\text{poten-v}}(r_s, d, \beta) = -4\pi\left(\frac{\mathcal{H}'}{\mathcal{H}^2} + \frac{2}{\mathcal{H} r_s}\right)\zeta_1^0(d) P_1(\cos\beta) \tag{6.46}$$

Where ζ_l^n is defined as follows

$$\zeta_l^n = \int dk k^n P_\zeta(k, z_s, z_s') j_l(kd). \tag{6.47}$$

We explicitly provide function P_ζ in Appendix. C.

6.1.8 All gravitational lensing contributions

Lets look into all contributions of gravitational lensing which are contained in the correlation function $\xi_{\Delta\Delta}^{\text{g}}$. We follow the same methodology as shown in subsection. 6.1.6. Here we won't give the show the cross-correlation function between galaxy overdensity gravitational and Doppler lensing term instead refer a reader to subsubsection. 6.1.7.3. Note that for gravitational lensing terms we considered the following expression

$$\begin{aligned}\Delta^{\text{g}} &= \int_0^{r_s} dr (r_s - r)\frac{1}{r r_s}\nabla_\perp^2(\Psi + \Phi) \\ &\approx \frac{3\Omega_{m0}\mathcal{H}_0^2}{2}\int_0^{r_s} dr (r_s - r)\frac{r}{r_s}\frac{\mu(z_s, k)}{a(z_s)}[1 + \gamma(z, k)]\Delta_m\end{aligned} \tag{6.48}$$

This approximation is due to the fact that our analysis is within sub-Hubble scale—since $\nabla_\perp^2 = r^2(\nabla^2 - \partial_r^2 - 2r^{-1}\partial_r)$ in sub-Hubble limit approximation we neglect the

last two terms to obtain $\nabla_\perp^2 \approx r^2\nabla^2$ keeping in mind the Poisson equation (6.6) and gravitational slip equation (6.7); making use of this information we get Eq. (6.48).

6.1.8.1 cross-correlation function between standard and gravitational lensing terms

We now execute the same derivation as in previous subsection for the galaxy overdensity cross-correlation function between standard and gravitational lensing term $\xi^{\text{st-g}}_{\Delta\Delta}$ which results in

$$\xi^{\text{st-g}}_{\Delta\Delta,0}(r_s,d,\beta) = \frac{4\pi}{3}\int_0^{r_s} dr(r_s-r)\frac{r}{r_s}\eta^2_{(I)0}(d)P_0(\cos\beta), \tag{6.49}$$

$$\xi^{\text{st-g}}_{\Delta\Delta,2}(r_s,d,\beta) = \frac{4\pi}{15\mathcal{H}}\int_0^{r_s} dr(r_s-r)\frac{r}{r_s}\eta^2_{2}(d)P_2(\cos\beta). \tag{6.50}$$

In the flat sky approximation, we express the cross-correlation between galaxy overdensity gravitational lensing and standard contribution term $\xi^{\text{st-g}}_{\Delta\Delta}$ as the total sum of monopole, dipole, quadrupole, octupole and hexadecapole which is given by

$$\xi^{\text{st-g}}_{\Delta\Delta} = \xi^{\text{st-g}}_{\Delta\Delta,0} + \xi^{\text{st-g}}_{\Delta\Delta,2} \tag{6.51}$$

6.1.8.2 Gravitational lensing auto-correlation function

We now execute the same derivation as in previous subsection for the galaxy overdensity gravitational lensing contributions $\xi^{\text{g-g}}_{\Delta\Delta}$ which results in

$$\xi^{\text{g-g}}_{\Delta\Delta} = \frac{4\pi}{15}\left[\int_0^{r_s} dr(r_s-r)\frac{r}{r_s}\right]^2 \eta^{-1}_{(II)0}(d)P_0(\cos\beta) \tag{6.52}$$

6.1.8.3 cross-correlation function between potentials and lensing terms

We now perform the same derivation as in previous subsection for the galaxy overdensity cross-correlation function between standard and gravitational lensing term $\xi^{\text{poten-g}}_{\Delta\Delta}$ which results in

$$\xi^{\text{poten-g}}_{\Delta\Delta,0}(r_s,d,\beta) = \frac{4\pi}{3}\int_0^{r_s} dr(r_s-r)\frac{r}{r_s}\eta^{-1}_{(III)0}(d)P_0(\cos\beta). \tag{6.53}$$

In the flat sky approximation, we express the cross-correlation between galaxy overdensity gravitational lensing and standard contribution term $\xi^{\text{poten-g}}_{\Delta\Delta}$ to be equal to

the monopole given above, which is given by

$$\xi^{\text{poten-g}}_{\Delta\Delta} = \xi^{\text{poten-g}}_{\Delta\Delta,0}. \tag{6.54}$$

6.1.9 Potentials contributions

Lets look into all contributions of gravitational lensing which are contained in the correlation function $\xi^{\text{poten}}_{\Delta\Delta}$. We follow the same methodology as shown in subsection. 6.1.6. Here we won't give the show the cross-correlation function between galaxy overdensity Doppler lensing and potentials term instead refer a reader to subsubsection. 6.1.7.4 and we also wont re-derive the cross-correlation function between potentials and gravitational lensing terms contribution subsubsection. 6.1.8.3.

6.1.9.1 cross-correlation function between standard and potentials terms

Let now provide the results for the cross-correlation function between standard and potentials terms $\xi^{\text{st-poten}}_{\Delta\Delta}$, which is given by

$$\xi^{\text{st-poten}}_{\Delta\Delta}(r_s, d, \beta) = 2\pi\left[\zeta^{1}_{(I)0}(d) + \frac{1}{3\mathcal{H}}\zeta^{1}_{0}(d)\right] + \frac{8\pi^2}{5}\zeta^{1}_{2}(d) \tag{6.55}$$

6.1.9.2 potentials auto-correlation functions

Let now provide the results for the auto-correlation function of the potentials contributions $\xi^{\text{poten-poten}}_{\Delta\Delta}$, which is given by

$$\xi^{\text{poten-poten}}_{\Delta\Delta}(r_s, d, \beta) = 2\pi\zeta^{-1}_{(II)0}(d) \tag{6.56}$$

6.1.10 Probing the Unified Dark Energy

Lets now see the behaviour of all contributions introduced above. We choose the following cosmological parameters; we adopt the present epoch matter density parameter $\Omega_{m0} = 0.308$, baryonic density parameter $\Omega_b = 0.048$ and the Hubble constant $H_0 = 67.8\,\text{km.s}^{-1}\text{Mpc}^{-1}$. We initialize all the evolution's at the photon-matter decoupling $a = 1/1 + z_d = 10^{-3}$. We adopt the primordial amplitude of power spectrum of about 2.2×10^{-9}, we adopt work by [104] to evaluate transfer function $T(k)$ and we assume similar bias evolution as shown [45, 47, 50]

6.1.10.1 Imprint of relativistic effects

Model $\mathcal{M}_I$

Here we analyze the behaviour of the clustering effects of Unified Dark Energy on galaxy overdensity—with respect to the Planck mass evolution rate α_M, which in this context is proportional to Compton wavelength parameter B_0 (where the superscript indicates evolutions today). We assume the state equation of UDE component of $w_x = -1$. The results we provide here are obtained by exploiting subsection. 6.1.4.1 into the multipoles.

In Fig. 6.2 (left panel), we show the amplitude of the octupole[4], given by Eq. (6.40); obtained by extracting each multipoles with it's appropriate Legendre polynomial, the octupole is plotted as a function of the comoving distance d at four various redshifts. We recognize that the octupole increase with an increase of the separation d and redshift at all scales.

Also in Fig. 6.2 (right panel), we show the amplitude of the octupole[5], given by Eq. (6.34); obtained by extracting each multipoles with it's appropriate Legendre polynomial, the hexadecapole is plotted as a function of the comoving distance d at four various redshifts. We see that at scale $d \lesssim 104\,\mathrm{h}^{-1}$Mpc hexadecapole increase with separation and start to decrease with an increase of separation at scale $d \gtrsim 104\,\mathrm{h}^{-1}$Mpc. Straightforward we see that octupole is 10 times greater that hexadecapole at all scales. The octupole and hexadecapole shown here are considered as the totals since their contributions appear only once in all contributions we worked out above, this is due to the fact that our correlations are strictly symmetric. We note that the standard-Doppler contribution and redshift differs strongly with due to the prefactor $(\mathcal{H}'/\mathcal{H}^2 + 2/\mathcal{H}r_s)$ decreases with redshift. Finally we hit that throughout the thesis the multipoles, i.e. monopole, dipole, quadrupole, octupole and hexacapole corresponds respectively to the quantities $d^2\xi_0^k, d^2\xi_1^k, d^2\xi_2^k, d^2\xi_3^k$ and $d^2\xi_4^k$ where superscript k denotes relation between (st,v,g,poten) evaluated in subsections. 6.1.6, 6.1.7, 6.1.8 and 6.1.9.

In Fig. 6.3 We show the behaviour and the amplitude of the monopole for different contributions; the standard-standard (blue), Doppler-Doppler (green), standard-lensing (red), lensing-lensing (magenta), potentials-lensing (cyan), standard-potentials (black) and potentials-potentials (yellow). The four different panels—top left, top right, bottom left and bottom right respectively corresponds to redshifts $z = 0.1, 0.3, 0.5$ and $z = 1$. In top left panel we see that the standard-standard contributions dominates at small

[4]This is extracted from the standard-Doppler contribution given in subsubsection. 6.1.7.1
[5]This is extracted from the standard-standard contribution given in subsection. 6.1.6

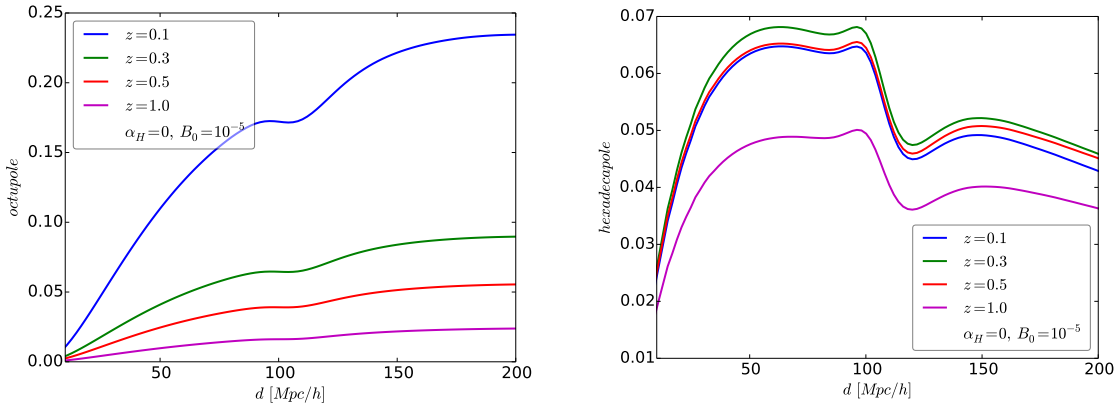

Fig. 6.2 *Left panel*: The plots of the amplitude of the octupole as function of the separation distance d, given by (6.40), for the values of the redshift $z = 0.1$ (blue), $z = 0.3$ (green), $z = 0.5$ (red) and $z = 1$ (magenta). *Right panel*: The plots of the amplitude of the hexadecapole as function of d, for four separate redshifts shown in the legend.

scale of about $d \lesssim 60\,\mathrm{h}^{-1}$Mpc but at larger scale $d \gtrsim 60\,\mathrm{h}^{-1}$Mpc standard-potentials contribution become more important. Similarly, in top right panel we see that the standard-standard contributions dominates at small scale of about $d \lesssim 60\,\mathrm{h}^{-1}$Mpc but at larger scale $d \gtrsim 60\,\mathrm{h}^{-1}$Mpc standard-potentials contribution become more relevant. Furthermore, in bottom left panel we note that at scale $d \lesssim 100\,\mathrm{h}^{-1}$Mpc standard-standard contribution is dominant but lensing-lensing contribution become very important at scale $d \gtrsim 100\,\mathrm{h}^{-1}$Mpc. And in bottom right panel we see that the standard-standard contributions dominates at small scale of about $d \lesssim 100\,\mathrm{h}^{-1}$Mpc but at larger scale $d \gtrsim 100\,\mathrm{h}^{-1}$Mpc standard-potentials contribution become more relevant. Thus, in all exhibitions the standard-standard contribution is more important than other contributions.

In Fig. 6.4 We show the behaviour and the amplitude of the dipole for different Doppler contributions; standard-Doppler contribution (blue), gravitational lensing-Doppler lensing (green) and potentials-Doppler contribution, plotted as a function of separation. The four different panels—top left, top right, bottom left and bottom right respectively corresponds to redshifts $z = 0.1, 0.3, 0.5$ and $z = 1$. At very small scales, we notice that standard-Doppler contribution blend in well with the redshift—this is because of the prefactor $(\mathcal{H}'/\mathcal{H}^2 + 2/\mathcal{H}r_s)$ decreases with redshift. But at large scales $d \gtrsim 104\,\mathrm{h}^{-1}$Mpc this contribution varies strongly with redshift. This also seems to be the case for gravitational lensing-Doppler and potentials-Doppler contributions.
Intriguingly, in Fig. 6.4 we realize that the standard-Doppler contribution for all

redshift and at all scales is more dominant than gravitational lensing-Doppler and potentials-Doppler contributions. This concurs with work by [50] that dipole provides a useful approach to probe relativistic corrections in large scale structure (LSS). Although gravitational lensing-Doppler and potentials-Doppler contributions remains subdominant, both are important in much higher redshifts.

In Fig. 6.5 we show the behaviour and the amplitude of the sum of all contributions for different multipoles; by considering standard-standard contribution, all Doppler contribution, all lensing contributions and all potentials contribution provided in in subsections. 6.1.6, 6.1.7, 6.1.8 and 6.1.9, i.e. for dipole we added standard-Doppler, lensing-Doppler and potentials-Doppler contributions $\xi^{\rm T}_{\Delta\Delta,1} = \xi^{\rm st\text{-}v}_{\Delta\Delta,1} + \xi^{\rm g\text{-}v}_{\Delta\Delta,1} + \xi^{\rm poten\text{-}v}_{\Delta\Delta,1}$. Various curves are indicted by monopole (blue), dipole (green), quadrupole (red), quadrupole (red), octupole (magenta) and hexadecapole (cyan). We realize that for redshift $z = 0.1$ (top left panel), $z = 0.3$ (top right panel) and $z = 0.5$ (bottom left panel) monopole is more influential than other multipoles. Moreover, for redshift $z = 1$ (bottom right panel) at scales $d \lesssim 100\,{\rm h}^{-1}$Mpc monopole is still dominant, but at scales $d \gtrsim 100\,{\rm h}^{-1}$Mpc hexadecapole become more important. This is due to the fact that both monopole and hexadecapole both contains standard contributions which are suppressed by the factor $(\mathcal{H}/k)^2$. We also notice that dipole and quadrupole remains always negative.

Fig. 6.6 shows the deviations of the sum of all contributions for different multipoles as ratios of their GR values, as function of separation d for four various redshifts indicated in different panels; $z = 0.1$ (top left), $z = 0.3$ (top right), $z = 0.5$ (bottom left) and $z = 1$ (bottom right). As we expected the difference depends not on separation d, the deviation to higher redshift decreases.

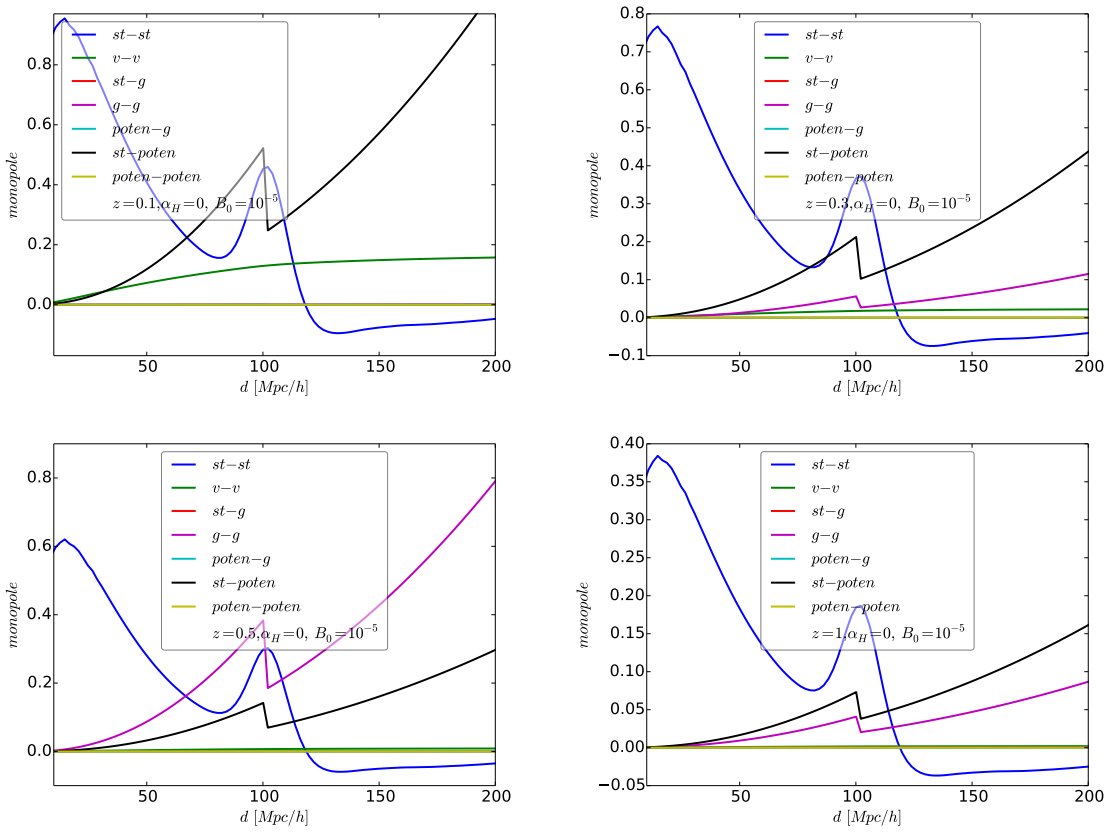

Fig. 6.3 We plot the different magnitudes of the monopoles as function of d, for the following contributions; the standard-standard (blue), Doppler-Doppler (green), standard-lensing (red), lensing-lensing (magenta), potentials-lensing (cyan), standard-potentials (black) and potentials-potentials (yellow). *Top left panel*: for redshift $z = 0.1$, *top right panel*: for redshift $z = 0.3$, *bottom left panel*: for redshift $z = 0.5$ and *bottom right panel*: for redshift $z = 1$.

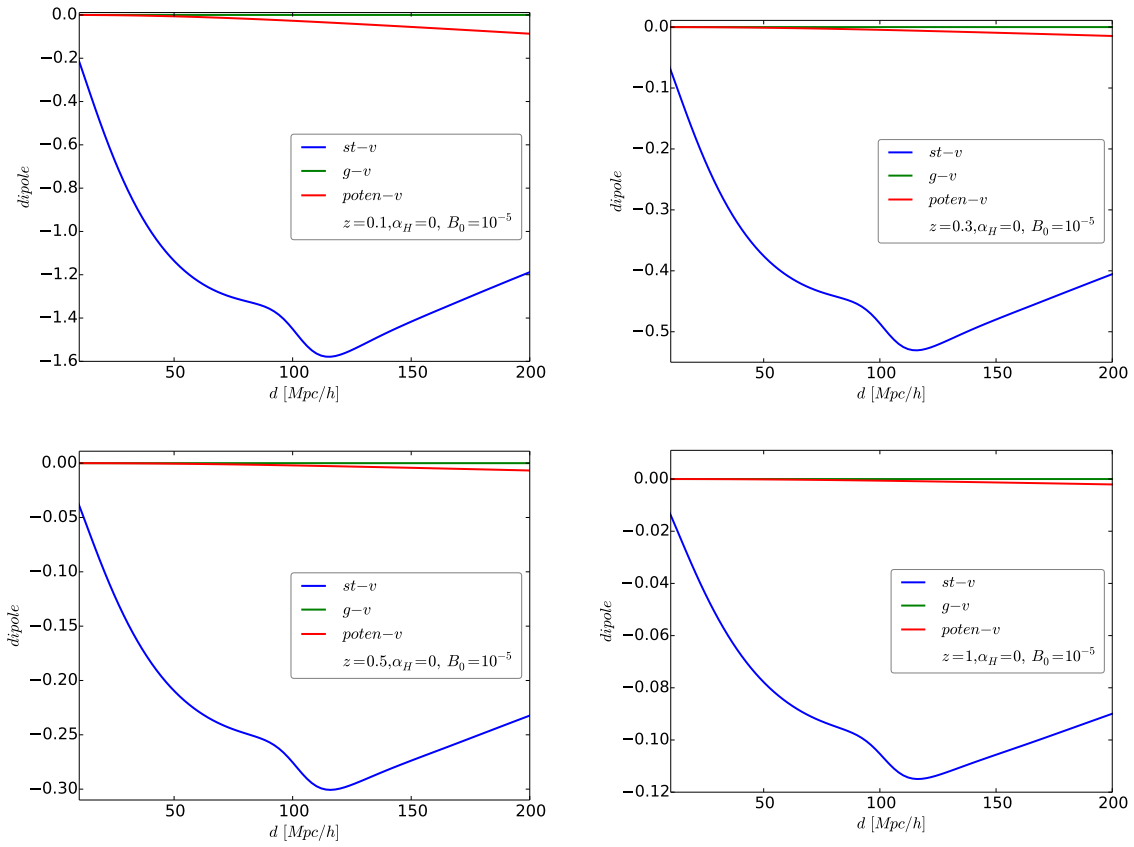

Fig. 6.4 We plot the different magnitudes of the dipoles as function of d, for the following contributions; standard-Doppler (blue), lensing-Doppler (green) and potentials-Doppler (red). *Top left panel*: for redshift $z = 0.1$, *top right panel*: for redshift $z = 0.3$, *bottom left panel*: for redshift $z = 0.5$ and *bottom right panel*: for redshift $z = 1$.

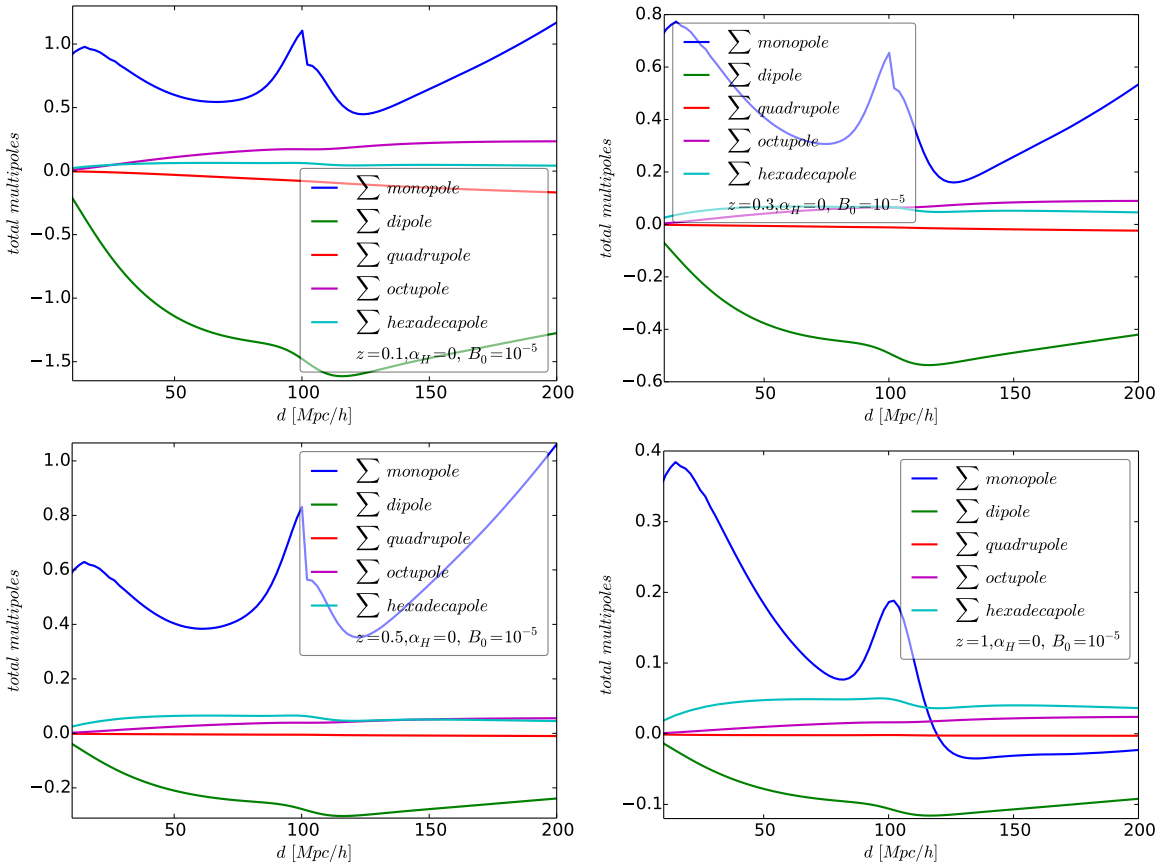

Fig. 6.5 We plot the amplitude of the sums of individual multipoles, i.e. monopole (blue), dipole (green), quadrupole (red), quadrupole (red), octupole (magenta) and hexadecapole (cyan) as function of d. *Top left panel*: for redshift $z = 0.1$, *top right panel*: for redshift $z = 0.3$, *bottom left panel*: for redshift $z = 0.5$ and *bottom right panel*: for redshift $z = 1$.

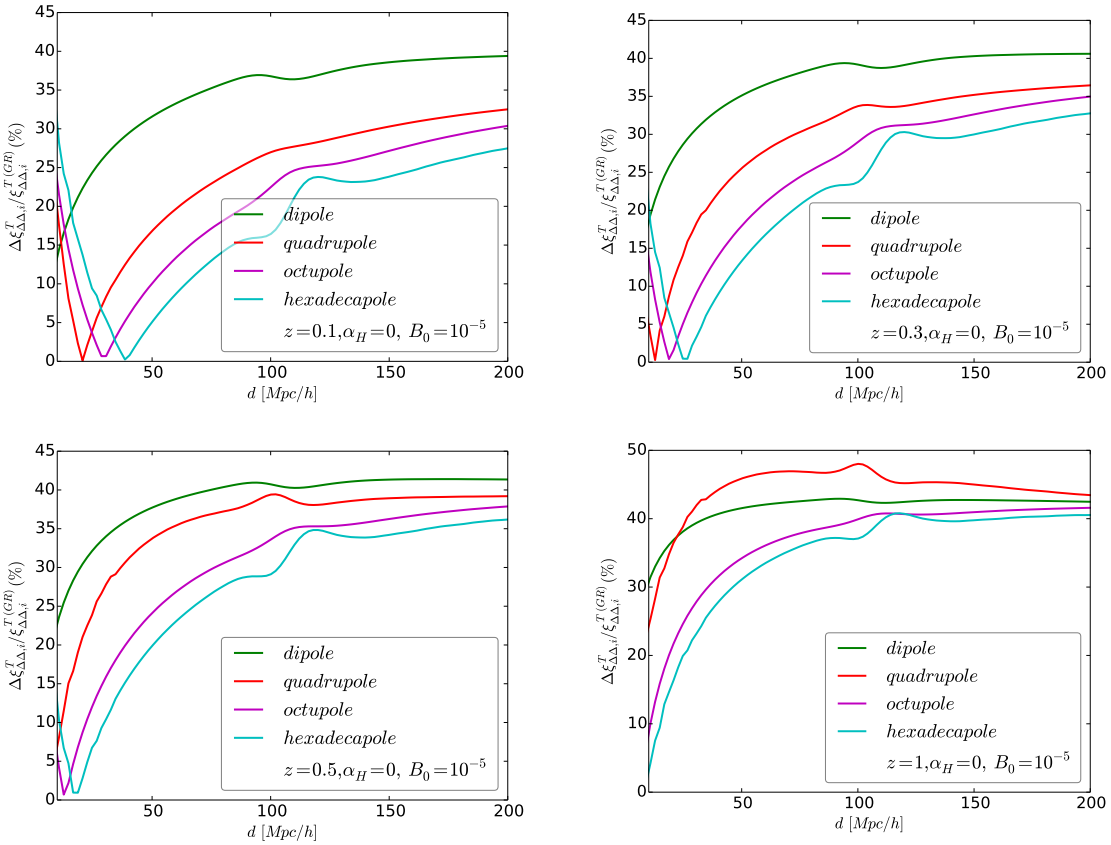

Fig. 6.6 We plot the fractional deviation of the sums of individual multipoles, i.e. dipole (green), quadrupole (red), octupole (magenta) and hexadecapole (cyan) as function of d. *Top left panel*: for redshift $z = 0.1$, *top right panel*: for redshift $z = 0.3$, *bottom left panel*: for redshift $z = 0.5$ and *bottom right panel*: for redshift $z = 1$.

Model $\mathcal{M}_{II}$

Here we explore beyond-Horndeski theories by adopting work by [217] at which the beyond-Horndeski parameter is nonzero ($\alpha_H \neq 0$), while braiding α_B depends on α_H and the tensor speed alteration is set to $\alpha_T = 0$ also the kineticity is chosen to be zero ($\alpha_K = 0$). For stability reasons we also have chosen $\Upsilon_1 = 0.5$ and $\Upsilon_2 = -0.3$ (see Table. 6.1 for more in formation on values used in this models), the results we provide here are obtained by exploiting subsection. 6.1.4.2 into the multipoles.

In Fig. 6.7 we show the behaviour and the amplitude of the sum of all contributions for different multipoles; by considering standard-standard contribution, all Doppler contribution, all lensing contributions and all potentials contribution provided in in subsections. 6.1.6, 6.1.7, 6.1.8 and 6.1.9, i.e. for dipole we added standard-Doppler, lensing-Doppler and potentials-Doppler contributions $\xi^{\rm T}_{\Delta\Delta,1} = \xi^{\rm st\text{-}v}_{\Delta\Delta,1} + \xi^{\rm g\text{-}v}_{\Delta\Delta,1} + \xi^{\rm poten\text{-}v}_{\Delta\Delta,1}$. Various curves are indicted by monopole (blue), dipole (green), quadrupole (red), quadrupole (red), octupole (magenta) and hexadecapole (cyan). We see that in top panels, the monopole is dominant at scales $d \lesssim 120\,{\rm h}^{-1}$Mpc and other multipoles remains subdominant, while on scales $d \gtrsim 120\,{\rm h}^{-1}$Mpc the octupole become more important. In bottom panels we notice that the once again the monopole is more dominant than other multipoles at scales $d \lesssim 120\,{\rm h}^{-1}$Mpc and the hexadecapole becomes more important in scales $d \gtrsim 120\,{\rm h}^{-1}$Mpc. Dipole and quadrupole remains always negative.

Fig. 6.8 shows the deviations of the sum of all contributions for different multipoles as ratios of their GR values, as function of separation d for four various redshifts indicated in different panels; $z = 0.1$ (top left), $z = 0.3$ (top right), $z = 0.5$ (bottom left) and $z = 1$ (bottom right). As we expected the difference depends not on separation d, the deviation to higher redshift decreases.

In figure. 6.9 we show the behaviour and the amplitude of the sum of all contributions for different multipoles; by considering standard-standard contribution, all Doppler contribution, all lensing contributions and all potentials contribution provided in in subsections. 6.1.6, 6.1.7, 6.1.8 and 6.1.9 plotted as function of redshift at a fixed at separation $d = 105\,{\rm h}^{-1}$Mpc considering models $\mathcal{M}_I$ (green), $\mathcal{M}_{II}$ (red) and ΛCDM (blue). We see that in top left panel at very small redshift model $\mathcal{M}_{II}$ is more important than model $\mathcal{M}_I$ and but at higher redshifts model $\mathcal{M}_I$ is dominant. In top right panel the quadrupoles, we notice that both models $\mathcal{M}_I$ and $\mathcal{M}_{II}$ are subdominant hence can be neglected. While bottom left panel indicates that the dipoles can strongly be measured by model $\mathcal{M}_I$ with $\mathcal{M}_{II}$ being subdominant. Lastly, in bottom right panel we see that octupole can strongly be measured by model $\mathcal{M}_{II}$.

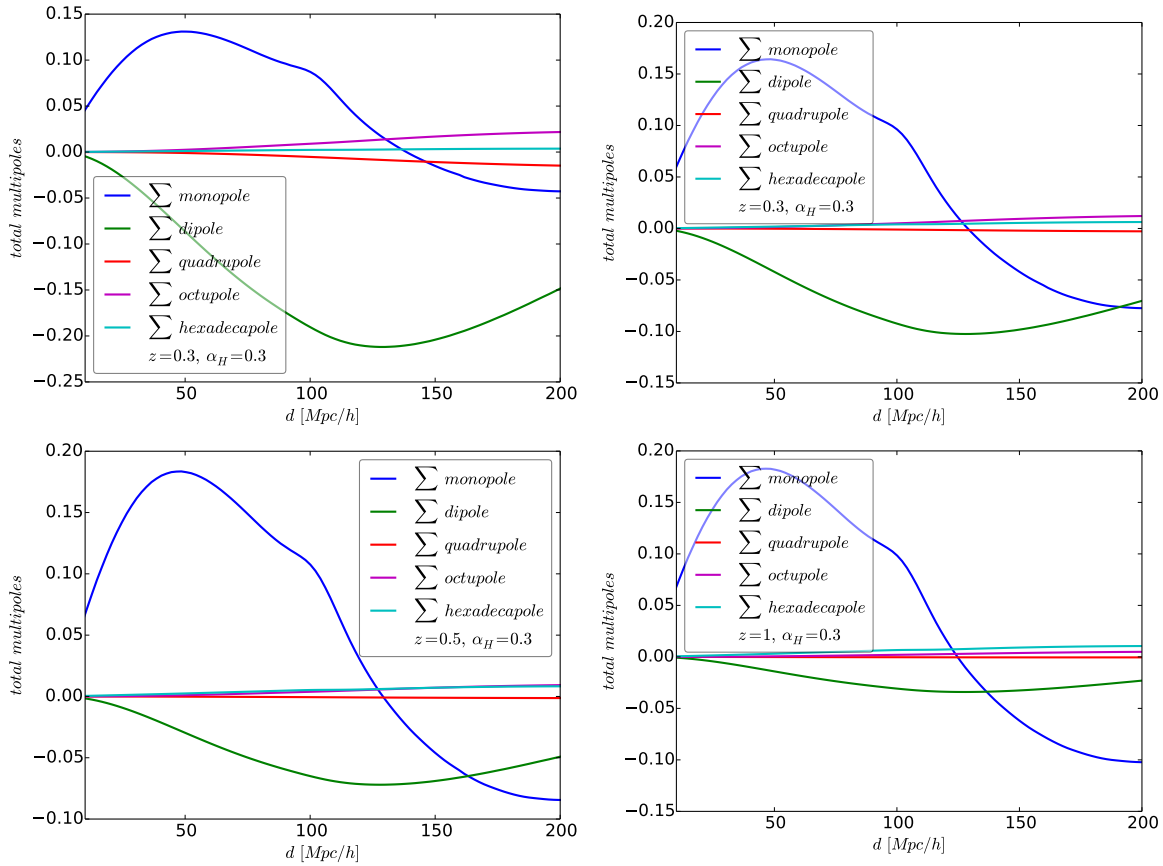

Fig. 6.7 We plot the amplitude of the sums of individual multipoles, i.e. monopole (blue), dipole (green), quadrupole (red), quadrupole (red), octupole (magenta) and hexadecapole (cyan) as function of d. *Top left panel*: for redshift $z = 0.1$, *top right panel*: for redshift $z = 0.3$, *bottom left panel*: for redshift $z = 0.5$ and *bottom right panel*: for redshift $z = 1$.

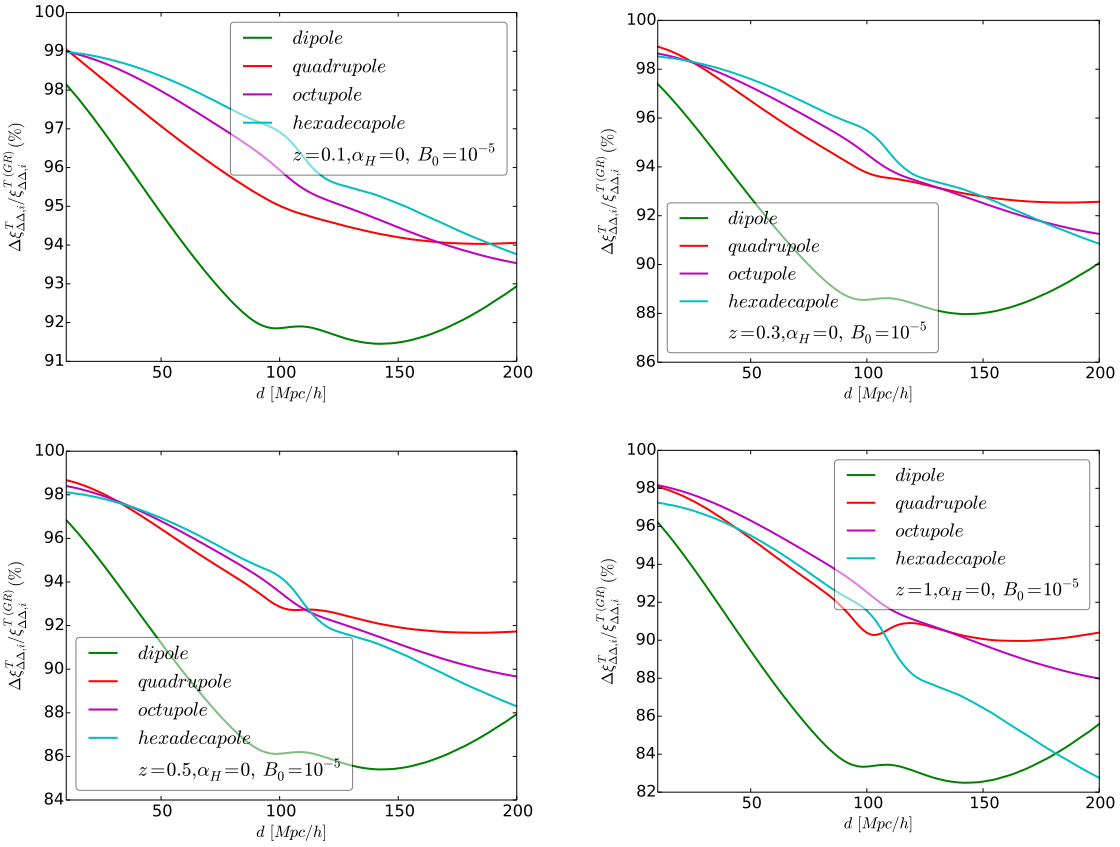

Fig. 6.8 We plot the fractional deviation of the sums of individual multipoles, i.e. dipole (green), quadrupole (red), octupole (magenta) and hexadecapole (cyan) as function of d. *Top left panel*: for redshift $z = 0.1$, *top right panel*: for redshift $z = 0.3$, *bottom left panel*: for redshift $z = 0.5$ and *bottom right panel*: for redshift $z = 1$.

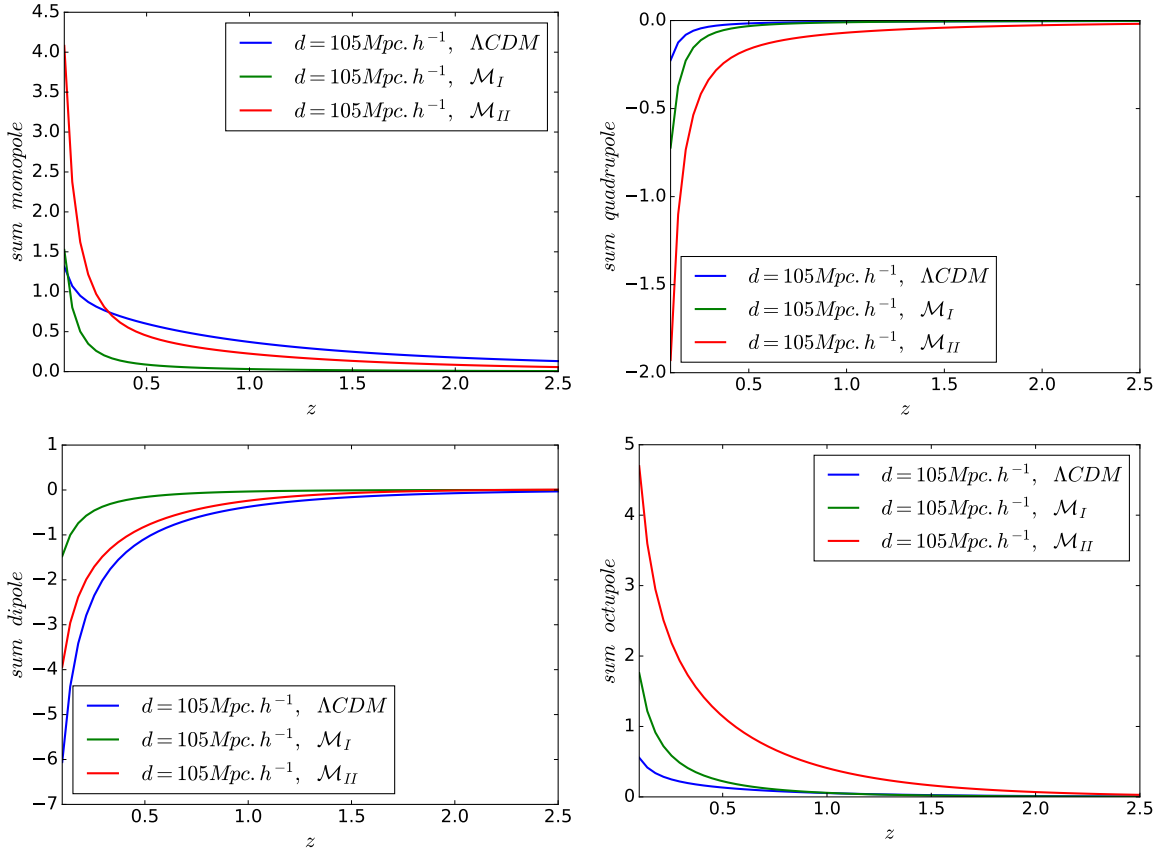

Fig. 6.9 We show the magnitude of the total of each multipoles as function of redshift at a fixed separation $d = 105\,\mathrm{h}^{-1}$Mpc considering models $\mathcal{M}_I$ (green), $\mathcal{M}_{II}$ (red) and ΛCDM (blue)

6.2 Testing General Relativity with the Doppler magnification effect

There have been many endeavors constructed seeking for some alternative models to explain the growth structure and cosmic acceleration today, without restoring back to the fine-tuned cosmological constant Λ. Build on braneworld models [163] tried to address the cosmological problem and the acceleration of the universe, few years later there was an attempt to distinguish general relativity GR from modified gravity, by developed a technique to compute the non-linear power spectrum while taking into account the mechanism that allows the model to recover GR on small scales [153]. Very recent approach by [115, 116, 119, 208] analyzing scalar-tensor theories in a broad class which is fully consistent on linear scales and not assuming quasi-static evolution this is encoded in the Horndeski Lagrangian. The studies of perturbation theory in modified gravity (MG) scenario in principle, can be classified in two different frameworks; the parametrization approach and the non-parametrization approach (see for more details [135, 251, 252]) here we consider the first approach.

In the past there existed several theories of parameterizations of MG i.e Brax-Davis-Li-Winther, Bertschinger-Zukin (B-Z) [33] and Hu-Sawicki model [26]. This type of parameterizations are satisfactory where the gravitational potential's time evolution can be neglected compared to their spatial gradient which is also know as quasi-static regime. The main motive of this thesis, is to potentially find a breakthrough on MG concept. Many Frameworks have been proposed to study different MG scenarios, such as the parameterized Post Friedmann PPF formalism including ref.[140, 141].

In this analysis, our work is part of the PPF framework work, which is generally developed to describe the three regimes of modified gravity theories and consists of a scale and time dependent function μ of the modified Poisson equation, with the function relating to the ratio of metric fluctuation γ and the effective parameter $\sum(z,k) = (1/2)(1+\gamma)\mu$. This function avoids a negative pressure to account for the late acceleration and is easy to move from a quasi-linear regime to a non-linear one where GR should be recovered.

On large-scale the peculiar velocity is a sensitive probe of the growth of structure and the nature of DE and powerful tool for constraining cosmological parameters. Although, peculiar velocities accuracy measurements are limited to lower redshift, since their uncertainties extend with distance [224]. In the past, several attempts has been carried out to estimate the distance with less uncertainties, such as Tully-Fisher and the fundamental plane methods [14, 86]—recently, [2, 139, 153, 240] developed a

σ_κ	z	SKA2 (95% CL)	DESI (95% CL)
0.3	0.15	$< 6.12 \times 10^{-6}$	$< 1.32 \times 10^{-5}$
	0.25	$< 9.70 \times 10^{-6}$	$< 2.14 \times 10^{-5}$
	0.35	$< 1.54 \times 10^{-5}$	$< 3.40 \times 10^{-5}$
	0.45	$< 2.44 \times 10^{-5}$	$< 5.30 \times 10^{-5}$
0.8	0.15	$< 1.49 \times 10^{-5}$	$< 3.44 \times 10^{-5}$
	0.25	$< 2.43 \times 10^{-5}$	$< 5.62 \times 10^{-5}$
	0.35	$< 3.91 \times 10^{-5}$	$< 8.93 \times 10^{-5}$
	0.45	$< 6.21 \times 10^{-5}$	$< 1.39 \times 10^{-4}$

Table 6.2 Marginalised constraints on the B_0 parameter, obtained at each redshift bin with two different values of σ_κ.

technique to evaluate the non-linear power spectra considering the mechanism that allows MG models to recover GR on small scales.

In this part of our work, we provide a new way to measure peculiar velocities directly at low redshifts, which allows one to utilize the cosmological GR testing[6]. In particular, we show that Doppler magnification effect will be detectable with the next generation of cosmological surveys given sufficient signal-to-noise to test GR on large scales. By evaluating the two point correlation function which will then give way for one to constrain the parameters with Fisher forecasts; which can be utilized by parametrised deviations from GR for forthcoming low-redshift galaxy surveys with DESI and SKA.

6.2.1 Growth function in PPF

In this subsection we demonstrate the key observable that enable us to differentiate between different modification of gravity models and dark energy are linear growth $f = d\ln D/d\ln a$. In general, for GR case the linear growth function only depends on time but not scale and its directly proportional to matter density through $f = \Omega_m(a)^{0.55}$, while for MG models the linear growth function depends on both scale and time which here we introduce as $f_\Psi(a,k), f_\Phi(a,k)$ and $f(a,k)$. Lets now give the explicit

[6]The apparent sizes and brightnesses of galaxies are correlated in a dipolar pattern around matter overdensities, appearing larger on their near side and smaller on their far side. The opposite effect occurs for galaxies around an underdense region. These patterns of apparent magnification induce dipole and higher multipole terms in the cross-correlation of galaxy number density fluctuations with their size/brightness

σ_κ	z	SKA2 (95% CL)	DESI (95% CL)
0.3	0.15	$< 2.82 \times 10^{-2}$	$< 6.05 \times 10^{-2}$
	0.25	$< 3.48 \times 10^{-2}$	$< 7.22 \times 10^{-2}$
	0.35	$< 4.43 \times 10^{-2}$	$< 8.80 \times 10^{-2}$
	0.45	$< 5.85 \times 10^{-2}$	$< 1.12 \times 10^{-1}$
0.8	0.15	$< 6.80 \times 10^{-2}$	$< 1.54 \times 10^{-1}$
	0.25	$< 8.12 \times 10^{-2}$	$< 1.80 \times 10^{-1}$
	0.35	$< 9.88 \times 10^{-2}$	$< 2.14 \times 10^{-1}$
	0.45	$< 1.24 \times 10^{-1}$	$< 2.66 \times 10^{-1}$

Table 6.3 Marginalised constraints on the E_{11} parameter, obtained at each redshift bin with two different values of σ_κ.

equations for $f_\Psi(a,k)$ and $f_\Phi(a,k)$ which are respectively given by

$$f_\Psi(a,k) = \frac{a\mu_d}{\mu D}\left[\mu_d\left(\mu\frac{dD}{da} + D\frac{d\mu}{da}\right) - \mu D\frac{d\mu_d}{da}\right], \tag{6.57}$$

and

$$f_\Phi(a,k) = \frac{aQ_d}{QD}\left[Q_d\left(Q\frac{dD}{da} + D\frac{dQ}{da}\right) - QD\frac{dQ_d}{da}\right]. \tag{6.58}$$

Denoting $Q \equiv \mu/\gamma$ and subscript d denotes the evaluation at decoupling.

In Fig. 6.10 We show the cosmic behaviour of the linear growth rate, which essentially serves as a test for any departures from the standard GR.In the case of modified gravity, we assume the same background evolution as ΛCDM. We have that our model deviates from ΛCDM at different epochs, i.e, $B_0 = 10^{-4}$ deviates at scales $k \lesssim 10^{-2}\,\mathrm{h/Mpc}$, while $B_0 = 10^{-5}$ deviates at scales $k \lesssim 0.04\,\mathrm{h/Mpc}$ and $B_0 = 10^{-6}$ deviates at scales $k \lesssim 0.088\,\mathrm{h/Mpc}$. However, at scales $k \gtrsim 10\,\mathrm{h/Mpc}$ all the value chosen tracks each other, at which all have deviated gradually from ΛCDM. Thus, accurate analysis of the structure growth rate as a function of time and scale might alleviate the well known standard model and alternative MG models.

In top panel of Fig. 6.11 we show the behaviour of the linear Φ and Ψ growth rate as function of scale factor, given by (6.57) and (6.58), at fixed Compton wavelength parameter $B_0 = 10^{-5}$ for different wavenumber $k = 0.05\,\mathrm{h.Mpc^{-1}}$ (dashed black), $k = 0.1\,\mathrm{h.Mpc^{-1}}$ (dashed yellow), $k = 0.15\,\mathrm{h.Mpc^{-1}}$ (dashed blue) and $k = 0.2\,\mathrm{h.Mpc^{-1}}$ (dashed green). We compare this curves with ΛCDM—which can be obtained by setting wavenumber to zero. In top left panel we have that from decoupling till late

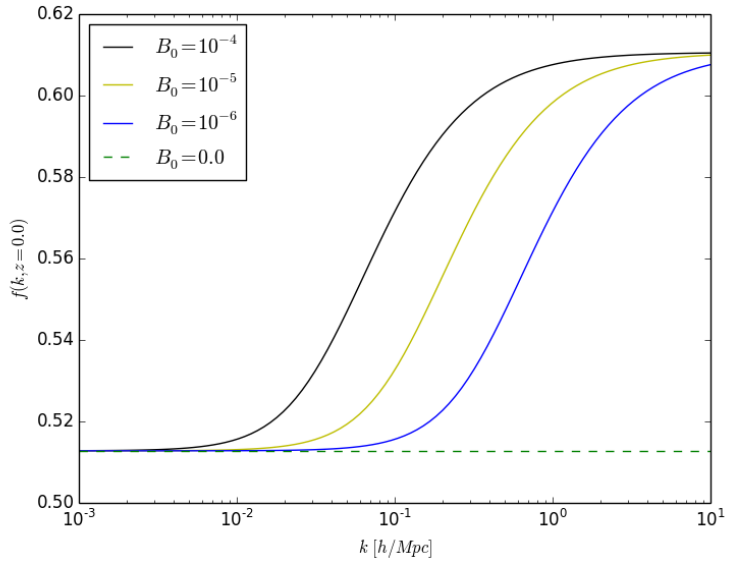

Fig. 6.10 Plots of the linear growth as function of scale for different Compton wavelength parameter $B_0 = 10^{-4}$ (solid black), $B_0 = 10^{-5}$ (solid yellow), $B_0 = 10^{-6}$ (solid blue) and $B_0 = 0$ (dashed green.)

epochs $z < 6$ the MG model track matter and start deviating away over matter on late epochs $z > 5$, but start to track matter at $z > 0$. n top right panel we have that from decoupling till late epochs $z < 6$ the MG model track matter and start deviating away under matter on late epochs $z > 5$, but start to track matter at $z > 0$. Additionally, bottom panel shows the behaviour of the linear Φ and Ψ growth rate as function of scale factor in third-dimension (3D).

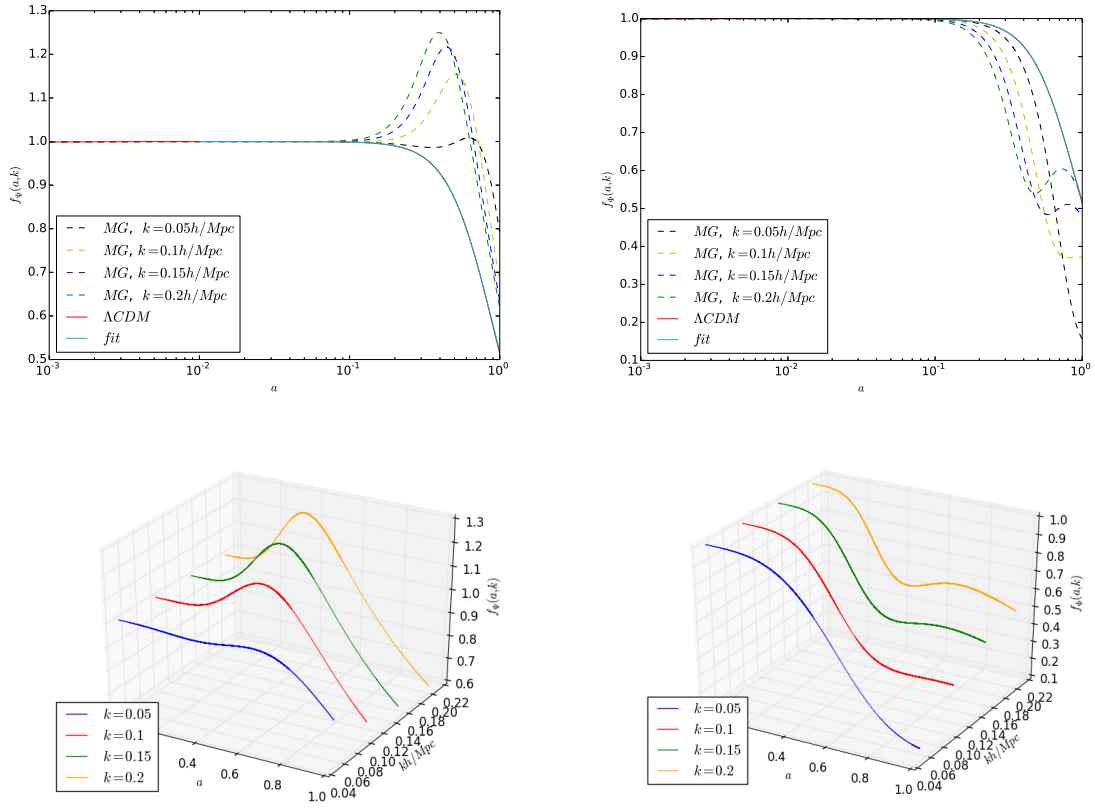

Fig. 6.11 *Top panel*: We show the linear growth rate for the two Bardeen potentials as function of scale factor, given by (6.57) and (6.58), at fixed Compton wavelength parameter $B_0 = 10^{-5}$ for different wavenumber $k = 0.05\,\mathrm{h.Mpc}^{-1}$ (dashed black), $k = 0.1\,\mathrm{h.Mpc}^{-1}$ (dashed yellow), $k = 0.15\,\mathrm{h.Mpc}^{-1}$ (dashed blue) and $k = 0.2\,\mathrm{h.Mpc}^{-1}$ (dashed green). We compare this curves with ΛCDM—which can be obtained by setting wavenumber to zero. We also add the fitting function $f = \Omega_m(a)^{6/11}$. *Bottom panel*: Shows the 3D view of the top panel

6.2.2 MG models

Lets now consider the two counterparts of the parametrisation of μ and γ to account for the test of modification of gravity on small scales. First we look into the well-worked model introduced by ref [3]

$$\mu(a,k) = 1+f_1(a)\frac{1+c_1(\lambda H/k)^2}{1+(\lambda H/k)^2} = 1+E_{11}\Omega_{DE}(a) \tag{6.59}$$

$$\gamma(a,k) = 1+f_2(a)\frac{1+c_2(\lambda H/k)^2}{1+(\lambda H/k)^2} = 1+E_{22}\Omega_{DE}(a) \tag{6.60}$$

Notice that for both expressions in the second equality we ignore scale dependence in this model, making this also an effective dark energy parametrisation. The second model we consider is an $f(R)$ model first given in [113, 140], which is given by

$$\mu(a,k) = \frac{1}{1-1.4\times10^{-8}|\lambda_1|^2a^3}\frac{1+\frac{4}{3}(\lambda k a^2)^2}{1+(\lambda k a^2)^2}, \tag{6.61}$$

$$\gamma(a,k) = \frac{1+\frac{2}{3}(\lambda k a^2)^2}{1+\frac{4}{3}(\lambda k a^2)^2}. \tag{6.62}$$

Where λ is the Compton wavelength, which we denote by $\lambda^2 = B_0c^2/(2H_0^2)$. This particular model is obtained by utilizing similar background expressions as the once provided in subsubsection. 6.1.4.1. We make a note that this two fiducial models can be considered as subclass of models introduced in section. 6.1.

6.2.3 Cross-correlation between standard galaxy overdensity and doppler convergence

In this subsection, we provide the the cross-correlation of the Doppler magnification and galaxy number count, for us to be able to constrain modified gravity using peculiar velocity. Fortunately for us this can be expressed in terms of subsubsection. 6.1.7.1 as follows

$$\xi^{\Delta\kappa_v}(r_s,d,\beta) = \frac{\left(1-\frac{1}{\mathcal{H}r_s}\right)}{\left(\frac{\mathcal{H}'}{\mathcal{H}^2}+\frac{2}{\mathcal{H}r_s}\right)}\xi^{\text{st-v}}_{\Delta\Delta}(r_s,d,\beta) \tag{6.63}$$

Where $\xi^{\text{st-v}}_{\Delta\Delta}$ is defined in Eq. 6.40. The signal of the dipole is simply given by the $P_1(\cos\beta)$. Now ref.[47] shown that the detectability of octupole, $P_3(\cos\beta)$ but this can be neglected in this case since its signal-to-noise is much lesser than that of dipole. However, the octupole can be detected by next generation of cosmological surveys.

Our two fiducial models contains specifically two parameters that we are interested in constrain, i.e. E11 and B0. In left panel of fig. 6.12 we show the magnitude of dipole at fixed redshift ($z = 0.15$) for various models, i.e. in full-sky $f(R)$ model (solid orange), scale independent model in (solid green) and ΛCDM (solid black)—in flat-sky $f(R)$ model (dashed orange), scale independent model in (dashed green) and ΛCDM (dashed black). Shaded dark grey and light grey lines represent errors when $\sigma_k = 0.3$ and $\sigma_k = 0.8$, respectively. The shaded regions show the error bars on the dipole, calculated with the specifications of a survey like SKA phase 2. We see that at very small scales $d \lesssim 20$ Mpc/h, $f(R)$ model and the scale-independent model deviates from GR. We also notice that flat-sky approximation tracks the full-sky approximation on scales $d \lesssim 80$Mpc/h and start deviating away from scales $d \gtrsim 80$ Mpc/h.

Also in Fig. 6.12 right panel we show the fractional deviation as the ratio between ΛCDM and both the $f(R)$ and scale-independent models. We see that at scales $d \lesssim 30$Mpc/h the ratio between $f(R)$ and ΛCDM decrease with an increase of redshift and separation d, while on the scales $d \gtrsim 30$Mpc/h the ratio increase with an increase of separation d but with an decrease of redshift. Clearly the scale-independent model does not depend on separation distance. As we expected, the fractional deviation decreases on higher redshifts, the suppresses deviations from GR at higher redshift are due to the function Ω_{DE}.

In Fig. 6.13 we show the fractional deviations as the ratio between ΛCDM and both the $f(R)$ and scale-independent models in the monopole and quadrupole of redshift-space-distortion (this monopole and quadrupole can be extracted from subsection. 6.1.6 by neglecting the term/s with bias). We see that the fractional deviation of $f(R)$ model, in the monopole (left panel) of RSD in comparison is much larger than that of dipole. However, this fractional deviation in the quadrupole (right panel) of RSD are much smaller than that of dipole. We also see that for scales $60\text{Mpc/h} \lesssim d \lesssim 130\text{Mpc/h}$ fractional deviation of monopoles at redshift $z = 0.15$ and $z = 0.55$ are equal. Even for monopole and quadrupole the scale-independent model does not depend on separation distance, and their magnitude does not differ much with the magnitude of the dipole.

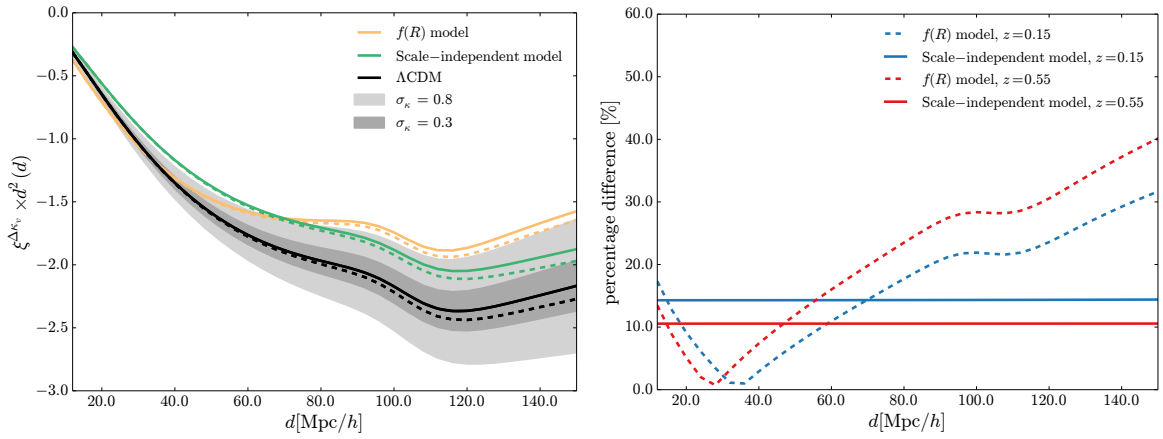

Fig. 6.12 The survey considered here is SKA2. *Left*: Full-sky dipole magnification for ΛCDM (solid black), $f(R)$ model (solid orange) and scale-independent model (solid green) against separation d at $z = 0.15$. Dashed lines are the flat-sky counterparts. Dark grey represents the errors when $\sigma_\kappa = 0.3$, light grey when $\sigma_\kappa = 0.8$. *Right:* The fractional deviation as ratio between $f(R)$ and ΛCDM is shown for $z = 0.15$ (dashed blue) and $z = 0.55$ (dashed red). Fractional deviation between the scale-independent model and ΛCDM is shown by solid lines. In both panels we have chosen $B_0 = 0.1$ and $E_{11} = 0.06$.

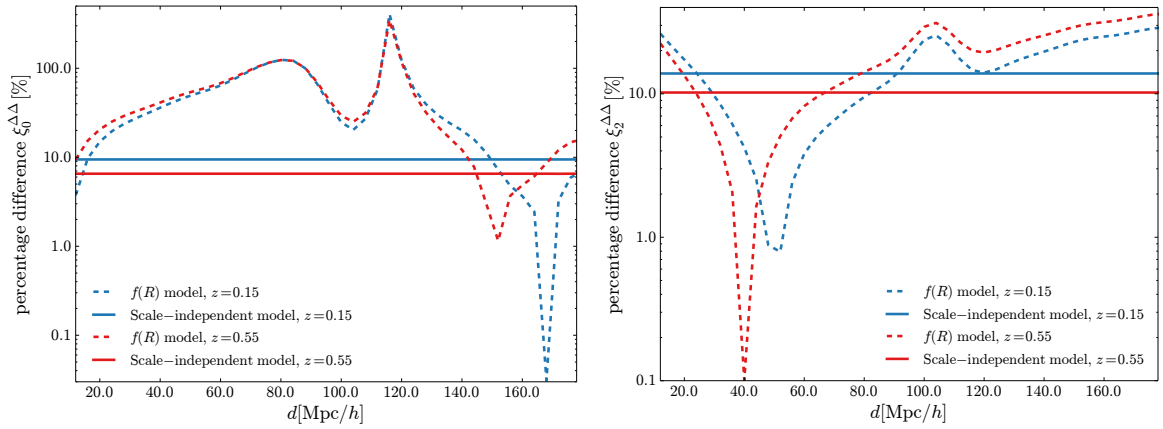

Fig. 6.13 Fractional deviation as ratio in the monopole (left) and quadrupole (right) of RSD between $f(R)$ and ΛCDM is shown for $z = 0.15$ (dashed blue) and $z = 0.55$ (dashed red). The fractional deviation between the scale-independent model and ΛCDM is shown by solid lines. In both panels we have chosen $B_0 = 0.1$ and $E_{11} = 0.06$. It is worth noting that the spike (around 120 Mpc/h) on the deviation related to the monopole is due to the fact that the two monopoles (ΛCDM and $f(R)$) change sign around that scale.

6.2.4 The next generation of cosmological surveys forecasts

Lets provide the cosmological parameter at which the predicted constraints in each models to show how–with Doppler magnification dipole deviations from GR can be constrained. We choose the following parameters h, Ω_m, Ω_b together with E_{11} for the scale-independent model and B_0 for the $f(R)$ model. The fiducial values we choose are those of ΛCDM+GR with $h = 0.68$, $\Omega_m = 0.3028$, $\Omega_b = 0.048$ and the MG parameters zero. We fix the other cosmological parameters to their fiducial value: $n_s = 0.96$, and $\sigma_8 = 0.83$.

6.2.4.1 Results

In the Fig. 6.14 left panel we show the $f(R)$ model connected constraint of Compton wavelength parameter B_0 and matter density Ω_m marginalised over the other parameters, considering DESI and SKA2 galaxy surveys. We see that the constraints are very sensitive to the value of the error on the size measurement as the difference between the choice of the two values of $\sigma_k = 0.3$ and $\sigma_k = 0.8$ by the factor of about 2. The marginalised constraints on B_0, obtained by combining the Doppler magnification dipole with Planck only, are $< 0.5 \times 10^{-3}$(95% CL) for $\sigma_k = 0.3$ and look very promising and exhibits the constraining power of SKA using the dipolar modulation as a probe.

Also in Fig. 6.14 right panel we show the scale-independent model connected constraint of function E_{11} and matter density Ω_m marginalised over the other parameters, considering DESI and SKA2 galaxy surveys. The constraints on $E_{11} < 2 \times 10^{-2}$(95% CL) provide a solid indication that Doppler magnification dipole is a powerful tool to probe departures from GR. Finally, in Fig. 6.15 we show the constraints for all parameters incorporated in $f(R)$ model and scale-independent model that we used in this work—note that for all the multipoles and forecast constraints does not involve the functions γ only functions $\mu(a, k)$, which are given in subsection. 6.2.2. In Table. 6.2 and 6.3 we show the marginalised constraints of the Compton wavelength parameter B_0 and parameter E_{11} given as function of redshift, respectively. More comprehensive details on this Fisher forecast constraints is given in [8].

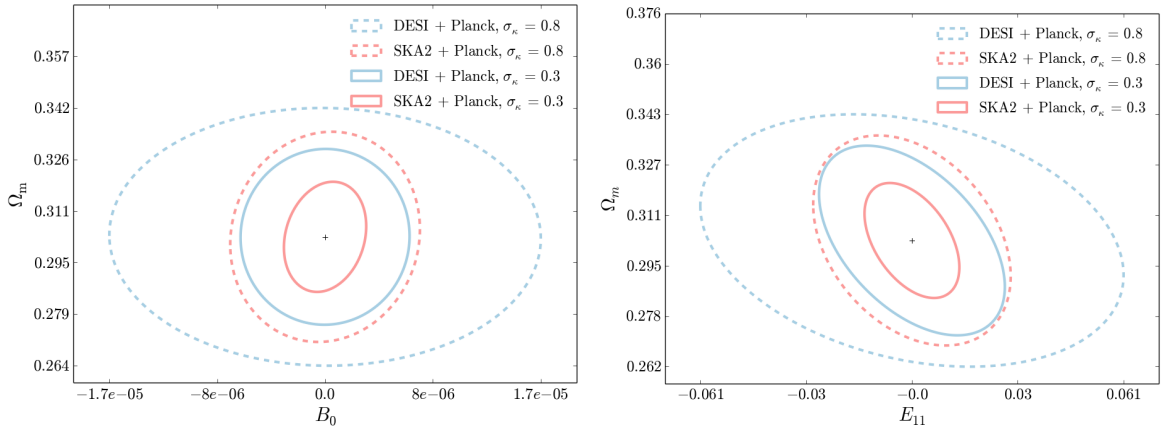

Fig. 6.14 Joint marginalised constraints $B_0 - \Omega_m$ for the $f(R)$ model (left) and $E_{11} - \Omega_m$ for the scale-independent model (right). Dashed blue and solid blue ellipses are 68% CL for the DESI survey, considering $\sigma_\kappa = 0.8$ and $\sigma_\kappa = 0.3$ respectively. Dashed red and solid red ellipses are 68% CL for the SKA2 survey, using $\sigma_\kappa = 0.8$ and $\sigma_\kappa = 0.3$ respectively.

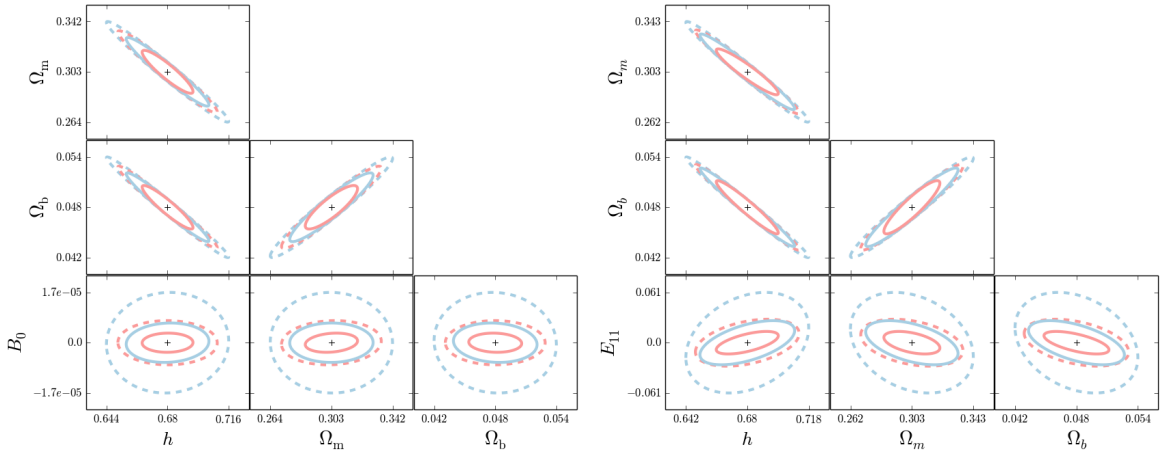

Fig. 6.15 Constraints on all the parameters in the $f(R)$ model (left) and the scale-independent model (right). All the ellipses are 68% CL. Dashed blue corresponds to DESI with $\sigma_\kappa = 0.8$, solid blue to DESI with $\sigma_\kappa = 0.3$, dashed red corresponds to SKA2 with $\sigma_\kappa = 0.8$ and solid blue to SKA with $\sigma_\kappa = 0.3$.

6.3 conclusions

In the first part of this work we presented a quasi-static approximation exploration of the linear cosmological perturbations of unified dark energy excluding the time derivatives of the metric potentials and velocity potential, quasi-static is a good approximation because it eases the computational demands of the coupled system of differential equations in the unified dark energy framework. We adopted the modified perturbed Einstein equations in the unified dark energy or effective field theory parameters formalism (for more details see [28, 116, 119]) and eliminating the scalar field and the time derivative of the modified perturbed Einstein equation provided in Appendix. D.2. We derived the energy-momentum equations and we also derived the new modified velocity potential, this newly derived equations accounts for all model classes including beyond-Horndeski models. We establish two generalized time and scale dependent free-parameters effective Newton's constant μ and gravitational slip γ which also depends on the five unified dark energy parameters.

We derived the auto-correlation functions of the galaxy overdensity, this provide a mixture of dominant term and subdominant term. One can easily express the convergence auto-correlation functions and the galaxy overdensity with convergence cross-correlation functions as function of galaxy overdensity auto-correlation functions. All this quantities are observables. Moreover, we examined the quasi-static approximation by computing the different multipoles measurements for various models of dark energy or modification of gravity, which involves the variation of the following contributions kineticity, braiding, tensor speed, beyond-Horndeski parameter and mass evolution parameter. For contributions which include the combination of the deviation between the speed of gravitational wave and the sound speed of light, braiding and kineticity being non-zero with other contributions set to zero we recover general relativity. We showed that for contributions where mass evolution parameter and braiding are non-zeros, mimics $f(R)$-gravity which we tested against general relativity and we could see that this model is closely related to ΛCDM model, we concluded this from the fractional deviation schematic. We also note that we recover general relativity when all unified general five-parameter α_i are set to zero.

Additionally, we have developed a new way that will allow us to potentially constrain in the near future the unified dark energy or effective field theory parameters μ and γ with the upcoming both wide field imaging and spectroscopic redshift surveys such as SKA, Euclid, DES, eBOSS, DESI, PFS, LSST and WFIRST.

The second part of this work we have adopted similar formalism prescribed by [47] to show the potential of probing Doppler magnification dipole, to evaluate the

deviations from general relativity, we considered the subclass models of Horndeski gravity as the toy modified gravity test in Parametrised post Friedmann formalism, this contains the extra scale and time parameter in the Poisson equation and due to the fact that dipole don't contains the gravitational slip parameter γ we've neglected this function in this case. On the horizon scales we consider this later relation is not testable.

Still in the quasistatic limit approximation within the scale of interest, we considered the cross-correlation function between standard contribution of galaxy overdensity and the Doppler convergence $\xi^{\Delta\kappa_v}$. We have compared the results of this quantity for two specified models with the general relativity scenario and we found out that their divergence with respect to general relativity is more pronounced on larger separation $d > 40$ Mpc/h in the case of scale-dependent departures from general relativity.

We note that in order to quantify any departure from GR the fiducial values of parameters in this work are those of ΛCDM. The constraints on B_0, from combining the dipole with Planck only, are comparable with the results in Fig. 6.14. We have also obtained good constraints on E_{11}. To get an idea of how sensitive to the errors on size measurement the constraints are, we have chosen optimistic and pessimistic cases with $\sigma_k = 0.3$ and $\sigma_k = 0.8$ respectively.

We have highlighted in this work that the Doppler magnification dipole, considering future surveys like SKA, has a great potential to investigate modification of gravity on sub-horizon scales.

Chapter 7

Conclusions and discussions

In modern cosmology various theoretical issues remains unresolved. However, on very small scales (Earth scales) to cosmological scales our comprehension of gravity yields remarkable accurate indication of the observations. The predominant issue among several is mapping cosmic expansion history with acceleration expansion, attribute to some sort of unknown energy density dubbed dark energy. In this thesis we addressed two related main methods to the hypothetical exploration of the dark energy. We also look into the Doppler lensing effect known as Doppler magnification, in the framework of the next generation of galaxy surveys, to explore how this probe could help strengthen the constrains on cosmological parameters and potentially provide the better understanding of the nature of dark energy.

In chapter. 2, we gave the foundation of modern cosmology; linear cosmological perturbations in FLRW Universe. We assessed the metric tensor, which describes the gravitational field space-time, we then gave the detailed derivation of the Einstein field equations, outlining the gravitational field equations and scalar, vector and tensor energy-momentum conservation equations, respectively, given in a particular gauge. Moreover, we gave a concise overview of the geodesics and their perturbations useful for derivation for galaxy number count given in Appendix. A and we also gave straight to the point standard model. We ended with the brief, basic description of the weak gravitational lensing—in order to introduced convergence which is useful in chapters. 5 and 6.

In chapter. 3, after a comprehensive discussion of the large-scale structure of our Universe, we discussed the initial conditions of the large-scale structure. Furthermore, we gave the overview on how the linear fluctuations evolves. We also described the Fourier decay of the density field; outlining the correlation function and the power spectrum. We gave a concise overview of the large-scale transfer function. We then

gave the discussion of the large-scale real and redshift space clustering. We ended with a discussion of the large-scale structure bias.

In chapter. 4, we gave the concise discussion of effective field theory, we also discussed the unitary gauge, outlining the basic background equations and scalar, vector and tensor modes perturbation equations. Lastly, we gave a brief discussion of unified dark energy parameter approach in unitary gauge—we introduced the effective field theory action which involve five free time dependent parameters $(\alpha_B, \alpha_M, \alpha_K, \alpha_T, \alpha_H)$—this are usually enough to describe the linear perturbations. This parameters describes beyond-Horndeski theories, this was firstly introduced in Horndeski theories which was represented by only four parameters $(\alpha_B, \alpha_M, \alpha_K, \alpha_T)$ [28, 116, 118, 119].

In the first method, described in chapter. 5, we analyzed the beyond-Horndeski theories approach which has been recently reconstructed in the dark energy scenario; dubbed the unified dark energy. We provided the scalar-tensor description of the interacting dark energy, we then gave the matter and unified dark energy background and perturbation relevant expressions. Furthermore, we tested numerically the unified dark energy by exploring the background and perturbations by varying the parameters α_{M0} and α_K. We also adapted the formalism by [47]; at which they analyze the two point cross-correlation dependency— between the size of the objects and the overdensity with separation distance d away from each other; which also provides the dipole and octupole signal. Moreover, we considered the standard contribution in the galaxy number count expression and Doppler contribution in the cosmic convergence expression; this is sufficient for the weak lensing effect analysis of the peculiar velocity. We calculated the two point cross-correlation in full-sky approximation and determined that it consists of the dipole and octupole terms for distance observer approximation. In order for us to determine the amplitude of the dipole and octupole, we adopted the estimator proposed by [47]—found that dipole remains one order magnitude larger than octupole in comparison, hence one can neglect octupole when analyzing the cosmological constraints for the next generation of cosmological surveys such as DES, Euclid, SKA and so on.

In the second method, described in chapter. 6, in the first part, we developed a quasi-static approximation treatment that reckon with large-scale velocity potential and the time derivatives of the metric potentials; in the linear cosmological perturbations of UDE. After acquiring the UDE formalism introduced by [28, 119], we derived the energy-momentum conservation equations from modified Einstein equation given in Appendix.D; obtained by eliminating the scalar field fluctuations, this depends on the free five parameters that describe the complete available model space, counting the

beyond-Horndeski gravity. Our work is within the framework of post parametrized Friedmann where we determined a both time and scale dependence of the effective modifications from the ΛCDM paradigm in the form of deviation in the standard Poisson equation and the difference between two Bardeen potentials and approximated the velocity potential and rate of growth of the matter density fluctuations; this sort of parametrization is useful in that it assist in recovering GR in non-linear regime. In this approach, we developed a way to potentially constrain the generalized modified gravity parameters μ and γ in the near future with the upcoming cosmological projects.

We have then computed the galaxy overdensity auto-correlation functions, convergence auto-correlation functions and the cross-correlation functions between the galaxy overdensity and the convergence, within scale of interest; taking care to include the full relativistic corrections of the observed overdensity. This three quantities are all observables. Thus, we have used similar formalism and estimator as one mentioned in chapter. 5 in order to numerically analyze the magnitude of various multipoles.

In the second part of chapter. 6, we focused on two particular sub-class of beyond-Horndeski gravity—First we considered a specialization of the model presented in [3] and secondly we considered the $f(R)$ model described by [113, 140], on the scale of interest. We then evaluated the cross-correlation function between the standard term of the galaxy overdensity and Doppler term of the convergence—which are both dominant contribution; following [47] we determined the amplitude of the dipole and octupole, then we found that dipole is one order magnitude larger than octupole and also dipole depends on bias and octupole doesn't. Therefore, we combined the dipole and *Planck*, and compared this with the results in [3] and [140]. We found very good constraints on B_0 and also on E_{11}. This approach provides the new way to get the insides of the nature of DE and gravity.

Appendix A

Detailed general relativistic evaluation of galaxy number count

A.1 Galaxy number count

In this section, we derive the expression for galaxy number count. Often galaxy number count or galaxy overdensity provide a promising probe of measuring the cosmological parameters. The intention is to infer the values of the parameters by measuring the abundance of the these large scale objects as a function of redshift at a given direction, then compare this with the theoretical predictions. Across the sky the one can measure the fluctuations in the number of galaxies. Let us assume that dN objects are observed in a redshift interval dz and solid angle. One can relate volume interval dV and the number galaxies dN by

$$\frac{dN}{dzd\Omega} \equiv \frac{dV}{dzd\Omega} \int dM \frac{dn}{dM} \tag{A.1}$$

Here n is the comoving number density at redshift z, V is the comoving the volume and M is the mass of the object. But per volume interval one can write the number galaxies counted by

$$\frac{dN}{dzd\Omega} \equiv N(z, \hat{\mathbf{n}}) \equiv nV(z, \hat{\mathbf{n}}) \tag{A.2}$$

Where $N(z, \hat{\mathbf{n}}) = nV(z, \hat{\mathbf{n}})$ is the number of object enumerated in a patch of sky centered by $(z, \hat{\mathbf{n}})$ with z being the redshift and $\hat{\mathbf{n}}$ is the direction of the observation. Then, the

galaxy number count can be given by [46, 48]

$$\Delta(z,\hat{\mathbf{n}}) \equiv \frac{N(z,\hat{\mathbf{n}}) - \bar{N}(z)}{\bar{N}(z)} \equiv \delta_z(z,\hat{\mathbf{n}}) + \delta_V(z,\hat{\mathbf{n}}) \tag{A.3}$$

Here $\delta_V(z,\hat{\mathbf{n}})$ is the volume contrast which is defined by $\delta_V(z,\hat{\mathbf{n}}) = \frac{\delta V}{\bar{V}}$ where $\frac{\delta V}{\bar{V}}$ is the fractional volume density perturbation, which can me worked out from

$$V(z,\hat{\mathbf{n}}) = \bar{V}(z) + \delta V(z,\hat{\mathbf{n}}), \qquad n(z,\hat{\mathbf{n}}) = \bar{n}(z) + \delta n(z,\hat{\mathbf{n}}), \qquad z = \bar{z} + \delta z \tag{A.4}$$

Below we provide the explicit equations for $\delta_z(z,\hat{\mathbf{n}})$ and $\delta_V(z,\hat{\mathbf{n}})$. Clearly the perturbed redshift and solid angle give rise to the volume perturbation, in addition, galaxy density $\delta(z,\hat{\mathbf{n}})$ measurement is independent of the observer gauge of choice.*redshift density perturbations* we start by computing the expression for $\delta_z(z,\hat{\mathbf{n}})$ distortion which we introduced above, this come about of this density distortion results from the redshift fluctuations at the source. To get a break though on this one need to relate the distortions in real space and redshift space, we start with the following

$$\begin{aligned} \delta_z(z,\hat{\mathbf{n}}) &= \frac{\rho(z,\hat{\mathbf{n}}) - \bar{\rho}(z)}{\bar{\rho}(z)} = \frac{\bar{\rho}(\bar{z}) + \delta\rho(z,\hat{\mathbf{n}}) - \bar{\rho}(z)}{\bar{\rho}(z)} = \frac{\bar{\rho}(z+\delta z) + \delta\rho(z,\hat{\mathbf{n}}) - \bar{\rho}(z)}{\bar{\rho}(z)} \\ &= \frac{\delta\rho(z,\hat{\mathbf{n}})}{\bar{\rho}(\bar{z})} - \frac{\delta z(z,\hat{\mathbf{n}})}{\bar{\rho}(\bar{z})}\frac{d\bar{\rho}}{dz} \end{aligned} \tag{A.5}$$

Where the $\bar{z} = 1/a - 1$ being the background redshift of FLRW Universe. Now here we need to use some of the information from the geodesics to obtain the redshift. Consider a photon which propagates from the source S which is to be seen by an observer O along the direction $\hat{\mathbf{n}}$, given that the photon can be spotted in any direction with our four-velocity u^α in the metric ds^2. In particular for a photon geodesic one can write the following

$$n^\alpha = (1 + \delta n^0, \bar{n} + \delta n^i) \tag{A.6}$$

Here $\bar{n}^0 = 1$ and $\sum_1^3 \bar{n}^i \bar{n}^i = 1$ we also have $\bar{n}^\alpha \bar{n}_\alpha = 0$. Then considering the FRW Universe with scalar perturbations in the gauge Newtonian the metric becomes

$$ds^2 = a^2[-(1+2\Psi)d\eta^2 + (1-2\Phi)\delta_{ij}dx^i dx^j] \tag{A.7}$$

Thus the geodesic equation gives

$$n^0(\lambda_O) - n^0(\lambda_s) \equiv \Phi\Big|_S^O + \Psi\Big|_S^O + \int_{\lambda_S}^{\lambda_O} \Phi'(\lambda)d\lambda + \int_{\lambda_S}^{\lambda_O} \Psi'(\lambda)d\lambda \tag{A.8}$$

and

$$n^i(\lambda_O) - n^i(\lambda_s) \equiv -\hat{\mathbf{n}}(\Phi_O - \Phi_S) - \hat{\mathbf{n}}(\Phi_O - \Phi_S) - \int_{\lambda_S}^{\lambda_O} \Phi_{,i}(\lambda)d\lambda - \int_{\lambda_S}^{\lambda_O} \Phi_{,i}(\lambda)d\lambda \tag{A.9}$$

Therefore, the redshift of the photon emitted though the gravitational field from the source S to the observer O reads

$$1+z = \frac{(g_{\alpha\beta}n^\alpha u^\beta)_S}{(g_{\alpha\beta}n^\alpha u^\beta)_O} = \frac{a_S}{a_O}(1+z) + \frac{a_S}{a_O}(1+z)\left[\delta(g_{\alpha\beta}n^\alpha u^\beta)\right]_S^O \tag{A.10}$$

Where $\frac{a_S}{a_O}(1+z) + \frac{a_S}{a_O}(1+z) \equiv 1+\bar{z}$, here $\bar{z}$ being the background redshift which relate to the perturbed reshift in this form $z = \bar{z} + \delta z$. We should notice that

$$\frac{\delta z}{1+z} = \delta(g_{\alpha\beta}n^\alpha u^\beta)\Big|_S^O \tag{A.11}$$

Making use of all above information and some couple of algebra the redshift becomes

$$1+z = (1+\bar{z})\left[1 + (\Phi + \Psi + V - \psi)\Big|_S^O - \int_S^O (\Phi' + \Psi')d\lambda\right] \tag{A.12}$$

From Eqs.(A.11) and (A.12), we can compute the following

$$\frac{\delta z}{1+\bar{z}} = -[\hat{\mathbf{n}}\cdot\mathbf{V} + \Phi + \Psi - \psi]_O^S + \int_O^{\bar{r}_s} (\Psi' + \Phi')d\bar{r} \tag{A.13}$$

Therefore, the perturbation δ_z yields,

$$\delta_z(z, \hat{\mathbf{n}}) = b\cdot\delta - 3\mathbf{V}\cdot\hat{\mathbf{n}} + 3\Psi - 3\frac{V}{k} - 3\int_{\bar{r}_S}^0 d\bar{r}(\Psi' + \Phi') \tag{A.14}$$

Volume perturbations secondly we evaluate the quantity δ_V we introduced in Eq. (A.3). Considering the infinitesimal element of the observed volume, meaning the spatial volume perceived by a source containing a metric ds[21] and 4-velocity u^μ, is expressed

[1]We work with the gauge-invariant potentials $\Phi = \phi - \mathcal{H}\sigma - \sigma'$, $\Psi = D + \frac{1}{3}\nabla^2 E + \mathcal{H}\sigma$ and $V = v + E'$ (see chapter. 2)

as [46, 48]

$$dV = \sqrt{-g}\,\epsilon_{\mu\nu\alpha\beta}u^{\mu}dx^{\nu}dx^{\alpha}dx^{\beta} \equiv V(z,\theta_O,\vartheta_O)dzd\theta_O d\vartheta_O \tag{A.15}$$

Here the total volume density V is defined by

$$V = \sqrt{-g}\,\epsilon_{\mu\nu\alpha\beta}u^{\mu}\frac{\partial x^{\nu}}{\partial z}\frac{\partial x^{\alpha}}{\partial \theta_S}\frac{\partial x^{\beta}}{\partial \vartheta_S}\left|\frac{\partial(\theta_S,\vartheta_S)}{\partial(\theta_O,\vartheta_O)}\right| \tag{A.16}$$

In a flat background FLRW Universe the geodesic are straight lines and the photon emission angles are equal i.e $\theta_S = \theta_O$ and $\vartheta_S = \vartheta_O$. Nevertherless, in a perturbed Universe these angles at the source are perturbed with respect to the observer's angles which are defined by

$$\theta_S = \theta_O + \delta\theta, \quad \vartheta_S = \vartheta_O + \delta\vartheta \tag{A.17}$$

Therefore, the determinant of Jacobian $\mathbf{J} = \frac{\partial(\theta_S,\vartheta_S)}{\partial(\theta_O,\vartheta_O)}$ yields

$$|\mathbf{J}| = 1 + \partial_\theta\delta\theta + \partial_\vartheta\delta\vartheta \tag{A.18}$$

Additionally, if we considering the determinant of metric $g_{\alpha\beta}$ introduced in subsubsection. 2.2.4.2, the metric of the determinant becomes

$$\sqrt{-g} = a^4\left(1 + \frac{1}{2}g_{\alpha\beta}\right) = a^4(1+\phi-3D) \tag{A.19}$$

Making using of the 4-velocity of the source $u = \frac{1}{a}(1-\phi, v^i)$, then we find that the non-dissipating terms of the total density volume yields

$$V = a^3(1-3D+\phi)\left[\frac{dr}{dz}r^2\sin\theta_S\,|\mathbf{J}| - \left(\frac{d\bar{r}}{d\bar{z}} + v_r\frac{d\eta}{d\bar{z}}\right)\bar{r}^2\sin\theta_O\right] \tag{A.20}$$

Where the change in comoving distance r with redshift along the photon geodesic is denoted by $\frac{dr}{dz}$, which can be expressed by [2]

$$\frac{dr}{dz} = \frac{d\bar{r}}{d\bar{z}} + \frac{d\delta r}{d\bar{z}} - \frac{d\delta z}{d\bar{z}}\frac{d\bar{r}}{d\bar{z}} \equiv \left(\frac{d\bar{r}}{d\eta} + \frac{d\delta r}{d\lambda} - \frac{d\delta z}{d\lambda}\frac{d\bar{r}}{d\bar{z}}\right)\frac{d\eta}{d\bar{z}} \tag{A.21}$$

[2]This is evaluated at linear order, which provide the distinction between redshift z and the background redshift $\bar{z}$

Note that the here we denoted $d\eta = -d\bar{r} = d\lambda$ by considering the lowest order along the photon geodesic $\frac{d\bar{r}}{d\bar{z}} = -\frac{d\eta}{d\bar{z}} = \frac{a}{\mathcal{H}}$, with this information one can re-write Eq. (A.20) as follows

$$V = \bar{V}\left[1 - 3D + (\cot\theta + \partial_\theta)\delta\theta - \mathbf{V}\cdot\hat{\mathbf{n}} + \partial_\vartheta\delta\vartheta - \frac{d\delta r}{d\lambda} + \frac{a}{\mathcal{H}}\frac{d\delta z}{d\lambda} + 2\frac{\delta r}{\bar{r}}\right] \tag{A.22}$$

Here we define $\bar{V} = a^4 r(\bar{z})^2 \mathcal{H}^{-1}\sin\theta_O$, subsequently one can hypothesizes that $d\bar{r}/dz = \bar{V}(-4 + \frac{2}{\bar{r}\mathcal{H}} + \frac{\mathcal{H}'}{\mathcal{H}^2})a$. Thus given Eq. (A.22) and $\delta_V = \frac{V-\bar{V}}{\bar{V}}$ and with some algebra the volume element becomes (see [48])

$$\begin{aligned}\delta_V &= -3D - \mathbf{V}\cdot\hat{\mathbf{n}} + (\cot\theta + \partial_\theta)\delta\theta + \partial_\vartheta\delta\vartheta + \frac{2\delta r}{r} - \frac{d\delta r}{d\lambda} + \frac{a}{\mathcal{H}}\frac{d\delta z}{d\lambda} \\ &- a\left(-4 + \frac{2}{\bar{r}\mathcal{H}} + \frac{\mathcal{H}'}{\mathcal{H}^2}\right)\delta z\end{aligned} \tag{A.23}$$

Here λ being the affine variable of the geodesic, we denote the radial perturbation along the geodesic by δr and $\delta\theta$, $\delta\vartheta$ are the transverse geodesic perturbations. In order to compute the full expression of the volume element δ_V Eq. (A.23), one need to take into consideration that the source and the source are encased by a sphere. Moreover, we require the relation of the cartesian coordinates x^μ and polar coordinates $\tilde{x}^\mu$ [95][3]. Making using of the null geodesic equation for n^μ one obtain

$$\delta x^i(\eta_S) = \int_O^{r_S} d\lambda(\delta g_{\alpha i}\bar{n}^\alpha + \delta g_{0\beta}\bar{n}^i\bar{n}^\alpha) + \frac{1}{2}\int_O^{r_S} d\lambda(r_S - r)(\delta g_{\alpha\beta,i} + \delta g'_{\alpha\beta}\bar{n}^i)\bar{n}^\alpha\bar{n}^\beta \tag{A.24}$$

Here we make a note that $\bar{r} = \lambda$, with this one can get to

$$\delta r = -\bar{n}_i\delta x^i = -\frac{1}{2}\int_O^{\bar{r}_S} d\lambda\delta g_{\alpha\beta}\bar{n}^\alpha\bar{n}^\beta = \frac{1}{2}\int_O^{\bar{r}_S} d\lambda(\Phi + \Psi) + \frac{B}{k} + \frac{1}{k^2}\left(\frac{dE}{d\lambda} - 2E'\right) \tag{A.25}$$

Now evaluating the derivative of δr can be obtained by using $d\eta = -dr = d\lambda$ and Eq. (A.25) we get the following

$$\frac{d\delta r}{d\lambda} = -(\Phi + \Psi) + \frac{dB}{kd\lambda} + \frac{1}{k^2}\left(\frac{d^2E}{d\lambda^2} - 2\frac{dE'}{d\lambda}\right) \tag{A.26}$$

[3]We define the 4-velocity displacement and spatial displacement vector of a particle in the polar coordinate are respectively given by

$$\delta\tilde{x}^\mu = \frac{\partial\tilde{x}^\mu}{\partial x^\nu}\delta x^\nu \quad \text{and} \quad \boldsymbol{\delta}\tilde{\mathbf{x}} = \delta r\mathbf{e}_r + \bar{r}\delta\theta\mathbf{e}_\theta + \bar{r}\sin\theta\delta\vartheta\mathbf{e}_\vartheta$$

Where $\{\mathbf{e}_r, \mathbf{e}_\theta, \mathbf{e}_\vartheta\}$ are the orthonormal unit vectors of the polar coordinates.

We make note that at lowest order $\bar{n}^i\partial_i X + \partial_\eta X = dX/d\lambda$ for every scalar X and $\bar{n}^i e_{\theta i} = \bar{n}^i e_{\vartheta i} = 0$ also $\bar{r}_S = \eta_O - \eta_S$. Preceding the similarly manner to Eq. (A.25), then the following yields

$$\bar{r}_S\delta\theta = \int_O^{\bar{r}_S} d\bar{r}\delta g_{i\beta}e^i_\theta\bar{n}^\beta - \frac{1}{2}\int_O^{\bar{r}_S} d\bar{r}\int_O^{\bar{r}_S} d\bar{r}(\bar{r}-\bar{r}_S)e^i_\theta\partial_i(\delta g_{\alpha\beta})\bar{n}^\alpha\bar{n}^\beta \tag{A.27}$$

$$\bar{r}_S\sin\theta\delta\vartheta = \int_O^{\bar{r}_S} d\bar{r}\delta g_{i\beta}e^i_\vartheta\bar{n}^\beta - \frac{1}{2}\int_O^{\bar{r}_S} d\bar{r}\int_O^{\bar{r}_S} d\bar{r}(\bar{r}-\bar{r}_S)e^i_\vartheta\partial_i(\delta g_{\alpha\beta})\bar{n}^\alpha\bar{n}^\beta \tag{A.28}$$

The second term in side the integral of Eqs. (A.27) and (A.27) are respectively rewritten as follows

$$\begin{aligned}\partial_i(\delta g_{\alpha\beta})e^i_\theta\bar{n}^\alpha\bar{n}^\beta &= \frac{1}{\bar{r}}[\partial_\theta(\delta g_{\alpha\beta}\bar{n}^\alpha\bar{n}^\beta) - \delta g_{\alpha\beta}\partial_\theta(\bar{n}^\alpha\bar{n}^\beta)] \\ &= \frac{1}{\bar{r}}[\partial_\theta(\delta g_{\alpha\beta}\bar{n}^\alpha\bar{n}^\beta) - 2\delta g_{\alpha i}\bar{n}^\alpha e^i_\theta]\end{aligned} \tag{A.29}$$

And

$$\begin{aligned}\partial_i(\delta g_{\alpha\beta})e^i_\vartheta\bar{n}^\alpha\bar{n}^\beta &= \frac{1}{\bar{r}\sin\theta}[\partial_\vartheta(\delta g_{\alpha\beta}\bar{n}^\alpha\bar{n}^\beta) - \delta g_{\alpha\beta}\partial_\vartheta(\bar{n}^\alpha\bar{n}^\beta)] \\ &= \frac{1}{\bar{r}\sin\theta}[\partial_\vartheta(\delta g_{\alpha\beta}\bar{n}^\alpha\bar{n}^\beta) - 2\delta g_{\alpha i}\bar{n}^\alpha e^i_\vartheta\sin\theta]\end{aligned} \tag{A.30}$$

By using the fact that $\partial_r = -\bar{n}^i\partial_i$, and after some algebra the angular contribution to the volume element yields (see comprehensive derivation [95])

$$\begin{aligned}(\cot\theta + \partial_\theta)\delta\theta + \partial_\vartheta\delta\vartheta &= -\left[\nabla^2 E - \left(\frac{d^2E}{d\lambda^2} - 2\frac{dE'}{d\lambda} + E''\right) + \frac{2}{r}\left(\frac{dE}{d\lambda} - E'\right)\right]\Bigg|_O^S \\ &+ \int_O^{\bar{r}_S} d\bar{r}(\bar{r}-\bar{r}_S)\frac{\bar{r}}{\bar{r}_S}\nabla^2_\perp(\Phi+\Psi)\end{aligned} \tag{A.31}$$

Where the angular Laplacian [15, 48, 95] $\nabla^2_\perp \equiv \nabla^2 - \partial^2_r - 2\bar{r}^{-1}\partial_r$ this is in a plane of the transverse to the line of sight. We applying Eqs. (A.25), (A.26) and (A.31) into (A.23) the following holds

$$\begin{aligned}\delta_V &= -4\mathbf{V}\cdot\hat{\mathbf{n}} - 2(\Phi+\Psi) + \int_O^{\bar{r}_S} d\bar{r}(\bar{r}-\bar{r}_S)\frac{\bar{r}}{\bar{r}_S}\nabla^2_\perp(\Phi+\Psi) + \left(3 + \frac{2}{\bar{r}_S}\right)\int_O^{\bar{r}_S} d\bar{r}(\Phi+\Psi) \\ &+ \frac{1}{\mathcal{H}}\left[\Psi' + \partial_r\Phi - \frac{d(\mathbf{V}\cdot\hat{\mathbf{n}})}{d\lambda}\right] + \left(\frac{\mathcal{H}'}{\mathcal{H}^2} + \frac{2}{\bar{r}_{S\mathcal{H}}}\right)\left[\Phi + \mathbf{V}\cdot\hat{\mathbf{n}} - \int_O^{\bar{r}_S} d\bar{r}(\Phi'+\Psi')\right]\end{aligned} \tag{A.32}$$

Combining Eq. (A.14) and (A.32) we obtain the observed overdensity of the galaxies which reads

$$\begin{aligned}\Delta(z,\hat{\mathbf{n}}) &= b\cdot\delta-\frac{1}{\mathcal{H}}\partial_r(\mathbf{V}\cdot\hat{\mathbf{n}})+\frac{1}{\mathcal{H}}\mathbf{V}'\cdot\hat{\mathbf{n}}+\left(1-\frac{\mathcal{H}'}{\mathcal{H}^2}-\frac{2}{\bar{r}\mathcal{H}}\right)\mathbf{V}\cdot\hat{\mathbf{n}}+\frac{1}{\mathcal{H}}\partial_r\Psi\\ &+ \int_O^{\bar{r}_S}d\bar{r}(\bar{r}-\bar{r}_S)\frac{\bar{r}}{\bar{r}\bar{r}_S}\nabla^2_\perp(\Phi+\Psi)+\left(\frac{\mathcal{H}'}{\mathcal{H}^2}+\frac{2}{\bar{r}\mathcal{H}}\right)\left[\Psi+\int_O^{\bar{r}_S}d\bar{r}(\Phi'+\Psi')\right]\\ &+ \int_O^{\bar{r}_S}d\bar{r}(\Phi+\Psi)+\Psi-2\Phi+\frac{1}{\mathcal{H}}\Phi'-3\frac{\mathcal{H}}{k}V \qquad (A.33)\end{aligned}$$

The break-down of each term is given in details on table. 5.1—the above expression is a consistent with (5.38).

A.2 Convergence

In this section, we provide the full general relativistic expression for convergence $\kappa(z,\hat{\mathbf{n}})$, similar to the galaxy number count $\Delta(z,\hat{\mathbf{n}})$ convergence is affected by the effects of relativistic (for more details and complete derivation see [15, 44, 45, 49, 214]) which is denoted by

$$\begin{aligned}\kappa(z,\hat{\mathbf{n}}) &= \frac{1}{2\bar{r}_S}\int_0^{\bar{r}_s}d\bar{r}(\bar{r}-\bar{r}_S)\frac{\bar{r}}{\bar{r}}\nabla^2_\perp(\Phi+\Psi)-\frac{2}{\bar{r}_s}\int_0^{\bar{r}_s}d\bar{r}\Psi\\ &+ \left(1-\frac{1}{r\mathcal{H}}\right)\left[\mathbf{V}\cdot\hat{\mathbf{n}}+\int_0^{\bar{r}_s}d\bar{r}(\Phi'+\Psi'\right]+\left(2-\frac{1}{r\mathcal{H}}\right)\Psi \qquad (A.34)\end{aligned}$$

The layout of the of each term is as follows: first term is the standard gravitational lensing, this is followed by the Shapiro time-delay, the third term is the combination of Doppler lensing and Integrated Sachs-Wolfe, and the very lastly term is known as Sachs-Wolfe.

Appendix B

Miscellanea

In this section of the appendix, we provide important formulae and some results which we have used in this thesis.

B.1 Hankel transform of correlation function and power spectra

We start by re-introducing the expression that relate power spectra and correlation function we introduced in section. 3.4.2 by Eq. (3.22) which here becomes a directional dependent function

$$P(\mathbf{k}) = \int d^3\mathbf{r}\, e^{-i\mathbf{k}\cdot\mathbf{r}}\xi(\mathbf{r}) \tag{B.1}$$

The multipoles coefficients of power spectra and correlation function can be related by making use of Rayleigh's expansion which is defined as

$$e^{-i\mathbf{k}\cdot\mathbf{r}} = 4\pi \sum_{LM} i^{-L} j_L(kr) Y^*_{LM}(\hat{\mathbf{k}}) Y_{LM}(\hat{\mathbf{N}}) \tag{B.2}$$

Hence one can write multipoles coefficients of power spectra and correlation function in spherical harmonic as (see [1] for more details)

$$P_L(k) = 4\pi i^{-L} \int_0^\infty r^2 dr j_L(kr)\xi_L(r), \quad \xi_L(r) = \frac{4\pi}{i^L}\int_0^\infty \frac{k^2 dk}{(2\pi)^3} P_{L.}(k) j_L(kr) \tag{B.3}$$

Where the imaginary units is denoted by i, index L specify the multipoles and $j_L(kr)$ being the spherical Bessel function which have provided in section. B.3. Due the

fact that we are dealing with 2-D clustering quantities we then can expect to write multipoles as

$$P_L(\mathbf{k}) = \sum_L \mathcal{P}_L(\mu) P_L(k), \quad \xi_L(\mathbf{r}) = \sum_L \mathcal{P}_L(\mu)\xi_L(r) \tag{B.4}$$

B.2 Clebsch-Gordan coefficients

The Clebsch-Gordan coefficients can be evaluated from the integral of three spherical harmonics over the sphere which are given as follows [98]

$$\mathcal{C}^{L_1\,L_2\,L_3}_{m_1\,m_2\,m_3} = \int d\Omega_{\hat{\mathbf{k}}} Y^*_{LM} Y^*_{2m}(\hat{\mathbf{k}}) Y^*_{1m'}(\hat{\mathbf{k}}) \tag{B.5}$$

$$= \sqrt{\frac{(2L_1+1)(2L_2+1)(2L_3+1)}{4\pi}} \begin{pmatrix} L_1 & L_2 & L_3 \\ 0 & 0 & 0 \end{pmatrix} \begin{pmatrix} L_1 & L_2 & L_3 \\ m_1 & m_2 & m_3 \end{pmatrix} \tag{B.6}$$

Where 3J-Wigner symbols are represented by 3×2 matrices. The Clebsch-Gordan coefficients are identically non-zero whenever the following properties are satisfied

$$|L_1 - L_2| \leq L_3 \leq L_1 + L_2, \quad m_1 + m_2 + m_3 = 0 \tag{B.7}$$

In addition, we need to also give a scenario where L and M are enforced by spherical harmonic to zero and together with two spherical harmonic which are respectively given by

$$\int d\Omega_{\hat{\mathbf{k}}} Y^*_{LM}(\hat{\mathbf{k}}) = \sqrt{4\pi}\delta_{L0}\delta_{M0} \tag{B.8}$$

And

$$\int d\Omega_{\hat{\mathbf{k}}} Y^*_{LM} Y^*_{2m}(\hat{\mathbf{k}}) = \delta_{L2}\delta_{Mm} \tag{B.9}$$

B.3 Spherical Bessel function

Generally spherical Bessel functions can be written as

$$j_L(x) = x^L \left(-\frac{1}{x}\frac{d}{dx} \right)^l \frac{\sin((x)}{x} \tag{B.10}$$

Where $x = kr$ and now we can explicitly write first five Bessel functions can easily calculated to yield

$$j_0(x) = \frac{\sin(x)}{x} \tag{B.11}$$

$$j_1(x) = \frac{\sin(x)}{x^2} - \frac{\cos(x)}{x} \tag{B.12}$$

$$j_2(x) = \frac{3\sin(x)}{x^3} - \frac{\sin(x)}{x} - \frac{3\cos(x)}{x^3} \tag{B.13}$$

$$j_3(x) = \left(1 - \frac{15}{x^2}\right)\frac{\cos(x)}{x} - \left(10 - \frac{105}{x^2}\right)\frac{\sin(x)}{x^2} \tag{B.14}$$

$$j_4(x) = \left[1 - \frac{\left(45 - \frac{105}{x^2}\right)}{x^2}\right]\frac{\sin(x)}{x} + \left(10 - \frac{105}{x^2}\right)\frac{\cos(x)}{x^2} \tag{B.15}$$

Where throughout the thesis we adopt $L \in \{0,1,2,3,4\}$.

B.4 Legendre polynomial

Form the ordinary differential equation [1] with some algebra we get the following solution

$$P_L(x) = \frac{1}{2^L L!}\frac{d^L}{dx^L}(x^2-1)^L \tag{B.17}$$

Then the first five Legendre polynomials are given by

$$P_0(x) = 1 \tag{B.18}$$

$$P_1(x) = x \tag{B.19}$$

$$P_2(x) = \frac{(3x^2-1)}{2} \tag{B.20}$$

$$P_3(x) = \frac{(5x^3-3x)}{2} \tag{B.21}$$

$$P_4(x) = \frac{(35x^4-30x^2+3)}{8} \tag{B.22}$$

[1]

$$\frac{d}{dx}\left[(1-x^2)\frac{P_L(x)}{dx}\right] + L(L+1)P_L(x) \tag{B.16}$$

Appendix C

Multipole expansions

DEFINING FUNCTIONS USED IN SUBSECTION. 6.1.5.
Here we define the following

$$P_{\nu}(k,z_s,z_s') = \frac{1}{(2\pi)^3}\frac{4}{9\Omega_{m0}^2\mathcal{H}_0^4}\frac{\mathcal{F}(z_s,k)\mathcal{F}(z_s',k)}{\mathcal{H}\mu(z_s,k)\mu(z_s',k)}\left(\frac{k}{k_\lambda}\right)^{n_s-1}T^2(k), \quad (C.1)$$

$$P_{\nu_{(I)}}(k,z_s,z_s') = \frac{1}{(2\pi)^3}\frac{4}{9\Omega_{m0}^2\mathcal{H}_0^4}\frac{b(z_s)D(z,k)\mathcal{F}(z_s',k)}{\mu(z_s,k)\mu(z_s',k)}\left(\frac{k}{k_\lambda}\right)^{n_s-1}T^2(k), \quad (C.2)$$

$$P_{\nu_{(II)}}(k,z_s,z_s') = \frac{1}{(2\pi)^3}\frac{4}{9\Omega_{m0}^2\mathcal{H}_0^4}\frac{bD(z_s,k)b(z_s')D(z_s',k)}{\mu(z_s,k)\mu(z_s',k)}\left(\frac{k}{k_\lambda}\right)^{n_s-1}T^2(k). \quad (C.3)$$

We also define

$$P_{\eta}(k,z_s,z_s') = \frac{a(z_s')\mu(z_s')}{(2\pi)^3}\frac{\mathcal{F}(z_s,k)D(z_s',k)}{a\mu(z_s,k)}[1+\gamma(z_s,k)]\left(\frac{k}{k_\lambda}\right)^{n_s-1}T^2(k), \quad (C.4)$$

$$P_{\eta_{(I)}}(k,z_s,z_s') = \frac{9\Omega_{m0}^2\mathcal{H}_0^4\mu(z_s',k)}{4a(2\pi)^3}\frac{bD(z_s,k)D(z_s',k)}{\mu(z_s,k)}[1+\gamma(z_s',k)] \times \left(\frac{k}{k_\lambda}\right)^{n_s-1}T^2(k), \quad (C.5)$$

$$P_{\eta_{(II)}}(k,z_s,z_s') = \frac{9\Omega_{m0}^2\mathcal{H}_0^4\mu(z_s',k)}{4aa(z_s')(2\pi)^3}D(z,k)D(z',k)[1+\gamma(z',k)] \times [1+\gamma(z_s,k)]\left(\frac{k}{k_\lambda}\right)^{n_s-1}T^2(k). \quad (C.6)$$

And

$$P_\zeta(k,z_s,z_s') = \frac{1}{(2\pi)^3}\frac{2}{3\Omega_{m0}\mathcal{H}_0^2\mu(z_s,k)}\mathcal{F}(z_s,k)\mathcal{L}(z_s,k)\left(\frac{k}{k_\lambda}\right)^{n_s-1}T^2(k), \quad \text{(C.7)}$$

$$\tilde{P}_\zeta(k,z_s,z_s') = \frac{1}{(2\pi)^3}\frac{2}{3\Omega_{m0}\mathcal{H}_0^2\mu(z_s,k)}\mathcal{F}(z_s,k)\mathcal{M}(z_s,k)\left(\frac{k}{k_\lambda}\right)^{n_s-1}T^2(k). \quad \text{(C.8)}$$

Where $\mathcal{L}$ and $\mathcal{M}$ are respectively defined by

$$\begin{aligned}\mathcal{L} &= \left(\frac{\mathcal{H}'}{\mathcal{H}^2}+\frac{2}{r_s\mathcal{H}}\right)\int_0^{r_s}dr\{\gamma'(z_s,k)+[1+\gamma(z_s,k)]D'(z_s,k)\}\\ &+ \frac{2}{r_s}\int_0^{r_s}dr[1+\gamma(z_s,k)]D(z_s,k)+\frac{1}{\mathcal{H}}[\gamma'(z_s,k)D(z_s,k)+\gamma(z_s,k)D'(z_s,k)]\\ &- 2\gamma(z_s,k)D(z_s,k)-\frac{2a\mathcal{H}}{\Omega_{m0}\mathcal{H}_0^2\mu(z_s,k)}\mathcal{F}(z_s,k)+\left(1+\frac{\mathcal{H}'}{\mathcal{H}^2}+\frac{2}{r_s\mathcal{H}}\right)D(z_s,k), \quad \text{(C.9)}\\ \mathcal{M} &= \left(1-\frac{2}{r_s\mathcal{H}}\right)\int_0^{r_s}dr\{\gamma'(z_s,k)+[1+\gamma(z_s,k)]D'(z_s,k)\},\\ &- -\frac{2}{r_s}\int_0^{r_s}dr\,D(z_s,k)+\left(2-\frac{1}{r_s\mathcal{H}}\right)D(z_s,k). \quad \text{(C.10)}\end{aligned}$$

And

$$P_{\zeta_{(I)}}(k,z_s,z_s') = \frac{1}{(2\pi)^3}\frac{2b}{3\Omega_{m0}\mathcal{H}_0^2\mu(z_s,k)}D(z_s,k)\mathcal{L}(z_s,k)\left(\frac{k}{k_\lambda}\right)^{n_s-1}T^2(k), \quad \text{(C.11)}$$

$$P_{\zeta_{(II)}}(k,z_s,z_s') = \frac{1}{(2\pi)^3}\mathcal{L}(z_s,k)\mathcal{L}(z_s',k)\left(\frac{k}{k_\lambda}\right)^{n_s-1}T^2(k). \quad \text{(C.12)}$$

Additionally we provide the following

$$P_{\eta_{(III)}}(k,z_s,z_s') = \frac{3\Omega_{m0}\mathcal{H}_0^2\mu}{2a(2\pi)^3}[1+\gamma(z,k)]D(z_s,k)\mathcal{L}(z_s',k)\left(\frac{k}{k_\lambda}\right)^{n_s-1}T^2(k), \quad \text{(C.13)}$$

C.1 Various contributions

Here we provide contributions contained in Eq.(6.28) last two terms which are respectively denoted as follows

$$\begin{aligned}
\xi^{\rm v}_{\kappa\kappa}(z,z',\theta) &= \langle\kappa^{\rm v}(z,\hat{\mathbf{n}})\kappa^{\rm v}(z',\hat{\mathbf{n}}')\rangle + 2\langle\kappa^{\rm g}(z,\hat{\mathbf{n}})\kappa^{\rm v}(z',\hat{\mathbf{n}}')\rangle \\
&+ 2\langle\kappa^{\rm poten}(z,\hat{\mathbf{n}})\kappa^{\rm v}(z',\hat{\mathbf{n}}')\rangle, \qquad \text{(C.14)} \\
\xi^{\rm g}_{\kappa\kappa}(z,z',\theta) &= \langle\kappa^{\rm g}(z,\hat{\mathbf{n}})\kappa^{\rm g}(z',\hat{\mathbf{n}}')\rangle + 2\langle\kappa^{\rm v}(z,\hat{\mathbf{n}})\kappa^{\rm g}(z',\hat{\mathbf{n}}')\rangle \\
&+ 2\langle\kappa^{\rm poten}(z,\hat{\mathbf{n}})\kappa^{\rm g}(z',\hat{\mathbf{n}}')\rangle, \qquad \text{(C.15)} \\
\xi^{\rm poten}_{\kappa\kappa}(z,z',\theta) &= \langle\kappa^{\rm poten}(z,\hat{\mathbf{n}})\kappa^{\rm poten}(z',\hat{\mathbf{n}}')\rangle + 2\langle\kappa^{\rm g}(z,\hat{\mathbf{n}})\kappa^{\rm poten}(z',\hat{\mathbf{n}}')\rangle \\
&+ 2\langle\kappa^{\rm v}(z,\hat{\mathbf{n}})\kappa^{\rm poten}(z',\hat{\mathbf{n}}')\rangle. \qquad \text{(C.16)}
\end{aligned}$$

And

$$\begin{aligned}
\xi^{\rm v}_{\Delta\kappa}(z,z',\theta) &= 2\langle\Delta^{\rm st}(z,\hat{\mathbf{n}})\kappa^{\rm v}(z',\hat{\mathbf{n}}')\rangle + \langle\Delta^{\rm v}(z,\hat{\mathbf{n}})\kappa^{\rm v}(z',\hat{\mathbf{n}}')\rangle \\
&+ 2\langle\Delta^{\rm g}(z,\hat{\mathbf{n}})\kappa^{\rm v}(z',\hat{\mathbf{n}}')\rangle + 2\langle\Delta^{\rm poten}(z,\hat{\mathbf{n}})\kappa^{\rm v}(z',\hat{\mathbf{n}}')\rangle, \qquad \text{(C.17)} \\
\xi^{\rm g}_{\Delta\kappa}(z,z',\theta) &= 2\langle\Delta^{\rm st}(z,\hat{\mathbf{n}})\kappa^{\rm g}(z',\hat{\mathbf{n}}')\rangle + \langle\Delta^{\rm g}(z,\hat{\mathbf{n}})\kappa^{\rm g}(z',\hat{\mathbf{n}}')\rangle \\
&+ 2\langle\Delta^{\rm v}(z,\hat{\mathbf{n}})\kappa^{\rm g}(z',\hat{\mathbf{n}}')\rangle + 2\langle\Delta^{\rm poten}(z,\hat{\mathbf{n}})\kappa^{\rm g}(z',\hat{\mathbf{n}}')\rangle, \qquad \text{(C.18)} \\
\xi^{\rm poten}_{\Delta\kappa}(z,z',\theta) &= 2\langle\Delta^{\rm st}(z,\hat{\mathbf{n}})\kappa^{\rm poten}(z',\hat{\mathbf{n}}')\rangle + \langle\Delta^{\rm poten}(z,\hat{\mathbf{n}})\kappa^{\rm poten}(z',\hat{\mathbf{n}}')\rangle \\
&+ 2\langle\Delta^{\rm v}(z,\hat{\mathbf{n}})\kappa^{\rm poten}(z',\hat{\mathbf{n}}')\rangle + 2\langle\Delta^{\rm g}(z,\hat{\mathbf{n}})\kappa^{\rm poten}(z',\hat{\mathbf{n}}')\rangle, \qquad \text{(C.19)} \\
& \qquad \text{(C.20)}
\end{aligned}$$

C.2 Comprehensive derivation of standard contribution auto correlation

In this section, we derive the galaxy overdensity standard term auto-correlation, we are interested in computing the following quantity

$$\xi^{\rm st}_{\Delta\Delta} = \langle\Delta(z,\hat{\mathbf{n}})\Delta(z',\hat{\mathbf{n}}')\rangle \qquad \text{(C.21)}$$

We can expand Eq. (C.21) as follows

$$\begin{aligned}
\xi^{\rm st}_{\Delta\Delta} &= b(z)b(z')\langle\Delta_m(z,\hat{\mathbf{n}})\Delta(z',\hat{\mathbf{n}}') + \frac{1}{\mathcal{H}(z)\mathcal{H}(z')}\langle\partial_r(\mathbf{V}\cdot\hat{\mathbf{n}})\partial_r(\mathbf{V}'\cdot\hat{\mathbf{n}}')\rangle \\
&- \frac{2b}{\mathcal{H}(z')}\langle\Delta_m(z,\hat{\mathbf{n}})\partial_r(z',\hat{\mathbf{n}}')\rangle \qquad \text{(C.22)}
\end{aligned}$$

The best way to evaluate the above quantity is to compute each term separately. We make use of the Fourier transform convention

$$f(\mathbf{x},\eta) = \int \frac{d^3k}{(2\pi)^3} e^{i\mathbf{kx}} f(\mathbf{k},\eta) \tag{C.23}$$

We can then express auto-correlation function of the first term in Fourier space as

$$\begin{aligned}\xi^{\mathrm{st}[1]}_{\Delta\Delta}(r,r',\theta) &= \frac{4bb(z')}{9\Omega^2_{m0}} \int \frac{d^3k}{(2\pi)^3}\frac{d^3k'}{(2\pi)^3} e^{i\mathbf{k}\cdot\mathbf{x}} e^{i\mathbf{k}'\cdot\mathbf{x}'} \\ &\times \left(\frac{k}{\mathcal{H}_0}\right)^2 \left(\frac{k'}{\mathcal{H}_0}\right)^2 \frac{D(z,k)D(z',k')}{\mu(z,k)\mu(z',k')} T(k)T(k')\langle\Psi_i(k)\Psi_i(k)\rangle \end{aligned} \tag{C.24}$$

We define $\langle\Psi_i(k)\Psi_i(k')\rangle = (2\pi)^3\delta_D(\mathbf{k}+\mathbf{k}')P_{\Psi_i}(k)$ where is given to be $P_{\Psi_i}(k) = A/k^3(k/k_\lambda)^{n_s-1}$, n_s is the scalar spectral in dex and A is the amplitude of initial power spectra. Applying this information in the auto-correlation the following yields

$$\xi^{\mathrm{st}[1]}_{\Delta\Delta}(r,r',\theta) = \frac{4bb(z')}{9\Omega^2_{m0}} \int \frac{d^3k}{(2\pi)^3} e^{i\mathbf{k}\cdot\hat{\mathbf{N}}d} \left(\frac{k}{\mathcal{H}_0}\right)^4 \frac{D(z,k)D(z',k)}{\mu(z,k)\mu(z',k)} T^2(k)P_{\Psi_i}(k) \tag{C.25}$$

Lets now introduce the P_1 and P_2 which are Legendre polynomial of the order 1 and 2 respectively, adopting the method in Ref.??, and expand the exponential together with the powers of $(\hat{\mathbf{k}}\cdot\hat{\mathbf{n}})$ and $(\hat{\mathbf{k}}\cdot\hat{\mathbf{n}})^2$ in terms of spherical harmonics

$$e^{i\mathbf{k}(\mathbf{x}'-\mathbf{x})} = 4\pi\sum_{LM} i^L j_L(kd) Y^*_{LM}(\hat{\mathbf{k}}) Y_{LM}(\hat{\mathbf{N}}) = e^{i\mathbf{k}\cdot\hat{\mathbf{N}}\cdot d} \tag{C.26}$$

$$(\hat{\mathbf{k}}\cdot\hat{\mathbf{n}}) = \frac{4\pi}{3}\sum_{m'=-1}^{1} Y^*_{1m'}(\hat{\mathbf{k}}) Y_{1m'}(\hat{\mathbf{n}}') = P_1(\mathbf{k}\cdot\hat{\mathbf{n}}) \tag{C.27}$$

$$(\hat{\mathbf{k}}\cdot\hat{\mathbf{n}})^2 = \frac{2}{3}\frac{4\pi}{5}\sum_{m'=-2}^{2} Y^*_{2m'}(\hat{\mathbf{k}}) Y_{2m'}(\hat{\mathbf{n}'}) + \frac{1}{3} = \frac{2}{3}P_2(\mathbf{k}\cdot\hat{\mathbf{n}}) + \frac{1}{3} \tag{C.28}$$

Exploiting the expansions provided above the auto-correlation function reads

$$\begin{aligned}\xi^{\mathrm{st}[1]}_{\Delta\Delta}(r,r',\theta) &= \frac{4bb(z')}{9\Omega^2_{m0}} \int \frac{dkk^2}{(2\pi)^3} 4\pi \sum_{LM} i^L j_L(kd) Y^*_{LM}(\hat{\mathbf{k}}) Y_{LM}(\hat{\mathbf{N}}) \\ &\times \left(\frac{k}{\mathcal{H}_0}\right)^4 \frac{D(z,k)D(z',k)}{\mu(z,k)\mu(z',k)} T^2(k)P_{\Psi_i}(k) \int d\Omega_{\hat{\mathbf{k}}} Y^*_{LM}(\hat{\mathbf{k}}) \end{aligned} \tag{C.29}$$

Now utilizing the following characteristic $\int d\Omega_{\hat{\mathbf{k}}} Y^*_{LM}(\hat{\mathbf{k}}) = \delta_{0L}\delta_{0M}$ the auto-correlation becomes

$$\xi^{\mathrm{st}[1]}_{\Delta\Delta} = \frac{bb(z')}{9\Omega^2_{m0}\pi^2}\int dk k^2 j_0(kd)\left(\frac{k}{\mathcal{H}_0}\right)^4 \frac{D(z,k)D(z',k)}{\mu(z,k)\mu(z',k)} T^2(k) P_{\Psi_i}(k) \quad \text{(C.30)}$$

Lets now look into the second term, applying the same set of step and with some algebra the auto correlation becomes

$$\begin{aligned}\xi^{\mathrm{st}[2]}_{\Delta\Delta} &= \frac{4aa'}{9\Omega^2_{m0}\mathcal{H}\mathcal{H}(z')}\int \frac{d^3k}{(2\pi)^3} e^{id\mathbf{k}\cdot\hat{\mathbf{N}}}\left(\frac{k}{\mathcal{H}_0}\right)^4 \frac{\mathcal{F}(z,k)\mathcal{F}(z',k)}{\mu(z,k)\mu(z',k)} T^2(k) P_{\Psi_i}(k) \\ &\times \left[\frac{4}{9}P_1(\hat{\mathbf{k}}\cdot\hat{\mathbf{n}})P_2(\hat{\mathbf{k}}\cdot\hat{\mathbf{n}}') + \frac{2}{9}P_2(\hat{\mathbf{k}}\cdot\hat{\mathbf{n}}) + \frac{4}{9}P_2(\hat{\mathbf{k}}\cdot\hat{\mathbf{n}}') + \frac{1}{9}\right] \quad \text{(C.31)}\end{aligned}$$

It's easy to see that that Eq. (C.31) composed of four integrals, which are due to the summation of the Legendre polynomials and the constant. We have to explicitly provide this integrals, lets start with the first integral based on first term of Eq. (C.31) which reads

$$\begin{aligned}\mathcal{I}^{[2]}_1 &= \frac{32}{365\pi^2}\int dk k^2\left(\frac{k}{\mathcal{H}_0}\right)^4 \frac{\mathcal{F}(z,k)\mathcal{F}(z',k)}{\mu(z,k)\mu(z',k)} T^2(k) P_{\Psi_i}(k) \\ &\times \left\{\left(1+\frac{2}{7}[\cos(2\alpha)\cos(2\beta)+\sin(2\alpha)\sin(2\beta)]+\cos(2\alpha)+\cos(2\beta)\right)\frac{225 j_4(kd)}{1792}\right. \\ &+ \left.\frac{5}{64}\left[1+\cos(2\alpha)\cos(2\beta)+\sin(2\alpha)\sin(2\beta)\right] j_0(kd).\right\} \quad \text{(C.32)}\end{aligned}$$

The second integration for works out to be

$$\begin{aligned}\mathcal{I}^{[2]}_2 &= -\frac{2}{90\pi^2}\int dk k^2\left(\frac{k}{\mathcal{H}_0}\right)^4 \frac{\mathcal{F}(z,k)\mathcal{F}(z',k)}{\mu(z,k)\mu(z',k)} T^2(k) P_{\Psi_i}(k) \\ &\times [1+3\cos(2\beta)] j_2(kd). \quad \text{(C.33)}\end{aligned}$$

The third term yields

$$\begin{aligned}\mathcal{I}^{[2]}_3 &= -\frac{2}{90\pi^2}\int dk k^2\left(\frac{k}{\mathcal{H}_0}\right)^4 \frac{\mathcal{F}(z,k)\mathcal{F}(z',k)}{\mu(z,k)\mu(z',k)} T^2(k) P_{\Psi_i}(k) \\ &\times [1+3\cos(2\alpha)] j_2(kd) \quad \text{(C.34)}\end{aligned}$$

Last we have

$$\mathcal{I}_4^{[2]} = \frac{1}{36\pi^2}\int dk k^2 \left(\frac{k}{\mathcal{H}_0}\right)^4 \frac{\mathcal{F}(z,k)\mathcal{F}(z',k)}{\mu(z,k)\mu(z',k)} T^2(k) P_{\Psi_i}(k) j_0(kd) \tag{C.35}$$

Therefor, collectively the above integrals produce a complete evaluation for second term auto-correlation which reads

$$\xi_{\Delta\Delta}^{\mathrm{st}[2]} = \frac{4aa'}{9\Omega_{m0}^2 \mathcal{H}\mathcal{H}(z')}(\mathcal{I}_1^{[2]} + \mathcal{I}_2^{[2]} + \mathcal{I}_3^{[2]} + \mathcal{I}_4^{[2]}) \tag{C.36}$$

Similarly, the last term of Eq. (C.31) works out to be

$$\begin{aligned}\xi_{\Delta\Delta}^{\mathrm{st}[3]} &= \frac{4b(z)a(z')}{9\Omega_{m0}\mathcal{H}}\int \frac{d^3k}{(2\pi)^3} e^{id\mathbf{k}\cdot\hat{\mathbf{N}}} \left(\frac{k}{\mathcal{H}_0}\right)^4 \frac{D(z,k)\mathcal{F}(z',k)}{\mu(z,k)\mu(z',k)} T^2(k) P_{\Psi_i}(k) \\ &\times \left[\frac{1}{3} + \frac{2}{3} P_2(\mathbf{k}\hat{\cdot}\hat{\mathbf{n}})\right]\end{aligned} \tag{C.37}$$

This also produce two separate integrals which yields

$$\mathcal{I}_1^{[3]} = \frac{1}{12\pi^2}\int dk k^2 \left(\frac{k}{\mathcal{H}_0}\right)^4 \frac{\mathcal{F}(z'S,k)D(z,k)}{\mu(z',k)\mu(z,k)} T^2(k) P_{\Psi_i}(k)] j_0(kd) \tag{C.38}$$

$$\begin{aligned}\mathcal{I}_2^{[3]} &= \frac{4}{15\pi^2}\int dk k^2 \left(\frac{k}{\mathcal{H}_0}\right)^4 \frac{\mathcal{F}(z',k)D(z,k)}{\mu(z',k)\mu(z,k)} T^2(k) P_{\Psi_i}(k)] \\ &\times [1 + 3\cos 2\alpha] j_0(kd)\end{aligned} \tag{C.39}$$

Thus, auto-correlation function for the third term yields

$$\xi_{\Delta\Delta}^{\mathrm{st}[3]} = \frac{4b(z)a'}{9\Omega_{m0}^2 \mathcal{H}(z')}(\mathcal{I}_1^{[3]} + \mathcal{I}_2^{[3]}) \tag{C.40}$$

Finally, we now have the complete galaxy overdensity standard term auto-correlation function which we define by

$$\xi_{\Delta\Delta}^{\mathrm{st}} = \xi_{\Delta\Delta}^{\mathrm{st}[1]} + \xi_{\Delta\Delta}^{\mathrm{st}[2]} + \xi_{\Delta\Delta}^{\mathrm{st}[3]} \tag{C.41}$$

Note that this expression is given in full sky approximation. Furthermore, in flat sky approximation Eq. (C.41) becomes consistent with Eq. (6.38).

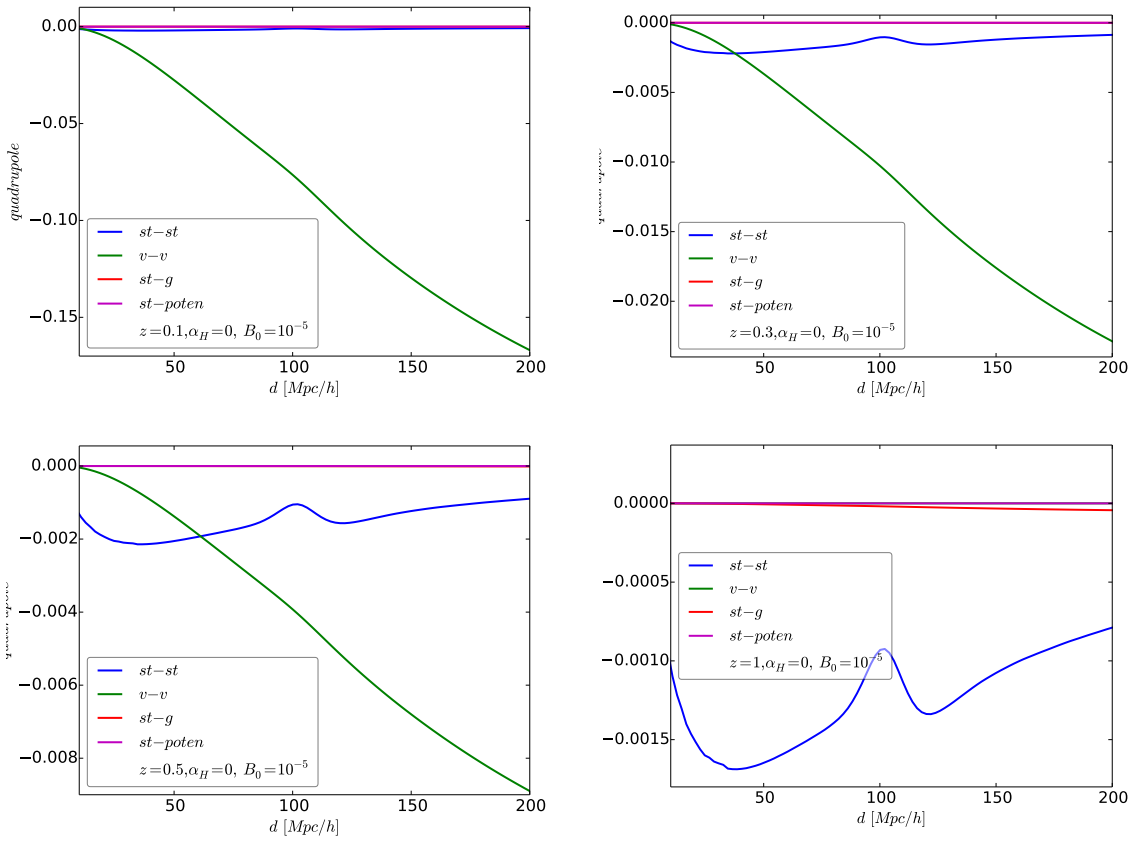

Fig. C.1 We plot different magnitudes of the quadrupoles as function of d, for the following contributions; standard-stardard (blue), doppler-doppler (green), standard-lensing (red) and standard-potentials (magneta). *Top left panel*: for redshift $z = 0.1$, *top right panel*: for redshift $z = 0.3$, *bottom left panel*: for redshift $z = 0.5$ and *bottom right panel*: for redshift $z = 1$.

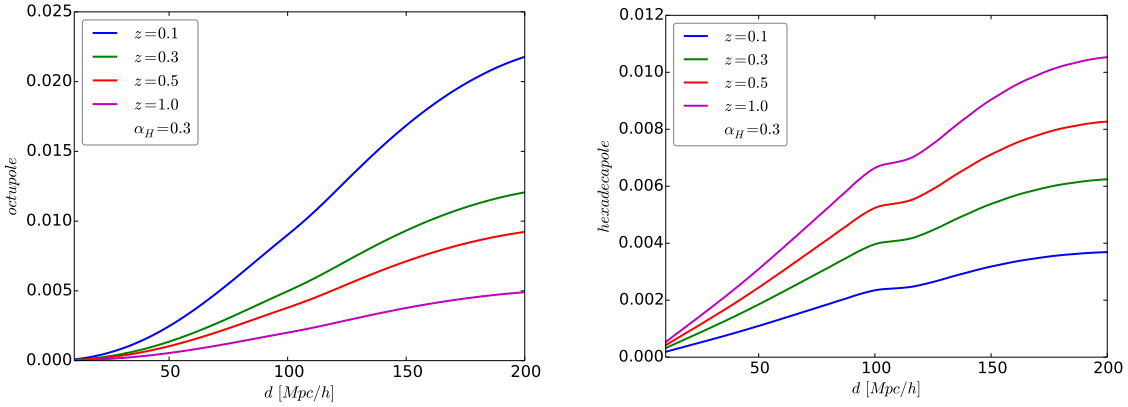

Fig. C.2 *Left panel*: The plots of the amplitude of the octupole as function of the separation distance d, given by (6.40), for the values of the redshift $z = 0.1$ (blue), $z = 0.3$ (green), $z = 0.5$ (red) and $z = 1$ (magneta). *Right panel*: The plots of the amplitude of the hexadecapole as function of d, for four separate redshifts shown in the legend.

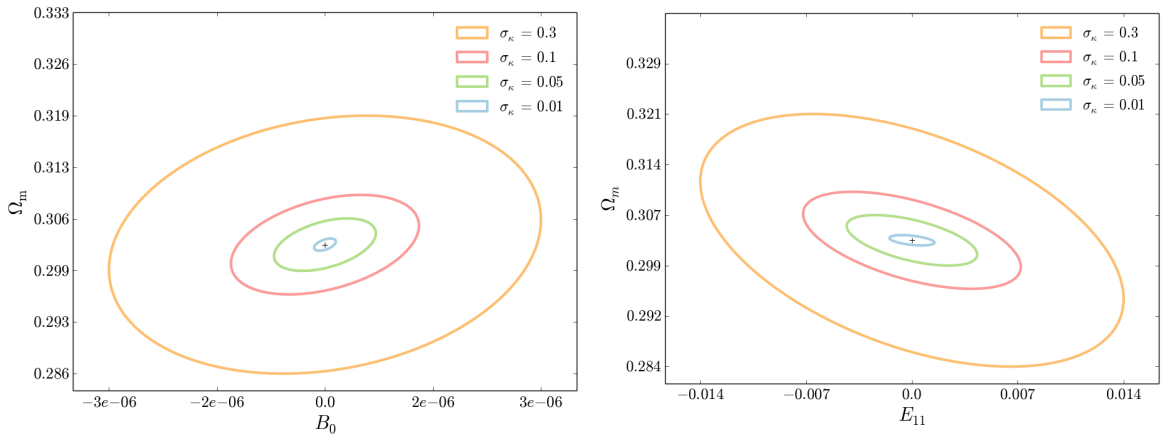

Fig. C.3 Constraints on $\Omega_{\rm m}$ and the B_0 parameter of the $f(R)$ model (left) and E_{11} parameter of the scale-independent model (right) for SKA2 + Planck (68% CL), for several different values of σ_κ.

C.3 Convergence auto-correlation functions

In this section we provide the all contributions of convergence auto-correlation functions $\xi^{\kappa\kappa}$—mentioned in introductory paragraph of chapter. 6. This can be expressed as the function of galaxy number count auto-correlation function, as shown on below quantities. Note that here we just provide final expressions in flat-sky approximation.

C.3.1 All Doppler lensing contributions

All the contributions here incorporate Doppler term

C.3.1.1 Doppler-Doppler terms correlation function

$$\xi^{\text{v-v}}_{\kappa\kappa}(r_s,d,\beta) = \frac{\left(1-\frac{1}{\mathcal{H}r_s}\right)^2}{\left(\frac{\mathcal{H}'}{\mathcal{H}^2}+\frac{2}{\mathcal{H}r_s}\right)^2}\xi^{\text{v-v}}_{\Delta\Delta}(r_s,d,\beta) \tag{C.42}$$

C.3.1.2 Gravitational lensing-Doppler terms correlation function

$$\xi^{\text{g-v}}_{\kappa\kappa}(r_s,d,\beta) = \frac{1}{2}\frac{\left(1-\frac{1}{\mathcal{H}r_s}\right)}{\left(\frac{\mathcal{H}'}{\mathcal{H}^2}+\frac{2}{\mathcal{H}r_s}\right)}\xi^{\text{g-v}}_{\Delta\Delta}(r_s,d,\beta) \tag{C.43}$$

C.3.1.3 Potentials-Doppler terms correlation function

$$\xi^{\text{poten-v}}_{\kappa\kappa}(r_s,d,\beta) = \tilde{\xi}^{\text{poten-v}}_{\Delta\Delta}(r_s,d,\beta) \tag{C.44}$$

The tilde means that we have replaced $\mathcal{L}$ with $\mathcal{M}$, i.e. We have use Eq. (C.8) instead of Eq. (C.7).

C.3.2 All Gravitational lensing contributions

All the contributions here incorporate gravitational lensing term

C.3.2.1 Lensing-lensing terms correlation function

$$\xi^{\text{g-g}}_{\kappa\kappa}(r_s, d, \beta) = \frac{1}{4}\xi^{\text{g-g}}_{\Delta\Delta}(r_s, d, \beta) \tag{C.45}$$

C.3.2.2 Poten-lensing terms correlation function

$$\xi^{\text{poten-g}}_{\kappa\kappa}(r_s, d, \beta) = \tilde{\xi}^{\text{poten-g}}_{\Delta\Delta}(r_s, d, \beta) \tag{C.46}$$

C.3.3 All potentials contributions

All the contributions here incorporate potentials term

C.3.3.1 Potentials-potentials terms correlation function

$$\xi^{\text{poten-poten}}_{\kappa\kappa}(r_s, d, \beta) = \tilde{\xi}^{\text{poten-poten}}_{\Delta\Delta}(r_s, d, \beta) \tag{C.47}$$

C.4 Convergence-galaxy number count auto-correlation functions

In this section we provide the all contributions of cross-correlation functions between galaxy number count and convergence $\xi^{\Delta\kappa}$—mentioned in introductory paragraph of chapter. 6. This can be expressed as the function of galaxy number count auto-correlation function, as shown on below quantities. Note that here we just provide final expressions in flat-sky approximation.

C.4.1 All Doppler lensing contributions

All the contributions here incorporate Doppler term

C.4.1.1 Standard-Doppler terms correlation function

$$\xi^{\text{st-v}}_{\Delta\kappa}(r_s, d, \beta) = \frac{\left(1 - \frac{1}{\mathcal{H}r_s}\right)}{\left(\frac{\mathcal{H}'}{\mathcal{H}^2} + \frac{2}{\mathcal{H}r_s}\right)}\xi^{\text{st-v}}_{\Delta\Delta}(r_s, d, \beta) \tag{C.48}$$

C.4.1.2 Doppler-Doppler terms correlation function

$$\xi^{\text{v-v}}_{\Delta\kappa}(r_s,d,\beta) = \frac{\left(1-\frac{1}{\mathcal{H}r_s}\right)^2}{\left(\frac{\mathcal{H}'}{\mathcal{H}^2}+\frac{2}{\mathcal{H}r_s}\right)^2}\xi^{\text{v-v}}_{\Delta\Delta}(r_s,d,\beta) \tag{C.49}$$

C.4.1.3 Standard-Doppler terms correlation function

$$\xi^{\text{g-v}}_{\Delta\kappa}(r_s,d,\beta) = \xi^{\text{g-v}}_{\Delta\Delta}(r_s,d,\beta) \tag{C.50}$$

C.4.1.4 Standard-Doppler terms correlation function

$$\xi^{\text{poten-v}}_{\Delta\kappa}(r_s,d,\beta) = \frac{\left(1-\frac{1}{\mathcal{H}r_s}\right)}{\left(\frac{\mathcal{H}'}{\mathcal{H}^2}+\frac{2}{\mathcal{H}r_s}\right)}\xi^{\text{poten-v}}_{\Delta\Delta}(r_s,d,\beta) \tag{C.51}$$

C.4.2 All gravitational lensing contributions

All the contributions here incorporate gravitational lensing term

C.4.2.1 Standard-lensing terms correlation function

$$\xi^{\text{st-g}}_{\Delta\kappa}(r_s,d,\beta) = -\frac{1}{2}\xi^{\text{st-g}}_{\Delta\Delta}(r_s,d,\beta) \tag{C.52}$$

C.4.2.2 Doppler-lensing terms correlation function

$$\xi^{\text{v-g}}_{\Delta\kappa}(r_s,d,\beta) = -\frac{1}{2}\xi^{\text{v-g}}_{\Delta\Delta}(r_s,d,\beta) \tag{C.53}$$

C.4.2.3 Lensing-lensing terms correlation function

$$\xi^{\text{g-g}}_{\Delta\kappa}(r_s,d,\beta) = -\frac{1}{4}\xi^{\text{g-g}}_{\Delta\Delta}(r_s,d,\beta) \tag{C.54}$$

C.4.2.4 Potential-lensing terms correlation function

$$\xi^{\text{g-g}}_{\Delta\kappa}(r_s, d, \beta) = -\frac{1}{4}\tilde{\xi}^{\text{g-g}}_{\Delta\Delta}(r_s, d, \beta) \tag{C.55}$$

C.4.3 All potentials contributions

All the contributions here incorporate potential term

C.4.3.1 Standard-potential terms correlation function

$$\xi^{\text{st-poten}}_{\Delta\kappa}(r_s, d, \beta) = \tilde{\xi}^{\text{st-poten}}_{\Delta\Delta}(r_s, d, \beta) \tag{C.56}$$

C.4.3.2 Doppler-potential terms correlation function

$$\xi^{\text{v-poten}}_{\Delta\kappa}(r_s, d, \beta) = \tilde{\xi}^{\text{v-poten}}_{\Delta\Delta}(r_s, d, \beta) \tag{C.57}$$

C.4.3.3 Gravitational-potential terms correlation function

$$\xi^{\text{g-poten}}_{\Delta\kappa}(r_s, d, \beta) = \tilde{\xi}^{\text{g-poten}}_{\Delta\Delta}(r_s, d, \beta) \tag{C.58}$$

Appendix D

The cosmological equations

D.1 The perturbation equations

In this appendix we provide the modified perturbed Einstein equations in UDE context which are all drawn from work by [28, 93, 119] which we made use of in section. (5.2) and. Here we consider the space-time metric[1] which is in contrary with [28, 93, 119], we adopt the total matter gauge (see [172]). We then can relate the two Bardeen potentials and the scalar fluctuations to metric perturbations by [119]

$$\Psi \equiv \delta N + \mathcal{H}\pi + \pi', \quad \Phi \equiv -\zeta - \mathcal{H}\pi, \quad \pi \equiv a^2\psi \tag{D.1}$$

With ψ being the metric scalar potential, δN is the metric temporal perturbation and metric spatial potential is denoted by ζ. The evolution of the unified dark energy momentum and energy density perturbation are respectively denoted by (note that we used this two equation to get equations. (5.33) and (5.35))

$$q_x' + 4\mathcal{H}q_x - (\bar{\rho}_x + \bar{p}_x)\Psi + \delta p_x - \frac{2}{3}k^2\sigma_x = \alpha_M \mathcal{H}\sum_A q_A \tag{D.2}$$

$$\delta\rho_x' + 3\mathcal{H}(\delta\rho_x + \delta p_x) - (\bar{\rho}_x + \bar{p}_x)\Phi' - k^2 q_x = \alpha_M \mathcal{H}\sum_A \delta\rho_A \tag{D.3}$$

[1] $ds^s = a^2[-(1+2\Psi)d\eta^2 + (1+2\Phi)d\vec{x}^2]$

Here the quantities q_A and σ_A respectively appears in eq. (5.27) and (5.28). We also define the following UDE perturbations

$$\begin{aligned}
V_x &\equiv \pi - \frac{2\alpha_B\mathcal{H}}{\bar{\rho}_x+\bar{p}_x}\mathcal{P}, && \text{(D.4)}\\
\sigma_x &\equiv \alpha_M a^{-2}M^2\mathcal{H}\pi - \alpha_T\mathcal{R} - \alpha_H\mathcal{P}, && \text{(D.5)}\\
\delta p_x &\equiv -[\bar{p}_x' + \alpha_M a^{-2}M^2\mathcal{H}(2\mathcal{H}'+\mathcal{H})]\pi - 2\alpha_M\mathcal{H}\mathcal{Q} - \frac{2}{3}k^2\sigma_x\\
&+ \left(\frac{\bar{\rho}_x+\bar{p}_x}{a^{-2}M^2} + 6\alpha_B\mathcal{H}^2\right)\mathcal{P} + 2\alpha_B\left(1+\frac{\alpha_B'}{\mathcal{H}\alpha_B}+\frac{\mathcal{H}'}{\mathcal{H}^2}+\frac{\mathcal{P}}{\mathcal{H}\mathcal{P}}\right)\mathcal{H}^2\mathcal{P}, && \text{(D.6)}\\
\delta\rho_x &\equiv 2k^2(\alpha_H\mathcal{R}+\alpha_B a^{-2}M^2\mathcal{H}\pi) + 3\mathcal{H}[(\bar{\rho}_x+\bar{p}_x)\pi + 2\alpha_B\mathcal{Q}]\\
&+ (\alpha_K - 6\alpha_B)\mathcal{H}^2\mathcal{P}. && \text{(D.7)}
\end{aligned}$$

Where we have the following parameters

$$\mathcal{P}\equiv\frac{M^2}{a^2}(\Psi-\pi'-\mathcal{H}\pi),\quad \mathcal{Q}\equiv\frac{M^2}{a^2}[\Phi'-\mathcal{H}\Psi+(\mathcal{H}^2-\mathcal{H}')\Pi],\quad \mathcal{R}\equiv\frac{M^2}{a^2}(\Phi-\mathcal{H}\pi) \text{(D.8)}$$

Note that the parameters are related to their physical counterparts by $\mathcal{P}=a^{-2}\mathcal{P}^{\rm phys}$, $\mathcal{Q}=a^{-1}\mathcal{Q}^{\rm phys}$ and $\mathcal{R}=a^{-2}\mathcal{R}^{\rm phys}$ we also have $\pi=a^{-1}\pi^{\rm phys}$—all the superscript *phys* denotes the physical quantities as given by [119].

D.2 Refined perturbed Einstein equations

The evolution equations for metric potentials are Φ and π, starting with Hamiltonian constraint which is given by

$$\begin{aligned}
&6(1+\alpha_B)\mathcal{H}\Phi' - (6-\alpha_K+12\alpha_B)\mathcal{H}^2\Psi + 2k_{\mathcal{H}}^2(1+\alpha_H)\mathcal{H}^2\Phi\\
-\;& 6\left[(1+\alpha_B)\left(\frac{\mathcal{H}'}{\mathcal{H}^2}-1\right)+\frac{\bar{\rho}_x+\bar{p}_x}{2a^{-2}M^2\mathcal{H}^{-2}}+\frac{k_{\mathcal{H}}^2}{3}(\alpha_H-\alpha_B)+\frac{\alpha_K}{6}-\alpha_B\right]\mathcal{H}^3\pi\\
=\;& -(6\alpha_B-\alpha_K)\mathcal{H}\pi' - \frac{\delta\rho_m}{a^{-2}M^2} \qquad \text{(D.9)}
\end{aligned}$$

Here $k_{\mathcal{H}}$ is equivalent to $\tilde{k}$ use by [119]; which is given to be $k_{\mathcal{H}}=k/\mathcal{H}$ .Then momentum and anisotropic constraints are respectively given by

$$\Phi' - (1+\alpha_B)\mathcal{H}\Psi + \alpha_B\mathcal{H}\pi' = -\left(1+\alpha_B-\frac{\mathcal{H}'}{\mathcal{H}^2}-\frac{\bar{\rho}_x+\bar{p}_x}{2a^{-2}M^2\mathcal{H}^{-2}}\right)\mathcal{H}^2\pi - \frac{a^2q_m}{2M^2}, \text{(D.10)}$$

$$(1+\alpha_T)\Phi + (1+\alpha_H)\Psi + [\alpha_M - (\alpha_H+\alpha_T)]\mathcal{H}\pi - \alpha_H\pi' = \frac{a^2\sigma_m}{2M^2}. \text{(D.11)}$$

Note we obtained Eq. (5.27) by making use of Eq. (D.4) and the expression for $\mathcal{P}$ provided by Eq. (D.8) into Eq. (D.11).

We provide the second order evolution of scalar field by [93]

$$\begin{aligned} \pi'' &+ (1+\alpha_1)\mathcal{H}\pi' + \alpha_3\mathcal{H}^2\pi - \phi' - \alpha_4\Phi' + \alpha_5\mathcal{H}\Psi - \alpha_6\mathcal{H}\Phi \\ &- 2\alpha_7\mathcal{H}\frac{a^2\sigma_m}{M^2} - 3\alpha_8\frac{a^2\delta p_m}{\mathcal{H}M^2} = 0 \end{aligned} \tag{D.12}$$

In addition to work by [119], we provide the evolution Ψ by considering the derivatives of Eq. (D.11) and combining the end product with Eqs. (D.10) and (D.12) the following yields

$$\Psi' + (1+\sigma_1)\mathcal{H}\Psi + \sigma_2\mathcal{H}\Phi - \sigma_3\mathcal{H}^2\pi - \sigma_4\frac{a^2 q_m}{2M^2} + \sigma_5\mathcal{H}\frac{a^2\sigma_m}{M^2} - \sigma_6\frac{3a^2\delta p_m}{\mathcal{H}M^2} \tag{D.13}$$

Where we have defined various α_i (with $i = 1, 2...$) parameters

$$\begin{aligned} \alpha_1\alpha &\equiv (3+\alpha_M)\alpha + \frac{\alpha_K'}{\mathcal{H}} + (6\alpha_B^2 + 2\alpha_K - 6\alpha_B)\left(\frac{\mathcal{H}'}{\mathcal{H}^2} - 1\right) + 6\alpha_B\left(\frac{\alpha_B'}{\mathcal{H}}\right. \\ &- \left.\frac{\bar{\rho}_m + \bar{p}_m}{2a^{-2}M^2\mathcal{H}^{-2}}\right) \end{aligned} \tag{D.14}$$

$$\begin{aligned} \alpha_2\alpha &\equiv -3\alpha_B\frac{a^3\bar{p}_m'}{M^2\mathcal{H}^3} + 6\left[\frac{\alpha_B'}{\mathcal{H}} + (1+\alpha_B)\left(\frac{\mathcal{H}'}{\mathcal{H}^2} - 1\right) + \frac{\bar{\rho}_m + \bar{p}_m}{2a^{-2}M^2\mathcal{H}^{-2}}\right]\left(\frac{\mathcal{H}'}{\mathcal{H}^2} - 1\right) \\ &- 2k_{\mathcal{H}}^2\left[1 + \alpha_T\alpha_B(1+\alpha_B) - (1+\alpha_H)(1+\alpha_M) + \frac{\alpha_B' - \alpha_H'}{\mathcal{H}}\right. \\ &+ \left.(1+\alpha_B-\alpha_H)\left(\frac{\mathcal{H}'}{\mathcal{H}^2} - 1\right) + \frac{\bar{\rho}_m + \bar{p}_m}{2a^{-2}M^2\mathcal{H}^{-2}}\right] \end{aligned} \tag{D.15}$$

$$\alpha_3 \equiv \alpha_1 + \alpha_2 + \frac{\mathcal{H}'}{\mathcal{H}^2} \tag{D.16}$$

$$\alpha_4\alpha \equiv 6\left[\frac{\alpha_B'}{\mathcal{H}} + (1+\alpha_B)\left(\frac{\mathcal{H}'}{\mathcal{H}^2} - 1\right) + \frac{\bar{\rho}_m + \bar{p}_m}{2a^{-2}M^2\mathcal{H}^{-2}}\right] + 2\alpha_H k_{\mathcal{H}}^2 \tag{D.17}$$

$$\begin{aligned} \alpha_5\alpha &\equiv -(3+\alpha_M)\alpha + \frac{\alpha_K'}{\mathcal{H}} + 6(1-\alpha_B)\frac{\alpha_B'}{\mathcal{H}} + 2k_{\mathcal{H}}^2(\alpha_H - \alpha_B) \\ &+ 3(1+\alpha_B)\frac{\bar{\rho}_m + \bar{p}_m}{a^{-2}M^2\mathcal{H}^{-2}} + \left[6\alpha_B^2 + 2\alpha_K - 12\alpha_B - 6\right]\left(\frac{\mathcal{H}'}{\mathcal{H}^2} - 1\right) \end{aligned} \tag{D.18}$$

$$\alpha_6\alpha \equiv 2k_{\mathcal{H}}^2\left[\alpha_M + \alpha_H(1+\alpha_M) - \alpha_T + \frac{\alpha_H'}{\mathcal{H}}\right] \tag{D.19}$$

$$\alpha_7\alpha \equiv \alpha_B k_{\mathcal{H}}^2, \quad \alpha_8\alpha \equiv \alpha_B \tag{D.20}$$

We also define the following

$$\sigma_1 \equiv \alpha_T+\alpha_H(\alpha_5+\alpha_4)+\alpha_B(1+\alpha_T-\alpha_H\alpha_4)-\frac{\alpha_H'}{\mathcal{H}\alpha_H}-\sigma_{1a}\left(\frac{1+\alpha_H}{\alpha_H}\right) \quad \text{(D.21)}$$

$$\sigma_2 \equiv \frac{\alpha_T'}{\mathcal{H}}-(1+\alpha_T)\frac{\alpha_H'}{\mathcal{H}\alpha_H}-\alpha_H\alpha_6-\sigma_{1a}\left(\frac{1+\alpha_H}{\alpha_H}\right) \quad \text{(D.22)}$$

$$\sigma_3 \equiv \sigma_{1b}+\sigma_{1a}\left(\frac{\alpha_M-\alpha_T}{\alpha_H}-1\right), \quad \sigma_4 \equiv 1+\alpha_T-\alpha_H\alpha_4 \quad \text{(D.23)}$$

$$\sigma_5 \equiv \alpha_M+\frac{\alpha_H'}{\mathcal{H}\alpha_H}-\frac{\sigma_m'}{\mathcal{H}\sigma_m}-2(1+\alpha_H\alpha_7)+\frac{\sigma_{1a}}{\alpha_H}, \quad \sigma_6 \equiv \alpha_H\alpha_8 \quad \text{(D.24)}$$

With

$$\sigma_{1a} \equiv \alpha_T+\alpha_B\sigma_4-\alpha_M-\alpha_H\alpha_1 \quad \text{(D.25)}$$

$$\sigma_{1b} \equiv (\alpha_M-\alpha_T)\frac{\alpha_H'}{\mathcal{H}\alpha_H}+(\alpha_H-\alpha_M+\alpha_H\alpha_4-1)\frac{\mathcal{H}'}{\mathcal{H}^2}+\frac{\alpha_T'-\alpha_M'}{\mathcal{H}}$$
$$- \alpha_H\alpha_3+\sigma_4\left(1+\alpha_B-\frac{\bar{\rho}_m+\bar{p}_m}{2a^{-2}M^2\mathcal{H}^{-2}}\right) \quad \text{(D.26)}$$

D.3 Defining beyond-Horndeski coefficients

We provide a catalogue of parameters we introduced in subsection. 6.1.1, for which we make an assumptions that ($\alpha_H \neq 0$)

$$\epsilon_n = -\frac{2}{\alpha}(\alpha_B-\alpha_H)^3, \qquad \epsilon_1=-3\alpha_B\frac{a^2\bar{\rho}_m}{2\mathcal{H}^2M^2}, \qquad \epsilon_2=\epsilon_1(\beta_3+\epsilon_{4_I}), \quad \text{(D.27)}$$

$$\epsilon_3 = -\frac{2}{\alpha_B-\alpha_H}\left(\frac{\alpha_B'}{\mathcal{H}\alpha_B}-\frac{\alpha_H'}{\mathcal{H}\alpha_H}+\frac{a^2\bar{\rho}_m}{4\mathcal{H}^2M^2}\right), \quad \text{(D.28)}$$

$$\epsilon_4 = \left[\beta_4-(1+\alpha_T)\left(\beta_2-\frac{\epsilon_2}{\epsilon_1}\right)\right]\epsilon_1, \quad \text{(D.29)}$$

$$\epsilon_{4_I} = \frac{\alpha_B'}{\mathcal{H}\alpha_B}-\frac{\alpha_H'}{\mathcal{H}\alpha_H}+1+\alpha_M-\left(\frac{\mathcal{H}'}{\mathcal{H}^2}-1\right)-\frac{1}{\alpha_B}\left[\left(\frac{\mathcal{H}'}{\mathcal{H}^2}-1\right)+\frac{a^2\bar{\rho}_m}{2\mathcal{H}^2M^2}\right] \quad \text{(D.30)}$$

$$\epsilon_6 = \beta_1\left\{\epsilon_7-\frac{2}{\alpha}[(\alpha_B-\alpha_H)\epsilon_3+\beta_2-\beta_3]\right\}-\frac{2\epsilon_1}{\alpha}\left\{(1+\alpha_B)\left[\left(2-\frac{\alpha_H}{\alpha_B}\right)\left(\frac{\mathcal{H}'}{\mathcal{H}^2}-1\right)\right.\right.$$
$$\left.- \alpha_M+\alpha_T\right]-\alpha_H\alpha_B\left(\frac{\alpha_B'}{\mathcal{H}\alpha_B^2}-\frac{\alpha_H'}{\mathcal{H}\alpha_H^2}\right)+\left.\frac{2(\alpha_B-\alpha_H)}{\alpha_B}\frac{a^2\bar{\rho}_m}{2\mathcal{H}^2M^2}\right\} \quad \text{(D.31)}$$

$$\epsilon_7 \equiv \frac{2\alpha_B}{\alpha}\left[2\left(\frac{\alpha_B'}{\mathcal{H}\alpha_B}-\frac{\alpha_H'}{\mathcal{H}\alpha_H}\right)-\epsilon_{4_I}+\frac{\alpha_H}{\alpha_B}\frac{a^2\bar{\rho}_m}{2\mathcal{H}^2M^2}\right] \quad \text{(D.32)}$$

We also have

$$
\begin{aligned}
\epsilon_5 &= \left[\left(\frac{\mathcal{H}'}{\mathcal{H}^2}-1\right)^2+\left(\frac{\mathcal{H}''}{\mathcal{H}^3}-4\frac{\mathcal{H}'}{\mathcal{H}^2}+2\right)\right](\alpha_B-(1+\alpha_H))\\
&+ \left[\frac{\epsilon_{5_I}}{\alpha}-\alpha_B(\alpha_M-\beta_3+3)-2(\alpha_M-\alpha_T-\frac{\alpha_H'}{\mathcal{H}})-(1+\alpha_M)\alpha_H\right]\frac{a^2\bar{\rho}_m}{2\mathcal{H}^2M^2}\\
&+ \left(\frac{\mathcal{H}'}{\mathcal{H}^2}-1\right)\left\{\epsilon_{5_{II}}+(1+\alpha_H)\left[\frac{1}{2}+\frac{1}{\alpha}(6\alpha_B-\alpha_K-3\alpha_H(1+\alpha_B))\right]\frac{a^2\bar{\rho}_m}{2\mathcal{H}^2M^2}\right\}\\
&+ \frac{1+\alpha_H}{4\alpha}\left(\frac{a^2\bar{\rho}_m}{2M^2\mathcal{H}^2}\right)^2(12\alpha_B-\alpha_K-6\alpha_H)+\frac{\alpha_H'}{\mathcal{H}\alpha_H}\frac{a^2\bar{\rho}_m}{2\mathcal{H}^2M^2}+\epsilon_{5_{III}}, \qquad \text{(D.33)}\\
\epsilon_{5_I} &= 6\alpha_B\alpha_H\left[\left(\alpha_M-\frac{\alpha_B'}{\mathcal{H}\alpha_B}\right)(1+\alpha_H)-\alpha_T-\frac{\alpha_H'}{\mathcal{H}}+\alpha_H\right]-(1+\alpha_H)\frac{\alpha_K'}{\mathcal{H}}\\
&+ \alpha_K\left[3(\alpha_H+\alpha_M)+2\alpha_B\left(\frac{\alpha_H'}{\mathcal{H}\alpha_H}-1\right)-\alpha_T(2(\alpha_B+1)-\alpha_H)\right.\\
&+ \left.\frac{\alpha_H'}{\mathcal{H}\alpha_H}-2\frac{\alpha_H'}{\mathcal{H}}+2\alpha_H\alpha_M+1\right], \qquad \text{(D.34)}\\
\epsilon_{5_{II}} &= -\alpha_B(3\alpha_M+2\alpha_T-\beta_3+5)-2(1+\alpha_H)\\
&+ 2(1+\alpha_B)\frac{\alpha_H'}{\mathcal{H}\alpha_H}+\left[3(1+\alpha_M)-2\frac{\alpha_B'}{\mathcal{H}\alpha_B}-\beta_3\right](1+\alpha_H), \qquad \text{(D.35)}\\
\epsilon_{5_{III}} &= (\alpha_B-\alpha_H)\left[2\left(1-\frac{\mathcal{H}'}{\mathcal{H}^2}+\alpha_M-\alpha_T\right)-(6\alpha_B\alpha_H+\alpha_K)\frac{a^2\bar{\rho}_m}{\alpha\mathcal{H}^2M^2}\right]\frac{\alpha_H'}{\mathcal{H}\alpha_H}\\
&+ \alpha_B\left[\alpha_T-\frac{\alpha_T'}{\mathcal{H}}+(3+\alpha_T+\alpha_M)(\alpha_M-\beta_3)+\beta_3-2(\alpha_M-2\alpha_T-1)\frac{\alpha_H'}{\mathcal{H}\alpha_H}\right]\\
&- \left\{2(\alpha_M-\alpha_T)\frac{\alpha_H'}{\mathcal{H}\alpha_H}+2\frac{\alpha_B'}{\mathcal{H}}(1+\alpha_T)+\alpha_H[\alpha_M(\alpha_M-\beta_3-2)-\frac{\alpha_M'}{\mathcal{H}}-\beta_3]\right.\\
&- \left.\frac{\alpha_M'}{\mathcal{H}}+2\frac{\alpha_H'}{\mathcal{H}}(1+\alpha_T)+\frac{\alpha_T'}{\mathcal{H}}+\alpha_T(\beta_3-1)+\alpha_M(\alpha_M-\alpha_T-\beta_3+1)\right\}\\
&+ 2\left[\alpha_M(1+\alpha_H)-\alpha_T+\alpha_H\right]\frac{\alpha_B'}{\mathcal{H}\alpha_B}+2\alpha_B-\alpha_B\frac{\alpha_M'}{\mathcal{H}}-\alpha_H, \qquad \text{(D.36)}\\
\epsilon_{79} &= \frac{2}{\alpha_B-\alpha_H}\left[\frac{a^2\bar{\rho}_m}{4M^2\mathcal{H}^2}-\frac{\alpha_M}{2}+\frac{\alpha_T}{2}+\frac{1}{2}\left(\frac{\mathcal{H}'}{\mathcal{H}^2}-1\right)\right]\\
&+ \epsilon_7+\epsilon_3-\frac{2\alpha_H}{\alpha}\frac{a^2\bar{\rho}_m}{2M^2\mathcal{H}^2}, \qquad \text{(D.37)}\\
\epsilon_{168} &= 3\left[\frac{2\alpha_B'\alpha_K-\alpha_B\alpha_K'}{\mathcal{H}\alpha}-\alpha_B\left(\epsilon_{4_I}-\alpha_M+\frac{\mathcal{H}'}{\mathcal{H}^2}+1\right)\right]\left[\alpha_M-\alpha_T-\left(\frac{\mathcal{H}'}{\mathcal{H}^2}+1\right)\right]\\
&- 3\alpha_B\left[\alpha_M(\alpha_M-\alpha_T)+\frac{\alpha_M'}{\mathcal{H}}-\frac{\alpha_T'}{\mathcal{H}}-\alpha_T\left(\frac{\mathcal{H}'}{\mathcal{H}^2}-1\right)-\left(\frac{\mathcal{H}''}{\mathcal{H}^3}-4\frac{\mathcal{H}'}{\mathcal{H}^2}+2\right)\right] \qquad \text{(D.38)}\\
& \qquad \text{(D.39)}
\end{aligned}
$$

And

$$\epsilon_{B1} = (1+\alpha_H)\left(\frac{\mathcal{H}'}{\mathcal{H}^2}+\frac{a^2\bar{\rho}_m}{2M^2\mathcal{H}^2}-1\right)+\alpha_B(1+\alpha_M), \tag{D.40}$$

$$\epsilon_{B3} = \frac{1}{2}\left(\frac{\mathcal{H}'}{\mathcal{H}^2}+\frac{a^2\bar{\rho}_m}{2M^2\mathcal{H}^2}-1\right), \quad \epsilon_{B4}=-3\alpha_B\left(\frac{\mathcal{H}'}{\mathcal{H}^2}-1\right). \tag{D.41}$$

Additionally we also define the following parameter

$$\mathcal{R}_1 = \left(\frac{\mathcal{H}'}{\mathcal{H}^2}-1\right)+\frac{\tilde{\beta}_{12}+\tilde{\beta}_3(\alpha_B-\alpha_H)^2k^2_{\mathcal{H}}}{\tilde{\beta}_1+k^2_{\mathcal{H}}(\alpha_B-\alpha_H)^2} \tag{D.42}$$

$$\mathcal{R}_2 = \frac{\tilde{\beta}_{14}+\tilde{\beta}_{15}k^2_{\mathcal{H}}+c^2_{sx}(\alpha_B-\alpha_K)^2k^4_{\mathcal{H}}}{\tilde{\beta}_1+k^2_{\mathcal{H}}(\alpha_B-\alpha_H)^2} \tag{D.43}$$

$$\mathcal{R}_3 = \frac{a^2\bar{\rho}_m}{2\mathcal{H}^2M^2}\frac{\tilde{\beta}_{16}+\tilde{\beta}_7k^2_{\mathcal{H}}}{\tilde{\beta}_1+k^2_{\mathcal{H}}(\alpha_B-\alpha_H)^2} \tag{D.44}$$

$$\mathcal{R}_4 = -\frac{a^2\bar{\rho}_m}{2\mathcal{H}^2M^2}\frac{\tilde{\beta}_{168}+\tilde{\beta}_{79}(\alpha_B-\alpha_K)^2k^2_{\mathcal{H}}+\alpha_H\epsilon_nk^4_{\mathcal{H}}}{\tilde{\beta}_1+k^2_{\mathcal{H}}(\alpha_B-\alpha_H)^2} \tag{D.45}$$

And

$$\mathcal{S}_1 = \frac{(1+\alpha_T)(\gamma_1+\alpha^2_Bk^2_{\mathcal{H}})+\frac{2\alpha_B}{\alpha}\gamma_9k^2_{\mathcal{H}}+\alpha_H\epsilon_{B1}k^2_{\mathcal{H}}}{\tilde{\gamma}_9+\alpha_H(\alpha_B-\alpha_H)k^2_{\mathcal{H}}} \tag{D.46}$$

$$\mathcal{S}_2 = \frac{\tilde{\beta}_1+(\alpha_B-\alpha_H)^2k^2_{\mathcal{H}}}{\tilde{\gamma}_9+\alpha_H(\alpha_B-\alpha_H)k^2_{\mathcal{H}}} \tag{D.47}$$

$$\mathcal{S}_3 = \frac{a^2\bar{\rho}_m}{\mathcal{H}^2M^2}\frac{\frac{\alpha_B}{\alpha}\gamma_9+\alpha_H\epsilon_{B3}}{\tilde{\gamma}_9+\alpha_H(\alpha_B-\alpha_H)k^2_{\mathcal{H}}} \tag{D.48}$$

$$\mathcal{S}_4 = -\frac{a^2\bar{\rho}_m}{2\mathcal{H}^2M^2}\frac{\frac{\alpha_B}{\alpha}\gamma_9+\alpha_H\epsilon_{B4}+\alpha_H(\alpha_B-\alpha_H)k^2_{\mathcal{H}}}{\tilde{\gamma}_9+\alpha_H(\alpha_B-\alpha_H)k^2_{\mathcal{H}}} \tag{D.49}$$

And the tilde betas are denoted by

$$\tilde{\beta}_i \equiv \beta_i+\alpha_H\epsilon_i, \qquad \tilde{\beta}_{1j}\equiv\beta_1\beta_j+\alpha_H\epsilon_j, \tag{D.50}$$

$$\tilde{\beta}_{79} \equiv 3\beta_7+\beta_9+\alpha_H\epsilon_{79}, \qquad \tilde{\beta}_{168}\equiv\beta_1(3\beta_6+\beta_8)+\alpha_H\epsilon_{168}. \tag{D.51}$$

D.4 Quasi-static approximation Coefficients

In this section, we define the Quasi-static approximation Coefficients that are introduced in the modified both scale and time parameters $\mu(a,k)$ and $\gamma(a,k)$ in Eq. (6.22) and (6.23), We start with the gamma's γ_i of the numerator of Eq. (6.23) which are defined

as follows:

$$\gamma_I = \alpha\tilde{\beta}_{16}\tilde{\beta}_1\left(\frac{\dot{\mathcal{H}}}{\mathcal{H}^2}-1\right)+2(\tilde{\beta}_{168}+\tilde{\beta}_{16})(\alpha\alpha_H\epsilon_{B3}+\alpha_B\gamma_9)\frac{a^2\bar{\rho}_m}{2M^2\mathcal{H}^2} \tag{D.52}$$

$$\gamma_{II} = (\alpha_B-\alpha_H)^2\Bigg[\alpha(\tilde{\beta}_{16}+\tilde{\beta}_1\tilde{\beta}_7)\left(\frac{\mathcal{H}'}{\mathcal{H}^2}-1\right)+2(\tilde{\beta}_{79}+\tilde{\beta}_7)(\alpha\alpha_H\epsilon_{B3}+\alpha_B\gamma_9) \times \frac{a^2\bar{\rho}_m}{2M^2\mathcal{H}^2}\Bigg] \tag{D.53}$$

$$\gamma_{III} = \alpha(\alpha_B-\alpha_H)^4\tilde{\beta}_7\left(\frac{\mathcal{H}'}{\mathcal{H}^2}-1\right)+\alpha_H\epsilon_n(\alpha\alpha_H\epsilon_{B3}+\alpha_B\gamma_9)\frac{a^2\bar{\rho}_m}{2M^2\mathcal{H}^2} \tag{D.54}$$

We also define the mu's μ_i of the numerator of Eq. (6.22) which are defined as follows:

$$\mu_I = -2\alpha_B\tilde{\beta}_{14}\gamma_9+[-2\alpha\alpha_H\epsilon_{B3}\tilde{\beta}_{14}+\alpha\tilde{\beta}_{16}(1+\alpha_T)\gamma_1]\left(\frac{\mathcal{H}'}{\mathcal{H}^2}-1\right), \tag{D.55}$$

$$\mu_{II} = [-2\alpha_B(\tilde{\beta}_{15}-\tilde{\beta}_{16})\gamma_9-2\alpha\tilde{\beta}_7(1+\alpha_T)\gamma_1+\alpha\alpha_B^2(1+\alpha_T)\tilde{\beta}_{16}+\alpha\alpha_B^2\tilde{\beta}_7(1+\alpha_T)\gamma_1 - 2\alpha\alpha_H\tilde{\beta}_{15}\epsilon_{B3}+\alpha\alpha_H\tilde{\beta}_{16}\epsilon_{B1}+\alpha\alpha_H(1+\alpha_T)\tilde{\beta}_7\gamma_1]\left(\frac{\mathcal{H}'}{\mathcal{H}^2}-1\right), \tag{D.56}$$

$$\mu_{III} = (\alpha_B-\alpha_H)^2[\alpha\alpha_B^2(1+\alpha_T)\tilde{\beta}_7+\alpha\alpha_H(\tilde{\beta}_7\epsilon_{B1}-2\epsilon_{B3}c_{sx}^2)+2\alpha_B(\tilde{\beta}_7 - c_{sx}^2)\gamma_9]\left(\frac{\mathcal{H}'}{\mathcal{H}^2}-1\right). \tag{D.57}$$

Finally, we define denominator of Eq. (6.22) which are defined as follows:

$$\begin{aligned}
\mu_{IV} &= [2\alpha_B\tilde{\beta}_{14}\gamma_9 + 2\alpha\alpha_H\epsilon_{B3}\tilde{\beta}_{14} + \alpha(1+\alpha_T)\gamma_1]\frac{a^2\bar{\rho}_m}{2M^2\mathcal{H}^2} \\
&+ \alpha\tilde{\beta}_1\tilde{\beta}_{14}\left(\frac{\mathcal{H}'}{\mathcal{H}^2}-1\right), \qquad \text{(D.58)} \\
\mu_V &= [\alpha\tilde{\beta}_{15}\tilde{\beta}_1 + (\alpha_B-\alpha_H)^2\tilde{\beta}_{14}]\left(\frac{\mathcal{H}'}{\mathcal{H}^2}-1\right) + [2\alpha_B(\tilde{\beta}_{15}+\tilde{\beta}_{168})\gamma_9 \\
&- \alpha\alpha_B\alpha_H\tilde{\beta}_{79}(1+\alpha_T)\gamma_1 + \alpha\alpha_B^2\tilde{\beta}_{79}(1+\alpha_T)\gamma_1 + \alpha\alpha_B^2\tilde{\beta}_{168} \\
&+ \alpha\alpha_H(\tilde{\beta}_{168}\epsilon_{B1} + 2\tilde{\beta}_{15}\epsilon_{B3}) + \alpha\alpha_H^2\tilde{\beta}_{79}(1+\alpha_T)\gamma_1]\frac{a^2\bar{\rho}_m}{2M^2\mathcal{H}^2}, \qquad \text{(D.59)} \\
\mu_{VI} &= \alpha(\alpha_B-\alpha_H)^2(\tilde{\beta}_{15}-\tilde{\beta}_1 c_{sx}^2)\left(\frac{\mathcal{H}'}{\mathcal{H}^2}-1\right) + [2\alpha_B(\alpha_B-\alpha_H)^2(\tilde{\beta}_{79}-c_{sx}^2)\gamma_9 \\
&+ \alpha\alpha_B^2\alpha_H(\tilde{\beta}_7\epsilon_{B1} - 2c_{sx}^2\epsilon_{B3}) + \alpha\alpha_H\tilde{\beta}_{79}(1+\alpha_T) - 2\alpha\alpha_B^3\alpha_H\tilde{\beta}_{79}(1+\alpha_T) \\
&+ \alpha\alpha_B^4\tilde{\beta}_{79}(1+\alpha_T) + \alpha\alpha_H^3(\tilde{\beta}_{79}\epsilon_{B1} + 2\epsilon_{B3}c_{sx}^2) \\
&+ \alpha\alpha_H\epsilon_n(1+\alpha_T)\gamma_1 - \alpha_B\alpha_H^2(\epsilon_{B3}c_{sx}^2 + 2\tilde{\beta}_{79}\epsilon_{B1})\frac{a^2\bar{\rho}_m}{2M^2\mathcal{H}^2}, \qquad \text{(D.60)} \\
\mu_{VII} &= +[\alpha\alpha_H\epsilon_n\alpha_B^2(1+\alpha_T) + \alpha\alpha_H^2\epsilon_n\epsilon_{B1} + 2\alpha_B\alpha_H\epsilon_n\gamma_9]\frac{a^2\bar{\rho}_m}{2M^2\mathcal{H}^2} \\
&+ \alpha(\alpha_B-\alpha_H)^4 c_{sx}^2\left(\frac{\mathcal{H}'}{\mathcal{H}^2}-1\right). \qquad \text{(D.61)}
\end{aligned}$$

We also define the gammas' and beta's we introduced in Eqs. (6.20) and (6.21) which are given by

$$\begin{aligned}
\mu_a &= \alpha_M^2 - \alpha_M + \left(\frac{\mathcal{H}'}{\mathcal{H}^2}-1\right)\left[4 + \left(\frac{\mathcal{H}'}{\mathcal{H}^2}-1\right) + \frac{\mathcal{H}''}{\mathcal{H}^3} - 4\frac{\mathcal{H}'}{\mathcal{H}^2} + 2\right] \qquad \text{(D.62)} \\
\mu_b &= \frac{3}{2}\alpha_M\left\{-\alpha_M - \left(\frac{\mathcal{H}'}{\mathcal{H}^2}-1\right)\left[\left(\frac{\mathcal{H}'}{\mathcal{H}^2}-1\right) + \frac{\mathcal{H}''}{\mathcal{H}^3} - 4\frac{\mathcal{H}'}{\mathcal{H}^2} + 2\right]\right\} \qquad \text{(D.63)} \\
\mu_c &= \frac{1}{2}\left\{\alpha_M^2 - 3\alpha_M\left(\frac{\mathcal{H}'}{\mathcal{H}^2}-1\right) - 4\alpha_M + \left(\frac{\mathcal{H}'}{\mathcal{H}^2}-1\right)\frac{a^2\bar{\rho}_m}{\mathcal{H}^2M^2}\right. \\
&+ \left. 2\left(\frac{\mathcal{H}'}{\mathcal{H}^2}-1\right)\left[\left(\frac{\mathcal{H}'}{\mathcal{H}^2}-1\right) + \frac{\mathcal{H}''}{\mathcal{H}^3} - 4\frac{'\mathcal{H}}{\mathcal{H}^2} + 2\right]\right\} \qquad \text{(D.64)}
\end{aligned}$$

$$\begin{aligned}
\gamma_a &= \alpha_M\left[2\alpha_M - 3 - 2\left(\frac{\mathcal{H}'}{\mathcal{H}^2}-1\right) + \left(\frac{\mathcal{H}'}{\mathcal{H}^2}-1\right)\frac{a^2\bar{\rho}_m}{\mathcal{H}^2M^2}\right] \\
&+ \left(\frac{\mathcal{H}'}{\mathcal{H}^2}-1\right)\left[4 + \left(\frac{\mathcal{H}'}{\mathcal{H}^2}-1\right) + \frac{\mathcal{H}''}{\mathcal{H}^3} - 4\frac{\mathcal{H}'}{\mathcal{H}^2} + 2\right] \qquad \text{(D.65)}
\end{aligned}$$

D.5 Adiabatic initial conditions

In this section we adopt the adiabatic initial conditions, this give some specifics on the condition of the vanishing gauge-invariant entropy perturbations S_{mx} (for more details see [92, 94, 95, 178]

$$S_{mx} \equiv 3\mathcal{H}\left(\frac{\bar{\rho}_m}{\bar{\rho}'_m}\Delta_m - \frac{\bar{\rho}_x}{\bar{\rho}'_x}\Delta_x\right), \quad S_{mx} = 0 \tag{D.66}$$

Note that at decoupling period $z = z_d$, and choosing the matter and UDE velocities to be same we get

$$V_m(z_d, k) = V_x(z_d, k) \tag{D.67}$$

Making use of information above that $S_{mx} = 0$ then we arrive at

$$S_{mx} = \frac{\Delta_m}{(1+w_m)} - \frac{\Delta_x}{(1+w_{x,\text{eff}})} = 0 \tag{D.68}$$

Results from the matter evolution perturbations meaning V_m and Δ_m, we get initial fluctuations at decoupling to be respectively denoted by

$$V_m(z_d, k) = \frac{2}{3\mathcal{H}(1+\Omega_m w_m + \Omega_x w_x)}\Psi(z_d, k) \tag{D.69}$$

$$\Delta_m(z_d, k) = \frac{1+w_m}{(1+\Omega_m w_m + \Omega_x w_{x,\text{eff}})}\left[\alpha_M \mathcal{H} V_x(z_d, k) + \frac{2k^2_{\mathcal{H}}}{3}\Phi(z_d, k)\right] \tag{D.70}$$

Using the Einstein de Sitter initial conditions at decoupling where $\Phi'(z_d, k) = 0$ provided that $\Omega_x \ll 1$ and given that $\pi'(z_d, k) = 0 = \sigma_m$ we get the following

$$\Phi(z_d, k) = -\frac{1+\alpha_H}{1+\alpha_T}\Psi(z_d, k) - \frac{\alpha_M - \alpha_T - \alpha_H}{1+\alpha_T}\mathcal{H}\pi(z_d, k) \tag{D.71}$$

Given that we have some parameter α_9 is define by

$$\alpha_9 \equiv 1 + \frac{2\alpha_B}{3(1+w_x)\Omega_x} \tag{D.72}$$

We then can finally write the initial fluctuations for $\pi(z_d, k)$ as follows

$$\pi(z_d, k) \equiv +\frac{1}{\alpha_9}V_x(z_d, k) + \frac{2\alpha_B}{3\alpha_9(1+w_x)\mathcal{H}\Omega_x}\Psi(z_d, k) \tag{D.73}$$

Note that the unified dark energy velocity fluctuations are denoted by

$$V_x(z_d,k) = -\frac{2}{3\mathcal{H}(1+\Omega_m w_m + \Omega_x w_x)}\Phi(z_d,k) \tag{D.74}$$

References

[1] Abramo, L. R., Reimberg, P. H., and Xavier, H. S. (2010). CMB in a box: causal structure and the Fourier-Bessel expansion. *Phys. Rev.*, D82:043510. (page 136)

[2] Adams, C. and Blake, C. (2017). Improving constraints on the growth rate of structure by modelling the density–velocity cross-correlation in the 6dF Galaxy Survey. *Mon. Not. Roy. Astron. Soc.*, 471(1):839–856. (page 114)

[3] Ade, P. A. R. et al. (2016). Planck 2015 results. XIV. Dark energy and modified gravity. *Astron. Astrophys.*, 594:A14. (page 2, 51, 86, 119, 128)

[4] Aghanim, N. et al. (2018). Planck 2018 results. VI. Cosmological parameters. *Astrophys. J.* (page 2, 76)

[5] Alcock, C. and Paczynski, B. (1979). An evolution free test for non-zero cosmological constant. *Nature*, 281:358–359. (page 4, 47)

[6] Amendola, L., Kunz, M., Motta, M., Saltas, I. D., and Sawicki, I. (2013). Observables and unobservables in dark energy cosmologies. *Phys. Rev.*, D87(2):023501. (page 86)

[7] Amendola, L. and Tsujikawa, S. (2010). *Dark Energy: Theory and Observations*. Cambridge University Press. (page 2, 11, 14)

[8] Andrianomena, S., Bonvin, C., Bacon, D., Bull, P., Clarkson, C., Maartens, R., and Moloi, T. (2018). Testing General Relativity with the Doppler magnification effect. *Mnras*. (page 85, 90, 96, 122)

[9] Arkani-Hamed, N., Cheng, H.-C., Luty, M. A., and Mukohyama, S. (2004). Ghost condensation and a consistent infrared modification of gravity. *JHEP*, 05:074. (page 51, 88)

[10] Armendariz-Picon, C., Damour, T., and Mukhanov, V. F. (1999). k - inflation. *Phys. Lett.*, B458:209–218. (page 51, 56, 58)

[11] Armendariz-Picon, C., Mukhanov, V. F., and Steinhardt, P. J. (2000). A Dynamical solution to the problem of a small cosmological constant and late time cosmic acceleration. *Phys. Rev. Lett.*, 85:4438–4441. (page 60)

[12] Armendariz-Picon, C., Mukhanov, V. F., and Steinhardt, P. J. (2001). Essentials of k essence. *Phys. Rev.*, D63:103510. (page 51, 56, 60)

[13] Arnowitt, R. L., Deser, S., and Misner, C. W. (2008). The Dynamics of general relativity. *Gen. Rel. Grav.*, 40:1997–2027. (page 9)

[14] B., T. R. and R, F. J. (2009). From distances to galaxy evolution and the dark matter problem. *aap*, 500:119–120. (page 114)

[15] Bacon, D. J., Andrianomena, S., Clarkson, C., Bolejko, K., and Maartens, R. (2014a). Cosmology with Doppler Lensing. *Mon. Not. Roy. Astron. Soc.*, 443(3):1900–1915. (page 59, 134, 135)

[16] Bacon, D. J., Andrianomena, S., Clarkson, C., Bolejko, K., and Maartens, R. (2014b). Cosmology with Doppler Lensing. *Mon. Not. Roy. Astron. Soc.*, 443(3):1900–1915. (page 69)

[17] Bacon, D. J., Refregier, A. R., and Ellis, R. S. (2000). Detection of weak gravitational lensing by large-scale structure. *Mon. Not. Roy. Astron. Soc.*, 318:625. (page 4)

[18] Bahcall, N. (1988). Large-scale strucrure in the universe indicated by galaxy clusters. *Annual review.* (page 35)

[19] Baker, T., Bellini, E., Ferreira, P. G., Lagos, M., Noller, J., and Sawicki, I. (2017). Strong constraints on cosmological gravity from GW170817 and GRB 170817A. *Phys. Rev. Lett.*, 119(25):251301. (page xix, 58, 76, 91)

[20] Baldauf, T., Seljak, U., Senatore, L., and Zaldarriaga, M. (2011). Galaxy Bias and non-Linear Structure Formation in General Relativity. *JCAP*, 1110:031. (page 59)

[21] Bardeen, J. M. (1980). Gauge Invariant Cosmological Perturbations. *Phys. Rev.*, D22:1882–1905. (page 11, 17, 42)

[22] Bartelmann, M. and Schneider, P. (2001). Weak gravitational lensing. *Phys. Rept.*, 340:291–472. (page 28)

[23] Bartolo, N., Matarrese, S., and Riotto, A. (2011). Relativistic Effects and Primordial Non-Gaussianity in the Galaxy bias. *JCAP*, 1104:011. (page 59)

[24] Bassett, B. A., Tsujikawa, S., and Wands, D. (2006). Inflation dynamics and reheating. *Rev. Mod. Phys.*, 78:537–589. (page 12)

[25] Battye, R. A. and Pearson, J. A. (2012). Effective action approach to cosmological perturbations in dark energy and modified gravity. *JCAP*, 1207:019. (page 51)

[26] Bean, R. and Tangmatitham, M. (2010). Current constraints on the cosmic growth history. *Phys. Rev.*, D81:083534. (page 114)

[27] Bekenstein, J. D. (1993). The Relation between physical and gravitational geometry. *Phys. Rev.*, D48:3641–3647. (page 51)

[28] Bellini, E. and Sawicki, I. (2014). Maximal freedom at minimum cost: linear large-scale structure in general modifications of gravity. *JCAP*, 1407:050. (page 50, 56, 57, 66, 87, 89, 92, 93, 124, 127, 151)

[29] Ben Achour, J., Crisostomi, M., Koyama, K., Langlois, D., Noui, K., and Tasinato, G. (2016). Degenerate higher order scalar-tensor theories beyond Horndeski up to cubic order. *JHEP*, 12:100. (page 51)

[30] Bernardeau, F., Bonvin, C., and Vernizzi, F. (2010). Full-sky lensing shear at second order. *Phys. Rev.*, D81:083002. (page 69)

[31] Bernardeau, F., Colombi, S., Gaztanaga, E., and Scoccimarro, R. (2002). Large scale structure of the universe and cosmological perturbation theory. *Phys. Rept.*, 367:1–248. (page 38)

[32] Bertacca, D., Bartolo, N., Bruni, M., Koyama, K., Maartens, R., Matarrese, S., Sasaki, M., and Wands, D. (2015). Galaxy bias and gauges at second order in General Relativity. *Class. Quant. Grav.*, 32(17):175019. (page 68)

[33] Bertschinger, E. and Zukin, P. (2008). Distinguishing Modified Gravity from Dark Energy. *Phys. Rev.*, D78:024015. (page 114)

[34] Bettoni, D. and Liberati, S. (2013). Disformal invariance of second order scalar-tensor theories: Framing the Horndeski action. *Phys. Rev.*, D88:084020. (page 51)

[35] Bettoni, D. and Liberati, S. (2015). Dynamics of non-minimally coupled perfect fluids. *JCAP*, 1508(08):023. (page)

[36] Bettoni, D. and Zumalacarregui, M. (2015). Kinetic mixing in scalar-tensor theories of gravity. *Phys. Rev.*, D91:104009. (page)

[37] Blas, D., Pujolas, O., and Sibiryakov, S. (2009). On the Extra Mode and Inconsistency of Horava Gravity. *JHEP*, 10:029. (page 58)

[38] Blas, D., Pujolas, O., and Sibiryakov, S. (2010). Consistent Extension of Horava Gravity. *Phys. Rev. Lett.*, 104:181302. (page 58)

[39] Bloomfield, J. (2013a). A Simplified Approach to General Scalar-Tensor Theories. *JCAP*, 1312:044. (page 51, 87)

[40] Bloomfield, J. K. (2013b). *COSMOLOGICAL MODELS OF MODIFIED GRAVITY*. PhD thesis, Cornell University. (page 4)

[41] Bloomfield, J. K. and Flanagan, E. E. (2012). A Class of Effective Field Theory Models of Cosmic Acceleration. *JCAP*, 1210:039. (page 51)

[42] Bloomfield, J. K., Flanagan, E. E., Park, M., and Watson, S. (2013). Dark energy or modified gravity? An effective field theory approach. *JCAP*, 1308:010. (page 50, 51, 55, 86, 87)

[43] Boggess, N. W. et al. (1992). The COBE mission - Its design and performance two years after launch. *Astrophys. J.*, 397:420–429. (page 11)

[44] Bolejko, K., Clarkson, C., Maartens, R., Bacon, D., Meures, N., and Beynon, E. (2013). Antilensing: The Bright Side of Voids. *Phys. Rev. Lett.*, 110(2):021302. (page 69, 135)

[45] Bonvin, C. (2008). Effect of Peculiar Motion in Weak Lensing. *Phys. Rev.*, D78:123530. (page 59, 81, 96, 102, 135)

[46] Bonvin, C. (2014). Isolating relativistic effects in large-scale structure. *Class. Quant. Grav.*, 31(23):234002. (page 59, 72, 99, 100, 130, 132)

[47] Bonvin, C., Andrianomena, S., Bacon, D., Clarkson, C., Maartens, R., Moloi, T., and Bull, P. (2017). Dipolar modulation in the size of galaxies: The effect of Doppler magnification. *Mon. Not. Roy. Astron. Soc.*, 472(4):3936–3951. (page 74, 81, 85, 96, 97, 98, 99, 100, 102, 120, 124, 127, 128)

[48] Bonvin, C. and Durrer, R. (2011). What galaxy surveys really measure. *Phys. Rev.*, D84:063505. (page 24, 59, 67, 70, 72, 73, 96, 130, 132, 133, 134)

[49] Bonvin, C., Durrer, R., and Gasparini, M. A. (2006). Fluctuations of the luminosity distance. *Phys. Rev.*, D73:023523. [Erratum: Phys. Rev.D85,029901(2012)]. (page 81, 135)

[50] Bonvin, C., Hui, L., and Gaztanaga, E. (2014). Asymmetric galaxy correlation functions. *Phys. Rev.*, D89(8):083535. (page 59, 75, 96, 97, 99, 100, 102, 105)

[51] Boubekeur, L., Creminelli, P., Norena, J., and Vernizzi, F. (2008). Action approach to cosmological perturbations: the 2nd order metric in matter dominance. *JCAP*, 0808:028. (page 51)

[52] Bouchet, F., Colombi, S., Hivon, E., and Juszkiewicz, R. (1995). Perturbative lagrangian approach to gravitational instability. *aap*, 296:575. (page 38)

[53] Brans, C. and Dicke, R. H. (1961). Mach's principle and a relativistic theory of gravitation. *Phys. Rev.*, 124:925–935. [,142(1961)]. (page 56)

[54] Brax, P. and Burrage, C. (2014). Constraining Disformally Coupled Scalar Fields. *Phys. Rev.*, D90(10):104009. (page 51, 68)

[55] Bruni, M., Matarrese, S., Mollerach, S., and Sonego, S. (1997). Perturbations of space-time: Gauge transformations and gauge invariance at second order and beyond. *Class. Quant. Grav.*, 14:2585–2606. (page 15)

[56] Carroll, S., Press, W., and Turner, E. (1992). The cosmological constant. *araa*, 30:499–542. (page 38)

[57] Carroll, S. M. (2004). *Spacetime and geometry: An introduction to general relativity.* American Physical Society. (page 60)

[58] Carroll, S. M., De Felice, A., Duvvuri, V., Easson, D. A., Trodden, M., and Turner, M. S. (2005). The Cosmology of generalized modified gravity models. *Phys. Rev.*, D71:063513. (page 56)

[59] Carroll, S. M., Duvvuri, V., Trodden, M., and Turner, M. S. (2004). Is cosmic speed - up due to new gravitational physics? *Phys. Rev.*, D70:043528. (page 56)

[60] Chagoya, J. and Tasinato, G. (2018). Compact objects in scalar-tensor theories after GW170817. *JCAP*, 1808(08):006. (page 58)

[61] Chakrabarty, H., Abdikamalov, A. B., Abdujabbarov, A. A., and Bambi, C. (2018). Weak gravitational lensing: a compact object with arbitrary quadrupole moment immersed in plasma. *Phys. Rev.*, D98(2):024022. (page 28)

[62] Challinor, A. and Lewis, A. (2011). The linear power spectrum of observed source number counts. *Phys. Rev.*, D84:043516. (page 39, 59, 67, 73)

[63] Cheung, C., Creminelli, P., Fitzpatrick, A. L., Kaplan, J., and Senatore, L. (2008). The Effective Field Theory of Inflation. *JHEP*, 03:014. (page 51, 55, 87)

[64] Clifton, T., Ferreira, P. G., Padilla, A., and Skordis, C. (2012). Modified Gravity and Cosmology. *Phys. Rept.*, 513:1–189. (page 51, 86)

[65] Cole, S., Fisher, K. B., and Weinberg, D. H. (1995). Constraints on Omega from the IRAS redshift surveys. *mnras*, 275:515–526. (page 97)

[66] Contreras, C., Blake, C., Poole, G. B., and Marin, F. (2013). Determining accurate measurements of the growth rate from the galaxy correlation function in simulations. *Mon. Not. Roy. Astron. Soc.*, 430(2):934–945. (page 97)

[67] Creminelli, P., D'Amico, G., Norena, J., and Vernizzi, F. (2009). The Effective Theory of Quintessence: the w<-1 Side Unveiled. *JCAP*, 0902:018. (page 50, 51)

[68] Creminelli, P., Lewandowski, M., Tambalo, G., and Vernizzi, F. (2018). Gravitational Wave Decay into Dark Energy. *JHEP*. (page 58)

[69] Creminelli, P., Luty, M. A., Nicolis, A., and Senatore, L. (2006). Starting the Universe: Stable Violation of the Null Energy Condition and Non-standard Cosmologies. *JHEP*, 12:080. (page 51, 87, 88)

[70] Creminelli, P. and Vernizzi, F. (2017). Dark Energy after GW170817 and GRB170817A. *Phys. Rev. Lett.*, 119(25):251302. (page 58)

[71] Crisostomi, M., Hull, M., Koyama, K., and Tasinato, G. (2016a). Horndeski: beyond, or not beyond? *JCAP*, 1603(03):038. (page 51)

[72] Crisostomi, M., Koyama, K., and Tasinato, G. (2016b). Extended Scalar-Tensor Theories of Gravity. *JCAP*, 1604(04):044. (page)

[73] D'Amico, G., Huang, Z., Mancarella, M., and Vernizzi, F. (2017). Weakening Gravity on Redshift-Survey Scales with Kinetic Matter Mixing. *JCAP*, 1702:014. (page 51)

[74] De Felice, A., Kobayashi, T., and Tsujikawa, S. (2011). Effective gravitational couplings for cosmological perturbations in the most general scalar-tensor theories with second-order field equations. *Phys. Lett.*, B706:123–133. (page 86)

[75] De Felice, A. and Tsujikawa, S. (2010). f(R) theories. *Living Rev. Rel.*, 13:3. (page 51, 61)

[76] de Putter, R. and Linder, E. V. (2007). Kinetic k-essence and Quintessence. *Astropart. Phys.*, 28:263–272. (page 58)

[77] de Rham, C. (2014). Massive Gravity. *Living Rev. Rel.*, 17:7. (page 50)

[78] Deffayet, C., Deser, S., and Esposito-Farese, G. (2009a). Generalized Galileons: All scalar models whose curved background extensions maintain second-order field equations and stress-tensors. *Phys. Rev.*, D80:064015. (page 51, 56)

[79] Deffayet, C., Esposito-Farese, G., and Vikman, A. (2009b). Covariant Galileon. *Phys. Rev.*, D79:084003. (page 56)

[80] Deffayet, C., Gao, X., Steer, D. A., and Zahariade, G. (2011). From k-essence to generalised Galileons. *Phys. Rev.*, D84:064039. (page 61)

[81] Deffayet, C., Pujolas, O., Sawicki, I., and Vikman, A. (2010). Imperfect Dark Energy from Kinetic Gravity Braiding. *JCAP*, 1010:026. (page 51)

[82] Dent, J. B. and Dutta, S. (2009). On the dangers of using the growth equation on large scales. *Phys. Rev.*, D79:063516. (page 65, 68)

[83] Deruelle, N. and Mukhanov, V. F. (1995). On matching conditions for cosmological perturbations. *Phys. Rev.*, D52:5549–5555. (page 10)

[84] Di Dio, E., Montanari, F., Durrer, R., and Lesgourgues, J. (2014). Cosmological Parameter Estimation with Large Scale Structure Observations. *JCAP*, 1401:042. (page 81)

[85] Dima, A. and Vernizzi, F. (2018). Vainshtein Screening in Scalar-Tensor Theories before and after GW170817: Constraints on Theories beyond Horndeski. *Phys. Rev.*, D97(10):101302. (page 58)

[86] Djorgovski, S. and Davis, M. (1987). Fundamental properties of elliptical galaxies. *apj*, 313:59–68. (page 114)

[87] Dodelson, S. (2003). *Modern cosmology*. Academic Press, San Diego, CA. (page 3, 11, 36, 73)

[88] Domenech, G., Mukohyama, S., Namba, R., Naruko, A., Saitou, R., and Watanabe, Y. (2015). Derivative-dependent metric transformation and physical degrees of freedom. *Phys. Rev.*, D92(8):084027. (page 51)

[89] Duniya, D. (2016a). Dark energy homogeneity in general relativity: Are we applying it correctly? *Gen. Rel. Grav.*, 48(4):52. (page 59)

[90] Duniya, D. (2016b). Large-scale imprint of relativistic effects in the cosmic magnification. *Phys. Rev.*, D93(10):103538. [Addendum: Phys. Rev.D93,no.12,129902(2016)]. (page)

[91] Duniya, D. (2016c). Understanding the relativistic overdensity of galaxy surveys. *JCAP*. (page)

[92] Duniya, D., Bertacca, D., and Maartens, R. (2013). Clustering of quintessence on horizon scales and its imprint on HI intensity mapping. *JCAP*, 1310:015. (page 59, 73, 159)

[93] Duniya, D. G., Clarkson, C., Weltman, A., Maartens, R., and Moloi, T. (2019). Probing beyond-Horndeski gravity on horizon scales. *In preparation.* (page 78, 81, 151, 153)

[94] Duniya, D. G. A., Bertacca, D., and Maartens, R. (2015). Probing the imprint of interacting dark energy on very large scales. *Phys. Rev.*, D91:063530. (page 59, 65, 67, 73, 81, 159)

[95] Duniya, Didam, G. A. (2015). *Relativistic Corrections to the Power Spectrum.* PhD thesis, University of the Western Cape. (page 11, 14, 18, 20, 23, 24, 35, 73, 133, 134, 159)

[96] Durrer, R. (1994). Gauge invariant cosmological perturbation theory: A General study and its application to the texture scenario of structure formation. *Fund. Cosmic Phys.*, 15:209–339. (page 11, 19)

[97] Durrer, R. and Tansella, V. (2016). Vector perturbations of galaxy number counts. *JCAP*, 1607(07):037. (page 59)

[98] Edmonds, A. R. (1996). *Angular momentum in quantum mechanics.* Princeton University Press. (page 137)

[99] Eingorn, M., Novák, J., and Zhuk, A. (2014). $f(R)$ gravity: scalar perturbations in the late Universe. *Eur. Phys. J.*, C74(8):3005. (page 61)

[100] Einstein, A. (1915). Die Feldgleichungen der Gravitation. *Sitzungsberichte der Königlich Preußischen Akademie der Wissenschaften (Berlin), Seite 844-847.* (page 25)

[101] Einstein, A. (1916). Die grundlage der allgemeinen relativitätstheorie. *Annalen der Physik*, 354:769–822. (page 25)

[102] Einstein, A. (1917). Kosmologische Betrachtungen zur allgemeinen Relativitätstheorie. *Sitzungsberichte der Königlich Preußischen Akademie der Wissenschaften (Berlin), Seite 142-152.* (page 25)

[103] Eisenstein, D. J. et al. (2005). Detection of the Baryon Acoustic Peak in the Large-Scale Correlation Function of SDSS Luminous Red Galaxies. *Astrophys. J.*, 633:560–574. (page 3, 42)

[104] Eisenstein, D. J. and Hu, W. (1997). Power spectra for cold dark matter and its variants. *Astrophys. J.*, 511:5. (page 91, 102)

[105] Ellis, G. F. R., Maartens, R., and MacCallum, A. H. (2012). *Relativistic cosmology.* Cambridge University Press, United Kingdom. (page 20)

[106] Endlich, S., Gorbenko, V., Huang, J., and Senatore, L. (2017). An effective formalism for testing extensions to General Relativity with gravitational waves. *JHEP*, 09:122. (page 51)

[107] Ezquiaga, J. M., Garcia-Bellido, J., and Zumalacárregui, M. (2016). Towards the most general scalar-tensor theories of gravity: a unified approach in the language of differential forms. *Phys. Rev.*, D94(2):024005. (page 51, 56)

[108] Ezquiaga, J. M. and Zumalacárregui, M. (2017). Dark Energy After GW170817: Dead Ends and the Road Ahead. *Phys. Rev. Lett.*, 119(25):251304. (page 58)

[109] Fang, W.-J. and Haiman, Z. (2007). Constraining Dark Energy by Combining Cluster Counts and Shear-Shear Correlations in a Weak Lensing Survey. *Phys. Rev.*, D75:043010. (page 4)

[110] Friedmann, A. (1924). On the Possibility of a world with constant negative curvature of space. *Z. Phys.*, 21:326–332. [Gen. Rel. Grav.31,2001(1999)]. (page 11)

[111] García-Bellido, J., Linde, A., and Linde, D. (1994). Fluctuations of the gravitational constant in the inflationary brans-dicke cosmology. *Phys. Rev. D*, 50:730–750. (page 35)

[112] Garriga, J. and Mukhanov, V. F. (1999). Perturbations in k-inflation. *Phys. Lett.*, B458:219–225. (page 60)

[113] Giannantonio, T., Martinelli, M., Silvestri, A., and Melchiorri, A. (2010). New constraints on parametrised modified gravity from correlations of the cmb with large scale structure. *Journal of Cosmology and Astroparticle Physics*, 2010(04):030. (page 119, 128)

[114] Glanza, J. (1917). Cosmic motion revealed. *Science*, 282:2156–2157. (page 25)

[115] Gleyzes, J., Langlois, D., Mancarella, M., and Vernizzi, F. (2015a). Effective Theory of Interacting Dark Energy. *JCAP*, 1508(08):054. (page 51, 114)

[116] Gleyzes, J., Langlois, D., Piazza, F., and Vernizzi, F. (2013). Essential Building Blocks of Dark Energy. *JCAP*, 1308:025. (page 50, 53, 62, 87, 88, 114, 124, 127)

[117] Gleyzes, J., Langlois, D., Piazza, F., and Vernizzi, F. (2015b). Exploring gravitational theories beyond Horndeski. *JCAP*, 1502:018. (page 66)

[118] Gleyzes, J., Langlois, D., Piazza, F., and Vernizzi, F. (2015c). Healthy theories beyond Horndeski. *Phys. Rev. Lett.*, 114(21):211101. (page 63, 87, 127)

[119] Gleyzes, J., Langlois, D., and Vernizzi, F. (2015d). A unifying description of dark energy. *Int. J. Mod. Phys.*, D23(13):1443010. (page 50, 51, 60, 61, 63, 65, 66, 86, 87, 89, 93, 94, 114, 124, 127, 151, 152, 153)

[120] Golovnev, A. (2013). ADM analysis and massive gravity. In *Modern Mathematical Physics. Proceedings, 7th Summer School: Belgrade, Serbia, September 9-19, 2012*, pages 171–179. (page 9)

[121] Grishchuk, L. P. (1975). The Amplification of Gravitational Waves and Creation of Gravitons in the Isotropic Universe. *Lett. Nuovo Cim.*, 12:60–64. [Erratum: Lett. Nuovo Cim.12,432(1975)]. (page 11)

[122] Groth, E. and Peebles, P. (1977). Statistical analysis of catalogs of extragalactic objects. *apj*, 217:385–405. (page 38)

[123] Gubitosi, G., Piazza, F., and Vernizzi, F. (2013). The Effective Field Theory of Dark Energy. *JCAP*, 1302:032. [JCAP1302,032(2013)]. (page 50, 51, 55, 86, 87, 93)

[124] Guth, A. H. (1981). Inflationary universe: A possible solution to the horizon and flatness problems. *Phys. Rev. D*, 23:347–356. (page 35, 41)

[125] Guth, A.H.and Pi, S.-Y. (1982). Fluctuations in the new inflationary universe. *Physical Review Letters*, 49:1110–1113. (page 41)

[126] Hamilton, A. (1992). Measuring omega and the real correlation function from the redshift correlation function. *apj*, 385:L5–L8. (page 97)

[127] Hassan, S. F. and Rosen, R. A. (2012a). Bimetric Gravity from Ghost-free Massive Gravity. *JHEP*, 02:126. (page 50)

[128] Hassan, S. F. and Rosen, R. A. (2012b). Confirmation of the Secondary Constraint and Absence of Ghost in Massive Gravity and Bimetric Gravity. *JHEP*, 04:123. (page 9)

[129] Hassan, S. F. and Rosen, R. A. (2012c). Resolving the Ghost Problem in non-Linear Massive Gravity. *Phys. Rev. Lett.*, 108:041101. (page)

[130] Hassan, S. F., Rosen, R. A., and Schmidt-May, A. (2012). Ghost-free Massive Gravity with a General Reference Metric. *JHEP*, 02:026. (page 9)

[131] Heath, D. (1977). The growth of density perturbations in zero pressure friedmann-lemaitre universes. *mnras*, 179:351–358. (page 27, 38)

[132] Heavens, A. F. and Taylor, A. N. (1995). A Spherical Harmonic Analysis of Redshift Space. *Mon. Not. Roy. Astron. Soc.*, 275:483–497. (page 46)

[133] Hebecker, A., Kraus, S. C., and Witkowski, L. T. (2014). D7-Brane Chaotic Inflation. *Phys. Lett.*, B737:16–22. (page 87)

[134] Hirano, S., Kobayashi, T., Tashiro, H., and Yokoyama, S. (2018). Matter bispectrum beyond Horndeski theories. *Phys. Rev.*, D97(10):103517. (page 58)

[135] Hojjati, A., Zhao, G.-B., Pogosian, L., Silvestri, A., Crittenden, R., and Koyama, K. (2012). Cosmological tests of General Relativity: a principal component analysis. *Phys. Rev.*, D85:043508. (page 114)

[136] Holder, G., Haiman, Z., and Mohr, J. (2001). Constraints on $omega_m$, $omega_l$, and $sigma_8$, from galaxy cluster redshift distributions. *Astrophys. J.*, 560:L111–L114. (page 4)

[137] Horava, P. (2009). Quantum Gravity at a Lifshitz Point. *Phys. Rev.*, D79:084008. (page 58)

[138] Horndeski, G. W. (1974). Second-Order Scalar-Tensor Field Equations in a Four-Dimensional Space. *International Journal of Theoretical Physics*, 10:363–384. (page 61)

[139] Howlett, C., Staveley-Smith, L., and Blake, C. (2017). Cosmological Forecasts for Combined and Next Generation Peculiar Velocity Surveys. *Mon. Not. Roy. Astron. Soc.*, 464(3):2517–2544. (page 114)

[140] Hu, B., Liguori, M., Bartolo, N., and Matarrese, S. (2013). Parametrized modified gravity constraints after Planck. *Phys. Rev.*, D88(12):123514. (page 114, 119, 128)

[141] Hu, B., Raveri, M., Frusciante, N., and Silvestri, A. (2014). Effective Field Theory of Cosmic Acceleration: an implementation in CAMB. *Phys. Rev.*, D89(10):103530. (page 50, 114)

[142] Hu, W. (2003). Self-consistency and calibration of cluster number count surveys for dark energy. *Phys. Rev.*, D67:081304. (page 4)

[143] Iyonaga, A., Takahashi, K., and Kobayashi, T. (2018). Extended Cuscuton: Formulation. *JHEP*. (page 58)

[144] Jeong, D. and Schmidt, F. (2012). Large-Scale Structure with Gravitational Waves I: Galaxy Clustering. *Phys. Rev.*, D86:083512. (page 67)

[145] Jeong, D., Schmidt, F., and Hirata, C. M. (2012). Large-scale clustering of galaxies in general relativity. *Phys. Rev.*, D85:023504. (page 67)

[146] Joyce, A., Jain, B., Khoury, J., and Trodden, M. (2015). Beyond the Cosmological Standard Model. *Phys. Rept.*, 568:1–98. (page 50)

[147] Kaiser, N. (1987). Clustering in real space and in redshift space. *mnras*, 227:1–21. (page 97)

[148] Kaiser, N. and Squires, G. (1993). Mapping the dark matter with weak gravitational lensing. *Astrophys. J.*, 404:441–450. (page 28, 45)

[149] Kase, R. and Tsujikawa, S. (2018). Dark energy scenario consistent with GW170817 in theories beyond Horndeski gravity. *Phys. Rev.*, D97(10):103501. (page 58)

[150] Kobayashi, T., Yamaguchi, M., and Yokoyama, J. (2011). Generalized G-inflation: Inflation with the most general second-order field equations. *Prog. Theor. Phys.*, 126:511–529. (page 61)

[151] Kodama, H. and Sasaki, M. (1984). Cosmological Perturbation Theory. *Progress of Theoretical Physics Supplement*, 78:1. (page 11, 20, 22)

[152] Kofman, L., Linde, A., and Starobinsky, A. A. (1994). Reheating after inflation. *Phys. Rev. Lett.*, 73:3195–3198. (page 35)

[153] Koyama, K. (2008). The cosmological constant and dark energy in braneworlds. *Gen. Rel. Grav.*, 40:421–450. (page 114)

[154] Koyama, K. (2016). Cosmological Tests of Modified Gravity. *Rept. Prog. Phys.*, 79(4):046902. (page 86)

[155] Kunz, M. (2009). The dark degeneracy: On the number and nature of dark components. *Phys. Rev.*, D80:123001. (page 51)

[156] KUTNER, M. L. (2003). Astronomy. a physical perspective. *Astronomische Nachrichten*, 310(3):186–186. (page 25)

[157] Lahav, O., Lilje, P., Primack, J., and Rees, M. (1991). ynamical effects of the cosmological constant. *mras*, 251:128–136. (page 27, 38, 46)

[158] Langlois, D. and Noui, K. (2016). Hamiltonian analysis of higher derivative scalar-tensor theories. *JCAP*, 1607(07):016. (page 51)

[159] Laureijs, R. et al. (2011). Euclid Definition Study Report. *Phys. Rev.* (page 5)

[160] Lemaitre, G. (1931). A homogeneous universe of constant mass and increasing radius accounting for the radial velocity of extra-galactic nebulae. *Mon. Not. Roy. Astron. Soc.*, 91:483–490. (page 11)

[161] Levine, E. S., Schulz, A. E., and White, M. J. (2002). Future galaxy cluster surveys: The Effect of theory uncertainty on constraining cosmological parameters. *Astrophys. J.*, 577:569–578. (page 4)

[162] Lewandowski, M., Maleknejad, A., and Senatore, L. (2017). An effective description of dark matter and dark energy in the mildly non-linear regime. *JCAP*, 1705(05):038. (page 51)

[163] Li, B., Barrow, J. D., and Mota, D. F. (2007). The Cosmology of Modified Gauss-Bonnet Gravity. *Phys. Rev.*, D76:044027. (page 114)

[164] Li, J., Carlson, B. E., and Lacis, A. A. (2014). Application of spectral analysis techniques in the inter-comparison of aerosol data. *Atmos. Meas. Tech.*, 7:2531–2549. (page 47)

[165] Li, X.-D., Park, C., Sabiu, C. G., Park, H., Weinberg, D. H., Schneider, D. P., Kim, J., and Hong, S. E. (2016). Cosmological constraints from the redshift dependence of the Alcock-Paczynski effect: application to the SDSS-III BOSS DR12 galaxies. *Astrophys. J.*, 832(2):103. (page 47)

[166] Lifshitz, E. (1946). Republication of: On the gravitational stability of the expanding universe. *J. Phys.(USSR)*, 10:116. [Gen. Rel. Grav.49,no.2,18(2017)]. (page 11)

[167] Lifshitz, E. M. and Khalatnikov, I. M. (1963). Investigations in relativistic cosmology. *Adv. Phys.*, 12:185–249. (page 11)

[168] Lightman, A. and Schechter, P. (1990). The omega dependence of peculiar velocities induced by spherical density perturbations. *apjs*, 74:831. (page 38)

[169] Linde, A. (1994). Hybrid inflation. *Phys. Rev. D*, 49:748–754. (page 35)

[170] Liu, J., Haiman, Z., Hui, L., Kratochvil, J. M., and May, M. (2014). The Impact of Magnification and Size Bias on Weak Lensing Power Spectrum and Peak Statistics. *Phys. Rev.*, D89(2):023515. (page 49)

[171] Lombriser, L. and Taylor, A. (2015a). Classifying Linearly Shielded Modified Gravity Models in Effective Field Theory. *Phys. Rev. Lett.*, 114(3):031101. (page 50, 66)

[172] Lombriser, L. and Taylor, A. (2015b). Semi-dynamical perturbations of unified dark energy. *JCAP*, 1511(11):040. (page 24, 51, 89, 151)

[173] Lopez-Corredoira, M. (2014). Alcock-Paczynski cosmological test. *Astrophys. J.*, 781(2):96. (page 4)

[174] Lopez-Honorez, L., Mena, O., and Rigolin, S. (2012). Biases on cosmological parameters by general relativity effects. *Phys. Rev.*, D85:023511. (page 67)

[175] Maartens, R., Abdalla, F. B., Jarvis, M., and Santos, M. G. (2015). Overview of Cosmology with the SKA. *PoS*, AASKA14:016. (page 5)

[176] Malik, K. A. (2001). *Cosmological perturbations in an inflationary universe*. PhD thesis, Portsmouth U. (page 11, 14, 18, 20, 22)

[177] Malik, K. A. and Matravers, D. R. (2008). A Concise Introduction to Perturbation Theory in Cosmology. *Class. Quant. Grav.*, 25:193001. (page 15)

[178] Malik, K. A. and Wands, D. (2004). Evolution of second-order cosmological perturbations. *Class. Quant. Grav.*, 21:L65–L72. (page 159)

[179] Malik, K. A. and Wands, D. (2009). Cosmological perturbations. *Phys. Rept.*, 475:1–51. (page 12, 15)

[180] Marian, L. and Bernstein, G. M. (2006). Dark energy constraints from lensing-detected galaxy clusters. *Phys. Rev.*, D73:123525. (page 4)

[181] Maselli, A., Silva, H. O., Minamitsuji, M., and Berti, E. (2015). Slowly rotating black hole solutions in Horndeski gravity. *Phys. Rev.*, D92(10):104049. (page 56)

[182] Massey, R., Kitching, T., and Richard, J. (2010). The dark matter of gravitational lensing. *Rept. Prog. Phys.*, 73:086901. (page 28)

[183] Matarrese, S., Mollerach, S., and Bruni, M. (1998). Second order perturbations of the Einstein-de Sitter universe. *Phys. Rev.*, D58:043504. (page 15)

[184] Menotti, P. (2017). Lectures on gravitation. *JHEP*. (page 51)

[185] Molnar, S. M., Haiman, Z., Birkinshaw, M., and Mushotzky, R. F. (2004). Constraints on the energy content of the universe from a combination of galaxy cluster observables. *Astrophys. J.*, 601:22–27. (page 4)

[186] Motohashi, H., Noui, K., Suyama, T., Yamaguchi, M., and Langlois, D. (2016). Healthy degenerate theories with higher derivatives. *JCAP*, 1607(07):033. (page 51)

[187] Mueller, E.-M., Bean, R., and Watson, S. (2013). Cosmological implications of the effective field theory of cosmic acceleration. *Phys. Rev.*, D87(8):083504. (page 51)

[188] Mukhanov, V. F., Feldman, H. A., and Brandenberger, R. H. (1992). Theory of cosmological perturbations. Part 1. Classical perturbations. Part 2. Quantum theory of perturbations. Part 3. Extensions. *Phys. Rept.*, 215:203–333. (page 11, 12, 20)

[189] Munshi, D., Valageas, P., Van Waerbeke, L., and Heavens, A. (2008). Cosmology with Weak Lensing Surveys. *Phys. Rept.*, 462:67–121. (page 4)

[190] Namikawa, T., Bouchet, F. R., and Taruya, A. (2018). CMB lensing bispectrum as a probe of modified gravity theories. *Phys. Rev.*, D98(4):043530. (page 58)

[191] Narayan, R. and Bartelmann, M. (1996). Lectures on gravitational lensing. In *13th Jerusalem Winter School in Theoretical Physics: Formation of Structure in the Universe Jerusalem, Israel, 27 December 1995 - 5 January 1996*. (page 28)

[192] Nicolis, A., Rattazzi, R., and Trincherini, E. (2009). The Galileon as a local modification of gravity. *Phys. Rev.*, D79:064036. (page 51)

[193] Novosyadlyj, B., Pelykh, V., Shtanov, Yu., and Zhuk, A. (2013). *Dark Energy: Observational Evidence and Theoretical Models*. Academperiodyka, Kyiv. (page 60)

[194] O'Raifeartaigh, C., O'Keeffe, M., Nahm, W., and Mitton, S. (2015). Einstein's cosmology review of 1933: a new perspective on the Einstein-de Sitter model of the cosmos. *Eur. Phys. J.*, H40(3):301–335. (page 39)

[195] P. Schneider, J. Ehlers, E. F. (1992). Gravitational lenses, xiv, 560 pp. 112 figs.. springer-verlag berlin heidelberg new york. also astronomy and astrophysics library. *Astronomische Nachrichten*, 314(4):314–315. (page 28)

[196] Pandolfi, S., Cooray, A., Giusarma, E., Kolb, E. W., Melchiorri, A., Mena, O., and Serra, P. (2010). Harrison-zel'dovich primordial spectrum is consistent with observations. *Phys. Rev. D*, 81:123509. (page 36)

[197] Park, M., Zurek, K. M., and Watson, S. (2010). A Unified Approach to Cosmic Acceleration. *Phys. Rev.*, D81:124008. (page 50, 51)

[198] Passaglia, S. and Hu, W. (2018). Scalar Bispectrum Beyond Slow-Roll in the Unified EFT of Inflation. *Phys. Rev.*, D98(2):023526. (page 58)

[199] Peebles, P. (1980). *The large-scale structure of the universe*. Princeton University Press. (page 1, 27, 45, 46)

[200] Peebles, P. (1993). *Principles of Physical Cosmology*. Princeton University Press. (page 25)

[201] Peiris, H. V. et al. (2003). First year Wilkinson Microwave Anisotropy Probe (WMAP) observations: Implications for inflation. *Astrophys. J. Suppl.*, 148:213–231. (page xiii, 37)

[202] Percival, W. J. (2005). Cosmological structure formation in a homogeneous dark energy background. *Astron. Astrophys.*, 443:819. (page 37)

[203] Perlick, V. (2010). Gravitational Lensing from a Spacetime Perspective. *Submitted to: Living Rev. Rel.* (page 28)

[204] Perlmutter, S. et al. (1999). Measurements of Omega and Lambda from 42 high redshift supernovae. *Astrophys. J.*, 517:565–586. (page 2, 3)

[205] Piazza, F., Steigerwald, H., and Marinoni, C. (2014). Phenomenology of dark energy: exploring the space of theories with future redshift surveys. *JCAP*, 1405:043. (page 87)

[206] Piazza, F. and Vernizzi, F. (2013). Effective Field Theory of Cosmological Perturbations. *Class. Quant. Grav.*, 30:214007. (page 50)

[207] Ratra, B. and Peebles, P. J. E. (1988). Cosmological Consequences of a Rolling Homogeneous Scalar Field. *Phys. Rev.*, D37:3406. (page 56)

[208] Renk, J., Zumalacarregui, M., and Montanari, F. (2016). Gravity at the horizon: on relativistic effects, CMB-LSS correlations and ultra-large scales in Horndeski's theory. *JCAP*, 1607(07):040. (page 59, 114)

[209] Riess, A. G. et al. (1998). Observational evidence from supernovae for an accelerating universe and a cosmological constant. *Astron. J.*, 116:1009–1038. (page 2, 3)

[210] Riotto, A. (2003). Inflation and the theory of cosmological perturbations. *ICTP Lect. Notes Ser.*, 14:317–413. (page 15)

[211] Robertson, H. P. (1936). Kinematics and World-Structure. 3. *Astrophys. J.*, 83:257–271. (page 11)

[212] Rogers, A. (2015). Frequency-dependent effects of gravitational lensing within plasma. *Mon. Not. Roy. Astron. Soc.*, 451(1):17–25. (page 28)

[213] Rogers, A. (2017). Gravitational Lensing of Rays through the Levitating Atmospheres of Compact Objects. *Universe*, 3:3. (page 28)

[214] Ruth, D. (2008). *The Cosmic Microwave Background*. Cambridge Graduate Texts. Cambridge University Press, Cambridge. (page 11, 18, 19, 20, 135)

[215] Ryden, B. (2016). *Introduction to cosmology*. Cambridge University Press. (page 25)

[216] Sakstein, J. and Jain, B. (2017). Implications of the Neutron Star Merger GW170817 for Cosmological Scalar-Tensor Theories. *Phys. Rev. Lett.*, 119(25):251303. (page xix, 58, 66, 76, 92)

[217] Sakstein, J., Wilcox, H., Bacon, D., Koyama, K., and Nichol, R. C. (2016). Testing Gravity Using Galaxy Clusters: New Constraints on Beyond Horndeski Theories. *JCAP*, 1607(07):019. (page xix, 66, 76, 92, 93, 110)

[218] Santoni, L., Trincherini, E., and Trombetta, L. G. (2018). Behind Horndeski: structurally robust higher derivative EFTs. *JHEP*, 08:118. (page 58)

[219] Sasaki, M. (1993). Cosmological gravitational lens equation: Its validity and limitation. In *Cosmological gravitational lens equation: Its validity and limitation.*, volume 90, pages 291–472. (page 28)

[220] Sawicki, I. and Bellini, E. (2015). Limits of quasistatic approximation in modified-gravity cosmologies. *Phys. Rev.*, D92(8):084061. (page 86, 94)

[221] Schlegel, D. J. et al. (2009). BigBOSS: The Ground-Based Stage IV Dark Energy Experiment. *Astron. Astrophys.* (page 3)

[222] Schmidt, B. P. et al. (1998). The High Z supernova search: Measuring cosmic deceleration and global curvature of the universe using type Ia supernovae. *Astrophys. J.*, 507:46–63. (page 3)

[223] Schmidt, F., Leauthaud, A., Massey, R., Rhodes, J., George, M. R., Koekemoer, A. M., Finoguenov, A., and Tanaka, M. (2012). A Detection of Weak Lensing Magnification using Galaxy Sizes and Magnitudes. *Astrophys. J.*, 744:L22. (page 4)

[224] Scrimgeour, M. I. et al. (2016). The 6dF Galaxy Survey: Bulk Flows on $50-70h^{-1}$ Mpc scales. *Mon. Not. Roy. Astron. Soc.*, 455(1):386–401. (page 114)

[225] Seljak, U. et al. (2005). Cosmological parameter analysis including SDSS Ly-alpha forest and galaxy bias: Constraints on the primordial spectrum of fluctuations, neutrino mass, and dark energy. *Phys. Rev.*, D71:103515. (page xiii, 37)

[226] Shirasaki, M., Hamana, T., and Yoshida, N. (2016). Probing cosmology with weak lensing selected clusters II: Dark energy and f(R) gravity models. *Publ. Astron. Soc. Jap.*, 68(1):4. (page 4)

[227] Song, Y.-S., Hu, W., and Sawicki, I. (2007). The Large Scale Structure of f(R) Gravity. *Phys. Rev.*, D75:044004. (page 92, 93)

[228] Springel, V., Frenk, C. S., and White, S. D. M. (2006). The large-scale structure of the Universe. *Nature*, 440:1137. (page 48)

[229] Sriramkumar, L. (2009). An introduction to inflation and cosmological perturbation theory. *Phys. Rev.* (page 22)

[230] Szapudi, I., Pan, J., Prunet, S., and Budavari, T. (2005). Fast edge corrected measurement of the two-point correlation function and the power spectrum. *Astrophys. J.*, 631:L1–L4. (page 81)

[231] Takada, M. and Bridle, S. (2007). Probing dark energy with cluster counts and cosmic shear power spectra: including the full covariance. *New J. Phys.*, 9:446. (page 4)

[232] Tegmark, M. et al. (2004). Cosmological parameters from SDSS and WMAP. *Phys. Rev.*, D69:103501. (page xiii, 36, 37)

[233] Tsujikawa, S. (2015). The effective field theory of inflation/dark energy and the Horndeski theory. *Lect. Notes Phys.*, 892:97–136. (page 50, 87)

[234] Turner, M. S. and Huterer, D. (2007). Cosmic Acceleration, Dark Energy and Fundamental Physics. *J. Phys. Soc. Jap.*, 76:111015. (page 3)

[235] Wagner, C., Muller, V., and Steinmetz, M. (2008). Constraining dark energy via baryon acoustic oscillations in the (an)isotropic light-cone power spectrum. *Astron. Astrophys.*, 487:63–74. (page 3)

[236] Wald, R. M. (1984). *General relativity.* Chicago Univ. Press, Chicago, IL. (page 10)

[237] Walker, R. M. (1984). On Milne's Theory of World-Structure. *Proceedings of the London Mathematical Society*, 42:90–127. (page 11)

[238] Wands, D. and Slosar, A. (2009). Scale-dependent bias from primordial non-Gaussianity in general relativity. *Phys. Rev.*, D79:123507. (page 68)

[239] Wang, L.-M. and Steinhardt, P. J. (1998). Cluster abundance constraints on quintessence models. *Astrophys. J.*, 508:483–490. (page 4)

[240] Wang, Y., Rooney, C., Feldman, H. A., and Watkins, R. (2018). The Peculiar Velocity Correlation Function. *Mon. Not. Roy. Astron. Soc.*, 480:5332. (page 114)

[241] Weinberg, D. H., Mortonson, M. J., Eisenstein, D. J., Hirata, C., Riess, A. G., and Rozo, E. (2013). Observational Probes of Cosmic Acceleration. *Phys. Rept.*, 530:87–255. (page 86)

[242] Weinberg, S. (2005). Quantum contributions to cosmological correlations. *Phys. Rev.*, D72:043514. (page 2)

[243] Weinberg, S. (2008). Effective Field Theory for Inflation. *Phys. Rev.*, D77:123541. (page 51)

[244] Weller, J., Battye, R., and Kneissl, R. (2002). Constraining dark energy with Sunyaev-Zeldovich cluster surveys. *Phys. Rev. Lett.*, 88:231301. (page 4)

[245] Wetterich, C. (1988). Cosmology and the Fate of Dilatation Symmetry. *Nucl. Phys.*, B302:668–696. (page 56, 92)

[246] Will, C. M. (2014). The Confrontation between General Relativity and Experiment. *Living Rev. Rel.*, 17:4. (page 51)

[247] Woodard, R. P. (2007). Avoiding dark energy with 1/r modifications of gravity. *Lect. Notes Phys.*, 720:403–433. (page)

[248] Woodard, R. P. (2015). Ostrogradsky's theorem on Hamiltonian instability. *Scholarpedia*, 10(8):32243. (page 51)

[249] Yoo, J. (2010). General Relativistic Description of the Observed Galaxy Power Spectrum: Do We Understand What We Measure? *Phys. Rev.*, D82:083508. (page 67)

[250] Yoo, J., Fitzpatrick, A. L., and Zaldarriaga, M. (2009). A New Perspective on Galaxy Clustering as a Cosmological Probe: General Relativistic Effects. *Phys. Rev.*, D80:083514. (page 67, 73)

[251] Zhao, G.-B., Giannantonio, T., Pogosian, L., Silvestri, A., Bacon, D. J., Koyama, K., Nichol, R. C., and Song, Y.-S. (2010). Probing modifications of General Relativity using current cosmological observations. *Phys. Rev.*, D81:103510. (page 114)

[252] Zhao, G.-B., Pogosian, L., Silvestri, A., and Zylberberg, J. (2009). Cosmological Tests of General Relativity with Future Tomographic Surveys. *Phys. Rev. Lett.*, 103:241301. (page 114)

[253] Zheng, Y. and Song, Y.-S. (2016). Study on the mapping of dark matter clustering from real space to redshift space. *JCAP*, 1608(08):050. (page 46)

[254] Zumalacarregui, M. and Garcia-Bellido, J. (2014). Transforming gravity: from derivative couplings to matter to second-order scalar-tensor theories beyond the Horndeski Lagrangian. *Phys. Rev.*, D89:064046. (page 51)